# PHARMACOLOGICAL AND BIOPHYSICAL DISSECTIONS OF THE TRAFFICKING AND INFECTION OF ADENO-ASSOCIATED VIRUS (AAV) *IN VITRO* AND *IN VIVO*

Ping-Jie Xiao

A dissertation submitted to the faculty of the University of North Carolina at Chapel Hill in partial fulfillment of the requirements for the degree of Doctor of Philosophy in the Department of Cell and Developmental Biology.

Chapel Hill
2013

Approved by:

R. Jude Samulski (Ph.D)

Ken Jacobson (Ph.D)

Keith Burridge (Ph.D)

Tal Kafri (Ph.D, M.D.)

Ellen R. Weiss (Ph.D)

## ABSTRACT

PING-JIE XIAO: Pharmacological and Biophysical Dissections of the Trafficking and Infection of Adeno-Associated Virus *In Vitro* and *In Vivo*.
(Under the direction of Dr. R. Jude Samulski)

Adeno-associated virus (AAV) is a defective and non-pathogenic human parvovirus that is dependent on the co-infection of a helper virus, such as Adenovirus or Herpes Virus, to fulfill its productive life cycle. While many traits of this virus have made it an attractive vector for gene therapy as well as the wide application in over 100 clinical trials, there remains a great need to further improve the performance of AAV in gene delivery. As a most promising solution to fit such need, development of novel AAV vectors with improved efficiency on cellular trafficking and processing was partially achieved by several strategies in the last decade, including isolation of natural serotypes, directed evolution, and rational design. Being a most effective approach for the development of new AAV vectors in the future, rational design requires extensive knowledge on AAV-host interaction, which is mainly a multi-step trafficking and intracellular processing from cell surface binding to nuclear entry. However, much is unknown about the details of interactions between AAV and its host, which has limited one's ability to improve the delivery efficacy of AAV vectors and therefore restricted their medical applications.

The primary goal of this dissertation is to advance our current knowledge of AAV-host interactions by developing new methodologies and providing more insights on how virion components and host machineries at molecular level affect the infectious pathway of

AAV. Typically, a successful transduction is achieved upon the accomplishment of virions on cell surface attachment, endocytosis and endosomal sorting, cytoplasmic trafficking, nuclear targeting, and genome processing. Prior to this work, an efficient method to quantitatively evaluate the intracellular trafficking of AAV particles is not available. Additionally, it was unknown how the AAV traverses the crowded cytoplasm in host cells prior to the nuclear entry. While microtubules (MTs) have been reported to facilitate the trafficking of many other viruses, it was unclear whether and how this cellular machinery may regulate the intracellular behavior of AAV. Therefore, we set out to build on the known foundation of AAV biology and hypothesize that MTs play an important role on AAV infection especially the cytoplasmic trafficking of this virus. In this thesis, we have established a method of computer-assisted quantitative 3D bio-distribution microscopy that samples the whole population of fluorescently-labeled vectors and documents their trafficking routes through cells and tissues. This method shall facilitate a quantitative evaluation of the effects of pharmacological reagents and vector variants on the delivery performance of viral vectors. With this method, we have demonstrated that AAV particles exploit MT-mediated endosome transportation to traverse the dense cytoplasm to reach the host nucleus. In addition, we have discovered a new cellular barrier composed of MTs at MTOC region that limits the nuclear entry and transduction of AAV virions, defining a novel defense mechanism by which host cells restrain viral invasion. On the basis of above findings, we have proposed a model to better illustrate the infectious pathway of AAV and its fine-tuning by MTs. Moreover, we have also documented the trafficking of AAV in animal tissues, providing new insights to the AAV biology and vectorology *in vivo*. While focusing on how AAV traffics through the subcellular maze, this work intersects areas of cell biology,

biophysics, virology, and gene delivery. This work provides valuable research tools, rationales, and assays for future exploration of the details of AAV trafficking and will contribute to the knowledge of AAV biology, facilitating the rational development of gene therapy vectors.

To my parents and wife,

who have been extremely patient and supportive to my Ph.D. study with love

## ACKNOWLEDGEMENTS

With the completion of this dissertation, I'd like to show my gratitude to the nurturing environment surrounding me in Chapel Hill and back home in Shanghai that has fostered my intellectual growth. I would like to specifically thank Dr. Jude Samulski for his guidance, his inspiration, and for setting an excellent scientific example for me to follow. Thank Dr. Samulski for providing a great environment to further foster my research independence that was initially established during my Master's study in Dr. Xu's lab at Fudan University in Shanghai. As an international student, I also received valuable help from him to improve my language. In the Gene Therapy Center and Department of Cell Biology there are many faculty members that go above and beyond their profession, as teachers and as mentors. In this regard, the Drs. Ken Jacobson, Keith Burridge, Tal Kafri, Ellen Weiss, Aravind Asokan have been outstanding. I would also like to thank Drs. Robert Bagnell, Ken Jacobson, Michael Chua, Aaron Neumann, and Vladimir Ghukasyan for the productive discussions on the principles and rationales of fluorescence microscopy.

Both my family and friends have also been providing tremendous supports in my development as a scientist as well as a person. My special gratitude also goes to my lovely wife and my parents, to my close friends in the interdisciplinary biomedical sciences program, to my friends both in and outside of lab. They have all done more for me than I could ever do in return, and I am truly grateful.

## TABLE OF CONTENTS

## LIST OF TABLES

## LIST OF FIGURES

## ABBREVIATIONS

| | |
|---|---|
| 3D | Three-dimensional |
| AAV | Adeno-associated virus |
| Ad | Adenovirus |
| BR1- | Basic region 1 mutation $^{120}$QAKKR/QANNR |
| BR2- | Basic region 2 mutation $^{140}$PGKKR/PGNNR |
| BR3- | Basic region 3 mutation $^{168}$PARKR/PANNR |
| CBA | Chicken beta actin |
| CF | Cystic fibrosis |
| CFTR | Cystic fibrosis transmembrane conductance regulator |
| CMV | Cytomegalovirus |
| CPV | Canine parvovirus |
| DAPI | 4′,6′-diamidino-2-phenylindole |
| DIC | Differential interference contrast |
| DMEM | Dulbecco's modified Eagle's medium |
| DMSO | Dimethyl sulfoxide |
| DNA | Deoxyribonucleic acid |
| EGFP | Enhanced green fluorescent protein |
| FIX | Factor IX |
| G551D | Glycine at position 551 mutated to aspartic acid |
| GFP | Green fluorescent protein |
| HD/AN | Histidine-aspartic acid mutated to alanine-asparagine |

| | |
|---|---|
| HEK | Human embryonic kidney |
| HIV | Human immunodeficiency virus |
| HS | Heparin sulphate |
| ITR | Inverted terminal repeat |
| Luc | Luciferase |
| MFI | Mean fluorescence intensity |
| MOI | Multiplicity of infection |
| mRNA | Messenger ribonucleic acid |
| MTOC | Microtubule organizing center |
| MVM | Minute virus of mice |
| NLS | Nuclear localization signal |
| ORF | Open reading frame |
| PBS | Phosphate-buffered saline |
| PCR | Polymerase chain reaction |
| PEI | Polyethyleneimine |
| $PLA_2$ | Phospholipase $A_2$ |
| qPCR | Quantitative polymerase chain reaction |
| rAAV | Recombinant adeno-associated virus |
| RPE65 | Retinal pigment epithelium-specific 65kD protein |
| SA | Sialic acid |
| siRNA | Short interfering ribonucleic acid |
| SV40 | Simian vacuolating virus 40 |
| TR | Terminal repeat |

| | |
|---|---|
| VP | Viral protein |
| VP3only | Capsids comprised of only VP3 subunits |

# CHAPTER 1

# INTRODUCTION TO GENE THERAPY AND AAV BIOLOGY

## Viral vectors for gene therapy

**Gene therapy**. The idea to treat heritable genetic disorders by delivering a functional copy of a mutant chromosomal gene was conceived as early as the 1970s (Osterman et al. 1971; Rogers 1971). Since then, the innovations in methods of gene delivery have expanded to include strategies, such as gene knockdown (i.e. shRNA delivery) and cell killing (i.e. cytotoxic gene delivery), to treat disorders resulting from gain-of-function or aberrant function mutations, in addition to rescuing loss-of-function genetic disorders. Spurred by the potential therapeutic impact of gene delivery and innovations in vector technology, the first clinical trial using gene therapy was reported in 1990 (Rosenberg et al. 1990). Since then, over 1700 clinical trials have been initiated with delivery methods spanning chemical carrier molecules to viral vectors and therapeutic targets including cardiovascular, neurological, muscular diseases, and cancer (www.wiley.co.uk/genmed/clinical). Adeno-associated virus (AAV) in particular possesses several biological properties that make it an ideal vector for gene delivery. Data from clinical trials demonstrate that AAV has a robust safety profile and therapeutic efficacy in several contexts. However, these data have also revealed that further improvement in the efficiency of delivery is needed. This has become one of the primary focuses of the field. Strategies of engineering the capsid to enhance AAV transduction offer a potential solution for improving therapeutic performance of this vector.

Developing a method to introduce therapeutic nucleic acids into specific cells or tissues within the body is not straightforward. Many different strategies have been employed. In general, all of these strategies can be classified into two categories based on the mechanism of delivery, non-viral or viral. Non-viral methods are typified by the delivery of naked nucleic acids (DNA or RNA) by physical means (e.g. gene gun or ultrasonic) or with the help of chemical reagents (e.g. cationic polymers) (Table 1). Viral methods rely on packaging nucleic acid encoding the functional protein or RNA inside of a viral particle and subsequent delivery to target cells via viruses' natural infection pathways.

**Non-viral delivery.** Delivery of 'naked' nucleic acid is probably the most straight forward approach to introducing genetic material into a cell (Kawabata et al. 1995). Delivery of naked nucleic acid (e.g. plasmid DNA (pDNA)) in this manner offers several desirable merits, including scalable production, low immunogenicity, and low rate of insertional mutagenesis (Wolff et al. 2005; Yazawa et al. 2006; Gray et al. 2008). However, the uptake and expression of pDNA is highly inefficient and is minimally tissue specific. This inefficiency of pDNA delivery is due to several factors. Naked nucleic acids are susceptible to degradation by nucleases present in the body (Pollard et al. 1998; Hoen et al. 2006; Liu et al. 2007). Additionally, the negative charge of these molecules causes electrostatic repulsive forces with the cell surface, partly accounting for the low level of uptake by cells (Bieber et al. 2002). Finally, once internalized into a cell, escape from endosomes/lysosomes as well as in the process of crossing the nuclear membrane is highly inefficient (Dean et al. 2005; Watson et al. 2005). To increase the efficiency of this delivery method, several strategies have been employed to protect the nucleic acid and improve cell entry. Cationic carrier molecules, including lipids and polymers (e.g. Polyethyleneimine), condense and protect

nucleic acids from exposure to nuclease degradation (Luo et al. 2000). These molecules coat the nucleic acid with excessive positive charges to improve association with the cell surface (Chen et al. 2007).The effect of these carriers is limited, however, due to promiscuous binding, which leads to low circulation times and the inability to target specific tissues or cell types (e.g. tumors) (Luo et al. 2000). Tissue specific delivery of naked nucleic acids can be achieved, to a certain degree, by conjugating specific ligands, such as transferrin, peptides, or growth factors (Gupta et al. 2005; Watson et al. 2005). The addition of these ligands targets the molecule to certain cell surface receptors, thus improving specificity. Sugars, such as galactose, mannose and saccharides, can also be added to enhance cellular uptake of nucleic acids and provide some level of specificity in tissue targeting (Hashida et al. 2001; Yu et al. 2009). However, most carriers and ligands do not assist crossing of the nuclear membrane and thus, transfer of plasmid to the nucleus only occurs when there is breakdown of the nuclear membrane during cell division (Wells 2010).

**Viral vectors for gene delivery.** Compared with non-viral methods, virus-mediated gene transfer can deliver genetic materials to cells or tissues with much higher efficiency and greater specificity. Several viruses have been explored for use as vectors for gene delivery. All of these viral systems rely on a similar approach, replacing part or all of the genome of the virus with the desired transgene, which can then be packaged and delivered to cells via the virus' natural transduction pathway. For this reason, each virus offers distinct advantages and disadvantages depending on the specific needs in the therapeutic protocols (e.g. target cells, size of transgene, etc.). Vectors have been developed based on Retroviruses, Adenoviruses, Herpes simplex viruses, and AAV.

**Table 1. Comparison of methods of gene delivery**

Table 1. Comparison of methods of gene delivery.

| Vectors | Naked DNA | Retrovirus (non-integrating lentiviral/ integrating) | Adenovirus | Herpes simplex virus | Adeno-associated virus |
|---|---|---|---|---|---|
| Genome type/ packaging limit | Plasmid/~10 kb | ssRNA/~8 kb | dsDNA/~35 kb | dsDNA/~150 kb | ssDNA/~4.6 kb |
| Particle size | <10 nm | ~100 nm | ~70–100 nm | ~180 nm | ~25 nm |
| Delivery efficacy[†] | - (low uptake and expression; lack of tissue specificity) | ++ (maybe limited to certain cell types) | +++ | + (limited to CNS) | +++ |
| Duration of expression[†] | - (transient) | +/++ (up to 9 months) | ++ (up to 2 years) | + (up to 7 months) | +++ (over 7.5 years) |
| Pathogenesis[†] | +++ (very low immunogenicity and integration) | ++/- (immune response and potential integration) | - (highly immunogenic and inflammatory) | - (immunogenicity and potentially toxic to CNS) | +++ (very low immunogenicity and integration) |

*[†]Relative rating of performance as a gene therapy vector for given traits (delivery efficacy, duration of expression and pathogenesis) from worst '-' to best '+++'.*

**Retroviruses.** Retroviruses are characterized by the ability to reverse transcribe a single-stranded RNA (ssRNA) genome into double-stranded DNA (dsDNA) and integrate into the host genome as part of their natural life cycle. The retroviral virion consists of an exterior envelope, averaging 80-100nm in diameter, which surrounds a protein capsid. The capsid contains two copies of the linear ssRNA genome, each 7-12kb in length (Osten et al. 2007). Viral infection begins with binding to the cell via interaction between glycoproteins on the viral envelope and specific receptors on the host cell surface. The viral envelope then fuses with the cell membrane and releases the capsid into the cytoplasm. Subsequently, the genetic material is released and transported to the nucleus with the aid of viral and cellular proteins. Once inside the nucleus, the viral genome integrates into the host chromosomes as a natural feature of its replication cycle.

Initially, vectors for gene delivery were derived from simple retroviruses, such as the gamma-retrovirus Moloney Murine Leukemia virus (MMLV). Long-term gene expression as a result of chromosomal integration was viewed as a significant advantage (Miller et al. 1990; Robbins et al. 1998). Such vectors were prominently featured in early gene therapy trials to treat X-linked SCID among other diseases (accounting for ~20% of clinical trials) (Gaspar et al. 2004; Chinen et al. 2007). However, the risk of insertional mutagenesis and failure of these vectors to infect non-dividing/differentiated cells have greatly limited their use (Miller et al. 1990; Robbins et al. 1998; Cavazzana-Calvo et al. 2007). In light of these concerns, vectors were developed based on “complex” retroviruses (e.g. lentiviruses HIV and SIV) (Miyoshi et al. 1998). In contrast to simple retroviral vectors, lentiviral vectors transduce non-dividing cells and can be engineered to have a much lower risk of insertional mutagenesis (Schnell et al. 2000; Bahner et al. 2007). Currently, lentiviral vectors have been

or are used in 2.3% clinical trials, treating diseases such as adrenoleukodystrophy (ALD), parkinson's disease, sickle cell anemia, and cancer immunotherapy (Bank et al. 2005; Li et al. 2005; Cartier et al. 2009; Williams 2009). Several advancements in vector engineering have made lentiviruses a viable option for clinical therapy. Among these, pseudotyping of vectors with different surface glycoproteins, such as vesicular stomatitis virus glycoprotein, has expanded targeting to a wider variety of cell/tissue types. Additionally, insights into the mechanism of vector integration have yielded non-integrating lentiviral (NIL) vectors that have nearly eliminated the risk of insertional mutagenesis. Despite these promising improvements, several hurdles remain. One problem is that these vectors are subject to transgene silencing (Bonci et al. 2003; Ellis 2005). The mechanism of this is not well understood, but long-term gene expression is limited. The innate immune response and preexisting immunity to glycoproteins used to pseudotype these vectors have also limited their efficacy (Towers 2007). Finally, a means of scalable production of clinical grade vector is lacking and challenges future advancement of this system.

**Adenovirus.** Adenovirus (Ad) possesses several properties that are desirable for a gene delivery vector and has been developed extensively for this purpose. In contrast to retroviruses, the Ad virion is made up of only a protein capsid of 70-100 nm in diameter and a 26-40 kb linear dsDNA genome (Campos et al. 2007). Transduction of Ad is mediated through interaction of the Fiber protein, which extends from the capsid surface, with the coxsackievirus and adenovirus receptor (CAR) on the cell surface. The virus is then internalized and transported to the nuclear envelop where its genome is released through the nuclear pore.

Development of Ad as a gene therapy vector has undergone several generational advancements. First generation vectors were created by removal of the E1 region of the genome. This deletion prevents replication of the virus and provides space in the genome for insertion of exogenous DNA (Kovesdi et al. 1997). To propagate these vectors, the E1 proteins must be provided in *trans.* The major concern with this method is that recombination events during vector production between the vector and complementing E1 sequence can result in restoration of wild type (WT) Ad. Second generation vectors remove a greater portion of the genome, including regions E2, E3, and E4. This reduces, but does not eliminate the risk of recombination events resulting in WT virus and expands the capacity for transgenes. Third generation 'gutless' vectors take this principle to the maximum by removing all non-essential sequence in the genome (Chen et al. 1997).

Ad-based vectors can infect dividing and non-dividing cells, have high transgene capacity, and a low rate of insertional mutagenesis. Additionally, scalable methods of production allow high titer preparations. Ad vectors have been widely used to treat a variety of diseases and account for ~24% of clinical trials ((Ghosh et al. 2006; Roth 2006; Gray et al. 2008; Mata-Espinosa et al. 2008); www.wiley.co.uk/genmed/clinical). The greatest hurdle to use of Ads is that they are highly immunogenic and inflammatory. Many patients have preexisting immunity to the virus and therapeutic effect of derived vectors can be limited by the host immune response (Douglas 2007). As a result, Ad vectors may be best suited for treating diseases in which only transient gene expression is needed, such as cancer.

**Herpes simplex virus.** Among members of the family *Herpesviridae*, the most progress toward developing gene therapy vectors has been made with herpes simplex virus (HSV). HSV is a large virus (~180 nm in diameter) comprised of an exterior envelope

containing a proteinaceous layer (i.e. tegument) and an icosahedral protein capsid. The packaged genome is a linear double-stranded DNA of ~152kb in length. Similar to retroviruses, HSV binds to specific receptors on target cells via glycoproteins on the surface of the viral envelope. The envelope then fuses with the cell membrane and the capsid and tegument are released into the cytoplasm. The capsid is trafficked to the nucleus with the aid of viral and cellular factors and the genome released through the nuclear pore. Once in the nucleus, the linear genome circularizes and persists in the cell as an extrachromosomal episome. Vectors derived from HSV are able to transduce dividing and non-dividing cells and can be targeted to various cell types by surface protein pseudotyping, much like retroviruses. Due to its size, HSV can deliver large pieces of exogenous DNA, the largest capacity among commonly used viral vectors (Fink et al. 1997; Geller 1997). HSV vectors account for ~3% of clinical trials. However, also much like retroviruses, a limitation of these vectors has been silencing of gene expression caused by DNA methylation, which has made these vectors less effective for long-term therapy (Kass et al. 1997; Lilley et al. 2001; Sun et al. 2003; Suzuki et al. 2008). Host immune responses to the vector and lack of scalable production have limited the application of these vectors as well (Fraefel et al. 1996).

In summary, the above viruses have been developed extensively as vectors for gene delivery to treat a number of human genetic disorders. Although each possesses desirable traits, several limitations confront their application in humans, including risk of insertional mutagenesis, host immune response, restricted tissue tropism, and limited duration of transgene expression. Further improvement of these vectors is required to overcome these challenges.

## AAV biology and vectorology

AAV shares many features in common with the viral vectors discussed above, however, it also has unique advantages that make it an exceptional vector for gene delivery. Unlike other viral systems, WT AAV is not associated with disease or pathology and derived vectors have an excellent safety profile in humans (Mueller et al. 2008). Moreover, the natural persistence of this virus in many tissues facilitates long-term transgene expression (Berns et al. 1975). A number of innovations have contributed to the success of AAV as a vector for gene therapy as well. For example, the ability to package AAV serotype-2 genome into capsids from various serotypes (transencapsidation) gives this vector a wide range of potential tissue tropisms (Rabinowitz et al. 2002). The following sections review the biology of AAV, successes and challenges that are already visible from clinical trials, and current strategies to improve AAV vectors further.

**AAV biology.** AAV was first discovered in 1965 as a contaminant in an Adenovirus preparation (Atchison et al. 1965; Hoggan et al. 1966). It was later classified as a member of the genus *Dependovirus* of the *Parvovirus* family because its replication depends on co-infection of a helper virus such as Adenovirus. AAV is a relatively small virus (~20nm) and consists of an icosahedral protein capsid containing the viral genome. The capsid possesses specificity for binding specific cell surface receptors and different serotypes have unique binding properties (McCarty et al. 2003; Ding et al. 2005). The viral genome is a single-stranded DNA (ssDNA) of ~4.7kb in length and is flanked by 145bp inverted terminal repeats (ITR). The ITR contains complementary sequences that result in formation of a 'T' shaped hairpin structure at both termini of the genome. This secondary structure facilitates synthesis of the second-strand and thus formation of a double-stranded molecule, which

severs as the template for transcription. The genome encodes open reading frames (ORF) *Rep* and *Cap* (Fig.I-1). *Rep*, is positioned 5' on the AAV genome and encodes four replication-related proteins, Rep78, Rep68, Rep52, and Rep40 (Kyostio et al. 1994). Rep78 and Rep68 interact with sequences within the ITR, termed the Rep-binding element (RBE), and are required for resolution of the secondary structures during replication. Rep52 and Rep40 are necessary for generation of single-stranded genomes and packaging. The *Cap* ORF is positioned 3' on the viral genome and encodes three structural proteins VP1, VP2 and VP3. These proteins assemble at a ratio of 1:1:10 (VP1:VP2:VP3) to form the viral capsid (Buning et al. 2004) consistent of 12 pentamers or 20 trimers of VP subunits (Fig.I-2). The three structural proteins share a common carboxyl terminal region, but have different amino-termini. This grants different functions to each of these proteins because the amino-terminus is involved in virus binding, entry, and intracellular trafficking (Johnson et al. 2010). Structural modules on the capsid surface and inside have to work accordantly for successful transduction. VP3 makes up the framework of the capsid, and the crystal structure portrays a rigid β-barrel core surrounded by eight loops (a.k.a variable regions), providing virions with interfacial interactions and receptor binding motifs on the capsid surface. The N-termini of VP1 and VP2 are more flexible than the β-barrel core and yet to be crystallized. While dispensable for virus assembly, genome packaging, cell surface binding and internalization, VP1 and VP2 are critical for productive infection and deletion of these proteins severely impairs the viral transduction. The structure of AAV2 icosahedral capsid is illustrated in figure I-2. Recently, coding for an additional protein, assembly activating protein (AAP), was described to overlap with the *Cap* gene and may be involved in AAV capsid assembly (Sonntag et al. 2010; Sonntag et al. 2011) (Fig. I-1).

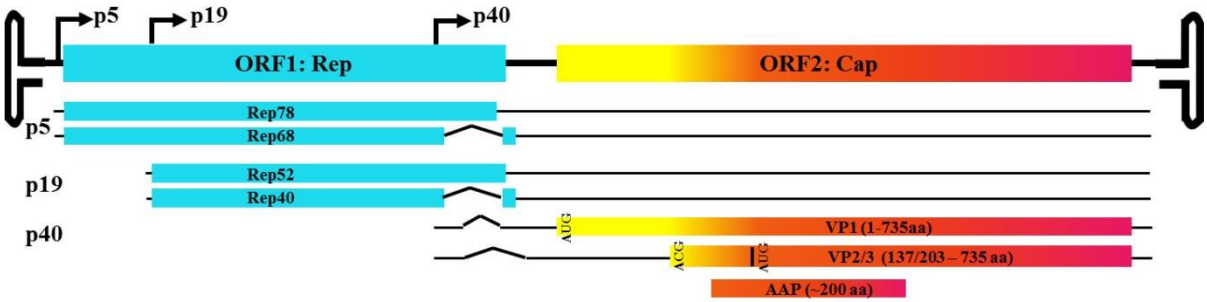


**Figure I-1. AAV genome.** Two open reading frames (ORFs) code proteins essential for virion replication and capsid composition. The left ORF '*Rep*' encodes four Rep proteins driven by two promoters. Both Rep78 (non-spliced) and Rep 68 (spliced) are initiated by the p5 promoter. Both transcripts of Rep 52 (non-spliced) and Rep 40 (spliced) are initiated by the p19 promoter. The right ORF '*Cap*' encodes three structural proteins (VP1-3) and one non-structural protein (AAV). Capsid transcripts are driven from the p40 promoter, which produces a minor splice variant for coding VP1 and a major splice variant for coding VP2 and VP3. Three capsid proteins exist in an overlapping reading frame with an identical C-terminus.

Current understanding of the AAV life cycle is derived primarily from the studies of serotype-2 (AAV2). Though many aspects are conserved among all serotypes, the reader should bear in mind that there are differences that make each unique. The life cycle of AAV2 involves receptor-mediated cell entry (Summerford et al. 1998), endosomal trafficking and escape (Ding et al. 2005), nuclear entry, and uncoating (Xiao et al. 2002; Grieger et al. 2006). Once the genome is released from the capsid, second-strand synthesis initiates from the 3' ITR. The secondary structure of the ITR is critical for this priming event as it positions the 3'end of single-stranded genome to act as the primer for the second strand. The resulting double-stranded molecule can then serve as the template for gene expression. In the absence of helper virus function the virus enters a state of latency (Samulski et al. 1991). In this state, viral gene expression is repressed and the genome persists episomally (Giraud et al. 1995). In the presence of Rep proteins, AAV DNA can integrate into a specific site in the human genome (chromosome 19), which shares homology with the ITR sequence and can be bound by the Rep proteins (Kotin et al. 1992; Miller et al. 2005; Nakai et al. 2005). It has been proposed that integration of AAV at this site may be part of the latent stage of AAV infection, aiding persistence in the absence of helper virus (Kotin et al. 1992). However, this has not been demonstrated conclusively. Genome replication commences with co-infection by a helper virus or other genotoxic stimuli (Atchison et al. 1965; Grossman et al. 1984; Yakobson et al. 1987; Yalkinoglu et al. 1988; Walz et al. 1997). Helper viruses provide several functions, including assisting transport to the nucleus, activation of transcription, and promoting an environment that is conducive to DNA replication (Chang et al. 1990; Shi et al. 1991; Duan et al. 1999; Xiao et al. 2002). For example, Ad proteins E1B55k and E4orf6 disrupt cell cycle regulatory proteins (Ferrari et al. 1996; Fisher et al. 1996). Similarly,

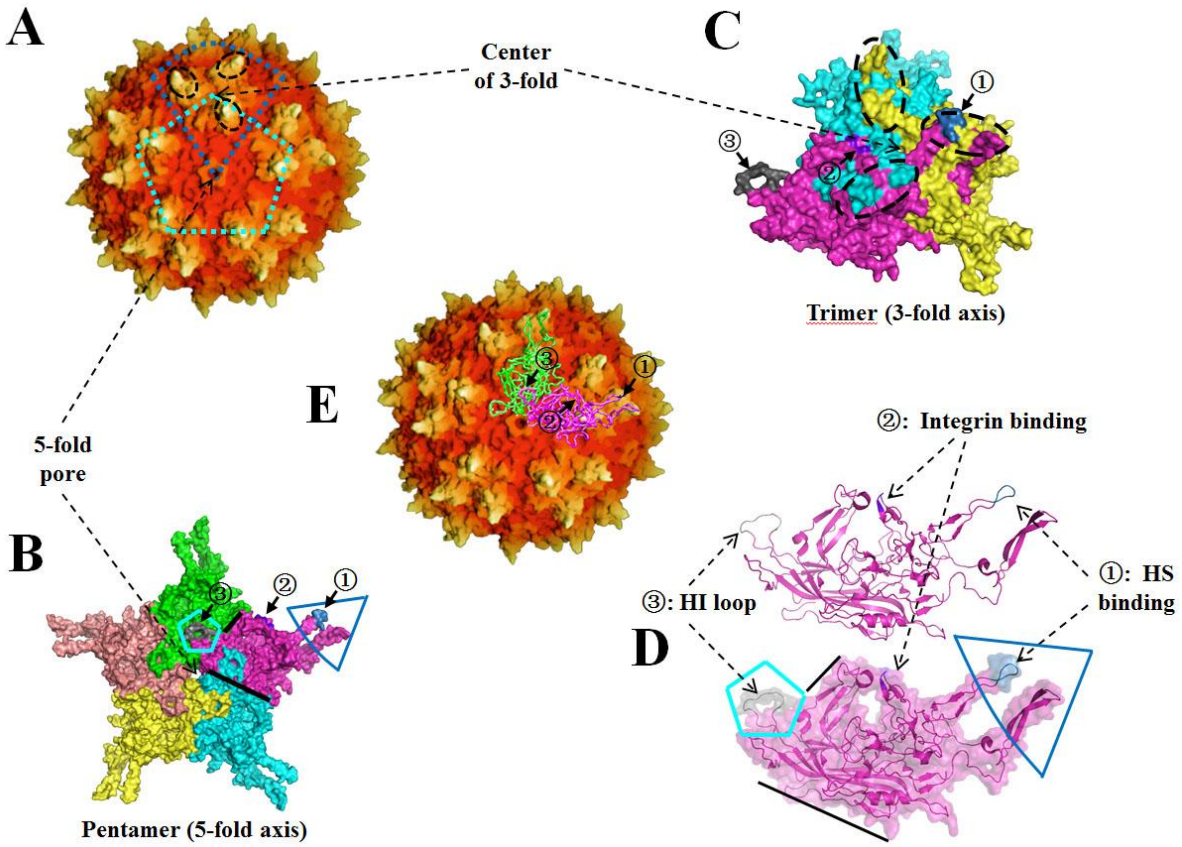


**Figure I-2. Structural dissection of the AAV capsid.** A) Model of icosahedral AAV capsid with highlighted pentamer (dashed cyan pentagon) and trimer (dashed blue 'triangle'). B) Surface representation of a pentamer composed of five VP3 subunits. C) Surface representation of a trimer composed of three VP3 subunits. Three 3-fold spikes in the trimer are highlighted by dashed black circles as in A). D) Top panel: Cartoon ribbon representation of a VP3 subunit of AAV2. Bottom panel: Cartoon ribbon representation is superimposed with the surface representation of a VP3 subunit. The positions of amino acid motif for HS binding, Integrin binding, and HI loop are highlighted in B-E. The parts of VP3 that form the 2-, 3-, and 5-fold axes of capsid symmetry are marked by black line, blue triangle, and cyan pentagon respectively in B and D. E) The AAV capsid is superimposed with the cartoon line representation of two VP3 subunits.

genotoxic stimuli, such as hydroxyurea or UV irradiation, can induce AAV replication as well (Grossman et al. 1984; Yakobson et al. 1987; Yalkinoglu et al. 1988).

**AAV vectorology.** Since generation of the first infectious clone of AAV2, the potential of recombinant AAV (rAAV) as a vector for gene therapy has become increasingly evident (Samulski et al. 1982; Samulski et al. 1983). Among many desirable attributes, AAV can transduce a variety of cell types, both dividing and non-dividing, and it is capable of long-term gene expression. Vectors derived from AAV retain only the ITR sequence, which is required for viral packaging and assembly, from the WT virus and do not express any viral genes (Xiao et al. 1997). This removes the possibility of unwanted consequences from introducing viral genes or genomic sequence. Additionally, scalable systems of production have been developed. Production of vector requires co-expression of *Rep*/*Cap* genes. Current methods supply these proteins as well as necessary helper virus proteins in *trans* and have virtually eliminated the risk of producing WT AAV (Samulski et al. 1989; Grieger et al. 2006). rAAV vectors utilize the same mechanisms and pathways of entry and trafficking as WT AAV, except that they do not integrate into the host chromosome due to the absence of the Rep proteins. Instead, the genomes form predominantly concatamers and persist as circular episomes (Miao et al. 1998; Nakai et al. 2001).

rAAV vectors have been tested for the treatments of a variety of disorders. In fact, more than 60 clinical trials have been initiated or completed with AAV-based vectors. The data from these trials establish an excellent safety profile for *in vivo* gene transfer, but also suggests that the efficiency of rAAV vectors bears further improvement.

## Applications and challenges of AAV in clinic

The first AAV vector to be delivered to human subjects carried the CFTR gene in a clinical trial to treat cystic fibrosis in 1995 (Flotte et al. 2003). Since then the number of AAV-based clinical trials has increased to more than 60. Here, I will briefly summarize these trials and discuss the challenges AAV vectors must overcome. A brief summary of these clinical trials is provided in Table 2.

**Cystic fibrosis.** Cystic fibrosis (CF) is an autosomal recessive disease that affects the lung most critically, but can also afflict the liver, pancreas, and intestine. This disease is caused by malfunction of the cystic fibrosis transmembrane regulator (CFTR), a chloride ion channel protein expressed in epithelial cells. Protein replacement therapy for a non-secreted protein such as CFTR is currently not feasible. As a result, gene therapy approaches to introduce a functional copy of the CFTR gene are being pursued as a strategy of treatment. In total, nine clinical trials have been initiated using AAV vectors to treat this disease (www.wiley.co.uk/genetherapy/clinical). The first was a phase I, dose-escalating trial, which introduced vector directly into the lung of 25 patients. Administration of the vector was well tolerated and only a mild neutralizing antibody response was detected in serum at the highest dosage (Flotte et al. 2003). However, the levels of gene expression observed were very low. Following this first attempt, subsequent trials have targeted the epithelium of the maxillary sinus for delivery in order to alleviate the symptom of persistent sinusitis associated with CF. As with delivery to the lung, targeting to this site had no significant side effects and the level of expression of CFTR, though insufficient for therapy, correlated with vector dose (Wagner et al. 1999; Wagner et al. 2002). More recent trials have tested introducing vector by inhaled aerosol. One such trial clearly demonstrated the safety of aerosolized delivery and, similar to

other methods of delivery, reported a dose-dependent response in gene expression (Aitken et al. 2001). In an attempt to reach therapeutic levels of expression, a multi-dose approach was conducted in which patients received multiple injections of vector. In this trial, repeated doses were well tolerated by the host immune system and an encouraging trend in improvement of pulmonary function was suggested by measurement of interleukin-8 (IL-8) and forced expiratory volume (Moss et al. 2004). However, a follow up study, which expanded treatment to additional patients, did not find the same effect, which brings into question the efficacy of this treatment protocol (Moss et al. 2007). Overall, these results provide data on the safety of rAAV delivery to the airway epithelium, but indicate that more efficient gene transfer is required to achieve therapeutic effect. A more comprehensive review can be found at Griesenbach et al (Griesenbach et al. 2012).

**Alpha1-antitrypsin deficiency.** Alpha1-antitrypsin (AAT) deficiency is an autosomal recessive disorder caused by reduced circulating levels of AAT protein (normally 1.5-3.5 mg/ml), which is secreted into the serum by hepatocytes and provides protease protection of the lung. Certain mutations of the AAT gene can also result in accumulation of abnormal protein in hepatocytes, causing disease of the liver. The symptoms of AAT-deficiency are emphysema, chronic obstructive lung disease, and liver damage. Current treatments include protein replacement therapy and avoidance of risk factors, such as smoking. Protein replacement therapy is costly and requires weekly infusions. Gene therapy has been explored for this disease primarily because restoration of only low levels of AAT (~800 μg/ml) can have therapeutic effect.

Based on successes in preclinical studies, several clinical trials have been initiated to treat AAT deficiency (Song et al. 2002; Lu et al. 2006). Two phase I trials are underway to test intramuscular delivery of rAAV expressing the AAT gene (Flotte et al. 2004; Brantly et al. 2009). Mild neutralization antibody and

## Table 2. Summary of AAV mediated clinical trials

**Table 2. Summary of gene therapy clinical trials utilizing adeno-associated virus vectors.**

| Disease | Phase trial | Vector/gene (administration route) | Safety data† | Immune response† | Delivery efficiency† | Therapeutic efficacy† |
|---|---|---|---|---|---|---|
| Cystic fibrosis | I | AAV2/CFTR (lung) | Safe | NAb | 0.002–0.5 vg/cell | N/A |
| | I[1a] | AAV2/CFTR (maxillary sinus) | Safe | NAb | 0.1–1 vg/cell | Insufficient |
| | II[1b‡] | AAV2/CFTR (maxillary sinus) | Safe | None | N/A§ | Insufficient |
| | I[2a‡] | AAV2/CFTR (lung via aerosol) | Minor adverse events | NAb | 0.1–0.6 vg/cell | N/A |
| | II[2b‡] | AAV2/CFTR (lung via aerosol) | Safe | NAb | 13–2303 vg/cell | Minor |
| | II[2c‡] | AAV2/CFTR (lung via aerosol) | Safe | NAb | N/A§ | Insufficient |
| AAT deficiency | I | AAV2/AAT (im. injection) | Safe | NAb | Up to 82nM serum AAT | Insufficient |
| | I | AAV1/AAT (im. injection) | Safe | NAb + T-cell response | 1.5–3.5 µg/ml serum AAT | Insufficient |
| | II | AAV1/AAT (im. injection) | Safe | NAb + T-cell response | 20 µg/ml serum AAT | Insufficient |
| Leber's congenital amaurosis | I | AAV2/RPE65 (subretinal injection) | Minor adverse events | NAb | N/A§ | Sufficient |
| Hemophilia B | I | AAV2/FIX (im. injection) | Safe | NAb | <2% | Insufficient |
| | I | AAV2/FIX (hepatic artery) | Safe | NAb + T-cell response | Therapeutic level of FIX | Minor |
| | I¶ | AAV2/FIX (hepatic artery) | N/A§ | N/A§ | N/A§ | N/A§ |
| | I | AAV8/FIXco (iv. injection) | Safe | T-cell response | 2–11% | Sufficient |
| Neurological diseases# | I | AAV2/ASPA (intracranial) | Safe | NAb | N/A§ | N/A§ |
| | I | AAV2/CERE-120 (intracranial) | Safe | None | N/A§ | Minor |
| | II | AAV2/AADC (intracranial) | Safe | NAb | N/A§ | Moderate |
| | I | AAV2/GAD65/67 (intracranial) | Safe | NAb | N/A§ | Moderate |
| | I | AAV2/CLN2 (intracranial) | Severe adverse events | NAb | N/A§ | Insufficient |
| Muscular dystrophy | I | AAV1/α-sarcoglycan (im. injection) | Safe | NAb + T-cell response | 57–62% positive fibers | Moderate |
| | I | AAV1/γ-sarcoglycan (im. injection) | Safe | NAb + T-cell response | 0.4–10.5% positive fibers | N/A§ |
| | I | AAV2.5/dystrophin (im. injection) | Safe | T-cell response†† | 0.01–2.56 vg/ diploid genome | N/A§ |

*†Some of these are the authors' summary based on the original reports to provide a general view of the outcome of these trials. The order of 'therapeutic efficacy' is: sufficient >moderate>minor> insufficient. For detailed information and exact conclusions, please refer to the text or the original reports.*
*‡For two consecutive clinical trials, '1b' is a follow-up one of '1a'; the same definition applies to '2a, 2b, 2c'.*
*§N/A represents one of the following cases: the information is not available in the original reports or authors are not able to make a brief conclusion based on the information presented in the original reports.*
*¶In this trial, immunosuppressive reagent was used.*
*#There are several other clinical trials for neurological disorders, but the details are currently not available or not accessible to the authors. A most recent review covers a general view of these trials (Weinberg, 2012).*
*††This T-cell response is against the transgene dystrophin, and the immune responses described for others trials are against the AAV capsid.*
*AADC: Aromatic amino acid decarboxylase; AAT: α1-anti-trypsin; ASPA: Aspartoacylase; CFTR: Cystic fibrosis transmembrane regulator; CLN2: Neuronal ceroidlipofuscinosis/tripeptidyl peptidase; FIX: Factor IX; GAD: Glutamic acid decarboxylase; im.: Intramuscular; iv.: Intravascular; N/A: Not available; NAb: Neutralizing antibody; RPE65: Retinal pigment epithelium-specific 65 kDa protein.*

T-cell immune response against the viral capsid were observed, but this did not adversely affect patient health and was dependent on vector dose. Although the level of AAT expression was below that required for therapeutic effect, transgene expression persisted for over 1 year and the safety data revealed no adverse reactions. These results suggest this method of delivery may produce therapeutic effect with increased vector dosage (Brantly et al. 2006; Brantly et al. 2009). This was tested in a subsequent study in which dose-escalation was performed in conjunction with IM delivery of rAAV serotype 1, shown to transduce muscle with high efficiency in animal models (Flotte et al. 2011). At three months of observation, vector administration was well tolerated, but all subjects developed neutralizing antibodies to AAV1 capsid. Antibody response was not observed against the transgene product, WT AAT. In this context, the level of transgene expression corresponded with vector dose and the level of circulating AAT in the serum reached >20 μg/ml in all patients (~2.5% of the required level). Thus, significant progress has been made toward developing a therapeutic for AAT deficiency, but further improvement is necessary to achieve rescue of function. Flotte et al provides a more comprehensive review on this disease (Flotte et al. 2011).

**Leber's congenital amaurosis.** Leber's congenital amaurosis (LCA) is a rare disease (estimated prevalence of about 1:80,000) in which vision is lost due to degeneration of the retina (Stone 2007). This disorder can be caused by mutations in one of more than a dozen genes. Mutation of the gene *RPE65* represents about 6% of all cases of LCA (den Hollander et al. 2008). Recent success has been achieved with gene therapy approaches to provide this gene. Sub-retinal injection of rAAV carrying *RPE65* has been demonstrated to restore vision in a canine model of LCA and expression of the protein has persisted for ~7.5 years (Acland

et al. 2001). When this strategy was extended into patients, restoration of vision was observed in most patients several weeks after treatment (Bainbridge et al. 2008; Cideciyan et al. 2008; Maguire et al. 2008). Continued observation revealed improvement in vision for up to 1.5 years and no adverse effects or pathology was observed (Simonelli et al. 2010). This is now regarded as the first successful AAV-based gene therapy trial in humans. These results demonstrate the safety and efficacy of delivering rAAV to the eye by sub-retinal injection and introduce a method of therapy that could potentially be used to treat other ocular diseases in addition to LCA. A more comprehensive review can be found at Stein et al (Stein et al. 2011).

**Hemophilia B.** Hemophilia B is an X-linked recessive disorder caused by defects in the gene encoding blood coagulation factor IX (FIX). Persons with a level of functional FIX less than 1% that of normal have severe hemophilia B and suffer from bleeding into the joints and soft tissues. This disease can even be fatal if bleeding occurs in the brain. Levels of FIX at 1-5% that of normal are associated with decreased bleeding episodes and levels over 5% provide normal function. Similarly to AAT deficiency, current treatment for Hemophilia B is protein replacement therapy, which is expensive and requires repeated intravenous injections. rAAV gene delivery may offer a more suitable strategy of treatment. rAAV vectors expressing the FIX gene have been administered to muscle and liver in animal models of Hemophilia B. Because the protein product is secreted to the blood stream, both tissues are suitable targets for expression. Based on data from these studies, four clinical trials have been initiated (High 2011). The first one attempted intramuscular injection. Although gene transfer and expression were not prevented by the pre-existing high titer of neutralization antibodies against the capsid, only limited transgene expression (<2%) was achieved at the highest dose

used (Kay et al. 2000; Manno et al. 2003). The second trial altered targeting to the liver via infusion through the hepatic artery. This approach did achieve expression of therapeutic levels of FIX, but only transiently (~2-4 weeks). Host immune response mediated by T lymphocytes against the vector capsid has been suggested to clear the transduced hepatocytes and thus limit the efficiency of delivery (Manno et al. 2006; Mingozzi et al. 2007). Based on these results, a third trial has been initiated using the same strategy as the second trial, targeting the liver, with co-administration of immunosuppressive drugs (High 2011). Results of this trial have not yet been reported, but it will be interesting to see if vector transduction is increased as a result. More recently, Nathwani and colleagues have taken a different angle to evade the immune system and increase gene expression, including utilization of serotype 8 capsid, which transduces the liver with higher efficiency and is less immunogenic than serotype 2 in animal models, and codon optimization of the transgene expression cassette (High 2011; Nathwani et al. 2011). With this strategy, therapeutic levels of FIX were observed (2-11% of normal) in all patients and gene expression persisted up to 16 months (Nathwani et al. 2011). Thus, efforts are close to a successful therapy. This evolution of treatment for FIX deficiency offers insight into the planning of future trials with AAV. Foremost, that there may be considerable flexibility in the immunogenicity and efficiency of transduction with capsids of different serotypes. High et al provides a more comprehensive perspective of gene therapy to treat this disease (High 2011).

**Neurological diseases.** rAAV vectors have been used to treat several diseases affecting the central nervous system (CNS), including Canavan's disease, Parkinson's disease (PD), Alzheimer's disease (AD), Batten's disease, and Epilepsy. To date, a total of twelve clinical trials have been conducted, six phase I, one phase I/II, and five phase II. The

first of these trials targeted Canavan's disease, a childhood form of leukodystrophy caused by mutations in the gene coding the enzyme aspartoacylase (ASPA). This disease causes irreversible brain damage and often death within the first decade of life (Leone et al. 1999). To treat this disease, rAAV expressing ASPA was injected intracranially into ten patients. This was the first attempt to deliver a rAAV vector to the CNS in humans and a considerable amount of data was collected to assess the safety of this approach. Importantly, no adverse side effects were experienced by any of the patients and host immune response to the vector was limited to a low level antibody response in patient serum (Janson et al. 2002; McPhee et al. 2006). Though data on the efficacy of treatment in this trial has not been reported, the safety information alone has paved the way for additional studies. Following this initial success, trials have been initiated for Parkinson's disease (PD) as well (Carlsson et al. 2007). PD is a progressive neurodegenerative disease caused by loss of dopaminergic neurons in the substantia nigra and a deficiency of the neurotransmitter dopamine. It appears in 5% of the population over 65 years of age and the predominant symptom is progressive loss of motor function. Strategies to reverse this disease have focused on providing either nerve growth factors (NGF) to reduce neuronal death or enzymes to enhance dopamine synthesis. To date, five clinical trials have been initiated with rAAV carrying the gene CERE-120 (i.e. neurturin) or the glial derived neurotrophic factor (GDNF) (Mochizuki et al. 2003). Delivery into patients had minimal adverse effects and a moderate reversal in disease state was observed (Marks et al. 2008). In another approach, rAAV expressing the enzyme aromatic amino acid decarboxylase (AADC) was used with the hope of increasing dopamine synthesis in patients. Administration of this vector was also shown to be safe and therapeutic effect was observed at six months after administration (Eberling et al. 2008; Christine et al. 2009; Muramatsu et

al. 2010). A third strategy is infusion of the subthalamic nucleus with rAAV expressing two isoforms of the enzyme glutamic acid decarboxylase (GAD65 and GAD67), which are responsible for the production of inhibitory neurotransmitter GABA (Luo et al. 2002). The subthalamic nucleus (STN) region of the brain has a central role in regulating movement and its dis-inhibition is believed to be responsible for the hyperkinetic motor activity symptoms in PD patients. The hypothesis is that introduction of these enzymes will alleviate the motor symptom of PD (Luo et al. 2002). As a result of this treatment most patients experienced significant improvement in motor function through one year post treatment (Kaplitt et al. 2007). A follow-up phase II trial with this approach is now underway. All the above results demonstrate the safety and long-term efficacy of rAAV for delivery into the CNS delivery. A more comprehensive review can be found at Weinberg et al (Weinberg et al. 2012).

**Muscular dystrophy.** Building on the experience of proceeding trials, in which the vector capsid was shown to be a significant factor in vector transduction, strategies to treat muscular dystrophy have exploited capsid serotypes specific for muscle. The first of these trials was designed to treat limb-girdle muscular dystrophy type 2D (LGMD-2D), which is caused by a defect in the synthesis of α-sarcoglycan. rAAV serotype 1, which transduces muscle with high efficiency, expressing α-sarcoglycan from a muscle specific promoter was introduced via IM injection (Mendell et al. 2009; Mendell et al. 2010). A ~5-fold increase was seen in the level of α-sarcoglycan and a corresponding increase in muscle fiber density was also observed. Gene expression was sustained in the muscle for six months. A later dose-escalating trial for LGMD-2C used a similar approach as the first trial, IM injection of rAAV1 expressing γ-sarcoglycan, but with a different muscle specific promoter (Herson et al. 2012). Data from 9 patients showed a mild antibody response against rAAV1 capsid with

one patient developing a T-cell immune response to the capsid. In addition to LGMD-2C, clinical efforts have begun to treat Duchenne muscular dystrophy (DMD), an X-linked disease caused by mutation of the gene that encodes dystrophin (Bowles et al. 2011; Mendell et al. 2011). In trial, six children with DMD were given vectors by intramuscular delivery. This trial was the first instance in which an engineered capsid (AAV2.5), derived from serotypes 1 and 2, has been used. The novel capsid did not elicit a significant host immune response and there were no unanticipated side effects from the treatment. However, the therapeutic dystrophin protein did elicit an auto-reactive T-cell response in one patient (Mendell et al. 2011). Diprimio et al provides a more comprehensive view on this disease (DiPrimio et al. 2010).

**Other diseases.** A number of clinical trials have been conducted using rAAV to treat diseases other than those described above as well, diseases such as inflammatory arthritis, heart disease, and metabolic diseases. Currently, there is one phase I trial to treat inflammatory arthritis using a vector to express a fusion protein of the human tumor necrosis factor-immunoglobulin Fc domain (TNFR:Fc), an antagonist of TNF-α. For delivery, vector was introduced into fifteen patients via intra-artery injection with the goal of reaching the joints (Mease et al. 2009). The objective of this trail was to determine safety, and though successful, was dosed too low to see therapeutic effect.

Efforts to treat heart disease have targeted heart failure patients, a major cause of morbidity and mortality in the United States. Serotype 1 encapsidated vector containing the SERCA2a gene was introduced via intra-coronary injection (Hajjar et al. 2008). SERCA2a is a calcium regulating protein expressed in cardiomyocytes and reduced level of this protein

has been linked with heart failure (Lipskaia et al. 2010). Results of this study have not yet been reported.

Lipoprotein lipase (LPL) deficiency, a monogenic metabolic disease leading to high serum triglyceride levels and pancreatitis, is another disease that may benefit from gene therapy. The approach in this trial was to introduce rAAV1 expressing LPL via IM injection. Eight patients were treated and three months after treatment average serum triglyceride levels were reduced by 27% and 41% in the low-dose and high-dose cohorts, respectively. Levels returned to baseline, however, at 18-31 months after treatment (Stroes et al. 2008). Transient expression in this trial may have been caused by a neutralization antibody and T-cell immune response against the capsid (Mingozzi et al. 2009).

**Challenges associated with AAV in clinic**

The clinical trials discussed above have demonstrated the safety, versatility, and adaptability of AAV-based gene therapy. On the other hand, they have also pointed out the current limitations and challenges for the future of AAV vectorology: cell/tissue specific targeting, efficiency of transduction, and immunogenicity. For example, in multiple trials (e.g. Hemophilia B and LPL) loss of gene expression occurred after only weeks and correlated with a T-cell immune response against the vector capsid (Manno et al. 2006; Stroes et al. 2008). For more detailed review on immune response to AAV vectors in clinical trials, please refer to Mingozzi et al (Mingozzi et al. 2011). In other trials (e.g. AAT and CF), though transgene expression was sustained for >1 year after delivery, the level in high-dose treated patients was still insufficient for therapeutic effect. Thus, more efficient vectors or routes of delivery are required (Flotte et al. 2011). For treatment of ocular diseases, targeting of specific types of cells in eye, such as retinal pigment epithelia (RPE), Müller cells, and

retinal ganglion cells (RGC), will require cell-type-specific vectors or promoters (Martin et al. 2002).

**Strategies for enhancing rAAV capsid**

The limitations of rAAV, learned from pre-clinical and clinical studies alike, have given momentum to efforts to improve this vector. Various strategies have been pursued, including development of novel capsids, transgene cassettes, and employment of pharmacological reagents to enhance gene delivery and expression. This section focuses on perhaps the most promising of these strategies, development of novel vector capsids to improve specific targeting and transduction efficiency (Table 3, Fig.I-3). The immune response associated with AAV vectors and potential strategies to tackle this issue have been extensively summarized in several most recent reviews (Bartel et al. 2011; Mingozzi et al. 2011; Rogers et al. 2011).

**Natural serotypes.** Over 100 natural serotypes of AAV have been isolated, many with unique properties of tropism and infectivity (Bantel-Schaal et al. 1984; Rutledge et al. 1998; Chao et al. 2000; Gao et al. 2002; Grimm et al. 2003; Gao et al. 2004; Mori et al. 2004; Pacak et al. 2006). A majority of clinical trials have been performed with rAAV encapsidated with serotype 2 capsid proteins largely because this serotype was the first to be isolated and characterized. Information about the transduction profiles of other serotypes is only beginning to come to light. New serotypes 1, 4, 5, 6, 7, 8, and 9 have been tested or are currently in testing with pre-clinical or clinical studies. rAAV1 shows high level of transduction of muscle tissues and has been used for intramuscular injection to treat AAT-deficiency and several cardiac/skeletal muscular diseases (Lu et al. 2006; Flotte et al. 2007; Hajjar et al. 2008; Brantly et al. 2009; Mendell et al. 2009; Herson et al. 2012). This serotype

has also been shown to have specificity for transducing non-neuronal cells in the retina. Alternatively, serotypes 4 and 5, though not tropic for muscle, have a greater specificity for transduction of the eye, specifically the retinal pigment epithelium (RPE), than 1 or other serotypes (Martin et al. 2002). rAAV5 is currently the most efficient for transduction of photoreceptor cells in the eye (Sun et al. 2010). Serotype 6 capsid has been shown to be efficient at transducing human airway epithelium cultures (Limberis et al. 2008). Based on these results, rAAV6 is currently in phase I clinical trial to deliver the human placental alkaline phosphatase gene to the upper airway in cystic fibrosis patients. Serotype 7 transduces muscle as efficient as AAV1, the most efficient serotype for muscle transduction identified so far (Gao et al. 2002).Serotype 8 displays ~100-fold higher transduction of the liver than serotype 2 and other serotypes (Gao et al. 2002; Cooper et al. 2009). rAAV8 is being used extensively in pre-clinical trials and has gone into patients to treat Hemophilia B (Nathwani et al. 2011). Serotypes 8 and 9 can also transduce myocardium much more efficiently (20-fold and 200-fold, respectively) than AAV1 (Pacak et al. 2006). In fact, AAV9 appears to be superior to other serotypes in a majority of tissues tested (Gao et al. 2004). A brief summary of AAV serotypes 1-9 is provided in Table 3.

**Mutagenesis-based directed evolution.** Directed evolution is a powerful tool to select for novel properties or to enhance pre-existing functions of the vector capsid. This process enriches for capsids able to succeed in the context of a designed selective pressure. Three steps are required to perform directed evolution: 1) Diversification; 2) Function-based selection; 3) Recovery. Diversification can be achieved by creating a large library of variants via randomized mutation or recombination. Function-based selection requires development of specific conditions of transduction that filter out vectors that do not have the desired

**Table 3. Summary of AAV serotypes 1-9**

| Table 3. Summary of AAV serotypes 1-9 | | | | |
|---|---|---|---|---|
| **Serotypes** | **Origins** | **Primary receptors** | **Tissue tropism** | **Clinical trials** |
| AAV1 | Laboratory cell culture | N-linked (SA) | Muscle, Lung, CNS, Eye, Pancreas | AAT, Muscular diseases, Heart failure, LPL deficiency, Inflammatory arthritis |
| AAV2 | Laboratory cell culture | HSPG | Liver, Muscle, CNS, Kidney, Eye | Most AAV-based trials |
| AAV3 | Laboratory cell culture | HSPG | Muscle | |
| AAV4 | Laboratory cell culture | O-linked SA | Eye, Lung, CNS | |
| AAV5 | Human | N-linked SA | Muscle, Lung, CNS, Eye | Muscular disease |
| AAV6 | Laboratory cell culture | N-linked SA; HSPG | Muscle, Lung, Heart | CF, Heart failure |
| AAV7 | Rhesus monkeys | N/A | Muscle, Lung, Eye, CNS | |
| AAV8 | Rhesus monkeys | N/A | Liver, Muscle, CNS, Heart, Eye, Pancreas | Hemophilia B |
| AAV9 | Human | N-linked galactose | Heart, Lung, Liver, Muscle, CNS, Eye, Pancreas, Kidney | |
| *AAT: α-anti-trypsin; AAV: Adeno-associated virus; CF: Cystic fibrosis; SA: Sialic Acid; HSPG: Heparan Sulfate Proteoglycan* | | | | |

property. Recovery is accomplished by subsequently amplifying the capsid variants that were successful. One of the first attempts to use this approach created a mutant capsid library (~10^6-10^7 variants) by error-prone PCR. For a function-based selection, the library was incubated with rabbit or human anti-AAV2 sera and transduced onto 293T or Hela cells, respectively (Maheshri et al. 2006; Perabo et al. 2006). This yielded two distinct groups of capsid variants, both with reduced reactivity with antibodies against serotype 2 (Maheshri et al. 2006; Perabo et al. 2006). A later design shuffled the *Cap* gene sequence among several natural serotypes in combination with error-prone PCR to create a potentially more diverse library (Grimm et al. 2008; Koerber et al. 2008; Li et al. 2008). Shuffling was performed between human serotypes 2, 4, 5, 8, and 9 along with avian, bovine, and caprine capsids. The resulting library was selected for transduction of human hepatocytes in the presence of human sera. A chimeric capsid of serotypes 2/8/9, AAV-DJ, was recovered (Grimm et al. 2008). This variant was shown to have higher efficiency of transduction than parent serotypes in several different tissues and transduced mouse liver much more efficiently than serotype 2.

The power of these biopanning studies is compromised, however, by the intrinsic bias associated with the method of selection, in these cases cultured cells. Cultured cells do not accurately reflect the obstacles to a vectors success *in vivo*, including inactivation by neutralizing antibodies, altered binding specificity in the sera, and physical barriers (e.g. endothelial cell layers and extracellular matrix) (Mingozzi et al. 2007; Asokan et al. 2010). To avoid this bias, two groups have adapted directed evolution to more relevant *in vivo* settings (Gray et al. 2009; Yang et al. 2009). In a screen of a library of capsids generated by shuffling serotypes 1-9 for muscle-tropic variants, Yang *et al.* recovered a heart-tropic vector

(AAVM41) with similar transduction efficiency to AAV9 in cardiac-muscle, but de-targeted from the liver and other tissues (Yang et al. 2009). Gray *et al.* also employed selection of a chimeric capsid library in the CNS of rats whose blood brain barrier (BBB) was compromised by kanic acid-induced seizure. Following recovery, a chimera (clone83) was obtained that efficiently transduces neurons and oligodendrocytes, while being de-targeted for most other tissues (Gray et al. 2009).

Directed evolution has proven to be a very efficient approach for generating novel vector capsids with enhanced transduction efficiency for specific tissues. This strategy may provide a way to advance clinical approaches otherwise limited by the tissue tropisms of parental rAAV vectors. For example, therapy for cystic fibrosis (CF) has been hindered by the low efficiency with which rAAV transduces the airway epithelium. Using a directed evolution approach, two groups were able to generate several AAV chimeras, which display significantly higher transduction of the apical airway compared with its parental serotypes (Excoffon et al. 2009; Li et al. 2009). Efforts using this method are ongoing and will likely make a significant contribution to AAV-based gene therapy in the future.

As an alternative to mutagenesis-based approach, directed evolution can also be applied using a peptide-insertion-based library to select for cell targeting properties. This approach, termed biopanning, has been applied to capsid libraries created by inserting peptides that have been randomized for sequence and size. The site of insertion was chosen to disrupt heparin-binding activity of the parent serotype in an effort to minimize binding to this receptor. Once the library is applied to target cells, only capsids capable of transduction will be recovered. In this way, capsids with specific tropism for myeloid, lymphoid leukemia, coronary endothelial, and other cell types have been developed (Muller et al. 2003; Perabo et

al. 2003; Waterkamp et al. 2006; Michelfelder et al. 2007). Similar approaches have also been used to select for vectors that survive circulation *in vivo*, where selective pressures more closely reflect those in patients (Michelfelder et al. 2007; Grimm et al. 2008; Michelfelder et al. 2009).

**Rational design.** For AAV vector, rational design is an engineering method to make artificial capsids with enhanced performance in gene delivery based on current understanding of AAV or other related materials' properties. To date, rational design of vector capsids has been used to enhance tissue-specific targeting, reduce non-specific targeting, and improve vector production (Zhang et al. 2002; Zhong et al. 2008; Petrs-Silva et al. 2009; Asokan et al. 2010; Bowles et al. 2011). Currently used strategies for rational design are illustrated as in figure I-3.

**Rational design by mosaic capsid.** Mosaic capsid engineering is a process of creating vectors with capsids made up of protein subunits from more than one serotype of AAV. In this technique, plasmids encoding capsid subunits of each serotype are mixed in specific ratios to achieve a desired proportion in the resulting mosaic capsid. Several studies have demonstrated the utility of this approach. Hauck *et al.* engineered several vectors using AAV1 and AAV2 capsid proteins in ratios of 9:1, 1:1, and 1:9 (Hauck et al. 2003). All of the resulting mutants exhibited transduction profiles with attributes from both parental serotypes, with efficient transduction of muscle (AAV1) and liver (AAV2). Similarly, Rabinowitz *et al.* carried out pair-wise combinations of AAV serotypes 1-5 at various ratios (Rabinowitz et al. 2004). One resulting mutant, AAV3/5, inherited the receptor binding profiles from both parent serotypes, heparin and mucin (Rabinowitz et al. 2004). Interestingly, inclusion of AAV5 capsid at levels as low as 10% was sufficient to confer mucin binding on mosaic

capsids AAV1/5, 2/5, or 3/5. In contrast, inclusion of AAV2 capsid as high as 75% was unable to make AAV2/5 bind to heparin. This phenomenon may be a result of binding affinities of those two capsids for their respective receptors, but this remains to be shown.

**Rational design by peptide insertion.** Peptides with specific cell binding properties, when inserting onto the surface of the vector, can alter the cell specificity of rAAV. It has been determined that the N-terminus of VP2 tolerates insertion of peptide sequences without disrupting capsid structure or vector production. Initially this was tested by insertion of peptides with known receptor binding properties or identified to bind specific targets in phage-display assays. Based on use of well-characterized peptides, insertion of the 14 amino-acid peptide L14 re-targeted vector to cells expressing integrin receptor, which were otherwise resistant to rAAV transduction (Girod et al. 1999). Similarly, insertion of the ligands for the serpin receptor or the luteinizing hormone receptor directed rAAV to lung epithelia and ovarian cancer cells, respectively (Wu et al. 2000; Shi et al. 2001). Alternatively, insertion of peptides identified by phage display has been used to generate tropism for CD13- and integrin-expressing cells, endothelial cells, brain, lung, and muscle tissues (Grifman et al. 2001; Nicklin et al. 2001; Shi et al. 2003; White et al. 2004; Work et al. 2006; White et al. 2008; Yu et al. 2009).

Despite numerous successes in retargeting rAAV by peptide insertion, it has proven difficult to eliminate the natural broad tropism of some serotypes, such as AAV2. Boucas *et al.* have found a solution to this problem by mutating the heparin binding motif (Boucas et al. 2009). However, modification of the heparin binding motif may not be sufficient to eliminate non-specific cell transduction, given the evidence that vectors selected for specificity to tumor or lung cells by insertion of targeting peptides at heparin binding sites transduced a number of

other tissues, including the heart (Michelfelder et al. 2009). This indicates that additional binding motifs exist on the capsid surface and contribute to the virus's natural tropism.

**Rational design by site mutation or domain swap.** Functional analysis and mutagenesis studies have mapped several conserved structural determinants on the AAV capsid (Girod et al. 1999; Kern et al. 2003; Opie et al. 2003; Bleker et al. 2005; Wu et al. 2006; DiPrimio et al. 2008). This information, together with crystal and cryo-EM structural data, has opened the door to the design of capsid based on the relationship among sequence, structure, and function (Kronenberg et al. 2001; Kaludov et al. 2003; Walters et al. 2004; Miller et al. 2006; Nam et al. 2007; Quesada et al. 2007; Lerch et al. 2009; Mitchell et al. 2009; O'Donnell et al. 2009). In this manner, Bowles *et al.* identified five amino acids on the AAV1 capsid that appear to be responsible for transduction of skeletal muscle and incorporated these into serotype 2 in an attempt to redirect the specificity of this capsid (Bowles et al. 2011). While has properties in common with both parental serotypes, the derived mutant, AAV2.5, displays high level transduction in skeletal muscle and lower reactivity to neutralizing antibodies specific for serotype 2. The increasing knowledge of the structure of AAV capsids gives insight into the physical aspects of AAV biology, but also provides a template with which to model specific capsid alterations and predict their impact (Xie et al. 2002; Nam et al. 2007). Asokan *et al.* identified and replaced a positively charged patch of amino acids (585-590) on the serotype 2 capsid, a surface loop known for its interaction with heparin sulfate, with the corresponding region of serotype 8, a serotype with highly efficient systemic transduction (Asokan et al. 2010). The resulting capsid (AAV2i8) exhibited significantly reduced (by a factor of 40) tropism for the liver and increased transduction in muscle cells compared with AAV2. These results support the notion that

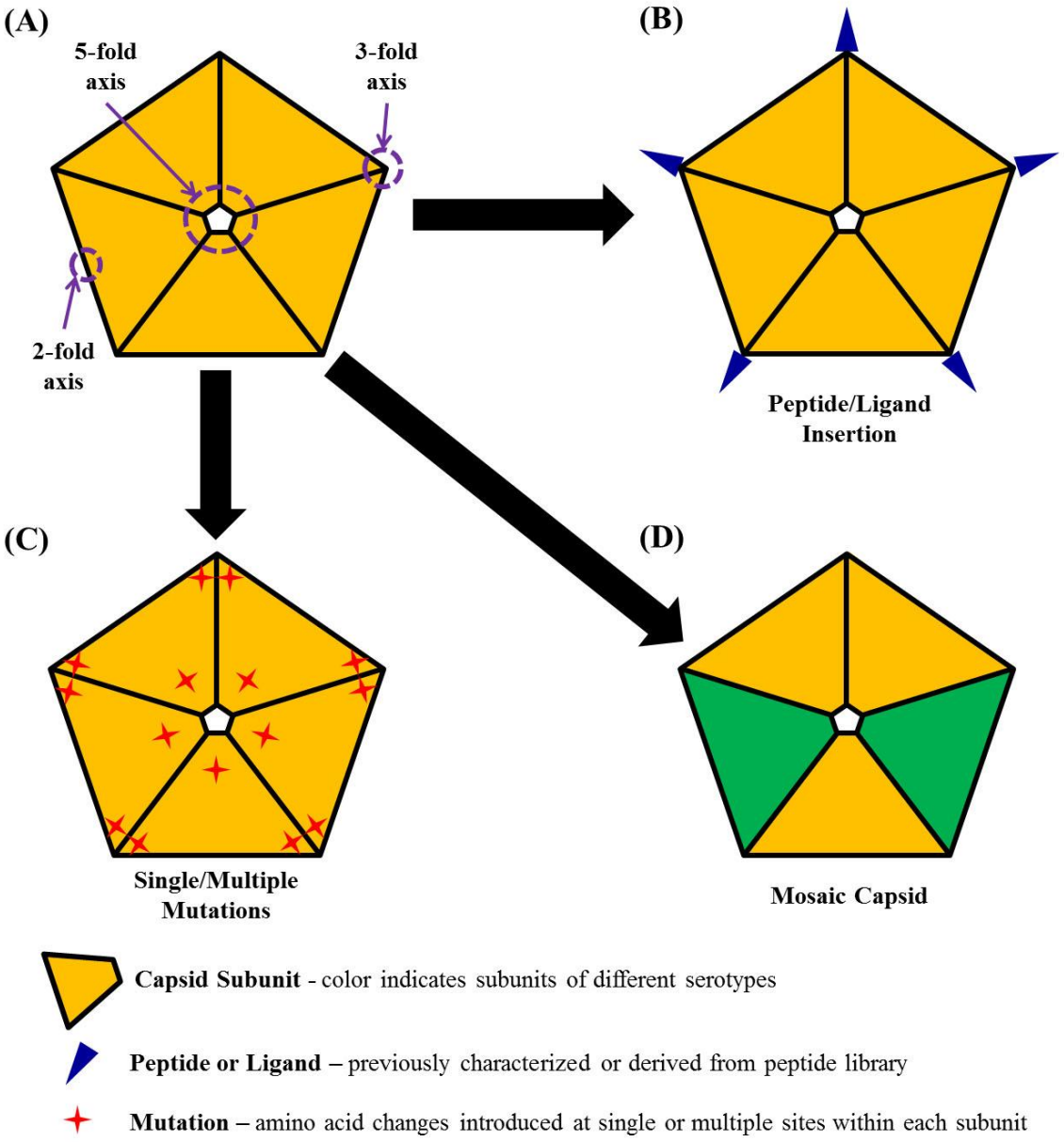


**Figure I-3. Illustration for capsid rational design.** (A) A pentamer of AAV capsid subunit. (B) Rational design by peptide insertion: Novel AAV variants with insertion of specific targeting ligand/peptide through strategy "peptide insertion". Both insertion at N-terminus of VP2 and receptor binding sites have been utilized for this strategy. (C) Rational design by mutations: Novel AAV variants with single or multiple site mutations and/or domain swaps through strategies including "mutagenesis based directed evolution" and "rational design by site mutation or domain swap". (D) Rational design by mosaic capsid: Novel AAV variants composed of heterogeneous capsid subunits from two or more different types of AAV. This strategy may equip the novel AAV capsid with the desired traits of its parental serotypes.

rational design can be used to derive new vectors well suited to clinical applications in gene therapy.

The use of AAV-based vectors continues to increase compared to other viral and non-viral gene transfer systems in clinical trials. Due to its unique properties, the ability to transduce a broad spectrum of dividing or non-dividing cells, low immunogenicity, and sustained gene expression, this vector is well suited to most gene therapy applications. The potential to treat human monogenic disorders has been demonstrated with recent successes in clinical trials for LCA and Hemophilia B. However, there is still a great need for improvement in the specificity and efficiency of gene delivery. In the last decade, significant advancement has been achieved with various methods of rAAV engineering to address these challenges. Increasing knowledge of AAV trafficking promises to extend strategies of capsid design to these processes of transduction as well (Johnson et al. 2008; Xiao et al. 2011; Kaminsky et al. 2012). In addition, our increased understanding of the interactions between AAV and the host immune system will allow further reduction of vector immunogenicity (Mingozzi et al. 2007; Bartel et al. 2011; Mingozzi et al. 2011; Rogers et al. 2011).

It is my personal prediction that rational design will be the most promising strategy for vector development and in the future clinical trials will include novel rAAV capsids from rational design to evade the host immune system and transduce target tissues with greater specificity and efficiency. However, it should be noted that our capacity to create new AAV vector through rational design is highly dependent on the knowledge regarding how each capsid motif functions in and interacts with host cells during viral transduction. To this end, intensive investigation to acquire sufficient knowledge on AAV and host interaction is critical and essential for further development of this vector.

## Subcellular events during AAV infection

Despite many advances in vector developments, administration of high dose viral particles is required to achieve efficient transduction due to rate-limiting steps including pre-existing immune response and non-specific targeting (Rogers et al. 2011). In addition to these limitations, host cells also exploit various cellular components as barriers to AAV productive infection, including the critical steps required for viral trafficking (e.g. cell surface uptake, cytoplasmic trafficking, endosomal escape, nuclear entry, etc.) (Wang et al. 2011). Better understanding of the AAV cellular trafficking will advance our knowledge in AAV biology and facilitate the development of enhanced AAV vectors.

To successfully transduce a cell, AAV virions have to travel through a variety of cellular structures and organelles consecutively, including cell surface binding and internalization, cytoplasmic trafficking, and finally nuclear entry. Like many other viruses, AAV have found a way to exploit host machineries for nuclear targeting to fulfill their own life cycle. Current understanding of the AAV life cycle is derived primarily from the studies of serotype 2 (AAV2). Though many aspects are conserved among all serotypes, there are differences that make each of them unique. The life cycle of AAV2 begins with docking to the host cell via interaction between viral capsid and heparin sulfate proteoglycan (HSPG) on the cell surface (Summerford et al. 1998). Entry of the cell involves the contribution of secondary receptors in addition to HSPG. Integrins and FGF receptors have both been identified to act as co-receptors for viral attachment and subsequent internalization (Qing et al. 1999; Summerford et al. 1999; Kaminsky et al. 2012). Internalization of the virus occurs via clathrin-mediated endocytosis (Summerford et al. 1998) as well as a clathrin independent route as suggested by a recent report (Nonnenmacher et al. 2011). The virus traffics through a variety of endosomal

compartments until acidification of the compartment triggers exposure of the amino-terminus of VP1 (Ding et al. 2005). It is suggested that the N-termini of VP1 and VP2 initially reside inside the capsid and are exposed on the surface in the acidic environment of the endosome (Bleker et al. 2005; Kronenberg et al. 2005), which allows virions to escape from these vesicles (Fig.I-4). It is believed that the N-terminus of VP1 carries phospholipase activity and facilitates the escape of the viral particle by breaking down the endosome membrane (Girod et al. 2002). This endosomal processing of AAV is required for successful infection (Vihinen-Ranta et al. 1998; Ding et al. 2005).

The N-termini of VPs are suggested to be very important for virus-host interactions. For instance, two functional elements of the capsid, a phospholipase A2 (PLA2) domain and several putative nuclear localization signals (NLSs), have been identified in that region. Most parvoviruses contain a motif of ~70 amino acids in VP1 highly homologous to the catalytic domain of PLA2, which is comprised of histidine and aspartic acid residues (75HD) (Zadori et al. 2001). Mutation of these residues to alanine and asparagine (75HD/AN) does not affect cell surface attachment or endocytosis, but strongly inhibits PLA2 activity and viral infectivity (Zadori et al. 2001). PLA2 activity is proposed to penetrate the endosomal membrane to permit the escape of AAV into the cytosol.

After endosomal escape, its genome is required to be delivered into the nucleus of the host cell. Typically, macromolecular traversing the nuclear envelope is an ATP-dependent event and is accomplished by the cooperation between cytoplasmic factors like Ran-1 and specific NLSs on target proteins (Nigg 1997; Gorlich et al. 1999). NLSs have been identified on N-terminus of VP1 from various parvoviruses and are integral to nuclear targeting (Vihinen-Ranta et al. 1997; Lombardo et al. 2000; Lombardo et al. 2002). While the first 10

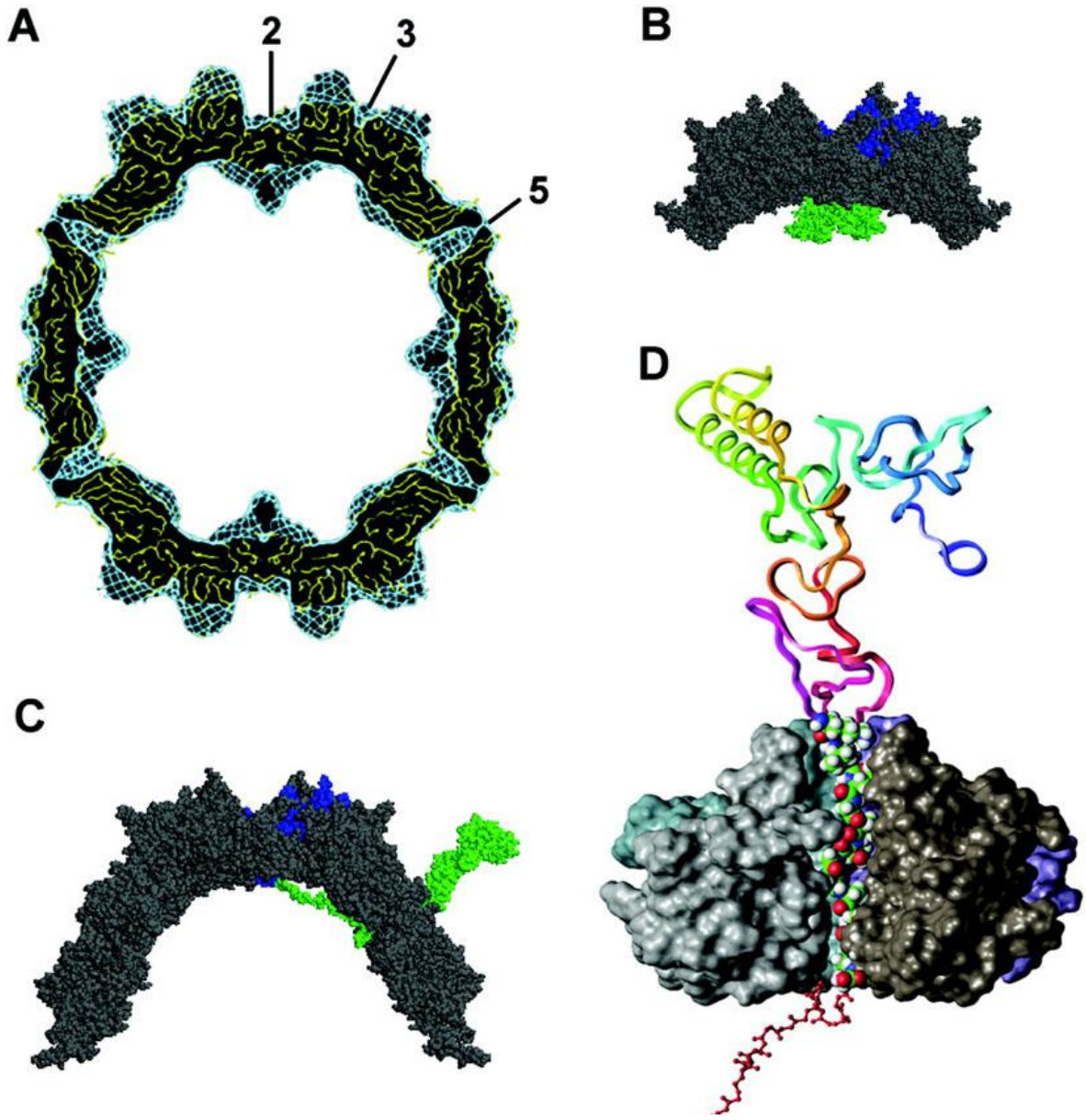


**Figure I-4. Exposure of VP1/2 N-termini through the 5-fold pore.** A) An equatorial slice of the capsid atomic model with 2-, 3-, and 5-fold axes of symmetry. B) 3D reconstruction of a portion of the AAV2 capsid where the unique N-terminus of VP1 is predicted to fold. C) Partial unfolding of VP1 after a capsid conformational change allows its exposure through a channel at a 5-fold axis. D) A model of VP1up exposure through the 5-fold axis (residues 1 to 185 become accessible). (Adapted from Kronenberg et al., 2005)

residues of VP1 in CPV and many other parvoviruses is a canonical NLS (Vihinen-Ranta et al. 1997), several conserved, hydrophilic, basic regions have been identified in AAV2 as potential NLSs, named BR1 ($^{120}$QAKKR), BR2 ($^{140}$PGKKR), and BR3 ($^{168}$PARKR) (Wu et al. 2000). Interestingly, one study shows that MVM is able to disrupt the nuclear envelope during infection, suggesting an alternative mechanism for the nuclear entry of parvovirus that PLA2 domain may also act at the nuclear membrane, in addition to the endosomal membrane (Cohen et al. 2006).

Upon reaching the nucleus, the virion must uncoat, while the details of this event and underlying mechanism are not well understood. It is unclear whether virion uncoating occurs prior to nuclear entry, concomitant with nuclear entry, or inside the nucleus. Intact capsids have been found to enter the nucleus, but whether the capsid disassembles completely or partially to release the genome and if this process is active or passive remain to be determined (Xiao et al. 2002; Grieger et al. 2006). The details of cellular trafficking of AAV are illustrated in figure I-5. More detailed information regarding the AAV trafficking may be found in two most recent reviews (Wang et al. 2011; Nonnenmacher et al. 2012).

Once the genome is released from the capsid, second-strand synthesis initiates from the 3' ITR. The secondary structure of the ITR is critical for this priming event as it positions the 3' end of single-stranded genome to act as the primer for the second strand. The resulting double-stranded molecule can then serve as the template for gene expression. In the absence of helper virus, AAV enters a state of latency (Samulski et al. 1991). In this state, viral gene expression is repressed and the genome persists episomally (Giraud et al. 1995). In the presence of Rep proteins, AAV DNA can integrate into a specific site in the human genome (chromosome 19), which shares homology with the ITR sequence and can be bound by the

Rep proteins (Kotin et al. 1992; Miller et al. 2005; Nakai et al. 2005). The episome scenario of AAV is exploited by gene therapy.

## Microscopy as a method to study viral trafficking

Therapeutic gene delivery is becoming one of the major strategies to improve human health. For example, both viral and non-viral vectors (e.g. adenovirus, AAV), liposomes and nanospheres) have recently been engineered to transfer therapeutic agents in an effort to treat human diseases (Warrington et al. 2006; Rissanen et al. 2007). Encapsulation of the intracellularly-acting materials (i.e. nucleotides, proteins) into specialized delivery vehicles (i.e. viral capsids, nanospheres) that can deliver these agents to specific organelle in a controlled manner is critical to achieve efficient and selective pharmacological effects (Torchilin 2006; Breunig et al. 2008). To accomplish such functions, these vectors have to partially or fully pass through a biological jungle, which is mainly a multi-step trafficking process from cell surface binding to nuclear entry (Bartlett et al. 2000; Brandenburg et al. 2007). As a result, development of therapeutic delivery vectors has concentrated on pharmacological reagents and vector variants that affect these pathways (Duan et al. 2000; Maheshri et al. 2006; Asokan et al. 2009; Yang et al. 2009). Effective achievement of such efforts requires quantitatively evaluating the biological effect(s) of those reagents or vector variants on these complex trafficking routes and bio-distribution of delivery vehicles.

Several sophisticated fluorescence microscopy techniques including confocal and total internal reflection fluorescence (TIRF) microscopy have dramatically advanced our knowledge on the trafficking of viruses in cultured cells during the past decades (Ding et al. 2006; Schelhaas et al. 2008; Vaughan et al. 2009). For instance, confocal microscopy with

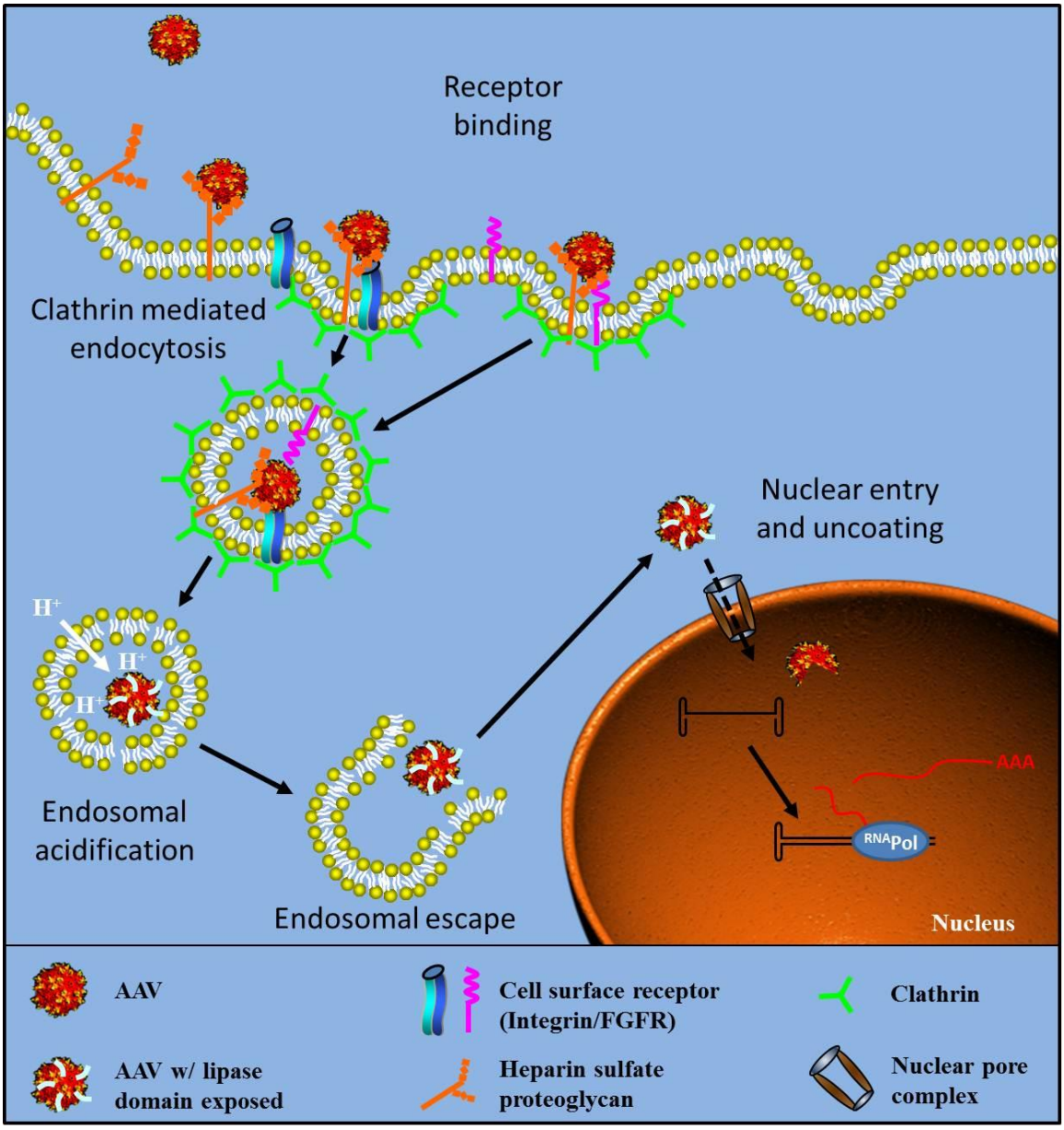


**Figure I-5. AAV trafficking scheme.** Binding and internalization: AAV virions attaches to the cell surface and then are internalized through endocytosis. After binding to the heparan sulfate proteoglycan (HSPG) on cell surface, AAV2 interacts with cell surface receptors (i.e. integrin and FGFR) and internalized through clathrin-mediated endocytosis. AAV5 has also been shown to utilize caveolae, and recently AAV2 has been also shown to use an endocytosis pathway independent of clathrin and caveolin. Endosomal trafficking and escape: AAV2 has been shown to utilize multiple types of endosome (i.e. early/recycling/late endosomes) for its intracellular trafficking. Endosomal escape is typically assisted by the exposure of N-terminus of VP1 on capsid triggered by the acidification of endosomes. It is currently still debatable whether the viral particles escape at the stage of late endosome or at an earlier one, both of which have been supported by previous studies. Viral degradation and capsid antigen presentation: Proteasomes have been shown to be the major machinery for

AAV degradation. Proteasome inhibitors can dramatically enhance AAV transduction. It is currently not clear if the capsid antigen presentation is mediated by lysosomal degradation or proteasome degradation. Nuclear entry and genome uncoating: Nuclear entry of viral genome is regarded as an essential event for successful AAV transduction. Currently, it remains unclear whether nuclear entry is through the nuclear pore complex or other routes. It is also unknown when, where and how genome uncoating takes place.

the assistance of 2D co-localization assay helped to demonstrate that AAV2 differentially traffics through late and recycling endosomes in a dose dependent manner (Ding et al. 2006), while TIRF microscopy assisted live cell imaging helped to show that actin disruption drugs could block the retrograde flow of Human papillomavirus on cell surface (Schelhaas et al. 2008).

Despite advances of 2D imaging and analysis (Seisenberger et al. 2001; Akita et al. 2004; Grieger et al. 2006), to date there is no method available to quantify the number and bio-distribution of nano-scaled viral particles in animal cells and tissues, which is essential in evaluating the effects of pharmacological reagents and viral vector variants on nanoparticle delivery. For example, many viral vectors have high particle-to-plaque forming unit (pfu) ratios, requiring hundreds to thousands of virions to successfully infect a single cell. This strongly suggests: 1) virions may take several different pathways during infection; 2) most viral entry and trafficking events may be futile (Brandenburg et al. 2007; Johnson et al. 2008), 3) a significant number of the particles are defective or not assembled properly (Zeltner et al. 2010). Before one can distinguish productive events from non-productive ones, it is essential to sample the entire population of intracellular viral particles without bias. Analysis of 2D images, utilized by current microscopy approaches, is not unbiased because it only samples one focal plane of viral particles within infected cells. In addition, each labeled particle is displayed as a discrete and intact multi-voxel fluorescent spot, and the distribution of particles in cells varies on each focal plane along the z-axis. 2D image from any focal plane selected for quantification is arbitrary, therefore classical pixel-by-pixel co-localization analysis is not suitable to examine intracellular distribution of viral particles that actually exist in 3D. Finally, current centroid-counting method fails to quantitate viral particles in

cells because of the fact that particles may aggregate or move into a sub-resolutional region like vesicles to give a single fluorescent spot, which is common for nanoparticle trafficking. As a result, no method to date is available for quantitatively determining the bio-distribution of nano-scaled vectors in three dimensions (such as outside or inside nucleus, or traversing nuclear membrane).

In Chapter-2, based on recent advances with computational image processing (Sedarat et al. 2004; Feng et al. 2007), we developed a sensitive and reliable methodology by integrating single particle imaging and 3D quantification into classical immunofluorescence to quantitate the trafficking kinetics and bio-distribution of nanoparticles in three dimensional animal cells and tissues. Using Cy5-labeled AAV as a working model, we quantitatively investigated the nuclear entry kinetics and bio-distribution of AAV2 in human cells and mouse tissues. This study demonstrates the potential of this methodology in screening pharmacological reagents and vector variants for the development of therapeutic-material delivery strategies, as well as in understanding the intracellular behavior of delivery viral vectors *in vitro* and *in vivo*.

## Microtubules in viral trafficking

Microtubules (MTs) are a component of cytoskeleton and are rope-like polymers of tubulins. MTs are highly dynamic as characterized by alternate phases of elongation and shrinkage, and play critical roles in a variety of cellular processes including maintaining cell structure, intracellular transportation, forming the spindle during mitosis, to name a few (Desai et al. 1997). Their roles in intracellular transport are usually achieved by either their own growth dynamics (Roohvand et al. 2009) or the activities of associated motor proteins,

particularly kinesin and dynein (Leopold et al. 2006). MTs forms a radial filamentous network with minus end anchored at a perinuclear site and plus end reaching cell surface area. This structural architecture of MTs allows the shuttling of intracellular molecules and vesicles between peri-nuclear region and other areas of a cell (Giannakakou et al. 2000; Niklinski et al. 2000) (Fig. I-6). For instance, intact MTs are required for the nuclear import of several transcription factors (e.g. p53, NF-kB, pRb) and on other hand, these structures are required to sequester other proteins (e.g. c-myc, MIZ-1, smad3) in the cytoplasm to block their nuclear entry (Giannakakou et al. 2000; Niklinski et al. 2000; Ziegelbauer et al. 2001; Roth et al. 2007; Gong et al. 2011).

Pathogens, especially DNA viruses (i.e. Ad, HSV, Baculovirus), hijack MT system to traverse dense cytoplasm and reach nucleus for their successful infection. Numerous studies have shown that both non-enveloped and enveloped viruses utilize MTs in infecting their host cells (Fig.I-6). This is typically exemplified by the utilization of dynein by viral particles to traffic through the crowded cytoplasmic environment to the nucleus, which is achieved in two ways: 1) virion itself binds to the MTs or MT-associated motors and then migrates on the MTs; 2) virions stay inside of membraneous endocytic vesicles that bind to and migrate on the MTs. AAV's helper viruses, both Ad and HSV, have to escape from the endosomes before trafficking on MTs. Both viruses can directly interact with both minus-end-directed and plus-end-directed MT motor proteins, allowing the bi-directional motions documented for both Ad and HSV on these filaments (Dodding et al. 2011; Engelke et al. 2011; Radtke et al. 2011). As these viruses escape from endosomes at an early stage, the infection of these viruses is not sensitive to the inhibition of endosomal acidification by Bafilomycin or Chloroquine as early as 20-30 minutes after viral inoculation (Greber et al. 1993). In contrast,

influenza virus migrates on the MTs towards the perinuclear region while staying inside of the endocytic vesicles (Lakadamyali, Rust et al. 2003). Acidification of endosomes is essential for escape of influenza virus from vesicles into cytoplasm, which can be blocked by Bafilomycin and Chloroquine.

For AAV, previous studies have reported that MT disruption impairs AAV transduction (Sanlioglu et al. 2000) and AAV can bind the cytoplasmic dynein in an *in vitro* binding assay (Kelkar et al. 2006). However, these studies were contrasted by another publication suggesting AAV transduction was not affected by the disrupted MT network or dynein motor activity (Hirosue et al. 2007). Additionally, it remains controversial whether AAV escapes from endosomes at early or late stage. As a result, the exact roles of MTs and endosomes on AAV transduction as well as the underling mechanisms are yet unclear.

In chapter 3, we have investigated the exact role(s) of MTs on AAV transduction and corresponding potential mechanisms using multiple techniques including confocal microscopy, live cell imaging, quantitative 3D microscopy, pharmacological reagents, and single particle tracking. Moreover, we also determine for the first time that AAV2 traffics on MTs in endosomal compartment and acidification of such structure is dependent on intact MTs. This study strongly supports an as yet undocumented model in which AAV2 exploits MTs for its rapid-directed cytoplasmic transportation towards the peri-nuclear sites where acidification of endosomes for viral escape takes place.

**Overcome cellular barriers: momentum of vector development**

Cells have many structures and machineries to protect themselves from exogenous infectious agents (e.g. viruses, bacteria etc.). For example, the plasma membrane is the first structure to restrict viral infection, and molecularly dense cytoplasm and the nuclear

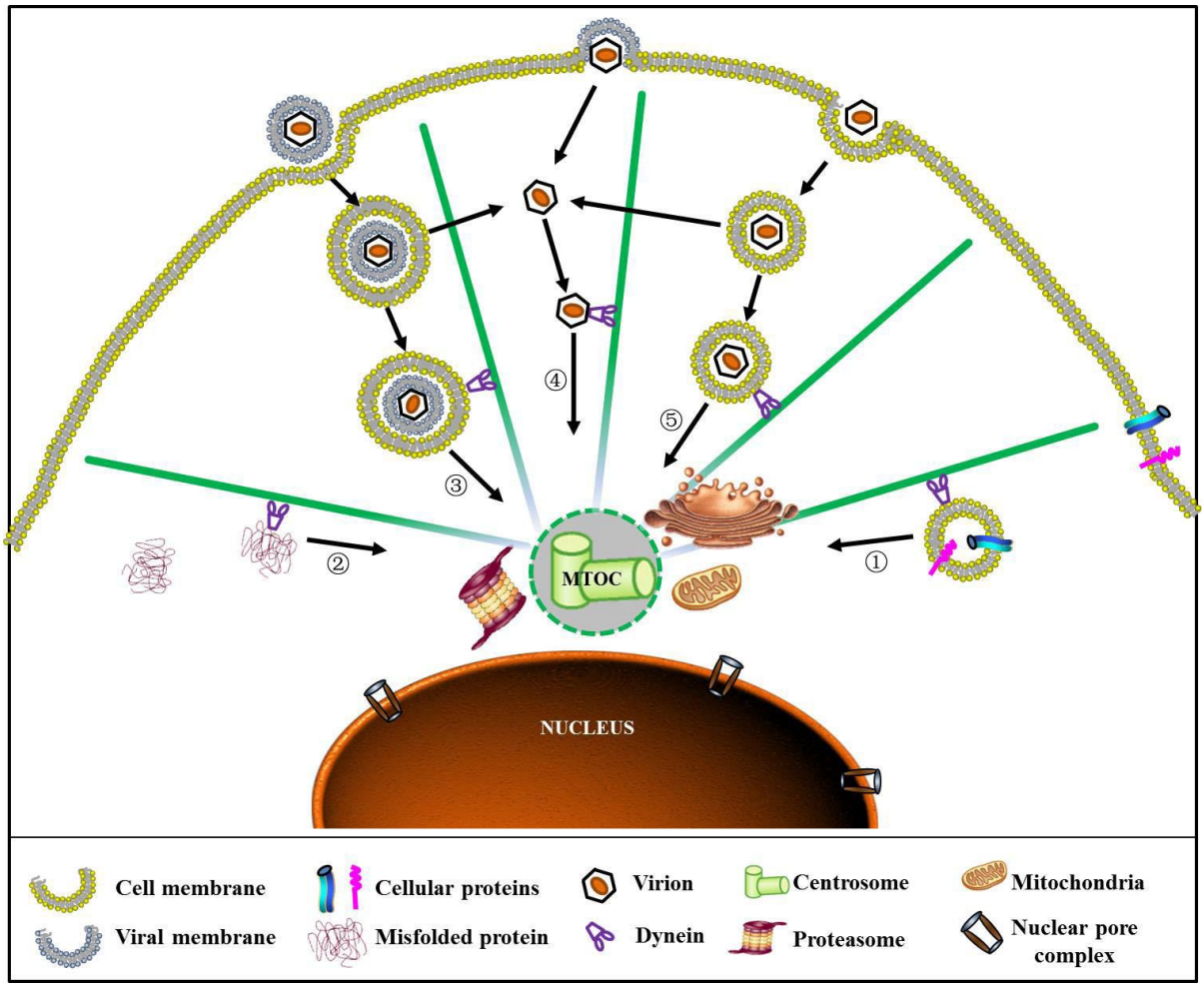


**Figure I-6. MT mediated trafficking of cellular factors and viruses.** Cellular materials like vesicles (route-1), proteins, and misfolded proteins (route-2) are transported on MTs. Viruses inside endocytic vesicles (route-3 and 5) or by itself (route-4) can also migrate on MTs.

envelope sever as additional barriers for viruses to reach their replication sites. As a consequence, viruses have to overcome these cellular barriers in host cells before delivering their genome to the target region for successful infection. Like many other viruses, AAV employs receptor-mediated endocytosis to penetrate the plasma membrane of host cells. Although not clear for AAV yet, many viruses exploit MTs as an effective strategy to traverse the crowded cytoplasm in order to deliver their genetic materials to the replication sites as discuss above. Moreover, like most DNA viruses, it is critical for AAV to deposit its genome in the nucleus. Typically there are three possible mechanisms for viruses to shuttle their genomes into the nucleus. The first mechanism, as exemplified by polyomavirus infection, is importing DNA into the nucleus through an intact virion, followed by intra-nuclear capsid uncoating and genome release (Whittaker et al. 2000). The second approach, as demonstrated by Herpes-simplex-virus (HSV) and Adenovirus (Ad), involves pre-steps of capsid uncoating before the viral genome itself is imported into the nucleus (Greber et al. 1997; Ojala et al. 2000). These two nuclear entry approaches are typically mediated by nuclear pore complex (NPC) on the nuclear envelope. Finally, as exemplified by retrovirus infection, some viruses utilize mitosis to import DNA into the nucleus. This presents a unique situation where the virus takes advantage of the breakdown of the nuclear envelope during the cell cycle.

Comprehensive knowledge in these barriers and virus-host interactions are critical to improve our understanding of basic virology and viral pathogenesis. Either strengthening these cellular barriers or weakening the viral capacity to penetrate these barriers presents potentially powerful means for inhibition of viral infection. On the other hand, attenuating

these barriers or designing capsid with enhanced ability to penetrate these barriers will offer promising opportunities to improve current vectors for gene therapy.

It has been documented that AAV2 enters the nucleus as an intact particle. Studies using nuclear injection of AAV monoclonal antibody (A20) can block viral transduction (Xiao et al. 2002; Sonntag et al. 2006). Sonntag and colleagues further demonstrated that most AAV genomes, unlike other parvoviruses such as MVM, are shuttled into nucleus by intact virions and subsequently uncoated there (Sonntag et al. 2006). Several nuclear localization signal (NLS) motifs including BR1-4 have been identified across the entire AAV capsid proteins VP1, VP2 and VP3. BR1-3 motifs at the N-terminus of VP1 protein have been shown to be critical for the nuclear targeting of post-entry virions (Grieger et al. 2006). Although some of these motifs have sufficient NLS activity to allow a protein to penetrate the nuclear envelope into the nucleus, the nuclear entry of AAV virions has been noted to be highly inefficient (Lux et al. 2005; Grieger et al. 2006; Sonntag et al. 2006; Xiao et al. 2011). These findings suggest that there may be another barrier besides nuclear envelope that limits the nuclear entry of AAV and successful transduction.

The Microtubule-Organization-Center (MTOC) is a subcellular structure at perinuclear region, from which microtubules (MTs) are nucleated to form a radial filamentous network with minus ends anchored at MTOC and plus end reaching cell surface area. Due to these features, MTs and MTOC coordinate, as a trafficking center, the transport of intracellular machineries between the perinuclear region and other areas of a cell (Fig. I-6). Numerous studies have shown that cellular misfolded proteins are also transported on the MTs towards MTOC region, where these misfolded proteins are sequestered or degraded by proteasomes and lysosomes at this region (Garcia-Mata et al. 2002; Wileman 2007).

Strikingly, during the early stage of infection, many incoming viruses are also delivered to and retained at a perinuclear site after entering the cells (Sodeik et al. 1997; Dohner et al. 2002; Suikkanen et al. 2002; Mani et al. 2006; Yea et al. 2007; Boisvert et al. 2010; Liu et al. 2012). This perinuclear site has been suggested to be co-localized with the MTOC region and as observed for cellular proteins, transport of these viruses is facilitated by dynein motors and transport along MTs (Fackler et al. 2006; Greber et al. 2006; Wileman 2007). Although this perinuclear retention of incoming virions seems to be a common phenomenon among many viruses, especially those that enter the nucleus, it remains unclear whether this accumulation is beneficial or inhibitory to viral infection (Wileman 2007).

In chapter 4, we have employed several recombinant viral vectors to investigate the role of perinuclear retention on the infection of both enveloped and non-enveloped viruses, and have further explored the detailed mechanism using Adeno-associated virus (AAV) as a model system. This study for the first time experimentally demonstrates that perinuclear accumulation of incoming virions at the MTOC is a barrier limiting infection of most nuclear viruses and more specifically restricting the nuclear entry of AAV, defining a novel defense mechanism by which host cells restrain viral invasion.

# CHAPTER 2

# QUANTITATIVE 3D TRACING OF GENE-DELIVERY VIRAL VECTORS IN HUMAN CELLS AND ANIMAL TISSUES


## Summary

Trafficking through a variety of cellular structures and organelles is essential for the interaction between gene delivery vectors (i.e. Adeno-associated Virus (AAV), Adenovirus, and liposomes) and host cells/tissues. Here we present a method of computer-assisted quantitative 3D bio-distribution microscopy that samples the whole population of fluorescently-labeled vectors and document their trafficking routes through cells and tissues. Using adeno-associated virus (AAV) as a working model, we first experimentally defined numerical parameters for the singularity of Cy5-labeled particles in a cellular environment by combining confocal microscopy and atomic force microscopy (AFM). We then developed a robust approach that integrates single-particle fluorescence imaging with 3D deconvolution and isosurface rendering to quantitate viral distribution and trafficking in human cells as well as animal tissues at the single particle level. Using this quantitative method, we uncovered an as yet uncharacterized rate-limiting step during viral cell entry, while delineating nuclear accumulation of virions during the first 8hrs post-infection. Further, our studies revealed for the first time that following intramuscular injection, AAV spread progressively across muscle tissues through endomysium between myofibers instead of traversing through target cells.

Such three-dimensional resolution and quantitative dissection of vector-host interactions at the subcellular level should significantly enhance our ability to resolve trafficking mechanisms of gene-delivery particles, and facilitate the development of novel viral vectors.

## Introduction

Therapeutic gene delivery is becoming one of the major strategies to improve human health. For example, both viral and non-viral vectors (e.g. adenovirus, adeno-associated virus(AAV), liposomes and nanospheres) have recently been adapted to deliver therapeutic agents in an endeavor to treat human disorders(Warrington et al. 2006; Rissanen et al. 2007). Encapsulation of the intracellularly-acting materials (i.e. nucleotides, proteins) into specialized delivery vehicles (i.e. viral capsids, nanospheres) that can deliver these agents to specific organelle in a controlled fashion is critical to attain efficient and selective pharmacological effects (Torchilin 2006; Breunig et al. 2008). To achieve such functions, these vectors have to partially or fully transverse a biological maze, which is mainly a multi-step trafficking process from cell surface binding to nuclear entry(Bartlett et al. 2000; Brandenburg et al. 2007). Consequently, development of therapeutic delivery vectors has concentrated on pharmacological reagents and vector variants that affect these pathways(Duan et al. 2000; Maheshri et al. 2006; Asokan et al. 2009; Yang et al. 2009). Effective achievement of such efforts requires quantitatively evaluating the biological effect(s) of those reagents or vector variants on these complex trafficking routes and bio-distribution of delivery vehicles.

During the past decades, several sophisticated fluorescence microscopy techniques including confocal and total internal reflection fluorescence (TIRF) microscopy have revolutionized our knowledge of specific viral trafficking events in cultured cells(Ding et al. 2006; Schelhaas et al. 2008; Vaughan et al. 2009). For example, confocal microscopy with the assistance of 2-dimensional co-localization assay helped to suggest that AAV2

differentially traffic through late and recycling endosomes in a dose dependent manner(Ding et al. 2006), while TIRF microscopy assisted live cell imaging helped to show that actin disruption drugs could block the retrograde flow of Human papillomavirus on cell surface(Schelhaas et al. 2008).

However, despite advances of 2D imaging and analysis (Seisenberger et al. 2001; Akita et al. 2004; Grieger et al. 2006), to date there is no method available to quantify the number and bio-distribution of nano-scaled viral particles in animal cells and tissues, which is essential in evaluating the effects of pharmacological reagents and viral vector variants on nanoparticle delivery. For example, many viral vectors have high particle-to-plaque forming unit (pfu) ratios, requiring hundreds to thousands of virions to successfully infect a single cell. This strongly suggest: 1) virions may take several different pathways during infection and, 2) most viral entry and trafficking events might be futile(Brandenburg et al. 2007; Johnson et al. 2008), 3) a significant number of the particles are defective or not assembled properly(Zeltner et al. 2010). Before one can distinguish productive events from non-productive ones, it is essential to sample the entire population of intracellular viral particles without bias. Analysis of 2D images, utilized by current microscopy approaches, is not unbiased because it only samples one focal plane of viral particles within infected cells. In addition, each labeled particle is displayed as a discrete and intact multi-voxel fluorescent spot, and the distribution of particles in cells varies on each focal plane along the z-axis. 2D image from any focal plane selected for quantification is arbitrary, therefore classical pixel-by-pixel co-localization analysis is not suitable to examine intracellular distribution of viral particles that actually exist in 3D. Finally, current centroid-counting method fails to quantitate viral particles in cells because of the fact that particles may aggregate or move into

a sub-resolutional region like vesicles to give a single fluorescent spot, as is common for nanoparticle trafficking. As a result, no method to date is available for quantitatively determining the bio-distribution of nano-scaled vectors in three dimensions (such as outside or inside nucleus, or traversing nuclear membrane).

Here, based on recent advances with computational image processing(Sedarat et al. 2004; Feng et al. 2007), we developed a sensitive and reliable methodology by integrating single particle imaging and 3D quantification into classical immunofluorescence to quantitate the trafficking kinetics and bio-distribution of nanoparticles in three dimensional animal cells and tissues. Using Cy5-labeled Adeno-associated virus (AAV) as a working model, we quantitatively investigated the nuclear entry kinetics and bio-distribution of AAV2 in human cells and mouse tissues. This study demonstrates the potential of this methodology in screening pharmacological reagents and vector variants for the development of therapeutic-material delivery strategies, as well as in understanding the intracellular behavior of delivery viral vectors *in vitro* and *in vivo*.

## Materials and Methods

**Production and purification of viruses.** Virus was produced in HEK-293 cells as previously described(Xiao et al. 1998). Briefly, using polyethylenimine (linear molecular weight, ~25,000), cells were triple transfected with pXR2, the pXX680 helper plasmid, and pTR-CMV-GFP containing the GFP reporter transgene flanked by inverted terminal repeats. At 60hrs post-transfection, cells were harvested and nuclei were isolated as previously described(Grieger et al. 2006). The nuclear pellet from 10 plates was resuspended in 10ml PBS with 0.5% Deoxycholate (DOC) and then sonicated for 1min. This suspension was incubated at 37℃ for 45 minutes in the presence of 100μg/ml DNase. Virus suspension was subjected to one round of cesium chloride (CsCl) step gradient density (1.3g/cm$^3$ and 1.5g/cm$^3$) fractionation. The viral fraction that resided in the interface between the two gradients was collected and subjected to another round of fractionation using CsCl continuous gradient density. Fractions that contained peak virus titers as determined by both slot dot blots and SDS-PAGE electrophoresis were dialyzed against 1× phosphate-buffered saline (PBS) supplemented with 5% sorbitol. Viral titers were determined by both dot blot(Grieger et al. 2006) and qPCR. The infectivity of AAV is determined to about 1 transduction unit per 100 particles.

**Cy5 labeling of viral particles.** AAV2 was covalently labeled with fluorophores as described(Bartlett et al. 1998). AAV2 labeling followed essentially the same protocol with slight modification. Briefly, purified AAV2 were incubated for 1hr at 4℃ in PBS with a ten-fold molar excess of Cy5 mono NHS esters (GE Healthcare) over the capsid protein units. Labeled viruses were separated from the free dyes by dialysis against PBS containing 5%

sorbitol and stored at -80℃ as small aliquots. The degree of labeling (DOL) was determined by spectophotometry using DOL= $A_{max}$ / ([virus] ×$E_{dye}$), with $A_{max}$ =absorbance of dye at absorbance maximum, [virus] =virus concentration, and $E_{dye}$ = extinction coefficient of the dye at its absorbance maximum. Please refer to the manufacturer's instructions for further details. Labeled viral titers were determined by both dot blot(Grieger et al. 2006) and qPCR.

**Vector administration and animal studies.** Housing and handling of BALB/c mice used in the current study were carried out in compliance with National Institutes of Health guidelines and approved by the IACUC at the University of North Carolina-Chapel Hill. Recombinant AAV2 vectors packaging GFP transgenes were administered through the intramuscular (2E+09vgs into the hind limb) in a volume of 20µl PBS. At 0.5, 2, 4 hours and 6 days after intramuscular injection, animals received an overdose of pentobarbital (100mg/kg intraperitoneally) and were perfused transcardially with ice-cold 100mM sodium PBS (pH 7.4), followed by 4% paraformaldehyde in PBS (pH 7.4). After muscle was post-fixed for 24hrs at 4 ℃ in paraformaldehyde/PBS (Xiao et al. 2007), 15µm cross sections were cut using a cyrosection microtome. Then the slides were directly sealed with mounting medium (Prolong Antifade Gold with DAPI [4',6'- diamidino-2-phenylindole]; Molecular Probes).

**Immunofluorescence.** Similarly to what we have previously described(Johnson et al. 2008), HeLa cells (3E+04 per well) were plated on 12-mm glass coverslips at 24hrs before infection. Next day, after incubation in DMEM containing 20mM HEPES at 4℃ for 5min, cells were incubated with Cy5-labeled virions (5,000 or 25,000 vgs/cell) at 4℃ for another 40min. Cells were washed three times with PBS to remove unbound viruses and transferred to 37℃ incubator (regarded as 0hr p.i.). At the indicated time points, cells were washed with

PBS and then fixed with 4% paraformaldehyde (PFA) for 15min at room temperature (RT). The cells were then permeabilized with 0.2% Triton X-100 in PBS for 5min at RT. Following four washes with PBS, the permeabilized cells were blocked with immunofluorescence buffer (IFB) (5% normal goat serum in PBS containing 0.05% Tween-20) for 1hr at RT. The cells were incubated with primary antibody to detect Lamp1 (monoclonal from Santa Cruz Biotechnology Inc.) diluted in 50% IFB for overnight at 4℃. The cells were then incubated in secondary antibody, diluted 1:2,000 in 50% IFB (anti-mouse Alexa-Fluor 488 [Molecular Probes]), for 1hr at RT. After six washes with PBS, coverslips were mounted cell side down on glass slides with mounting medium (Prolong Antifade Gold with DAPI [4',6'- diamidino-2-phenylindole]; Molecular Probes).

**3D confocal fluorescence microscopy and 3D blind deconvolution.** The labeled Hela cells were examined by use of a Zeiss LSM710 laser scanning confocal microscope equipped with a Zeiss Plan-Apochromat 63×/NA 1.40 oil objective. The confocal pinhole aperture was set to the diameter of the first Airy disk. Stacks of 20-30 focal planes were captured at 0.31μm z-intervals through the depth of the cell. 3D images of the cells were reconstructed by using the image stacks. The Nyquist theorem, which utilizes the limitation of the microscope optics [full-width half-maximum (FWHM)] to dictate adequate sampling, was used to determined that pixel dimensions of 0.13×0.13×0.31μm (X, Y, Z) were required to properly sample the data.

Deconvolution was performed by AutoDeblur software (Media Cybernetics Inc.), using iterative and constrained algorithms. The procedure started with a theoretical PSF derived from the actual setting of Zeiss710 confocal microscope. To generate the theoretical PSF, AutoDeblur took the following factors into consideration: NA of the microscope

objective, refractive index of the medium, excitation wavelength, emission wavelength, confocal pinhole radius, pixel size, z-axis interval, microscope type (i.e., wide field, confocal), and number of excitation photons. A new adjusted adaptive PSF derived from the previous deconvolution round was used to generate next adaptive PSF that fits the real imaging data better than the previous one (termed as one iteration or deconvolution round(Pawley 2006)). The number of iterations may serve as a regularization factor. In general, the remaining restoration error decreases with an increasing number of iterations. At the same time, the error due to noise amplification increases. The procedure should be stopped at an iteration number in which the sum of both errors is minimal(Vandervoort et al. 1995). To determine the optimal number of iteration, intracellular Cy5-AAV2 particles were deconvolved up to 50 rounds and the resulting images were saved every 5 rounds. The resulting images from 10 deconvolution rounds (number of iteration) displayed the highest SNR, best spatial resolution and most closely resemble the fluorescence signal from a point light source (Fig.II-2). This iteration number (10 rounds) was then used to deconvolve all the confocal images in this paper.

**Computer assisted 3D visualization and analysis.** All deconvolved image stacks was processed using IMARIS software package (Bitplane AG, Zurich, Switzerland) for visualization and quantification purpose. Briefly, a deconvolved image stack was reconstructed using a volume rendering module and smoothened by a 3D-median filter. Subsequently, an isosurface rendering module was applied through thresholding by the fluorescence intensity that is slightly higher than background. For Cy5-AAV2, the isosurface rendering was thresholded at the fluorescence intensity of 1000a.u. (the upper boundary of background). For AF488-Lamp1, the fluorescence intensity of 530a.u. was used. For DAPI,

isosurface rendering was thresholded at the fluorescence intensity of 2500a.u.. The parameters (volume, MFI, TFI) for these isosurface coated Cy5-AAV2 objects were extracted from the IMARIS program and analyzed as described in result section. The localization of Cy5-AAV2 in nucleus or lysosomes was analyzed as described in result section. Aberrations caused by refractive index mismatch results in a suboptimal z resolution. FWHM changes of the point spread functions of the two channels (DAPI and Cy5) differed one voxel ($0.13 \times 0.13 \times 0.31\ \mu m^3$) in XY- and Z-directions, while no significant changes was observed between AF488 and Cy5. The channel registration difference between DAPI and Cy5 was fixed by adjusting the DAPI channel using channel shift module in IMARIS to avoid potential false-positive localization results.

**AFM.** After imaging with confocal microscope, the coverslips were removed from glass slides and gently rinsed with PBS. The coverslips were quickly rinsed in ddH2O, blotted dry and then slightly dried under a stream of nitrogen. The images were captured in air with a Nanoscope IIIa (Digital Instruments) microscope in tapping mode. Pointprobe tapping mode silicon probes (Molecular Imaging Corporation) with spring constants of ~50 N/m and resonance frequencies ~170 kHz were used for all imaging. The images were collected at a speed of 4Hz, a size of 4μm × 4μm, and a resolution of 512 × 512 pixels.

**Electron microscopy (EM).** Purified and dialyzed virus particles in 1× PBS were pipetted onto a glow-discharged copper grid. The grid was washed twice with water and then stained with 2% uranyl acetate. EM images were taken with a LEO EM 910 transmission electron microscope (TEM) at various magnifications.

## Results

**Quantitative 3D distribution microscopy.** To precisely tracking and localize labeled particles in cells and tissues, we developed an object-based quantitative 3D distribution microscopy which is composed of two steps: 1) assess the localization of particles, 2) quantitate the number of particles in each cellular structure. Here we used localization of particles in nucleus as an example to explain this method. As diagramed in Figure II-1A-a, five nanoparticles (P1-P5 in four groups G1-G4) are differentially localized in a cell, with P1 inside the nucleus, P2 transversing nuclear membrane, P3-P5 outside of the nucleus, and especially P4 and P5 associated with a sub-resolutional region (i.e. vesicles with diameter less than 200nm). Confocal microscope is used to create a z-stack sectioning through the entire cell and generate 3D fluorescence images. Image distortions are a natural aspect of an optical microscope (noise, scatter, glare and blur) and diminish the contrast and resolution of raw images, thus impairing the accuracy of quantitative image analysis. To counteract these problems, restorative 3D deconvolution is used to reverse the optical distortions, negating the effects of the optical system that are represented by its point spread function (PSF, Fig.II-2A). After 3D deconvolution, the fluorescence images are visualized by 3D volume rendering as shown in Figure II-1A-b, with four fluorescence spots (#1-#4) formed by corresponding particles.

To determine the localization of each particle in an object-by-object manner, we first employ isosurface rendering by thresholding fluorescence intensity to distinguish signal from the background (Fig.II-2A, dashed blue line). With this method, we will create a Volume of Interest (VOI) for each fluorescence spot from an optically resolvable particle

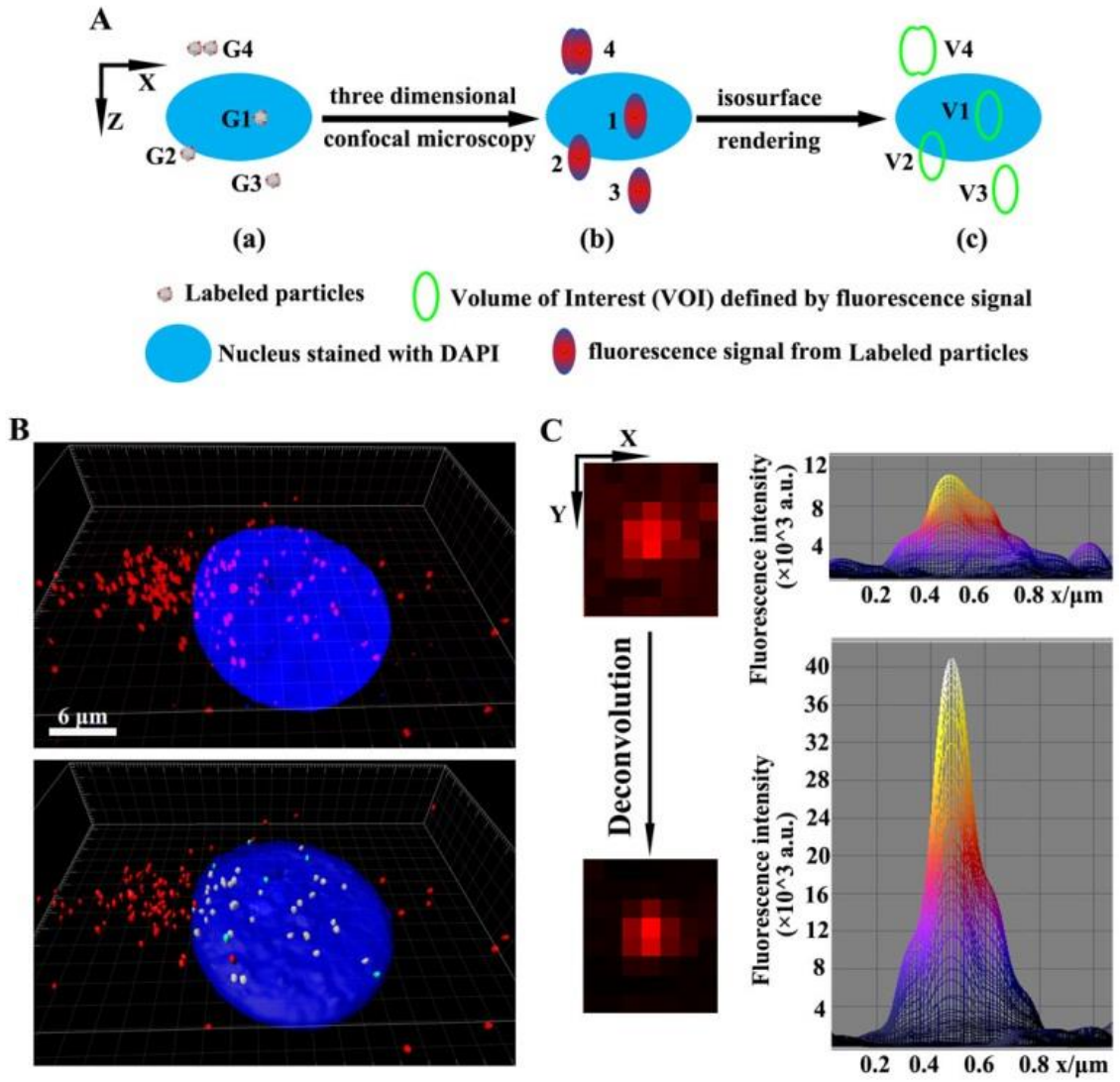


**Figure II-1. Object-based quantitative 3D distribution microscopy.** A) Working model for object-based 3D bio-distribution measurement is shown in X/Z dimensions. (a) actual localization of labeled particles and nucleus, with five particles localized in four optically resolvable groups (G1-G4), (b) expected fluorescence signal (spots #1-#4) from four groups of labeled particles by 3D confocal microscopy, and (c) four volume of interest (V1-V4) defined by the fluorescence spots in (b) with the assistance of isosurface rendering. B) Distribution of Cy5-AAV2 particles in Hela cells at 6hrs post infection (p.i.). Upper panel is the fluorescence signal from 3D confocal microscopy, with red Cy5-AAV2 and blue DAPI-stained nucleus. Scale bar represents 6µm. Lower panel is the isosurface rendering and shows the different localization of viral particles: red is in cytoplasm, cyan is traversing nuclear membrane and yellow is inside of nucleus. C) Example of 3D deconvolution of fluorescence signal of Cy5-AAV2 particles. This improves the Signal-to-Noise Ratio (SNR) and dimensional resolution of fluorescence signal from a single Cy5-AAV2. 3D surface plots (right panel) of the fluorescence signal from a single particle before and after deconvolution were generated by Image J. Pixel size in X and Y is 0.13×0.13 µm.

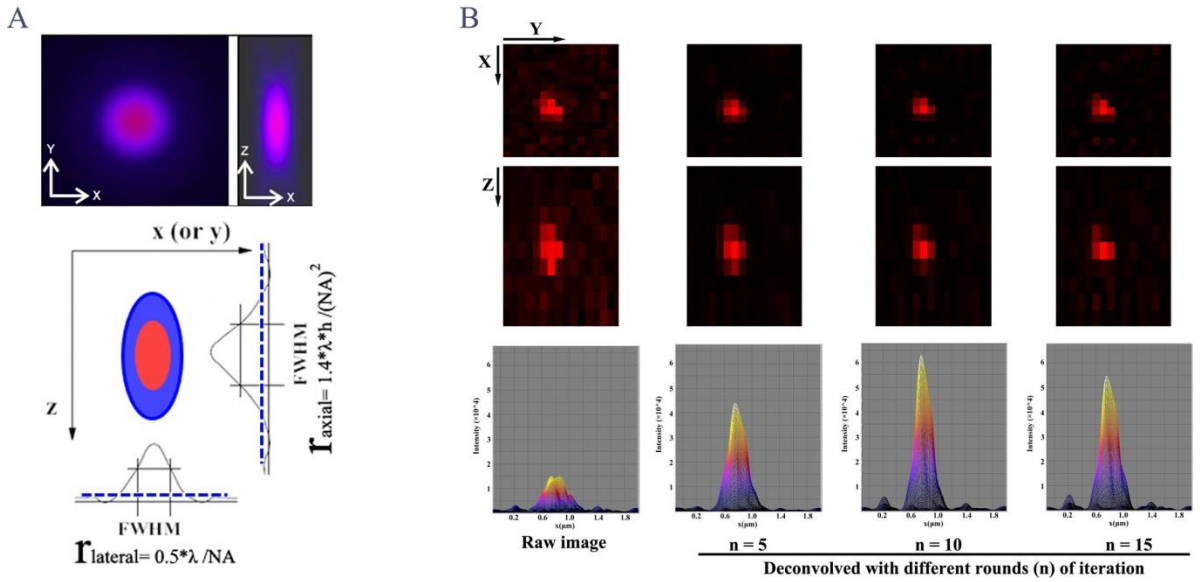


**Figure II-2. Theoretical point spread function (PSF) of confocal images and optimization of 3D deconvolution.** A) Theoretical confocal PSF displayed in X/Y and X/Z dimensions (top). In the bottom figure, the red region usually represents 84% of fluorescence signal from a point light source and defined by full-width-at-half-maximum (FWHM: indicator of resolution defined by Rayleigh criteria) in all three dimensions. The blue region is usually defined as the threshold separating the real signal from background (dotted blue line) and represents 95% of fluorescence signal. B) A single Cy5-AAV particle within cells was imaged as described in Methods. Z-stack images were processed with different iteration numbers (5, 10, 15) of 3D blind deconvolution. a) Micrographs of fluorescence signal from pre- and post-deconvolved images were displayed in X/Y and X/Z dimensions. b). 3D surface plot of corresponding fluorescence signal was generated by Image J and suggested ~3-4 fold improvement in Signal-to-Noise Ratio (SNR).

group (Fig. II-1A-a: G1-G4). The localization of each particle is then determined by the amount of DAPI signal within its VOI (Fig. II-1A-c: V1-V4). Specifically, the mean fluorescence intensity (MFI) of DAPI in V1 is the same as that in nucleus, demonstrating that P1 is inside the nucleus; the MFI of DAPI in V3 and V4 is the same as that in the cytoplasm, but much lower than that in nucleus, demonstrating that P3-P5 are outside the nucleus; and the MFI of DAPI in V2 is between those in nucleus and in cytoplasm, demonstrating that P2 is traversing the nuclear membrane.

To count the number of particles, classical centroid counting method fails when several particles associate with a sub-resolutional region and display as a single fluorescent spot (Fig. II-1A-b: spot #4), which is very common in nanoparticle trafficking. In addition, the amount of dyes (or dye-labeled particles) should be calculated by the number of emitted photon or fluorescence intensity instead of fluorescence volume(Akita et al. 2004; Chen et al. 2008), since there is no linear correlation between the amount of dyes and fluorescence volume ((Pawley 2006) and Fig.II-3). To quantitate particles including those within sub-resolutional regions, we calculate such number using the total fluorescence intensity (TFI) of each fluorescence spot by the formula: number of particles in structure-X $=\sum TFI_{strX}/mTFI_s$, in which $TFI_{strX}$ denotes the TFI of fluorescence spots formed by labeled particles in cellular structure X, and $mTFI_s$ denotes the mean value of TFI experimentally calculated from fluorescence spots formed by a single particle. Using quantitatively labeled fluorescence beads (InSpect Image Intensity Calibration beads from Invitrogen), we demonstrated that TFI but not volume linearly correlated with the amount of dyes on beads (Fig.II-3A) and the number of dye-labeled objects can be precisely calculated from TFI (Fig.II-3B), which validated the accuracy of this intensity-based quantification. In addition, compared with

**A**

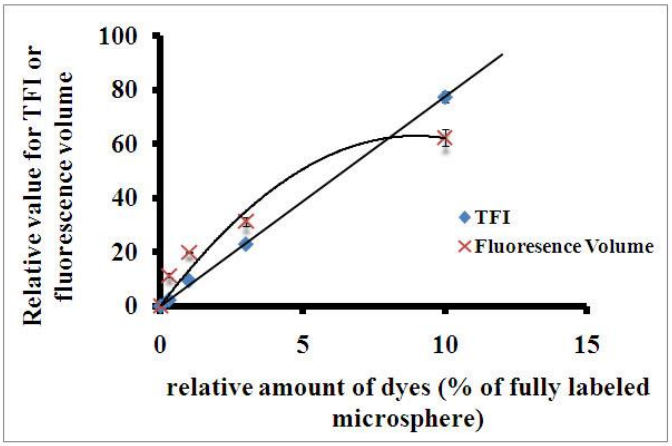


**B**

| | The labeling degree of fluorescence beads | | | |
|---|---|---|---|---|
| | 0.30% | 1% | 3% | 10% |
| TFI of beads in singlet | (2.4E+06) ± (2.8E+05) | (9.5E+06) ± (1.0E+06) | (2.3E+07) ± (1.2E+06) | (7.8E+07) ± (2.0E+06) |
| TFI of beads in doublet | (4.6E+06) ± (4.3E+05) | (1.9E+07) ± (6.7E+05) | (4.4E+07) ± (2.1E+06) | (1.5E+07) ± (3.8E+06) |

**Figure II-3. Total fluorescence intensity (TFI) is proportional to the amount of dyes and dye-labeled beads.** A) Differentially labeled fluorescence beads (0.3%, 1%, 3% and 10% of maximum labeled beads obtained from Invitrogen Inc.) were imaged for 3D quantification, and both TFI and fluorescence volume are plotted against the labeling degree of these fluorescence beads. This panel shows that only TFI is proportional to the labeling degree of these beads but fluorescence volume is not. B) Calculated TFI of fluorescence signal from single beads or those in doublets. For beads of any labeling degree, the TFI of beads in doublets is always 2 times of that of single beads, further demonstrating the linear correlation between TFI and the number of labeled particles.

earlier studies (Akita et al. 2004; Chen et al. 2008), this object-by-object quantification method only calculates the signal from viral particles but not the automatically system-generated noise signal prevalent in the digital images, because these noise are usually bright fluorescence sports with only one or two pixels/voxels that are filtered away from the particle-formed fluorescence spots with 10 or more voxels (Fig. II-1B, II-5C, II-7A). Such feature further improves the precision of this method.

**AAV particle labeling, localization and quantification.** With this method, one is able to quantitate the bio-distribution of nano-scaled particles in cells/tissues by specifying the number and localization of particles in each cellular structure. In the following context, we will quantitate the distribution of Cy5-AAV2 particles in Hela cells at 6hrs post infection (p.i.) to fully demonstrate this method.

Labeling viruses with fluorochromes has been used in imaging particle trafficking (Pelkmans et al. 2001; Schelhaas et al. 2008; Vaughan et al. 2009). We chemically conjugated viral particles with Cy5 to minimize autofluorescence in cells and tissues. Electron microscopy data demonstrated that the physical morphology of AAV2 was not affected by Cy5 conjugation and most of the labeled virions remained as single particles (Fig.II-4A). Labeling did not impact transduction efficiency significantly as indicated by GFP reporter gene assay (Fig.II-4B,C). SDS-PAGE and fluorography of Cy5-AAV2 demonstrated that fluorochromes were specifically coupled to all three capsid proteins (VP1,2,3) as indicated by three fluorescence bands (Fig.II-4D). This specificity of labeling was validated in human cells using mouse monoclonal antibody A20 which only recognizes the intact AAV2 particles (Fig.II-4E). These results demonstrated that both morphology and functionality (A20 binding and infectivity) of these labeled virions are the same as un-labeled ones.

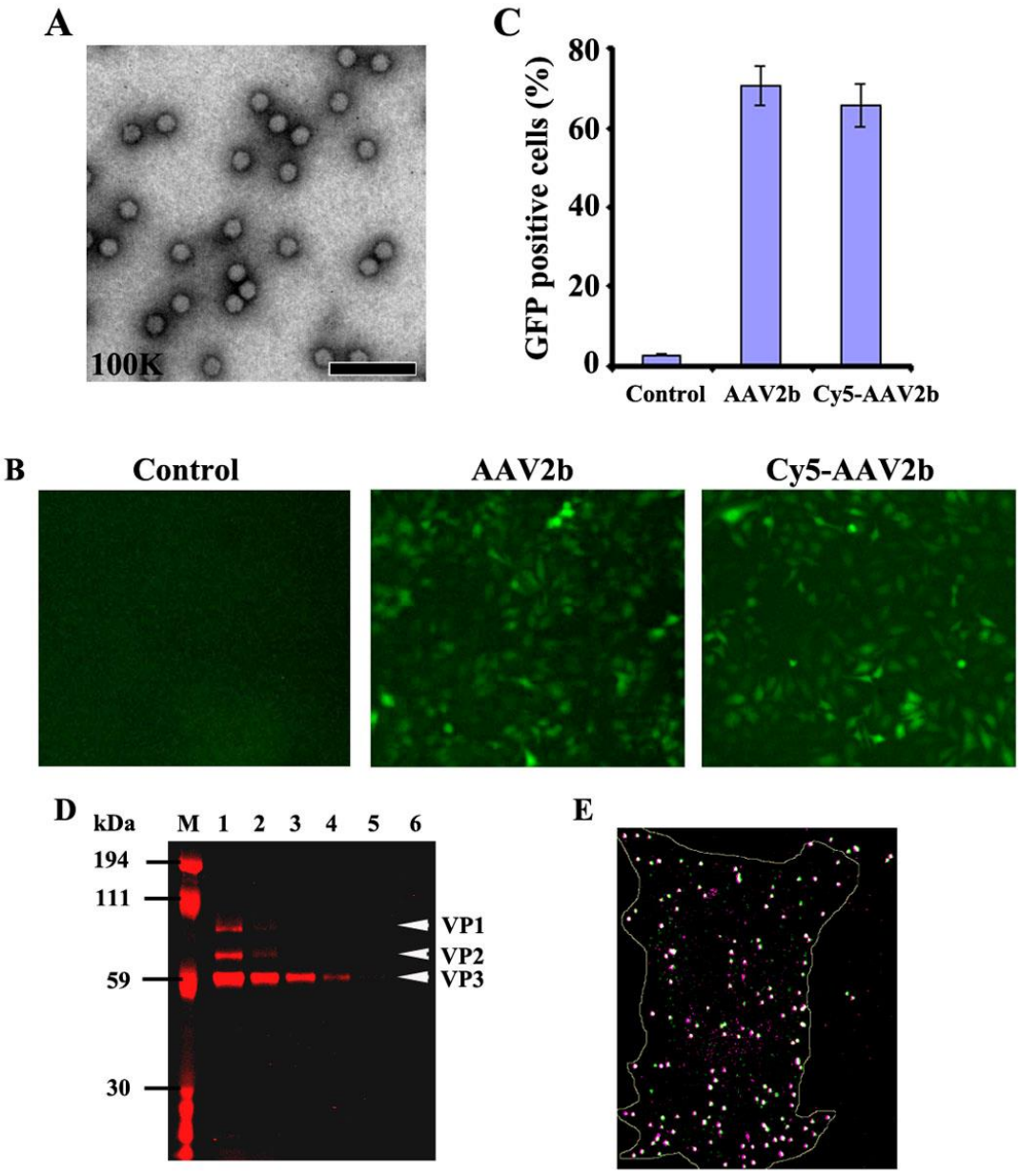


**Figure II-4. Evaluation of AAV2 morphology and infectivity after chemical conjugation with Cy5.** A) Electron micrographs of Cy5-AAV2. Scale bar represents 0.1μm. B) and C) Hela cells were incubated with PBS, AAV2 or Cy5-AAV2 (2,000 vgs/cell). B) GFP transgene expression captured with epi-fluorescence microscope. C) Histogram indicating percentage of GFP positive cells determined by flow cytometry analysis 24 hours p.i.. Error bars represent the standard deviation (STDEV) for three independent experiments. D) SDS-PAGE electrophoresis of Cy5-AAV2 capsid and directly detect Cy5 signal using LI-COR Odyssey. M: protein marker, 1: 2E+09, 2: 1E+09, 3: 5E+08, 4: 2.5E+08, 5: 1.25E+08, 6: 6.25E+07 vector genomes as determined by QPCR. E) Hela cells were infected with Cy5-AAV2 at 5,000 vgs/cell for 40 minutes, and visualized for Cy5 signal (Red) and monoclonal antibody A20 staining of intact capsids (Green). Cell edge is outlined with white line.

At 6hrs p.i. with Cy5-AAV2 at 5,000 vector genomes per cell (vgs/cell), Hela cells were fixed and their nuclei were stained with DAPI. A Zeiss710 confocal fluorescence microscope was used to create a z-stack sectioning through the entire cell for each fluorochrome at the optimal z-step (well-characterized Nyquist Sampling Frequency). We employed AutoDeblur software (Media Cybernetics Inc.) for the deconvolution using an iterative constrained blind algorithm to remove out-of-focus haze, blur and noise. After 3D deconvolution, the fluorescence signal from AAV particles was visualized by 3D volume rendering (Fig.II-1B). Consistent with theoretical confocal point spread function (PSF(Pawley 2006)), the fluorescence signal from a labeled particle is shaped as prolate-spheroid in 3D, with an approximate equatorial radius a = 0.2-0.3μm and polar radius b = 0.3-0.4μm, which resulted in the volume range of less than $0.13\mu m^3$. These signals with prolate-spheroid-shape had improved Signal-to-Noise Ratio (SNR) up to 3-4 fold (Fig.II-1C). Resolution was also enhanced in all three dimensions evaluated by FWHM (Full Width at Half Maximum: 0.15-0.2μm in X/Y and 0.3μm in Z compared with standard confocal resolution limit of 0.3-0.4μm in X/Y and 0.6μm in Z, Fig.II-1C, II-2). We then employed isosurface rendering module in IMARIS software (Bitplane Inc.) to generate VOIs for the signals from each optically resolvable Cy5-AAV2 group and thereafter determined the localization of Cy5-AAV2 particles to nucleus by DAPI signal. As shown in lower panel of Figure II-1B, red spots represent the particles outside of nucleus, cyan spots represent the particles associated with nuclear membrane and yellow spots represent the particles inside of nucleus. $\sum TFI_{strX}$ was then calculated by the $TFI_{strX}$ for each fluorescence spot. To quantitate the particles in each type of localization, we will derive the value of $mTFI_s$ in the following studies.

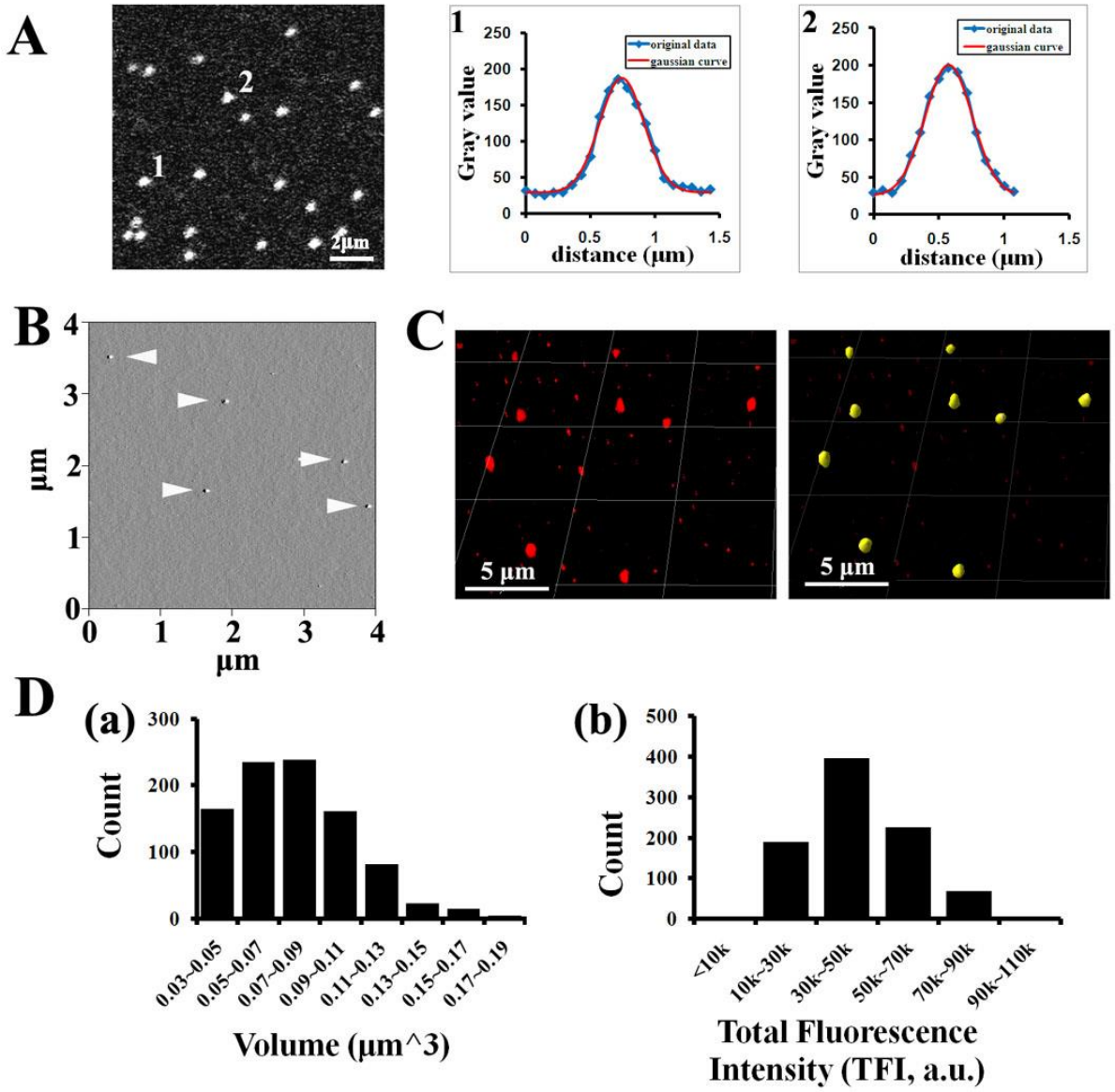


**Figure II-5. Characterization of fluorescence signal for single Cy5-AAV2 particles.** A) Representative confocal image (left) of Cy5-AAV2 bound to coverslip. Scale bar represents 2µm. Representative fluorescence intensity profiles (right 1-2) of two Cy5-AAV2 particles (indicated at left). B) Atomic force microscopy image of Cy5-AAV2 particles (arrowheads) from the same glass coverslip as in A demonstrated the dispersity of viral particles on the coverslip. C) 3D reconstruction of deconvolved confocal images (left: Cy5-AAV2 in red) and subsequent 3D isosurface rendering images (right: Cy5-AAV2 in yellow). Bars represent 5µm. D) Histograms of volume (a) and TFI (b) for all Cy5-AAV2 particles recorded from the coverslip in A and B. The mean values of TFI was 44834 ± 16447.3 a.u..

We characterized the fluorescent signal of a single Cy5-AAV2 particle by three parameters (volume, mean fluorescence intensity (MFI) and TFI). 4-6e+07 Cy5-AAV2 particles were loaded onto grid coverslips to yield a distribution of approximately 1 particle per 5$\mu m^2$. Uniformly labeled particles were obtained as indicated by confocal microscopy of Cy5-AAV2 on the coverslip (Fig.II-5A, left). Profiles of fluorescence signal intensity for two representative Cy5-AAV2 particles follow Gaussian distribution (Fig.II-5A, right), suggesting that fluorescence signal was from single particles(Schelhaas et al. 2008). The fluorescence signal (thresholded as dashed blue line in Fig.II-2A) from Cy5-AAV2 had a diameter of 0.5-0.6μm, comparable to the fluorescence signal generated by other nano-scaled viruses (e.g. SV40) (Pelkmans et al. 2001; Schelhaas et al. 2008). 3-5 regions from each coverslip were imaged using the microscope settings for quantitative analysis (see Methods), and 2-3 Z-stack images were taken for each region. The distribution of Cy5-AAV2 on the same regions was verified using atomic force microscopy (AFM). Only the regions on which the minimum distance between every two physically dissociated Cy5-AAV2 particles was larger than 0.5μm (Fig.II-5B) were chosen for later quantification. Thus, we demonstrated that each fluorescence spot visualized by fluorescence microscopy represented a single Cy5-AAV2 particle. Images from these chosen regions were processed with 3D deconvolution, reconstruction and isosurface rendering (Fig.II-5C). Three statistics (volume, Cy5 MFI and Cy5 TFI) of each isosurface coated fluorescence spot were used to define the singularity of labeled particles. Volume was plotted for all fluorescent objects (Fig.II-5D-a), and could fit to a Gaussian curve indicating a normal distribution. According to theoretical confocal PSF (Pawley 2006), we defined Cy5-AAV2 objects with volume smaller than 0.13$\mu m^3$ as the 3D fluorescence pattern for a single Cy5-AAV2. These defined single

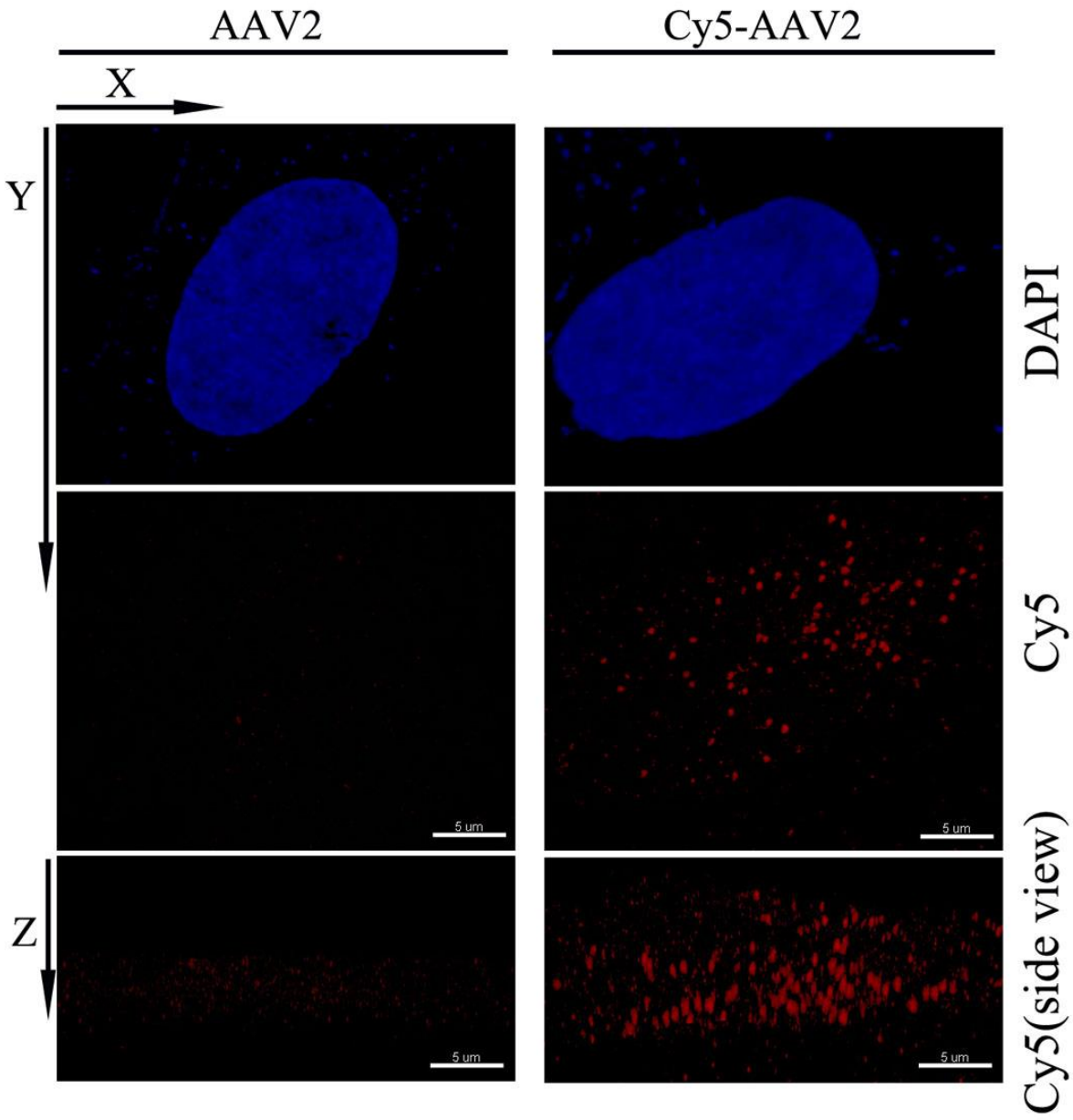


**Figure II-6. Visualization of Cy5-AAV2 particles within cells by fluorescence microscopy.** Hela cells were incubated with AAV2 or Cy5-AAV2 (5,000 vgs/cell) at 4℃ for 40 minutes and then moved to 37℃ after washing. Cells were fixed with 4% PFA at 13 hours and nuclei were stained with DAPI. Stacks of images throughout the whole cells were taken using Zeiss710 confocal microscope at sampling frequency of 0.13×0.13×0.31μm in X/Y/Z dimensions. All images were subjected to 3D deconvolution. 3D reconstructed images are displayed. Bottom panels are side view of Cy5 channel in X/Z dimensions. Bars represent 5μm.

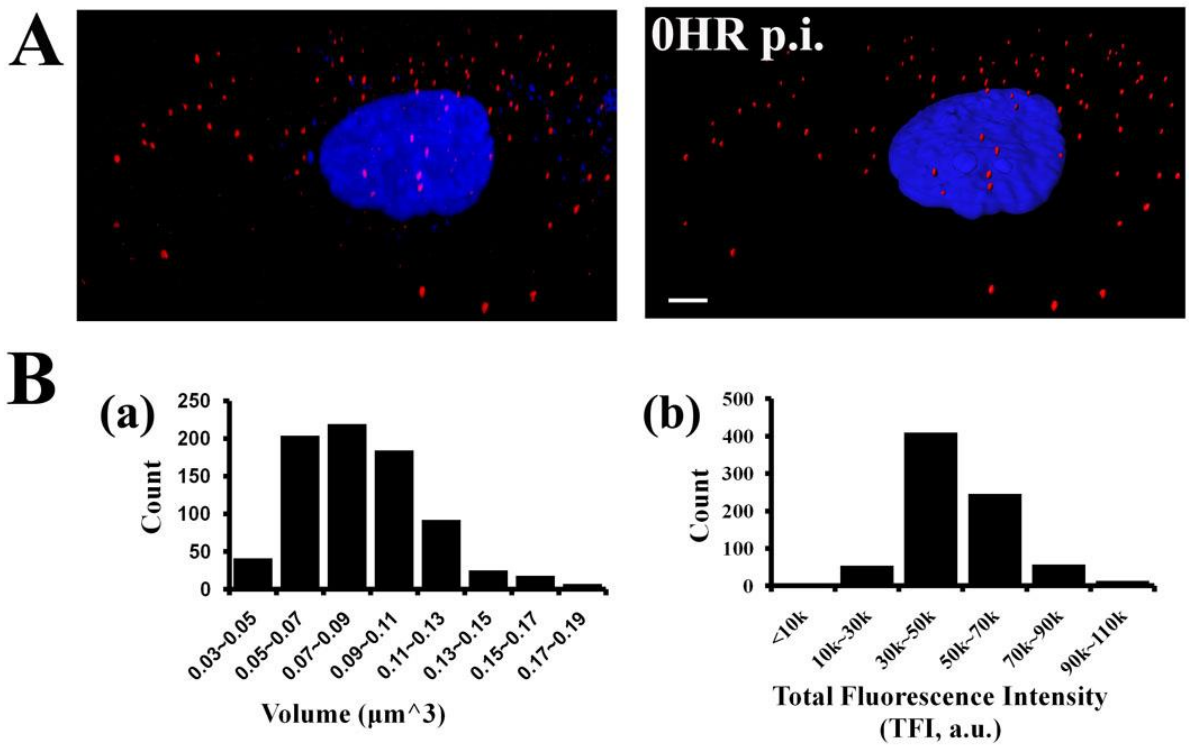


**Figure II-7. Fluorescence properties of single Cy5-AAV2 particles within cells.** Hela cells were incubated with Cy5-AAV2 (5,000 vgs/cell) and fixed and nuclei were stained with DAPI. Stacks of images throughout the cells were taken using a Zeiss710 confocal microscope. A) Representative 3D confocal image of Cy5-AAV2 within cells after being deconvolved and reconstructed (left). Right panel shows the corresponding 3D isosurface rendered image. Scale bar represents 5μm. B) Histograms of volume (a) and TFI (b) for all Cy5-AAV2 particles within cells (n = 5) as calculated by Imaris program. The mean value of TFI was 47568 ± 13345.5 a.u..

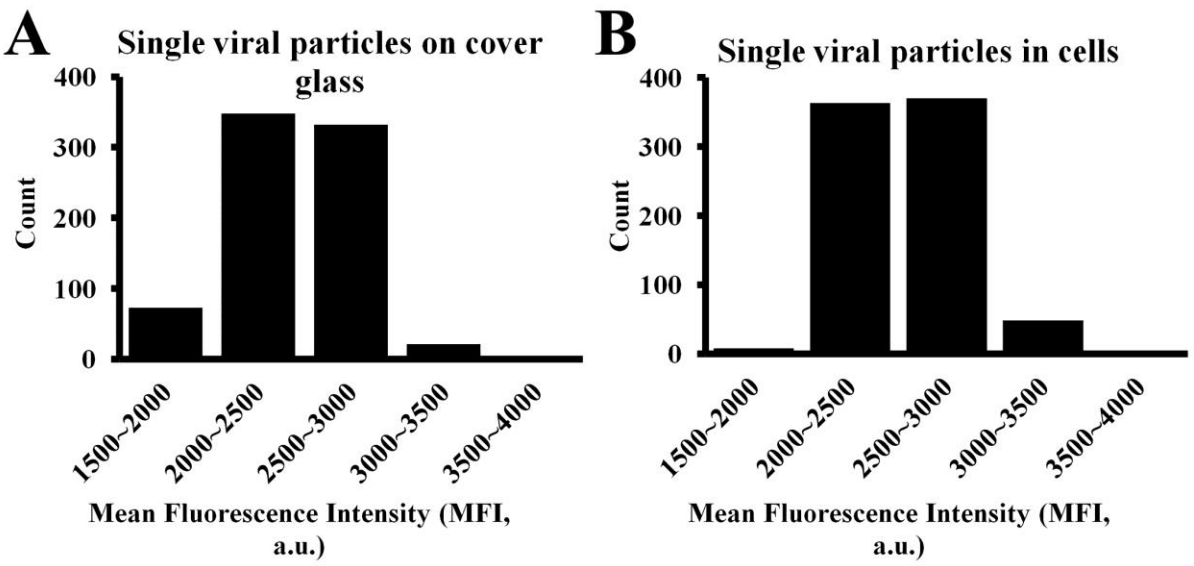


**Figure II-8. Mean fluorescence intensity of single Cy5-AAV2 on coverslips and in cellular environment.** While determining both volume and TFI of the fluorescence signal from Cy5-AAV2, we also calculated the corresponding MFI value: A) single Cy5-AAV2 on coverslips has a mean value of MFI at 2438 ± 310.6 a.u., and B) single Cy5-AAV2 on coverslips has a mean value of MFI at 2516 ± 256.5 a.u..

Cy5-AAV2 objects had a mean value of Cy5 TFIs at 44834 ± 16447.3 a.u. (Fig.II-5D-b), and a mean value of Cy5 MFI at 2438 ± 310.6 a.u. (Fig.II-8A).

The complexity of the cellular environment may affect the fluorescent properties from a single Cy5-AAV2. We analyzed whether single Cy5-AAV2 particles on glass had similar fluorescent properties on cells. Briefly, we incubated 5,000 Cy5-AAV2 per Hela cells (over a surface area of ~2000 $\mu m^2$) at 4℃ for 40 minutes to allow a dispersed distribution of Cy5-AAV2 particles over the cell surface (Fig.II-7A). Specificity of viral fluorescence signal was verified by comparison to non-labeled AAV2 infected cells (Fig.II-6). We then collected the imaging data and analyzed the three parameters (volume, MFI and TFI) exactly as described above for *in vitro* characterization. The distribution of volumes was almost identical to the results from the analysis on coverslip (Fig.II-5D-a, II-7B-a). The same range of volumes (<= 0.13$\mu m^3$) was used to define the fluorescence signal from single Cy5-AAV2 in cells. In the cellular environment, single Cy5-AAV2 objects have a mean value of Cy5 TFIs at 47568 ± 13345.5 a.u. (II-7B-b) and Cy5 MFI at 2516 ± 256.5 a.u. (Fig.II-8B), which is not significantly different from the values determined on coverslip. Consistency between the fluorescent signal from coverslip and cell culture supports that our characterization and quantification by this method is reliable. With this calculated mTFIs (=47568 a.u.), we then determined the number of Cy5-AAV for each location at 6hrs p.i.: 150 in the whole cell, 37 in nucleus, 6 associated with nuclear membrane and 107 localized in cytoplasm (Fig.II-1B).

With this scenario, the subset of Cy5-AAV2 fluorescence spots with specific nuclear localization can be quantitated by DAPI fluorescence signal within each viral VOI and calculated mTFIs. By applying isosurface rendering to the nuclear DAPI signal, the relative localization between AAV2 particles and nucleus can be easily and unambiguously

visualized. Compared with previous studies (Akita et al. 2004; Grieger et al. 2006; Chen et al. 2008), this method not only allows one to assess the viral distribution from the view of entire population but also allows one to locate each individual particle into finer sub-cellular structures (i.e. inside/outside nucleus or traversing nucleus, as shown in Fig.II-1B). By determining the fluorescence parameters for single particles, this method also first time allows one to quantitate the number of virions in various cellular structures. For example, including nuclear targeting, co-localization of AAV2 with other specific cellular structures (e.g. AAV-cell membrane, AAV-lysosome) and corresponding trafficking kinetics were quantitatively investigated using this method.

**Kinetics of AAV2 trafficking in endo/lyso vesicles and nucleus.** Intracellular trafficking in small vesicles like endosomes and lysosomes is essential for productive viral infection. For example, AAV2 has been shown to undergo successive endosomal trafficking and sorting after viral entry (Ding et al. 2006). We tested the applicability of this method toward elucidating these essential events using lysosomal association of AAV2 as an example. Hela cells were incubated with Cy5-AAV2 (5,000 vgs/cell) at 4℃ for 40 minutes. After removing unbound virions, cells were incubated at 37℃ and harvested at 0hr, 2hrs, 4hrs, 8hrs and 13hrs p.i., and fixed with paraformaldehyde. Lysosomes were labeled with monoclonal Lamp1 antibody. Z-stack images were captured through the entire cell using a Zeiss LSM710 laser scanning confocal microscope. After 3D deconvolution and reconstruction of image stacks, we measured the association between lysosomes and AAV2 particles over time. Our results demonstrated that about 40% of intracellular AAV2 consistently associated with lysosomes between 2hrs and 13hrs after infection (Fig.II-9).

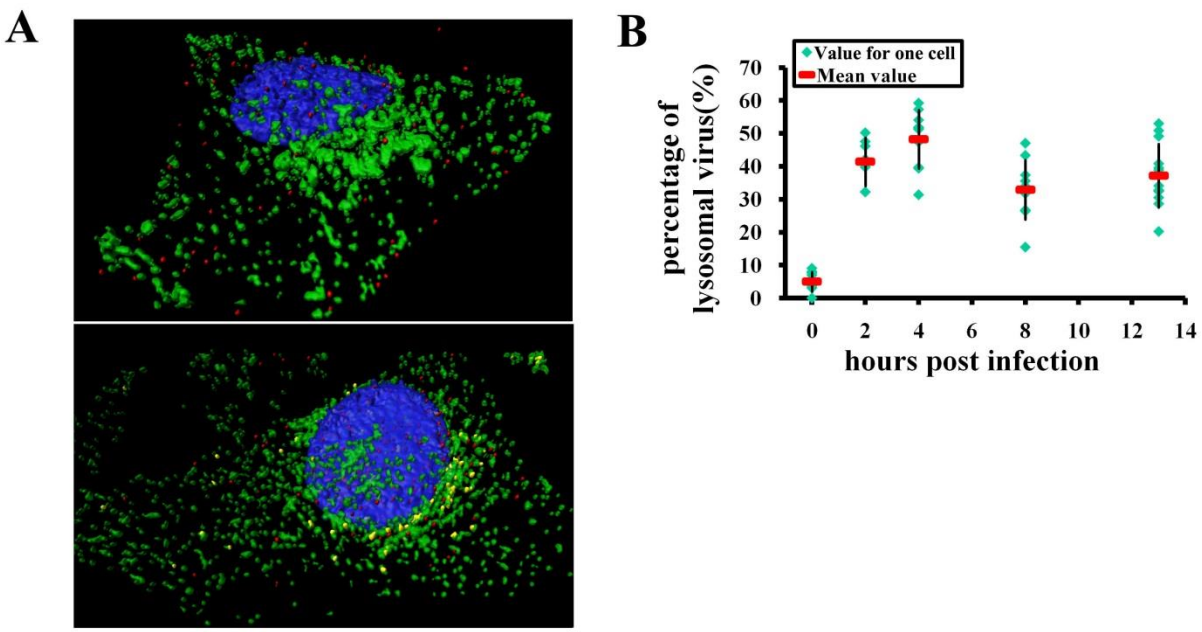


**Figure II-9. Association of Cy5-AAV2 with the lysosomes.** A) Representative 3D isosurface images of Cy5-AAV2 within cells at 0hr and 8hrs p.i.. Nuclei are stained in blue, and viral particles (red) associated with lysosomes (green) are highlighted as yellow. B) The percentage of viral particles associated lysosomes was plotted. Cyan diamonds represent data from individual cells (n = 10-15), red bars represent mean value of each time point (0hr, 2hr, 4hr, 8hr and 13hr), and error bars represent the standard deviation (STDEV).

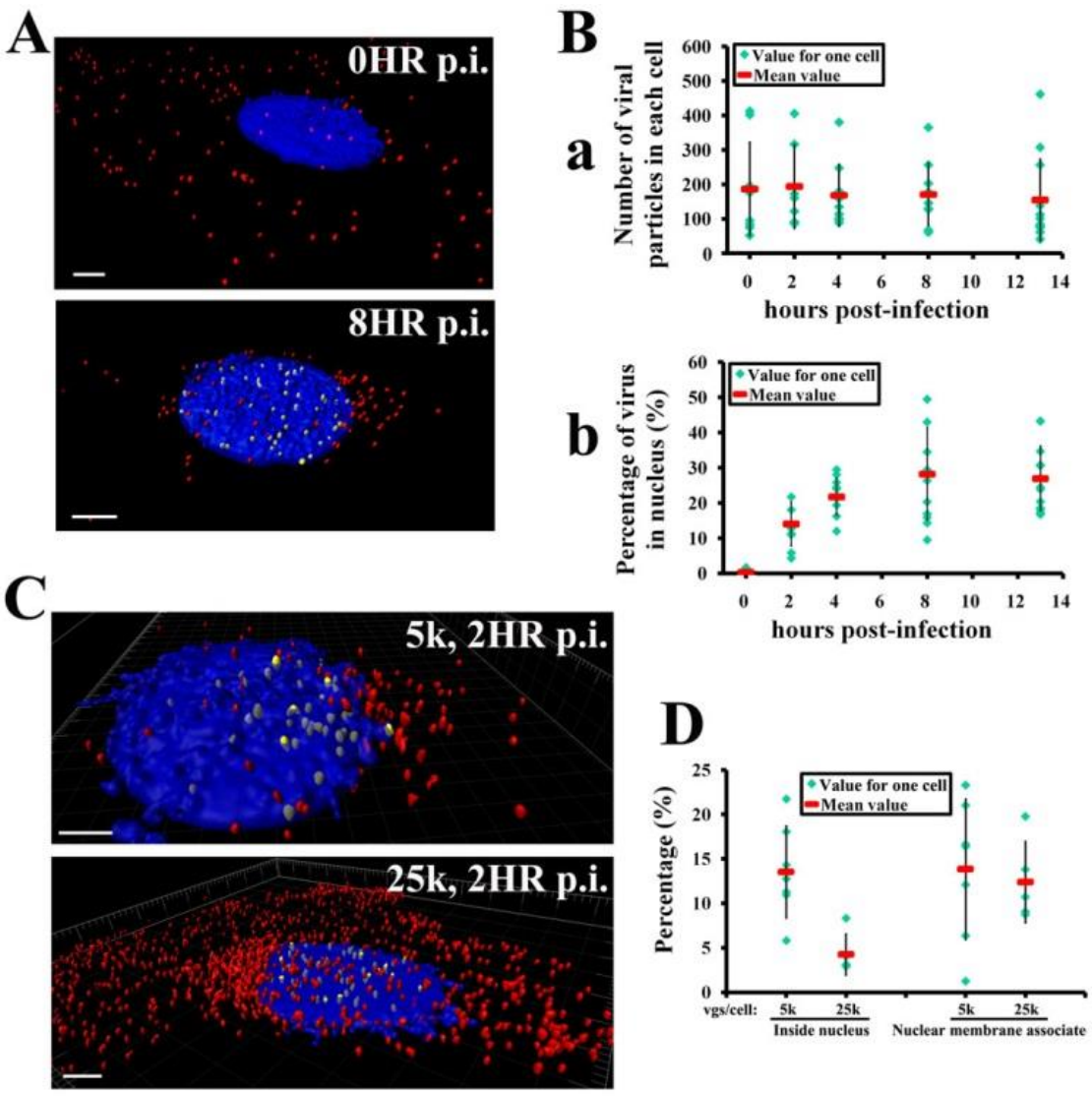


**Figure II-10. Kinetics of Cy5-AAV2 nuclear targeting.** Hela cells were incubated with Cy5-AAV2 (A+B: 5,000 vgs/cell, C+D: 5,000 or 25,000 vgs/cell) at 4℃ for 40 minutes and then transferred to 37℃ incubator. Cells were then fixed at 0, 2, 4, 8 and 13 hours and nuclei were stained with DAPI. The number of viral particles within cells was calculated using the mean value of Cy5 TFI (47568 a.u.) determined in Fig.II-7B-b. A) Representative 3D isosurface images of Cy5-AAV2 within cells at 0hr and 8hrs p.i.. Viral particles in nuclei are highlighted as yellow. Scale bars represent 5μm. B) Plots of total number of viral particles (a) and percentage of intra-nuclear viral particles (b) in each cell. C) Representative 3D isosurface images of cells infected at 5,000 or 25,000 vgs/cell at 2hrs p.i.. Viral particles in nuclei are highlighted as yellow. Scale bars represent 5μm. D) Percentage of intra-nuclear and nuclear membrane associated viral particles as shown in C. Cyan diamond represents data from individual cells (n=10-20), red bars represent mean value of each time point, and error bars represent the standard deviation (STDEV).

Nuclear entry of either viral proteins or genetic material, following the small vesicle trafficking, is one of the rate-limiting steps in most viral infection. Extensive effort has been made to block this step in antivirus strategies or to improve the efficiency of this step for more efficient gene delivery (Haffar et al. 2005; Hindley et al. 2007; Suzuki et al. 2007; Johnson et al. 2008; Greber et al. 2009). Like several DNA viruses (Hindley et al. 2007; Greber et al. 2009), AAV2 has to enter the cell nucleus to complete its life cycle (Sonntag et al. 2006; Johnson et al. 2008). However, such trafficking kinetics as well as the mechanism through which AAV enters nucleus remains unknown due to the lack of a quantitative method to study this process. Here we demonstrated the use of 3D tracking of single viral particles to explore the dynamics of AAV2 nuclear entry in cultured cells.

Experiments were carried out as lysosomal association studies, and nuclei were stained with DAPI. After 3D deconvolution and reconstruction of image stacks, we quantitatively documented the kinetics of AAV2 nuclear targeting (Fig.II-10, & Movie S3-S5). We observed that the number of viral particles (~200) associated with the cell did not change significantly over the time period we observed (Fig.II-10B-a). On average, 0% and 14% of total intracellular viral particles were found in the nucleus at 0hrs and 2hrs p.i. respectively, and this percentage increased to 22% at 4hrs, 28% at 8hrs and 27% at 13hrs (Fig.II-10B-b). With the previous measured mean value of Cy5 TFI (47568 a.u.) for a single Cy5-AAV2, the corresponding viral particle numbers in the nucleus were 27, 38, 48 and 41 at 2hrs, 4hrs, 8hrs and 13hrs respectively (data not shown). These results suggest the following dynamics of AAV2 nuclear targeting: 1) Half of the nuclear targeting events happened within the first 2hrs p.i., with the remainder occurring between 2-8 hrs p.i. . This correlates well with the fact that reporter gene (GFP) expression can be detected as early as

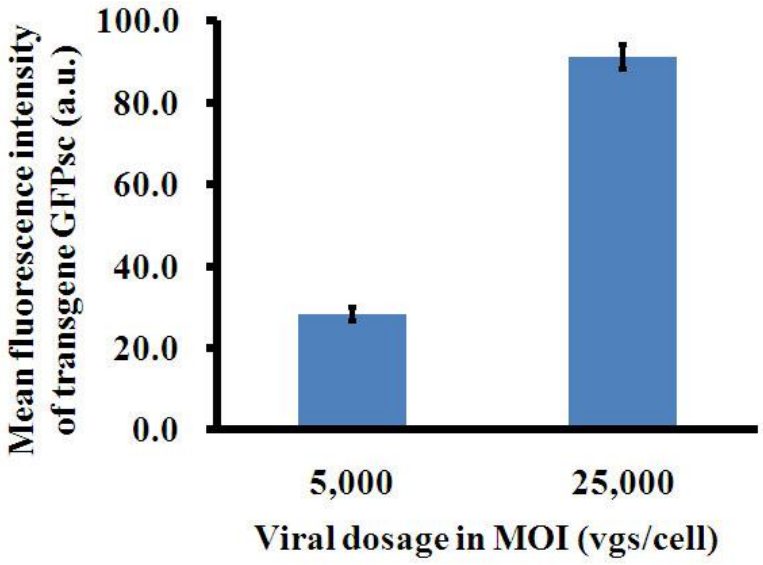


**Figure II-11. The level of transgene EGFPsc expression at two different virion dosages** (MOI=5,000 vgs/cell and MOI=25,000 vgs/cell). The relative mean fluorescence intensity (RMFI) at 5,000 vgs/cell is about 28.2 a.u., and RMFI at 25,000 vgs/cell is about 91.2 a.u..

6-8hrs p.i.. 2) The relative number of AAV2 in the nucleus appears to level off at 8hrs p.i., with about 30% (48 out of 170) intracellular AAV2 particles on average located in the nucleus. This result is consistent with an earlier report which found that a similar percentage of AAV genome (~30%) ended up in the nucleus (Zhong et al. 2008). These results were summarized into an *in vitro* model (Fig.II-13A) and quantitatively documented in a table (Fig.II-13C: Table1). Remarkably, the percentage of AAV2 associated with the nuclear membrane (~12%) at 2hrs p.i. did not change when the viral dosage was increased to 25,000 vgs/cell. However, nuclear entry efficiency at 2hrs p.i. with 25,000 vgs/cell (~4%) was significantly decreased (3 fold) compared to that with 5,000 vgs/cell (~14%) (Fig.II-10C,D). These results suggest that limited sites for viral entry are available on the nuclear membrane or limited trafficking routes are available for AAV2 to enter nucleus. In accordingly, the transduction efficiency measured by transgene GFPsc expression at 25,000 vgs/cell is only about three folds of that at 5,000 vgs/cell (Fig.II-11).

**Trafficking kinetics in mouse muscle.** The ultimate goal of studying particle trafficking is to elucidate the behavior of viral and non-viral vectors in tissues and animals. The *in vivo* setting provides the most applicable information for the development of efficient gene delivery vectors. Current method of studying the distribution of viral vectors *in vivo* using reporter gene assays tracks only the virions that successfully transduce cells. Given that the vast majority of virions are likely to be futile in infection, reporter gene imaging provides a biased understanding of virion distribution that can easily lead to mis-interpretation of the pharmacology of these agents, resulting in failed development of anti-viral and therapeutical delivery vectors (Hofherr et al.; Brandenburg et al. 2007). To circumvent this problem, we have tracked all AAV particles, both infectious and abortive, in mouse muscle over time.

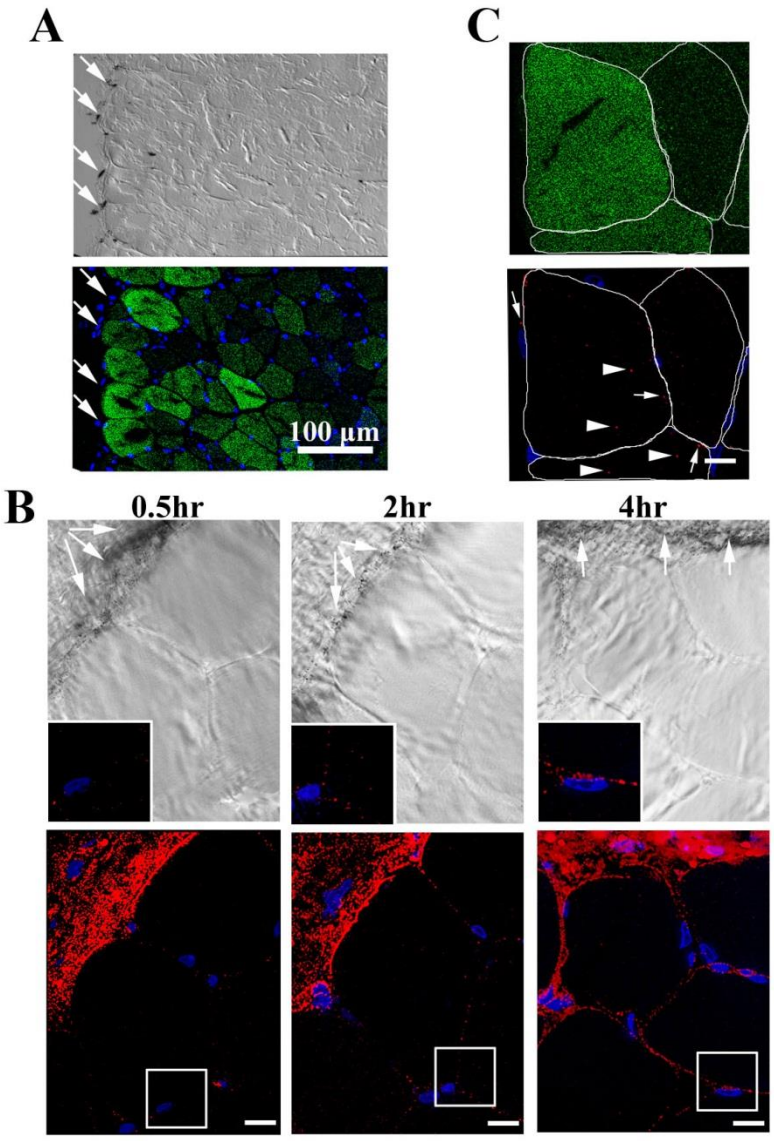


**Figure II-12. Trafficking of AAV2 in mouse muscle.** A) Site of AAV injection is visualized by Indian ink (black spots in upper panel) and is indicated by arrows, and corresponding reporter gene GFP expression (Green) in muscle at 6 days post-injection (lower panel). Scale bar represents 100µm. B) Distribution of Cy5-AAV2 particles in mouse muscle at 0.5, 2 and 4hrs post-injection. Upper panel shows the DIC images with the injection site indicated by arrows. Lower panel shows the localization of Cy5-AAV2 particles (red) and nuclei (blue). The inserts in upper panel are the magnified view of selected regions in lower panel (white boxes). Scale bars represent 10µm. C) Cy5-AAV2 particles were detected inside the muscle fibers at 6 days post-injection. Upper panel shows the expression of reporter gene GFP in muscle fibers. Lower panel shows the Cy5-AAV2 particles (red) and nuclei (blue). Individual muscle fibers are outlined by curved white-lines. Arrowheads indicate the viral particles inside the fibers and arrows indicate the viral particles along the side of muscle fibers. Scale bar represents 10µm.

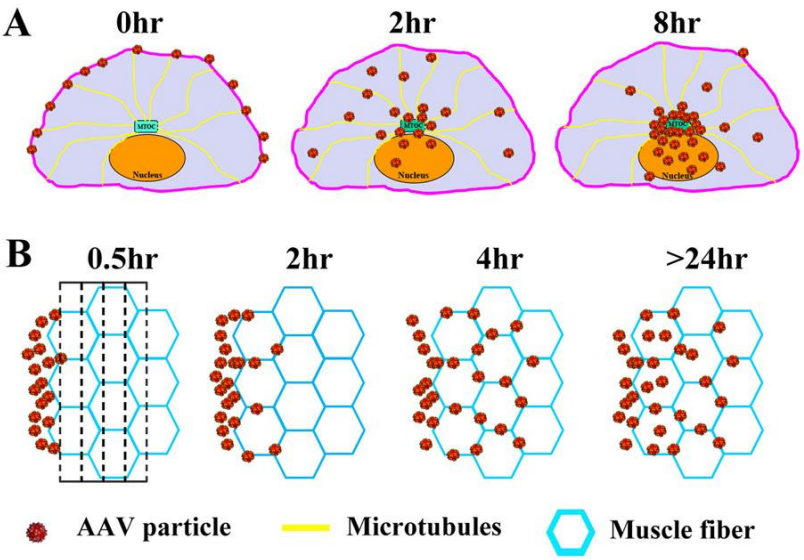


C

| In Vitro (MOI=5,000vgs/cell) | | | | | |
|---|---|---|---|---|---|
| | Total number of AAV | AAV traversing nuclear membrane | | AAV in Nucleus | |
| | Mean number/per cell | Mean number per cell | Mean percentage (%) | Mean number per cell | Mean percentage (%) |
| 0hr | 186 | 0 | 0 | 0 | 0 |
| 2hr | 193 | 29 | 15 | 27 | 14 |
| 4hr | 168 | 21 | 12 | 38 | 22 |
| 8hr | 170 | 24 | 14 | 48 | 28 |
| 13hr | 152 | 23 | 14 | 41 | 27 |

| In Vivo (2E+09 vgs/injection) | | | | | | | |
|---|---|---|---|---|---|---|---|
| | Total number of AAV within the region | | Number of AAV traversing nuclear membrane per nucleus | | No. of AAV in nucleus per nucleus | | |
| Hours p.i. | 2hrs | 4hrs | 2hrs | 4hrs | 2hrs | 4hrs | 6days |
| Region I | 758 | 3252 | 14 | 27 | 13 | 148 | Not detectable in most nuclei |
| Region II | 597 | 2518 | 4 | 27 | 6 | 23 | |
| Region III | 54 | 1186 | 0 | 12 | 0 | 10 | |
| Region IV | N.A. | 699 | N.A. | 1 | N.A. | 4 | |

**Figure II-13. Schematic and quantitative documentation of AAV2 trafficking in vitro and in vivo.** A) Model for AAV2 infection in cell culture. After binding to the cell surface at 0hr, AAV2 particles are transported via microtubules toward the perinuclear region (typically Microtubule Organization Center, MTOC) within the first 8 hours after viral inoculation. Progressive nuclear entry is observed during the first 8 hours p.i., with about 30% of viral particles in the nucleus at 8 hours p.i.. B) Model for AAV2 trafficking mouse muscle shown in cross-sectioned view. AAV2 particles traffic from the injection site to distal myofibers through the endomysium between those fibers. Some AAV particles penetrate the muscle fibers, but only at later time point (>=24hrs). To quantitatively document the intra-muscular trafficking in C (Table 2), four regions (I-IV) were defined from the injection site to distal myofibers, and the width of each region is about half of myofiber's diameter. C) Quantitative documentation of AAV2 distribution and trafficking kinetics in cultured Hela cells (Table 1) and mouse muscles (Table 2).

After injection with Cy5-AAV2 particles, mouse limb muscle was collected at various times. Reporter gene (GFP) expression spread up to several muscle fibers away from the injection site, indicated by Indian ink (arrows in Fig.II-12), and was stronger in those fibers closer to the injection site than in the fibers distal from injection site at six days p.i. (Fig.II-12A). The immediate question is whether this distribution pattern represents the spreading of GFP molecules or viral particles across the muscle fibers. Our results showed that, in contrast to Indian ink remained local to the site of injection (Fig.II-12B upper panel), AAV particles migrated from the injection site into the neighboring fibers (three muscle fibers away from the injection site). We observed that numbers of AAV particles in the surrounding fibers and in nuclei increased from 0.5hr to 4hrs (Fig.II-12 lower panel). Almost all Cy5-AAV2 particles were located at the site of injection after 0.5hr post-injection. A few viral particles were observed on the side of fibers (sarcoplasm) adjacent to the injection site at 2hrs post-injection. A large amount of viral particles appeared on the side of fibers close to (3 muscle fibers away from) the injection site at 4hrs post-injection. Such trafficking kinetics was summarized in an *in vivo* trafficking model (Fig.II-13B) and quantitatively documented in a table (Fig.II-13C: Table 2). During this time period, viral particles were only observed along the side of muscle fibers (sarcoplasm) but not inside the fibers prior to 4hrs post-injection (Fig.II-12B lower panel) and the number of AAV capsids in nucleus was increased over time (Fig.II-13C). This observation suggests that viral particles after intra-muscular injection are likely to spread through the endomysium between muscle fibers, rather than by transcytosis. In addition, at six days p.i., AAV capsids were only observed along and inside the muscle fibers but not detectable in most of the nuclei (Fig.II-12C, II-13C). This observation suggested that most AAV genome should be readily released rapidly *in vivo*.

## Discussion

Understanding how nanoparticles travel through the cellular structures and how pharmacological reagents can affect viral trafficking is essential for the development of enhanced gene therapy vectors (e.g. polymers, Adenovirus and AAV) (Torchilin 2006; Breunig et al. 2008). Fluorophore labeling of particles has been mainstay in studying the dynamics of particle trafficking (Pelkmans et al. 2001; Ding et al. 2006; Schelhaas et al. 2008). While a fancy research tool, current molecular tracking and 2D imaging analyses have significant limitations in studying classical viral trafficking and bio-distribution (Seisenberger et al. 2001; Grieger et al. 2006), in which temporal resolution is not the primary interest. For example, sampling all intracellular viral particles and quantitatively studying their distribution and trafficking kinetics in 3D animal cells and tissues has not yet been achieved. Although investigation of bio-distribution and trafficking kinetics of DNA carrier vectors have been attempted previously (Akita et al. 2004; Grieger et al. 2006), these studies are 2D imaging analyses that have limitations in quantitatively characterizing the viral behavior in 3D cellular structures. For example, classical 2D imaging and analysis can lead to arbitrary results, since the distribution patterns in different focal planes vary along the z-axis of confocal images. As a result, neither distribution data gained from a specific focal plane nor that simply summed up from all focal planes is able to correctly reflect the behavior of virus in cells. Recently, Chen *et al* studied the trafficking kinetics of plasmid carriers by measuring the volume of fluorescence spot generated by labeled particles (Chen et al. 2008). As known, the amount of dye molecules (or dye-labeled particles) in a subresolutional region (diameter < 150nm) should be calculated by the amount of emitted

photons linearly reflected by fluorescence intensity in confocal images (Pawley 2006; Zenklusen et al. 2008) but not by fluorescence volume, since there is no linear correlation between number of dye molecules (or labeled particles) and fluorescence volume (Fig.II-3A). As a result, the amount of emitted photons or fluorescence intensity instead of fluorescence volume should be used to quantitate dye-labeled subresolutional-sized particles (Fig.II-3). The method described in this study directly uses fluorescence intensity information to quantitatively determine the number and distribution of nano-scaled particles in three dimensions (Fig.II-3, II-5D-b, II-7B-b), which is fundamentally different from the volume-based method (Chen et al. 2008). In addition, restorative 3D deconvolution was also applied to appropriately counteract the image distortions caused by optical systems to increase the accuracy of this three dimensional image analysis ((Pawley 2006), Fig.II-2). In brief, this method has employed multiple strategies including iso-surface assisted object-by-object analysis (Fig.II-1B), intensity-based calculation (Fig.II-3) and restorative 3D deconvolution (Fig.II-2) to significantly improve the accuracy of 3D image quantification. Compared with previous studies, including the improved precision of image quantification, this method not only allows one to view the particle trafficking from an entire viral population (Fig.II-10, II-13C), but also for the first time allows one to locate each individual particle into finer sub-cellular structures (i.e. inside/outside nucleus or traversing nucleus, as shown in Fig.II-1B and detailed localization in muscle as shown in Fig.II-12C). By determining the fluorescence parameter for a single Cy5-AAV2 virion (Fig.II-5, II-7), this method also allows one to quantitate the absolute number of particles in each cellular structure such as nucleus (Fig.II-10), microtubules and cell surface as well as sub-resolutional vesicle structures like endo/lysosomes (Fig.II-9), which have never been reported previously. Finally and

importantly, this method for the first time allows one to quantitatively investigate particle bio-distribution/trafficking in animal tissues (Fig.II-12), which have not been documented by any of above method.

Our electron microscopy data demonstrates that almost all Cy5-AAV2 virions we used in this study are full particles (Fig.II-4A). The labeled virions are shown to preserve the capsid integrity as determined by A20 antibody binding (Fig.II-4E), and have similar infectivity as non-labeled AAV2 (Fig.II-4B,C). These labeled virions are also shown to have the normal ability to bind heparan sulfate and migrate on microtubules (data not shown). Using these Cy5-AAV2 that preserve the same morphology and functionality as unlabeled ones, we have generated a body of interesting and biologically meaningful results consistent with previous reports as well as several novel observations that have never been documented previously. For example, we have quantitatively demonstrated that the majority of AAV2 are bound to the cell surface as single particles even at a high MOI and the binding of AAV2 can be blocked by incubating the virus with heparin or incubating cells with heparanase (data not shown), supporting previous reports showing heparan sulfate is the primary receptor for AAV2 (Summerford et al. 1998; Bartlett et al. 2000). We then demonstrated that AAV2 can migrate on microtubules and that disruption of the microtubule network impaired the nuclear targeting of AAV2 (Chapter-4). The kinetics of AAV2 trafficking in small vesicles like lysosomes was illustrated using this quantitative microscopy method (Fig.II-9). In addition, we also explored the kinetics of AAV2 nuclear trafficking, one of the most important events in AAV infection, by quantitate the number and percentage of AAV particles in nuclei over time (Fig.II-1B, II-10, and II-13C). Importantly, we have for the first time quantitatively characterized the trafficking behavior of AAV2 in mouse muscle tissue (Fig.II-12B, II-13C)

providing rationale for the pattern of viral transgene expression *in vivo*. We will discuss some of these findings in detail in the following text.

Nuclear entry is regarded as the most critical and rate-limiting step for the life cycle of most DNA viruses (e.g. adenovirus, herpesvirus and parvovirus) (Whittaker et al. 2000; Greber et al. 2009). Blocking the nuclear entry is an alternative way to block viral replication (Haffar et al. 2005; Boulo et al. 2007; Hindley et al. 2007; Greber et al. 2009), and on the other hand, facilitating the nuclear entry of viruses has been a promising strategy to improve viral vectors for gene delivery (Hansen et al. 2000; Suzuki et al. 2007; Johnson et al. 2008; Mudhakir et al. 2009). Several groups have suggested that AAV entered nucleus as intact virions (Bartlett et al. 2000; Sonntag et al. 2006; Johnson et al. 2008). For example, the Kleinschmidt group demonstrated that intact AAV2 particles enter the nucleus, since nuclear injection of the A20 antibody can block AAV2 infection and disassembled AAV particles are not detected by B1 antibody until 20hrs after infection (Sonntag et al. 2006). Our group showed that AAV enters the nucleus as intact virions and nuclear virions could be extracted and used to re-infect new cells (Johnson et al. 2008). These most recent studies suggest that AAV enters nucleus as intact virions and then uncoats there. However, the kinetics of AAV nuclear targeting has not been precisely documented and the exact route/site for viral nuclear entry is highly controversial. The method described herein was used to quantitatively investigate the viral nuclear entry step. Our microscopy analysis of AAV documented the kinetics of nuclear entry over 13hrs post infection (Fig.II-10 and Fig.II-13C: Table 1), summarized in the in vitro model (Fig.II-13A). The result showing that about 30% of bound AAV2 particles entered nucleus, together with the observation showing that only about 4-5% (~200 out of 5,000 virions/cell) of particles in the medium attached to cell surface, suggests

that only 1-2% of AAV2 virions will eventually enter the nucleus and express. Such binding efficiency was verified by quantitative PCR (data not shown), and also reported by other studies for other AAV serotypes (Shen et al.). This low binding efficiency is due to the nature of biochemical reaction between ligands (AAV2) and receptors (heparan sulfate on cell surface), rather than the quality of AAV prep because the unbound particles remaining in the medium can be transferred to successfully infect new cells as well. These results propose the existence of a non-infectious trafficking pathway as another reason for the high particle-to-pfu phenomena in AAV infection in addition to the defective particles in AAV preparations. We also noticed a wide variation in the number of nuclear particles per cell at every time point (Fig.II-10B). This supports a highly heterogeneous susceptibility of each cell to AAV2 infection and explains the variation of AAV2 transgene GFP expression among individual cells. As a result, by quantitating the number of virions in a single cell as accessible by this method, one will be able to correlate the number of viral particles in a cell with the amount of transgene expression to address questions like how many virions are needed to express a certain amount of transgene. Typically, one will be able to observe the expression of double-stranded GFP transgene *in vitro* at about 6-8 hours after infection. Given the several hours required for the maturation of a GFP molecule to give fluorescence (Heim et al. 1995), such observation indicate that viral particle should enter nucleus and release genome within couple hours p.i.. The kinetics of AAV nuclear trafficking revealed in this study clearly demonstrated the early AAV2 nuclear entry events within 2 hours p.i. (Fig.II-10B), which provides a molecular rational for such a gene expression profile. In dose response studies, the number of virions in the nucleus does not increase linearly with the number of nuclear membrane associated virions at 2hrs p.i. (Fig.II-10D). This result suggests that there may be

limited sites/routes for AAV2 nuclear entry through the nuclear membrane, and provides a sound explanation for the observation that the fold increase in virion dosage does not translate to equivalent fold increase in transduction (Fig.II-11). Experiments to confirm this hypothesis are ongoing. With such scenario, this method enables one to quantitate the effects of pharmacological drugs and AAV variants on the nuclear transportation of AAV particles to facilitate the direction towards improving this vector's performance.

Similar to the documentation of nuclear entry dynamics, the kinetics of viral trafficking through other cellular structures (i.e. small vesicles, cell surface, microtubules) can also be documented with this method (Fig.II-6). The spatial-temporal distribution of all viral particles within the host cells throughout the entire trafficking pathway can be determined by integrating all the information regarding the kinetics of virions in various cellular structures. It is noted that about 1:100 rAAV2 particles are infectious consistent with a recent report (Zeltner et al. 2010), suggesting that only 1 out of 100 viral particles in culture medium will successfully infect a cell in the culture dish. Our study shows that only about 5% of rAAV2 in the medium will attach to the cell surface for internalization (as suggested by Fig.II-10B). Our heparin competition and heparanase treatment studies demonstrate that all particles tracked in these experiments were 100% positive for first step in infectious pathway (i.e. viral binding), making the above observations relevant irrespective of the particle-to-infectious-unit ratio.

Understanding the distribution of viral and non-viral vectors *in vivo* is extremely valuable to advance current drug/DNA delivery strategies. In this study, we have successfully applied our quantitative 3D microscopy method to study the distribution of AAV2 particles in animal tissues. We and other groups have observed the limited spreading of AAV2

transduction around the needle track as indicated by the expression pattern of various reporter genes (Fig.II-12A, and (Kessler et al. 1996; Fisher et al. 1997; Pruchnic et al. 2000)). However, there is no direct evidence on AAV2 trafficking that provides the molecular rationale for such transgene expression profiles *in vivo*. To address this question, we used the quantitative microscopy method to directly quantitate the distribution of AAV2 particles in mouse muscle over time. Our results for the first time showed that the AAV2 particles were localized at the injection site during the first 30 minutes and then uniformly spread through tissues up to three muscle fibers away from the injection site over 4hrs (Fig.II-12B). This result is significant in that it allows one to correlate viral spread with expression and should provide insight into vector tropism when studying capsid variants specific for muscle or various tissues such as brain and eye (Kessler et al. 1996; Fisher et al. 1997; Davidson et al. 2000; Gregorevic et al. 2004; Sun et al. 2005; Wang et al. 2005). Another important question is how the viruses traffic to the cells distal from the injection site (Kotchey et al.; Kessler et al. 1996; Fisher et al. 1997; Davidson et al. 2000; Gregorevic et al. 2004; Sun et al. 2005; Wang et al. 2005; Di Pasquale et al. 2006). Transcytosis has been proposed as a mechanism for the spreading of various viruses, including HIV, poliovirus and AAV, and most of these studies involved epithelial cell barriers using *in vitro* transwell cell culture (Kotchey et al.; Ouzilou et al. 2002; Bomsel et al. 2003; Di Pasquale et al. 2006; Bhat et al. 2007). However, little information is available regarding the mechanism of trafficking for AAV particles *in vivo*. Our studies using this quantitative 3D microscopy method show that almost all viral particles localized to the boundary of the muscle fibers (sarcoplasm) but not inside the fibers when trafficking to the distant fibers (Fig.II-12B). This observation strongly suggests that most AAV2 particles traffic through the endomysium between muscle fibers instead of

traversing through myofibers. These virions between muscle fibers, we believe, are infectious as indicated by the transgene expression in these muscle cells (Fig.II-12A). It is also noteworthy that the trafficking kinetics showing virions in muscle nuclei at 30min to 4hrs (Fig.II-12B) combined with the absence of AAV2 in nuclei at 6 days p.i. (Fig.II-12C) suggests that nuclear AAV2 vectors release their genomes quite rapidly. Previous reports demonstrated that the expression of AAV2 transgenes in muscle did not reach the peak until around 5 weeks p.i. (Fisher et al. 1997; Chao et al. 2000). These studies in combination may support that, after uncoating, AAV2 transduction may be impacted by other cellular factors such as the rate-limiting step of second strand synthesis (Ferrari et al. 1996; Fisher et al. 1996; McCarty et al. 2001). Additionally, at 6 days after injection, AAV2 particles were also detected inside of the muscle fibers/cells (Fig.II-12C). This observation supports a hypothesis that, unlike in cultured cells, viral particles *in vivo* can persist in myofibers potentially providing a temporal reservoir of virus. And these virions may traffic to the nucleus and contribute to viral transduction at later times (over 2 weeks), which also could be an explanation to the observed AAV transduction profile in muscle (Fisher et al. 1997; Chao et al. 2000).

This quantitative 3D distribution microscopy approach presented here was originally designed to quantitatively examine how pharmacological reagents and viral genetic variants impact the trafficking kinetics and bio-distribution of viral vectors. With this approach, we have generated a panel of very interesting and biological meaningful results consistent with previous reports as well as several novel observations that have not been previously documented. These findings both support the current working knowledge of AAV biology and provide a better mechanistic insight into the behavior of this viral vector *in vitro* and *in*

*vivo*. It will be of particular interest to quantitatively compare the trafficking behavior of various AAV serotypes and chimeric vectors, as well as mutant capsids defective/enhanced in viral trafficking. Data from such studies should provide guidance for the rational design of optimal gene therapy vectors. Therefore, such an ability to quantitate the distribution and trafficking kinetics of nanoparticles (Fig.II-13C) should facilitate a quantitative evaluation of the effects of pharmacological reagents and vector variants on the delivery performance of these particles in cultured cells as well as animal tissues. Finally, in combination with pharmacological tools and live cell imaging, this 3D quantitative distribution microscopy approach will provide a comprehensive and powerful method to understand the physiological life cycle of gene-delivery vectors, as well as the intracellular behavior of other nanoparticles *in vitro* and *in vivo*.

# CHAPTER 3

# CYTOPLASMIC TRAFFICKING, ENDOSOMAL ESCAPE, AND PERI-NUCLEAR ACCUMULATION OF AAV2 PARTICLES ARE FACILITATED BY MICROTUBULE NETWORK


## Summary

Understanding AAV trafficking is critical to advance our knowledge in AAV biology and exploit novel aspects of vector development. Similar to most DNA viruses, after receptor binding and entry, AAV traverse the cytoplasm and deposit the viral genome in cell nucleus. In this study, we examined the role of microtubule (MT) network on AAV productive infection. Using pharmacological reagents (e.g. Nocodazole), live cell imaging, and flow cytometry analysis, we demonstrated that AAV2 transduction was reduced by at least 2-fold in the absence of MT network. Cell surface attachment and viral internalization were not dependent on intact MT network. In treated cells at 2hrs post-infection, quantitative 3D microscopy determined a reproducible difference in number of intracellular particles associated with nuclear membrane or the nucleus compared to controls (6-7% *vs* 26-30% respectively). Confocal microscopy analysis demonstrated a direct association of virions with MTs, further supporting a critical role on AAV infection. To investigate the underling mechanisms, we employed single particle tracking (SPT) to monitor the viral movement in real-time. Surprisingly, unlike other DNA viruses (i.e. Ad and HSV) that display bi-directional motion on MTs, AAV2 displays only uni-directional movement on MTs towards

the nuclei with peak instantaneous velocities at 1.5-3.5μm/s. This rapid and uni-directional motion on MTs lasts for about 5-10 seconds and resulted in AAV particles migrating more than 10 μm in the cytoplasm reaching the nucleus very efficiently. Furthermore, electron microscopy analysis determined that, unlike Ad and HSV, AAV2 particles were transported on MTs within membraneous compartments, and surprisingly the acidification of AAV2 containing endosome was delayed by the disruption of MTs. These findings altogether suggest an as yet undescribed model in which after internalization, AAV2 exploits MTs for rapid cytoplasmic trafficking in endosomal compartments uni-directionally towards peri-nuclear region where most acidification events for viral escape take place.

## Introduction

Adeno-associated virus (AAV), a member of *parvovirus* family, is unique in that it requires helper virus (e.g. Ad, HSV) for productive replication. This non-enveloped icosahedral protein capsid (~20nm in diameter) packages a 4.7kb single-stranded genomic DNA. The capsid is composed of three overlapping subunit proteins, encoded by the *Cap* gene, at a ratio of 1:1:10 (Vp1:Vp2:Vp3). Due to its unique properties including non-pathogenicity, ability to transduce dividing and non-dividing cells, breadth of tissue tropism, and sustainable transgene expression, several recombinant AAV capsids especially serotype 2 (rAAV2) have been extensively exploited as gene therapy vectors (Wu et al. 2006). The potential of this vector has been well demonstrated by recent successes in several clinical trials including treating Leber's congenital amaurosis (Maguire et al. 2008) and Hemophilia B (Nathwani et al. 2011). Despite many advances in vector developments, administration of high dose viral particles is required to achieve efficient transduction due to rate-limiting steps including pre-existing immune response and non-specific targeting (Rogers et al. 2011). In addition to these limitations, host cell also exploits various cellular components as barriers to AAV productive infection, including the critical steps required for viral trafficking (e.g. cell surface uptake, cytoplasmic trafficking, endosomal escape, nuclear entry, etc.) (Wang et al. 2011). Better understanding of the AAV cellular trafficking will advance our knowledge in AAV biology and facilitate the development of enhanced AAV vectors.

To successfully transduce a cell, AAV virions have to travel through a variety of cellular structures and organelles consecutively, including cell surface binding and internalization, cytoplasmic trafficking, and finally nuclear entry. It is known that AAV2

virions bind to its primary receptor Heperan Sulfate Proteoglycan (HSPG) on cell surface (Summerford et al. 1998) and internalized through clathrin-dynamin mediated pathway (Duan et al. 1999; Bartlett et al. 2000), which are facilitated by co-receptors including integrins (Summerford et al. 1999) and FGF receptors (Qing et al. 1999). After entry, the virus remains associated with endosomes until acidification of the compartment which triggers exposure of the N-terminus of Vp1 protein (Sonntag et al. 2006). The N-terminus of Vp1 carries phospholipase activity and facilitates viral particles escaping by breaking down the endosomal membrane (Sonntag et al. 2006). Successful transduction of AAV requires that its genome be delivered into the nucleus, which is believed to be achieved by nuclear localization signals on the capsid subunit Vp1 (Grieger et al. 2006). However, little is known about how the viral particles traverse across the dense cytoplasm micro-environment from the cell peripheral to nuclear proximity, where AAV enters the nucleus.

Microtubules (MTs) are a component of cytoskeleton and are rope-like polymers of tubulins. MTs are highly dynamic as characterized by alternate phases of elongation and shrinkage, and play critical roles in a variety of cellular processes including maintaining cell structure, intracellular transportation, forming the spindle during mitosis, to name a few (Desai et al. 1997). Their roles in intracellular transport are usually achieved by either their own growth dynamics (Roohvand et al. 2009) or the activities of associated motor proteins, particularly kinesin and dynein (Leopold et al. 2006). Numerous studies have shown that both non-enveloped and enveloped viruses utilize MTs in infecting their host cells. This is typically exemplified by the utilization of dynein by viral particles to traffic through the crowded cytoplasmic environment to the nucleus. For AAV, previous studies have reported that MT disruption impairs AAV transduction (Sanlioglu et al. 2000) and AAV can bind the

cytoplasmic dynein in an *in vitro* binding assay (Kelkar et al. 2006). However, these studies were contrasted by another publication that AAV transduction was not affected by the disrupted MT network or dynein motor activity (Hirosue et al. 2007). As a result, the exact roles of MTs on AAV transduction as well as the underling mechanisms are yet unclear.

In this study, we have investigated the exact role(s) of MTs on AAV transduction and corresponding potential mechanisms using multiple techniques including confocal microscopy, live cell imaging, quantitative 3D microscopy, pharmacological reagents, and single particle tracking. Data from live cell imaging and flow cytometry analysis demonstrated that the viral transduction was impaired in the presence of several chemicals used to disrupt MTs. This result was further supported by the measurements from quantitative microscopy that the proportions of AAV particles associated with nuclear envelop or inside the nucleus, were significantly diminished upon MT disruption. In single particle tracking experiments, we observed that AAV virions display three classical types of particle motions such as confined diffusion, normal diffusion, and directed motion. For the first time, we demonstrated the fast and uni-directional migration of AAV2 on MTs with peak instantaneous velocity up to 1.5-3.5 μm/s, which is consistent with the motion mediated by dynein motor. Furthermore, our observations from electron microscopy and pharmacological studies determined for the first time that AAV2 traffics on MTs in endosomal compartment and acidification of such structure is dependent on intact MTs. Above data altogether have strongly supported an as yet undocumented model in which AAV2 exploits MTs for its rapid-directed cytoplasmic transportation towards the peri-nuclear sites where acidification of endosomes for viral escape take place.

## Materials and Methods

**AAV2 production, purification and labeling.** AAV2 was produced in HEK-293 cells as previously described (Grieger et al. 2006). Briefly, cells were transfected with three plasmids: pXR2, pXX680, and pTR-CMV-GFP containing the GFP reporter transgene flanked by two ITRs. At 60hrs after transfection, cells were harvested and nuclei were isolated using hypotonic buffer and Kontes homogenizer (Grieger et al. 2006). AAV2 particles were recovered by resuspending the nuclear pellet in PBS with 0.5% Deoxycholate (DOC) and then sonicated for 1min. Highly pure virus was then retrieved as described previously (Xiao et al. 2011). Briefly, after DNase treatment, virus suspension was subjected to one round of cesium chloride (CsCl) step gradient density fractionation and another round of fractionation using CsCl continuous gradient density. Determination of peak viral fractions, dialysis of virus, and measurement of viral titers by qPCR were done as described (Grieger et al. 2006). The infectivity of AAV is determined to about 1 transduction unit per 100 particles.

AAV2 was covalently labeled with Cy5 or 1.4nm Nanogold particles as described in manufacture's protocol with slight modification. Briefly, purified AAV2 were incubated for 2hr at 4℃ in PBS with a 20-fold molar excess of Mono-NHS-Cy5 (GE Healthcare) or Mono-NHS-Nanogold (Nanoprobes) over the capsid protein units. Free dyes or Nanogold were removed from labeled viral particles by dialysis against PBS containing 5% sorbitol and viral solutions were stored at -80℃ as small aliquots. The degree of labeling (DOL) of Cy5-AAV2 was determined by spectrophotometry as described by manufacturer's instructions. Labeled

viral titers were determined by both dot blot (Grieger et al. 2006) and qPCR. Infectivity of the viral particles was determined by GFP reporter gene assay.

**Cell culture and drug treatment.** Hela cells (American Type Culture Collection) were grown in Dulbecco's modified Eagle medium (DMEM, Invitrogen) with 10% FBS in 5% CO2 incubator. All cells were passaged every 2-3 days for up to ten passages and new aliquots of frozen cells were recovered from liquid nitrogen. To disrupt microtubules, the cells were incubated with medium containing 30μM Nocodazole or 10μM Vinblastine for 30-60 minutes before experiments. For lysosomotropic reagents, 50μM Chloroquine or 64nM Bafilomycin A1 were administrated to block the acidification of endosomes. The drugs were maintained in the culture throughout the experiments.

**Pulse infection and Immunofluorescence.** Pulse infection of AAV2 was performed as previously described (Xiao et al. 2011). Briefly, HeLa cells were seeded on 12-mm glass coverslips at 24hrs before infection. Next day, after incubation in DMEM containing 20mM HEPES at 4℃ for 5min, cells were inoculated with Cy5-AAV2 (~5,000 vgs/cell) at 4℃ for another 40min. Cells were washed with PBS to remove unbound virions and transferred to 37℃ incubator (regarded as 0hr p.i.).

For immunofluorescence, cells were washed with PBS and then fixed with 4% paraformaldehyde (PFA) for 15min at room temperature (RT). The cells were then permeabilized with 0.2% Triton X-100 in PBS for 5min at RT. After blocked with immunofluorescence buffer (IFB) (5% normal goat serum in PBS containing 0.05% Tween-20) for 1hr at RT, the cells were incubated with primary antibody to detect tubulin (Rat monoclonal from Abcam Inc.) diluted in 50% IFB for overnight at 4℃. The cells were then incubated in secondary antibody, diluted 1:2,000 in 50% IFB (anti-mouse Alexa-Fluor 488

[Molecular Probes]), for 1hr at RT. After six washes with PBS, coverslips were mounted cell side down on glass slides with mounting medium (Prolong Antifade Gold with DAPI [4',6'-diamidino-2-phenylindole]; Molecular Probes).

**Reporter gene assay and live cell imaging.** At three hours after pulse infection of self-complementary AAV2 containing TR-CMV-GPF, Hela cells were transferred to the stage of Olympus IX-70 for recording the GFP expression in real-time. The camera was set to take a frame of GFP expression in DMSO or Nocodazole treated cells every five minutes. The snapshots of GFP expression were taken at the indicated time points from the video and the level of GFP expression were measured by the mean fluorescence intensity of GFP using Image J program.

**Quantitative 3D microscopy.** Hela cells pulse infected with Cy5-AAV2 were fixed by PFA and mounted to glass slides as described above. The distribution of viral particles in Hela cells were examined using a Zeiss LSM710 laser scanning confocal microscope equipped with a Plan-Apochromat 63×/NA 1.40 oil objective. Stacks of 20-30 focal planes were captured at 0.31μm z-intervals through the depth of the cell. 3D images of the cells were reconstructed by using the image stacks. All images were acquired at pixel dimensions of 0.13×0.13×0.31μm (X, Y, Z) to fulfill the Nyquist sampling.

Deconvolution was performed by AutoDeblur software (Media Cybernetics Inc.) using iterative and constrained algorithms as described previously (Xiao et al. 2011). The procedure started with a theoretical PSF derived from the actual setting of Zeiss710 confocal microscope, including NA of the microscope objective, refractive index of the medium, excitation wavelength, emission wavelength, confocal pinhole radius, pixel size, z-axis interval, and microscope type (i.e., wide field, confocal). A new adjusted adaptive PSF

derived from the previous deconvolution round was used to generate next adaptive PSF that fits the real imaging data better than the previous one (termed as one iteration or deconvolution round). A 12-round of iteration was used to deconvolve all the confocal images in this study.

All deconvolved image stacks was processed using IMARIS software package (Bitplane AG, Zurich, Switzerland) for visualization and quantification as described previously (Xiao et al. 2011). Briefly, each deconvolved image stack was reconstructed using a volume rendering module and smoothened by a 3D-median filter. Subsequently, an isosurface rendering module was applied through thresholding by the fluorescence intensity that is slightly higher than background. For Cy5-AAV2, the isosurface rendering was thresholded at the fluorescence intensity of 1500a.u. (the upper boundary of background). For DAPI, isosurface rendering was thresholded at the fluorescence intensity of 2900a.u.. Parameters (volume, MFI, TFI) for these isosurface coated Cy5-AAV2 objects were extracted from the IMARIS program and analyzed to determine the localization of particles as described previously (Xiao, 2011).

**Internalization assay.** Pulse infection and immunofluorescence on Hela cells were carried out as described above, except that the cells were not permeabilized when incubating with mouse monoclonal antibody A20 to specifically probe the viral capsids on cell surface. The co-localization between A20 and Cy5 signal was examined by 3D microscopy as described above. In this scenario, A20 positive Cy5-AAV2 presents the virion on cell surface and A20 negative Cy5-AAV2 presents the virion inside the cells.

**Single particle tracking and analysis.** For fluorescence imaging, Hela cells were cultured in phenol red-free DMEM with 10% FBS in Petri dishes with poly (L-lysine)-coated

glass coverslips on the bottom. Before fluorescence experiments, cells were washed in serum-free, phenol red-free medium supplemented with 20mM HEPES (pH 8.0). The movement of Cy5-AAV2 particles was recorded by an Olympus IX-81 microscope equipped with Hammatsu Camera.

The trajectories of AAV particles were generated by the "cell" module in the IMARIS program. The location of each viral particle was computed as the centroid of the bright spot. The parameters (instantaneous speed, displacement, displacement length) of the viral trajectories were directly extracted from the program as following:

Instantaneous speed at time index *t*: $S(t) = \frac{\sqrt{D_x(t,t-1)^2 + D_y(t,t-1)^2}}{T(t) - T(t-1)}$ with $D_x(t_1,t_2) = P_x(t_1) - P_x(t_2)$; where $T(t)$ is time in seconds at time point *t*, $P_x(t)$ is x-position of particle at time index *t*.

Displacement of particles at time $\Delta t$ after initial time point $t_0$:

$$D^2(\Delta t) = D_x^2(t_0+\Delta t, t_0) + D_y^2(t_0+\Delta t, t_0)$$

Displacement length of a viral trajectory: $D(t_L, t_0) = \sqrt{D_x(t_L, t_0)^2 + D_y(t_L, t_0)^2}$ , where $t_L$ is the last time index of the trajectory.

MSD plot analysis was carried out as described previously (de Bruin et al. 2007; Akita et al. 2010). For each trajectory of an AAV particle, the MSD for each time interval was calculated by the following formula:

$$MSD(n \cdot \Delta t) = \frac{1}{N-n} \sum_{i=0}^{N-n-1} \left\{ [D_x(i \cdot \Delta t + n \cdot \Delta t, i \cdot \Delta t)]^2 + \left[ D_y(i \cdot \Delta t + n \cdot \Delta t, i \cdot \Delta t) \right]^2 \right\}$$

Where *N* is the total number of frames in the video, $\Delta t$ is the time interval between two successive frames, and *n* and *i* are positive integers.

**Transmission electron microscopy (TEM).** For negative staining of AAV2 and Nanogold-AAV2, viral particles in PBS were pipetted onto a glow-discharged copper grid. The grid was washed twice with water and then stained with 2% uranyl acetate. For visualizing Nanogold-AAV2 in cells, infected Hela cells were fixed at room temperature in 2% glutaraldehyde (in 0.15M sodium phosphate buffer, pH7.4) for 20-30 minutes, followed by 1hr in 1% OsO4. Silver enhancement was applied on the ultrathin sections. Electron microscopy images were taken with a LEO EM910 transmission electron microscope at various magnifications.

## Results

**Microtubule disruption impairs AAV2 transduction.** Microtubule (MT) network has been shown to be required for successful infection and replication of viruses, including CPV and BPV. To investigate the role of MTs on AAV's infection, we first examined whether MT disruption affects viral transduction. Recombinant AAV2 (rAAV2) carrying self-complementary GFP transgene cassette was used in reporter gene assays to evaluate the level of viral transduction. Self-complementary AAV2 (scAAV2) was designed to overcome the step of second strand synthesis of viral DNA for successful transduction (McCarty et al. 2001). AAV2 particles were incubated with cells at 4 $^{o}$C for about 40 minutes and unbound particles were then removed by washing before transferring cells to 37 $^{o}$C for subsequent viral events. This procedure is defined as "pulse infection" to synchronize viral infection, which was used in all experiments throughout this study. In this study, we used mean fluorescence intensity (MFI) reflecting the average number of GFP molecules per cell to measure the level of AAV2 transduction. To better understand the viral transduction profiles, videos were taken on an IX70 microscope to record the expression of the viral transgene GFP in real-time. Briefly, three hours after pulse infection with scAAV2-GFP, Hela cells were transferred to the microscope stage for live imaging up to 21hrs p.i.. Snapshots were taken from the videos at 3hrs, 6hrs, 8hrs, 12hrs, 16hrs, and 21hrs after infection (Fig.III-1A). The GFP expression by AAV2 can be detected as early as 6-8hrs p.i. in DMSO treated cells, but was only barely detectable at 8hrs p.i. in Nocodazole treated cells. The quantitative data on the GFP mean fluorescence intensity (MFI) agrees with such observation (Fig.III-1B). To test if Nocodazole reduces AAV transduction in a viral dose-dependent manner, different MOIs of AAV were used to pulse infect the Hela cells in the presence of Nocodazole or DMSO and

GFP expression were measured by flow cytometry. To exclude the potential effects of dead cells on the quantification, we washed the cells in each well three times with PBS before harvesting them for flow cytometry analysis to remove any floating or loosely attached cells (typically are dead ones). With this experiment procedure, we ensured that about 95% of the cells subject to flow cytometry analysis are viable (data not shown). The histogram in figure III-1C demonstrates that Nocodazole treatment before AAV inoculation reduced the viral transduction at all tested dosages from 80 vgs/cell to 10,000 vgs/cell (Fig.III-1C and III-2). There was no significant difference between pulse infections at 37 $^{o}$C and at 4 $^{o}$C on the reduction of viral transduction by Nocodazole treatment (Fig.III-1C and III-3).

Nocodazole induced MT disassembly could have reduced the viral transduction by impairing either the viral trafficking or the promoter activity of transgene cassette. To examine the potential effects of Nocodazole on the promoter activity of AAV transgene cassette, we measured the GFP expression from plasmid transfection of corresponding transgene cassette in AAV in the presence of DMSO or Nocodazole. Our data show that level of GFP expression from plasmid transfection in the Nocodazole treated cells is not significantly different from that in DMSO treated cells (Fig.III-4). This observation suggests that Nocodazole treatment does not alter the activity of promoter in transgene cassette, but instead, affects the AAV transduction most probably at the level of viral trafficking or processing. Importantly, the reduction of viral transduction was not limited to the Nocodazole treatment but also observed with other MT-disassembly drugs including colchicine and vinblastine (Fig.III-5). This result further demonstrates that it is MT disruption but not the side-effect of Nocodazole impairs the viral transduction.

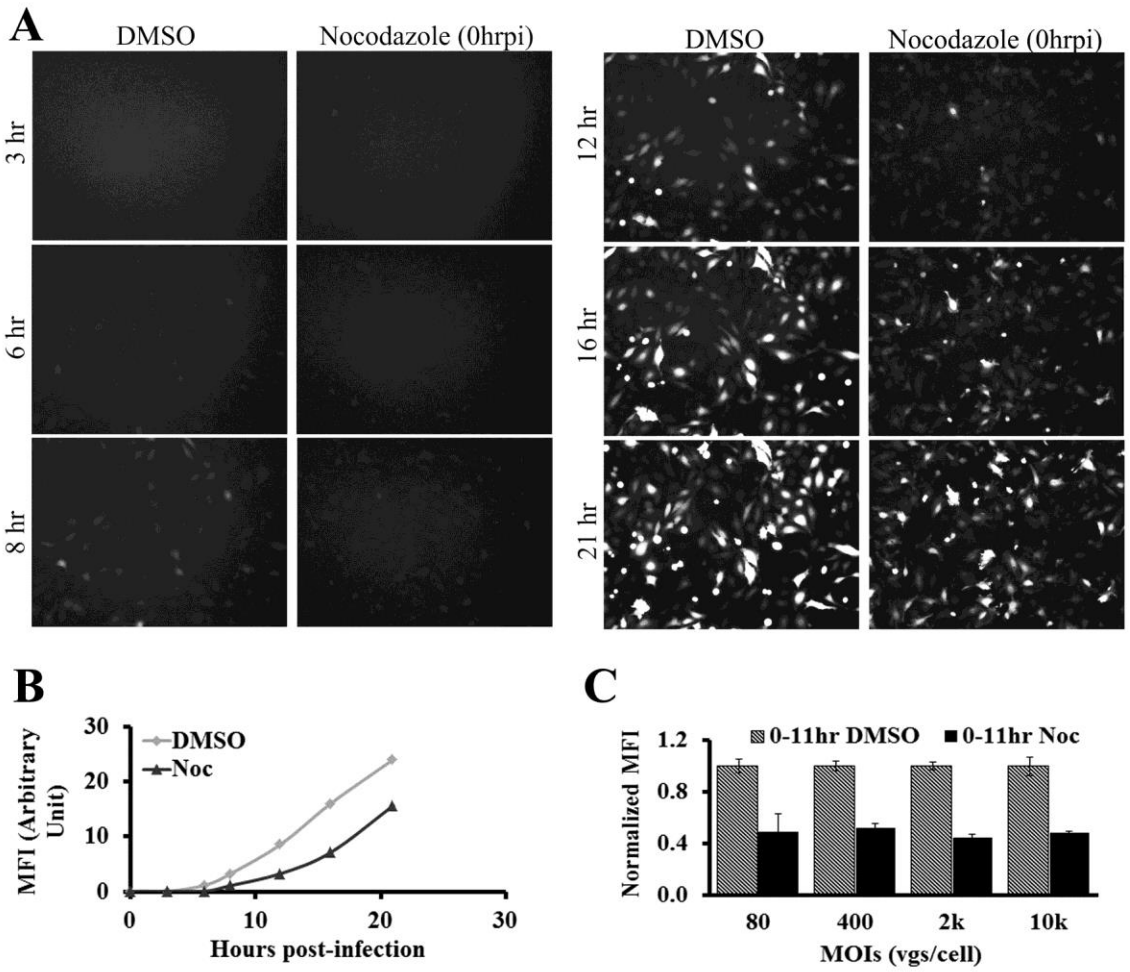


**Figure III-1. Microtubule disruption before viral inoculation reduces early AAV2 transduction.** At 30-60 min after pre-treatment with DMSO or Nocodazole, Hela cells were incubated with AAV2-CMV-GFPsc (scAAV2-GFP) particles at 4 $^{o}$C for 40 min and unbound virions were washed out before transferring Hela cells to 37 $^{o}$C ("pulse infection"). A video was taken of the GFP expression from 3hrs to 21hrs after pulse infection. A) Snapshots of the video were taken at 3, 6, 8, 12, 16, 21hrs p.i. B) Quantification of GFP fluorescence intensity in the snapshots by Image J. C) Hela cells were treated with DMSO or Nocodazole 30-60 min before pulse infection with scAAV2-GFP at different dosages (80, 400, 2000, 10000 vgs/cell). GFP expression was measured by flow cytometry at 11 hours p.i. and mean fluorescence intensity (MFI) was normalized to that of DMSO treatment. Normalized ratio of the percentage of GFP positive cells is shown in figure III-2.

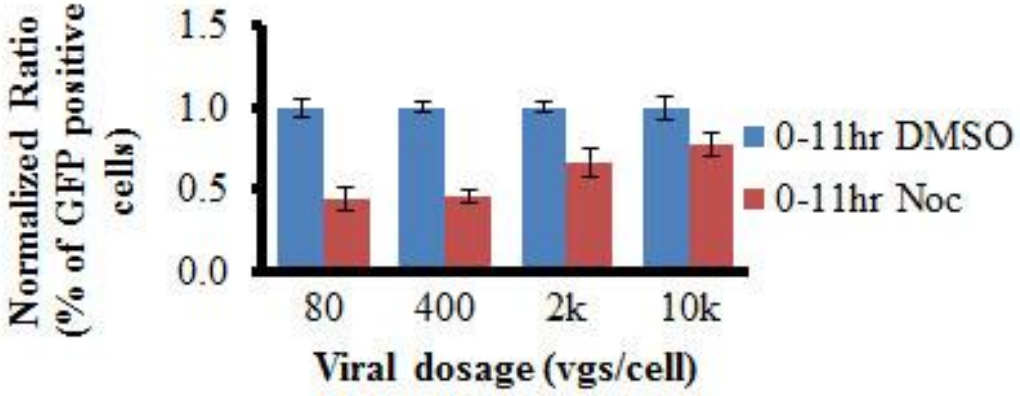


**Figure III-2. Normalized ratio of the percentage of GFP positive cells at various viral dosages** (80, 400, 2000, 10000 vgs/cell).

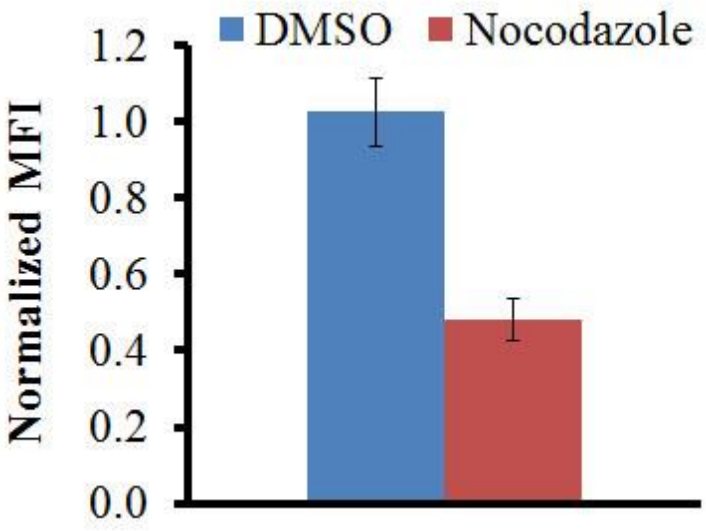


**Figure III-3. MT disruption by Nocodazole impaired viral transduction after the cells were pulse infected with AAV2 at 37 degree.** Histogram shows the normalized GFP MFI in the DMSO or Nocodazole treated cells.

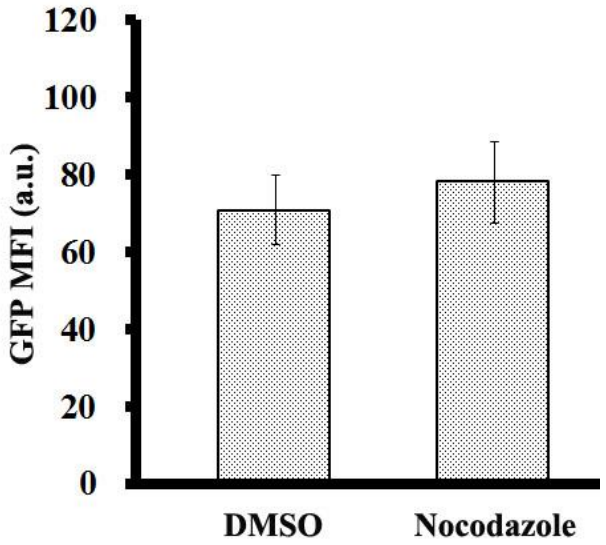


**Figure III-4. MT disruption by Nocodazole does not interfere with the activity of promoter in viral transgene cassette.** At 16-20hrs after transfected with Plasmid TR-CMV-GFP using Polyethyleneimine (PEI), Hela cells were treated with DMSO or Nocodazole. At 10-12hrs after drug treatments, cells were harvested for flow cytometry analysis to measure the GFP expression. The histogram shows that there were no significant difference on GFP expression between DMSO and Nocodazole treated cells.

**AAV2 attachment and internalization on the cell surface are not affected by MT disruption.** MTs have been previously demonstrated to be critical for clathrin-dynamin mediated viral entry as well as cytoplasmic trafficking of viruses (Van de Walle et al. 2001; Gilbert et al. 2004; Greber et al. 2006; Clemente et al. 2009). Here we examined whether intact MTs are required for the attachment and internalization of AAV2 particles on cell surface. Immediately after pulse infection, cells were harvested and subjected to viral genome extraction. The average number of viral genomes per cell was measured by quantitative PCR (Fig.III-6A). The histogram in figure III-6A shows that the amount of viral particles attached to the Nocodazole-treated cells is comparable to that of control cells, demonstrating that intact MT network is not required for cell surface binding of AAV2. To test if internalization of AAV2 particle was affected by the disruption of MTs, we employed both Cy5-AAV2 particles and a mouse monoclonal antibody A20, which can specifically recognize intact viral particles. For immunofluorescence on the cells with intact cell membrane before permeabilization, antibody will not be able to enter the cell and only probe the viral particles on cell surface. Under this scenario, Hela cells were pulse infected with Cy5-AAV2 and fixed with paraformaldehyde at 0hr or 1hr after infection. Without permeabilization, cells were probed with A20 antibody and co-localization between Cy5 and A20 signal were imaged with confocal microscopy (Fig.III-6B). Cy5 signal represents all the viral particles on cell surface and inside the cells, and A20 signal only highlight the viral particles on cell surface. As a result, A20 positive Cy5-AAV2 particles are on cell surface and A20 negative Cy5-AAV2 particles are internalized and inside the cells (Fig.III-6C). Maximum intensity projection (MIP) was applied to display 3D information of co-localization between A20 and Cy5 signal in 2D images (Fig.III-6B). Figure III-6B shows

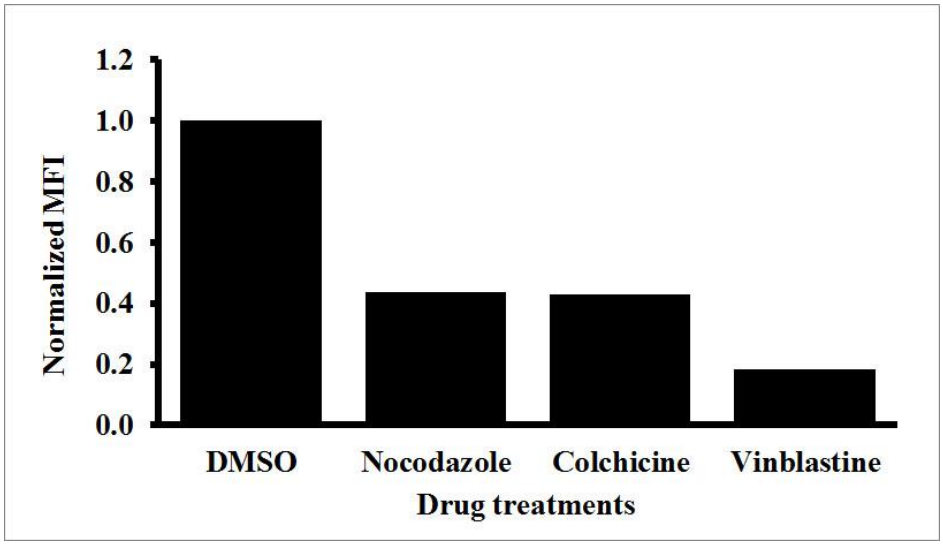


**Figure III-5. Various anti-microtubule drugs can impair AAV2 transduction.** At 1hr after treatment with various anti-microtubule drugs (Nocodazole, Colchicine, and Vinblastin), Hela cells were pulse infected with scAAV2-GFP at 2,000 vgs/cell. GFP expression was measured by flow cytometry at 10hrs p.i. and mean fluorescence intensity (MFI) was normalized to that of DMSO treatment. The histogram shows that all these anti-microtubule drugs can impair the viral transduction.

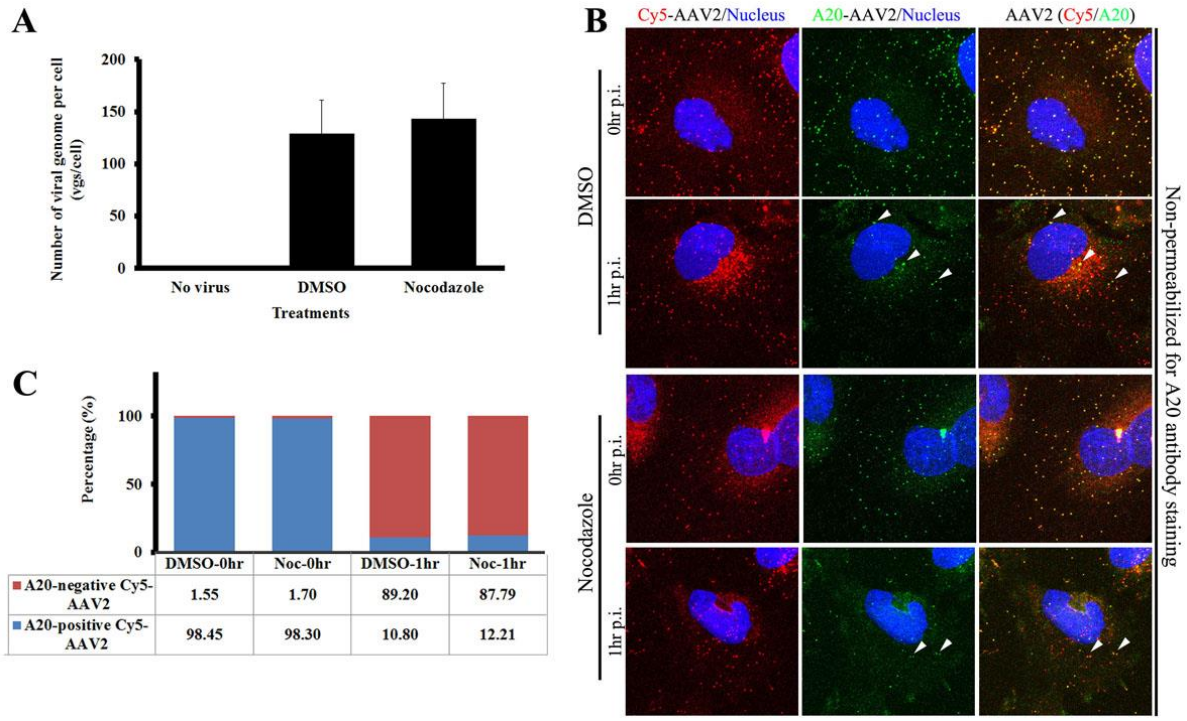


**Figure III-6. MT disruption does not impair the attachment and internalization of AAV2.** Hela cells were pre-incubated with DMSO or Nocodazole for 30-60 min before pulse infection of Cy5-AAV2. A) To determine the binding efficiency, cells were harvested at 0hr p.i. for viral genome extraction. The number of viral genomes per cell (vgs/cell) was determined by quantitative-PCR. B) and C) Cells were fixed at 0hr or 1hr p.i. without permeabilization. Nuclei were stained with DAPI (blue) and AAV2 capsids were stained with monoclonal antibody A20 (green). Before membrane permeabilization, A20 antibody is not able to access the viral particles inside of the cells and thus only binds to the un-internalized AAV2 virions (yellow in the merged figures). B) Representative images from maximum intensity projection (MIP) show the co-staining between A20 and Cy5 signal. Several representative un-internalized AAV2 particles are highlighted by arrowheads. C) Quantification of co-localization between Cy5 and A20 as a measurement of viral particles remaining on cell surface and those which have internalized.

that almost all Cy5-AAV2 particles were also stained with A20 antibody on both control and Nocodazole-treated cells at 0hr after infection, which is consistent with the fact that almost all viral particles should be on cell surface without internalization at 0hr p.i.. At 1hr p.i., majority of Cy5-AAV2 particles were not stained with A20 antibody and only about 12% of viral particles were stained with A20 in the Nocodazole treated cells, which is comparable to that in control cells (Fig.III-6B,C). These data determine that neither binding nor internalization of AAV2 particles on cell surface is dependent on intact MT network.

**MT disruption reduces the peri-nuclear accumulation and nuclear entry of AAV2.** Above results demonstrate that MT disruption before viral inoculation reduced the viral transduction by at least 2-fold and neither viral attachment nor internalization was impaired by Nocodazole treatment, suggesting the reduced transduction is more likely caused by the altered viral trafficking or processing (i.e. cytoplasmic trafficking, nuclear entry). For most DNA viruses, cytoplasmic trafficking from cell periphery to the peri-nuclear region is critical for the nuclear entry of viral components. As nuclear entry of AAV2 is known to be pre-requisite for successful viral transduction, we examined the efficiency of these events under Nocodazole or DMSO treatment. Here, we used Cy5-AAV2 particles generated by covalent labeling of purified AAV2 capsids with Cy5 fluorophores as described previously (Xiao et al. 2011). After pretreatment with Nocodazole or DMSO for 30-60min to allow fully disruption of MT by Nocodazole, Hela cells were pulse infected with Cy5-AAV2 and the localization of viral particles were examined at 2hrs p.i. using confocal fluorescence microscopy (Fig.III-7). Figure III-7A shows the representative distribution of AAV2 particles upon DMSO or Nocodazole treatment for 2hrs. To quantify such distribution, we used 3D quantitative microscopy as described previously (Xiao et al. 2011) and figure III-7B shows

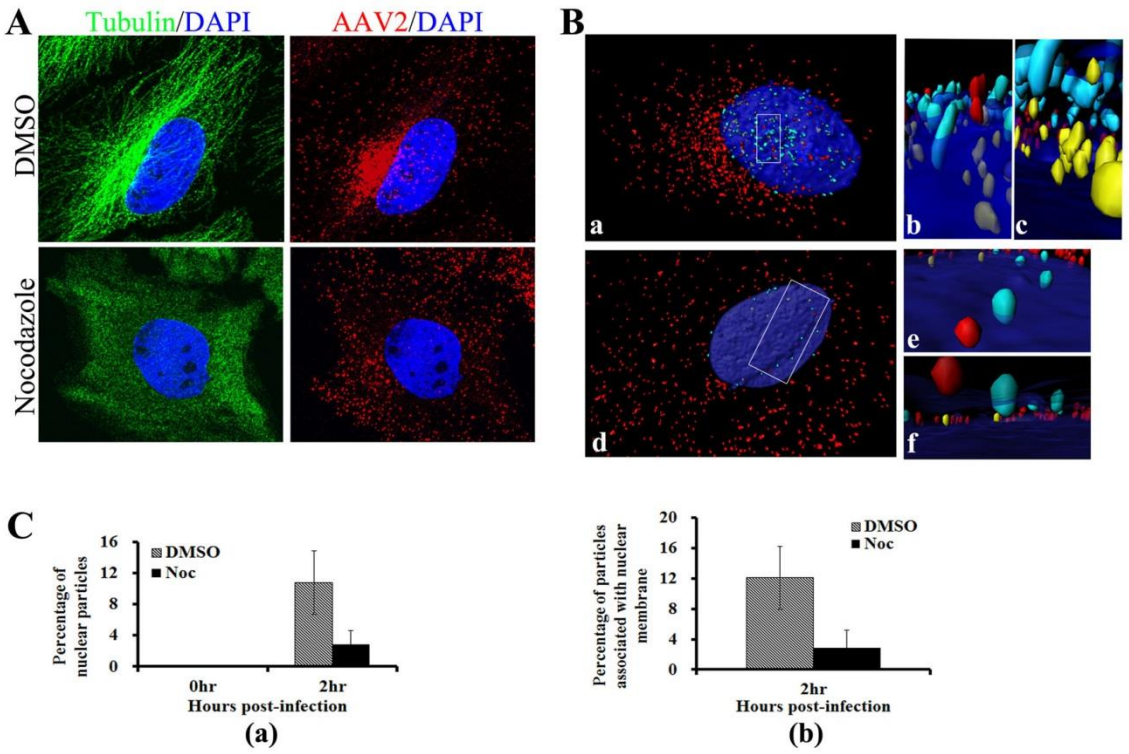


**Figure III-7. Early peri-nuclear accumulation and nuclear entry is reduced by the disruption of MT network.** Hela cells were pre-incubated with DMSO or Nocodazole 30-60 min before the pulse infection of Cy5-AAV2. Cells were fixed at 0hr or 2hrs p.i.. Nuclei were stained with DAPI (blue) and MTs were stained with alpha-tubulin antibody (green). A) Representative 2D images show the distribution of Cy5-AAV2 particles (red) at 2hrs p.i. in the cells treated with DMSO or Nocodazole. B) Representative images illustrate the quantification of viral distribution using 3D microscopy in the cells treated with DMSO (a-c) or Nocodazole (d-f) as described previously (Xiao et al. 2011). a and d are top views. b-f are magnified side views of insets in a and d. b and e are side views observed above the nucleus (nuclear envelope indicated by blue layer based on DAPI signal). c and f are side views observed inside the nucleus (between the top and bottom nuclear envelopes). AAV2 particles in cytoplasm are highlighted as red, these associated with nuclear envelope are cyan, and these inside the nucleus are yellow. More details about viral distribution in these cells are shown in supplemental videos S3 and S4. C) Histogram shows the percentages of AAV2 particles in the nuclei (a) and these associated with nuclear envelope (b) calculated from 15-20 cells in each group based on the quantification illustrated in B).

the representative images to illustrate the actual quantification by presenting the views from different angles of the 3D images (Fig.III-7B). The quantitative data are presented in figure III-7C. In DMSO treated cells, AAV2 particles were distributed normally: about half of intracellular particles localized at nuclear periphery, 10-15% in the nucleus (with 39 particles per nucleus on average) and remaining particles were in the cytoplasm (Fig.III-7B, C). In the cells where MTs were fully disrupted by Nocodazole, only about 3% of viral particles were in the nucleus (about 12 particles per nucleus on average) and remaining 97% particles were scattered across the cytoplasm (Fig.III-7B,C). In the aspect of nuclear targeting, viral particles seem to get lost in the cytoplasm and randomly localize in the Nocodazole-treated cells. It is known that the nuclear envelope is one of the cellular structures that AAV2 particles have to interact with before their nuclear entry. Figure III-7 clearly shows that a much smaller proportion of intracellular AAV2 virions localized at the peri-nuclear region in the Nocodazole-treated cells than that in DMSO-treated cells (Fig.III-7A, B). We then tested if reduced peri-nuclear localization of AAV2 has led to the reduced proportion of virions associated with nuclear membrane. Using the quantification method established previously (Xiao et al. 2011), we determined that only about 3% of AAV2 particles associated with nuclear membrane in the Nocodazole-treated cells compared to over 10% in the control cells (Fig.III-7C). This data suggest that the cytoplasmic trafficking from cell periphery to peri-nuclear region may facilitate the virus to interact with nuclear membrane. All of these data support a model where MT disruption reduces the proportions of AAV2 particles in the peri-nuclear and nuclear region, and thus reduces the viral transduction.

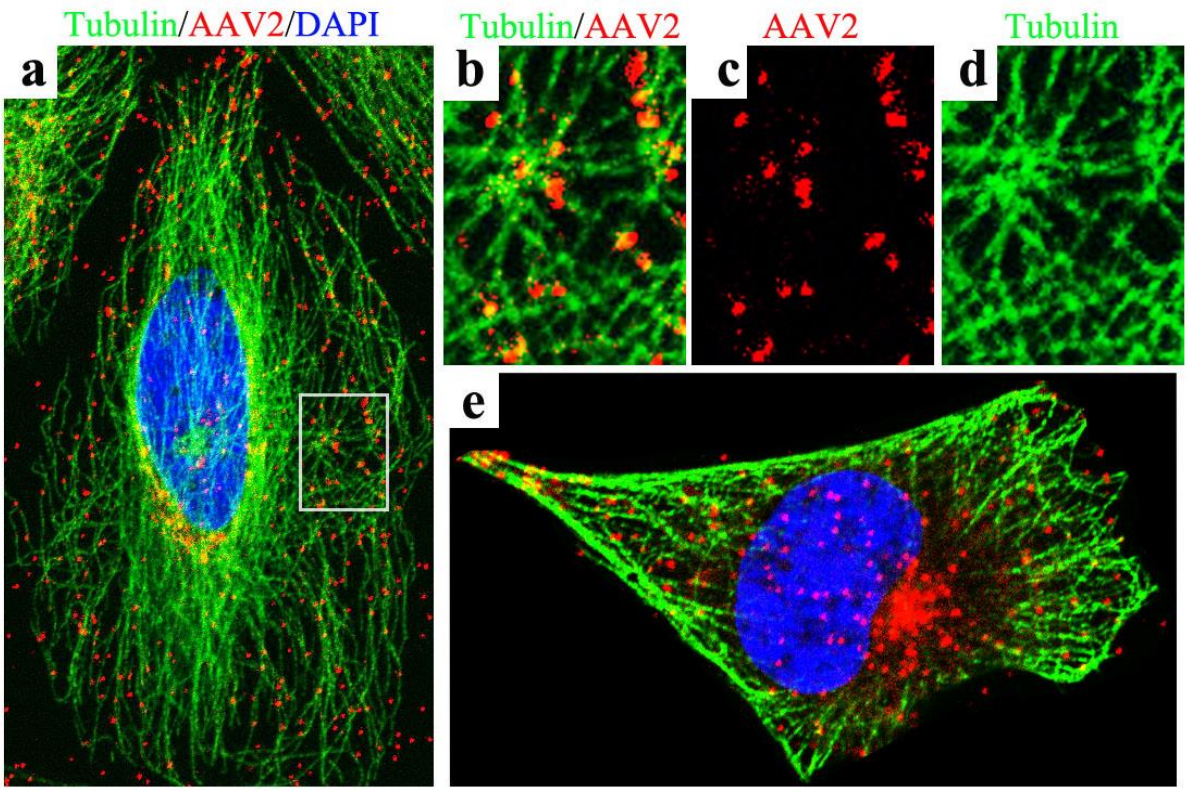


**Figure III-8. AAV2 co-localizes with MTs.** Cells were fixed at 30min (a-d) or 2hrs (e) after pulse infection with Cy5-AAV2. Nucleus was stained with DAPI (blue) and MTs were stained with alpha-tubulin antibody (green). The localization of Cy5-AAV2 (red) on MTs (green) is shown in a and e. b-d show the magnified view of the inset in a.

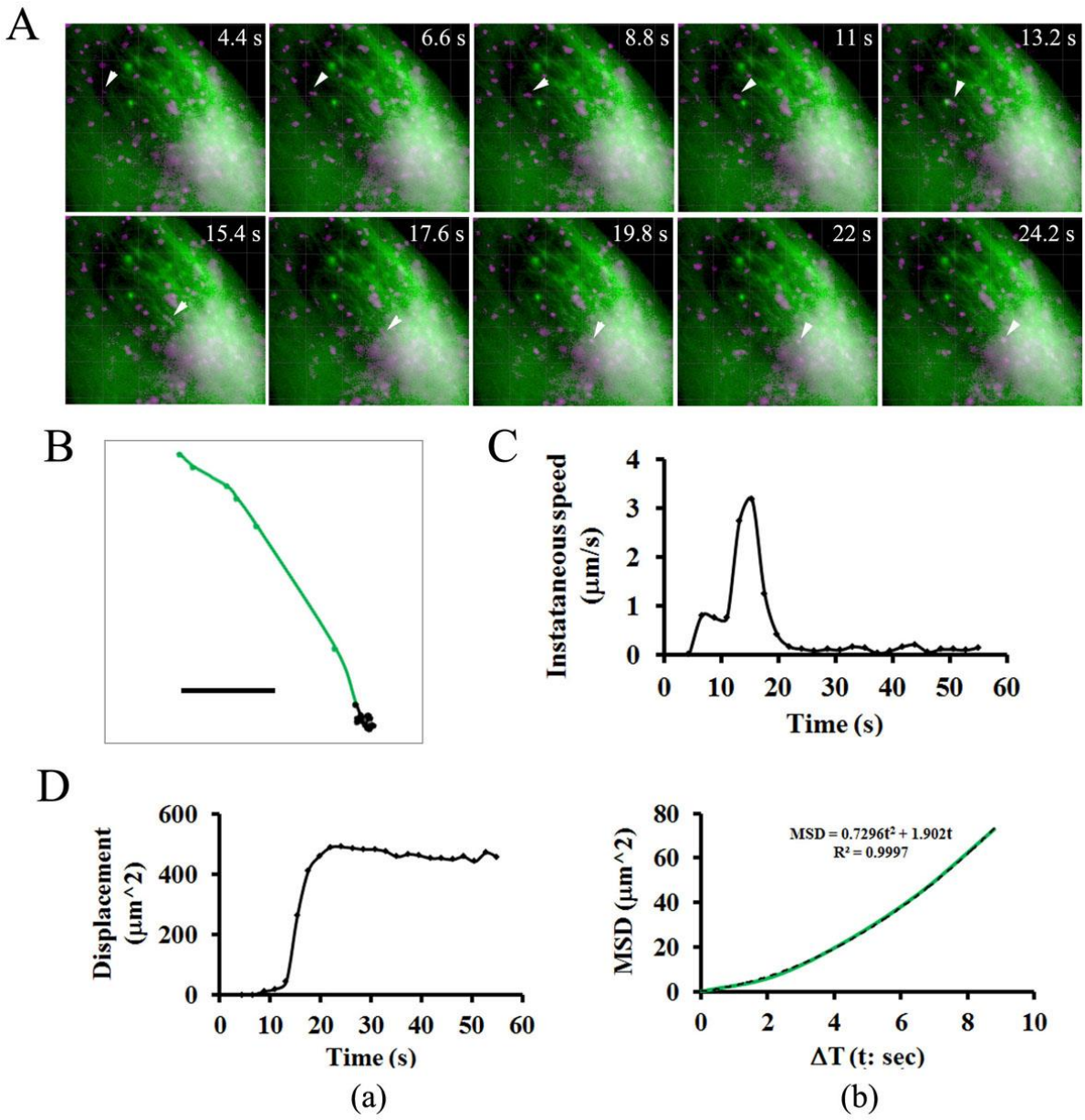


**Figure III-9. Fast and uni-directional movement of AAV2 towards the peri-nuclear region.** Videos were taken at 1hr after pulse infection of Cy5-AAV2 using Olympus IX81 inverted fluorescence microscope. A) snapshots of consecutive frames with 2.2s time interval shows the fast and directed movement of Cy5-AAV2 (purple and indicated by arrowheads) on microtubule (green) towards peri-nuclear region. B) Trajectory of Cy5-AAV2 particle indicated by arrowheads in A. Frames subject to the directional transport are shown as green points and lines, and those with confined motion in peri-nuclear region are indicated as black points Bar represents 5 μm. C) The instantaneous velocity of the particle (indicated by arrowheads in A) over time. D) The displacement from the starting position (a) and mean square displacement (MSD) (b) are plotted for the particle indicated by arrowheads in A. In (b), the plot between MSD and time interval (ΔT) is fitted by a quadratic curve (dotted line: $MSD = 0.7269t^2 + 1.902t$) with $R^2 = 0.9997$.

**AAV2 exploits MTs for rapid and uni-directional trafficking from cell periphery to peri-nuclear region.** The reduced peri-nuclear accumulation and nuclear entry are most likely caused by the impaired MT-mediated cytoplasmic trafficking as evidenced for other viruses (Sodeik et al. 1997; Leopold et al. 2000; Greber et al. 2006). To further investigate the potential role of MTs on AAV2 infection, we first examined the co-localization between virions and MTs in cells. At 30min or 2hrs after pulse infection with Cy5-AAV2, Hela cells were fixed with paraformaldehyde and MTs were probed with α-tubulin antibody. A confocal microscope was used to image the localization of AAV2 particles on MT filaments (Fig.III-8). At 30min p.i., the majority of AAV2 were localized on the MTs at cell periphery. At 2hrs p.i., about 30% of viral particles were localized on the MTs at cell periphery, about 50% of viral particles finished trafficking from cell periphery to the peri-nuclear region and over 10% of intracellular particles have entered nucleus (Fig.III-8 and (Xiao et al. 2011)).

Next, we tested whether the role of MTs during AAV infection works at the step of cytoplasmic trafficking from cell periphery to peri-nuclear region. To this end, single particle tracking (SPT) in live cells was used to study the trafficking of AAV2 in the cytoplasm. From the previous SPT studies for other viruses including Ad and influenza (Lakadamyali et al. 2003; Akita et al. 2010), it is known that cytoplasmic transportation is usually characterized by fast and directional movements on MT filaments. In our SPT experiments in the non-treated cells, Cy5-AAV2 particles displayed rapid and uni-directional movements from the cell periphery to the peri-nuclear region (Fig.III-9A, B). This is different from the bi-directional movement of Ad or HSV on MTs. Figure III-9A suggests that such directed motion is on the MT tracks. Consistent with previous studies about MT-mediated trafficking

(Lakadamyali et al. 2003), the Cy5-AAV2 particle migrated with instantaneous velocities at 1.5-3.5 μm/sec when moving from cell periphery to the peri-nuclear region (Fig.III-9C). This movement persisted for only 5-10 seconds (Fig.III-9C), and allowed for a large displacement between the initial and final position of the particle (Fig.III-9D-a). Mean square displacement (MSD) analysis was employed to verify that the observed motion of the Cy5-AAV2 particle is an active transportation event rather than passive diffusion of virion in the cytoplasm. MSD analysis is typically used to describe three types of particle motions: confined diffusion, normal diffusion, and directed motion (Fig.III-11B). Active transportation on MTs is one type of directed motion, which can be described by a quadratic dependence of MSD on time interval ΔT (Fig.III-11B). The MSD-ΔT plot of the viral particle indicated by arrowheads in figure III-9A can be fitted into a quadratic curve, demonstrating that the movement of this particle is directed motion and is consistent with dynein-mediated retrograde trafficking on MTs (Fig.III-9D-b).

**Rapid-directional motion of AAV2 particle is ablated by MT disruption.** To further investigate that such directed movement is mediated by MTs, we examined the viral trafficking in the presence of Nocodazole. Videos of viral trafficking were taken at 1-1.5 hours after pulse infection of Cy5-AAV2 particles at about 1 frame/second. Compared with control cells, directional movement was completely ablated in the Nocodazole-treated cells (Fig.III-10, III-11). Based on MSD plot analysis (Fig.III-11B), the directed movement of AAV2 particle indicated by quadratic curve was only observed in the control cells but not in Nocodazole-treated cells (Fig.III-11C). Both normal diffusion characterized by linear dependence of MSD on ΔT and confined diffusion indicated by

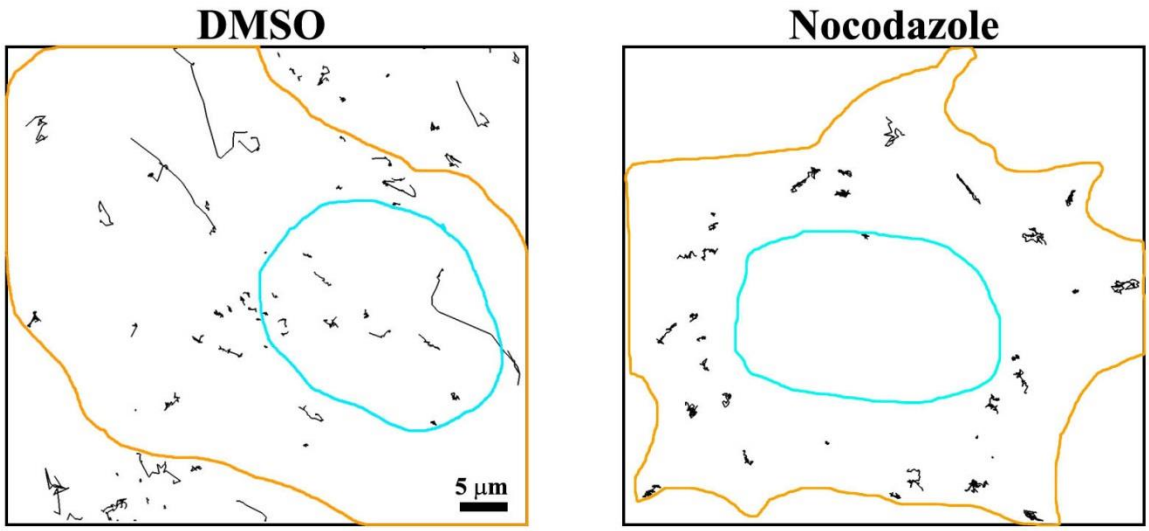


**Figure III-10. Trajectories of AAV2 trafficking.** Trajectories (black curves) were generated for the viral particles continuously tracked over 20 frames in the supplemental movies S6 and S7. Brown lines highlight the outline of cells and cyan line highlight the outline of the nucleus.

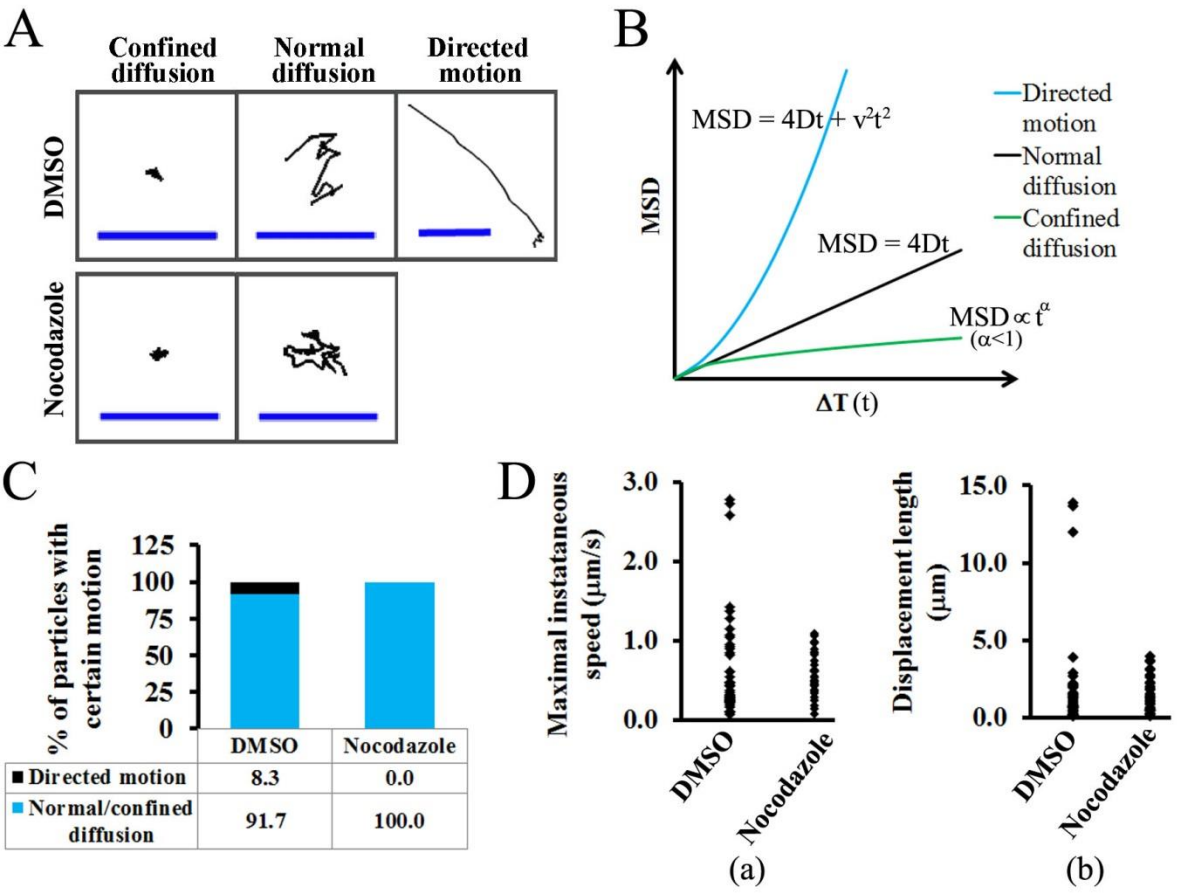


**Figure III-11. Fast and uni-directional movement of AAV2 particles is dependent on intact microtubules.** A) Representative trajectories for AAV2 in the DMSO or Nocodazole treated cells as shown in videos S6&S7. Bars represent 5 μm. B) Three simulated MSD plots for various types of particle motion. The mean square displacement (MSD) is plotted against time interval ΔT (*t*). Normal diffusion is usually described by a linear plot given by formula: $MSD = 4Dt$ (*D* is diffusion coefficient). Directed motion is usually described by a quadratic curve given by formula: $MSD = 4Dt + v^2t^2$ (*v* is mean velocity of the motion). An asymptotic behavior with $MSD \propto t^{\alpha}$ ($\alpha<1$) indicates confined diffusion. C) Histogram showing the proportions of viral particles with directed motion or diffusion from MSD analysis. D) The maximal instantaneous speed (a) and displacement length (b) of each AAV2 track. For C) and D), trajectories were generated only for these viral particles continuously tracked over 20 frames and about 40-60 trajectories were analyzed for each group.

asymptotic behavior of MSD on ΔT were not disrupted in the presence of Nocodazole. Particle motions with peak instantaneous velocities over 1.5 μm/sec were totally lost in the presence of Nocodazole (Fig.III-11D-a). Correspondingly, particles motions resulting in large displacement (> 10 μm) responsible for particle transportation from cell periphery to peri-nuclear region were also only observed in the control cells but not in the cells lack of intact MT network (Fig.III-11D-b). Above data demonstrate that rapid and uni-directional trafficking of AAV2 from cell periphery to peri-nuclear region requires intact MTs. Our data also suggest that intact MT network is unlikely to be involved in either confined or normal diffusions (Fig.III-11C).

**AAV2 migrates on MTs in the endosomes and the acidification of these structures is delayed by MT disruption.** After internalization through clathrin-dynamin mediated endocytosis, several DNA viruses including parvoviruses have to escape from the endosomes upon the acidification of these membraneous structures. It is known that Adenovirus (Ad) escape from the endosome in an early stage during infection (within 30min p.i.) before these particles migrate on MTs (Leopold et al. 1998; Leopold et al. 2000). In contrast, little is known about the timing of endosomal escape and MT-mediated trafficking of parvoviruses. Our electron microscopy data demonstrates that AAV2 particles were inside the endosomes when migrating on MTs (Fig.III-12A). This observation is the first one to show that AAV2 particles, distinct from Ads, usurp the MT-mediated endosomal trafficking for their nuclear targeting. It is also known that the maturation of endosomes takes place during their trafficking on MTs from the cell periphery to the peri-nuclear region, where most matured late endosomes with low pH locate (Vonderheit et al. 2005; Huotari et al. 2011). We used pharmacological studies to further test whether MTs mediated transportation

is required for the acidification of AAV-containing endosomes. Consistent with earlier report (Bartlett et al. 2000), chemicals (Bafilomycin and Chloroquine) that block endosomal acidification inhibited AAV transduction (Fig.III-12B-a). It was demonstrated previously that Adenovirus escapes from early endosome before migrating on MTs and its infection is not sensitive to the inhibition of endosomal acidification as early as 20-30 minutes after viral inoculation (Cassimeris et al. 1986; Leopold et al. 1998). Notably, our data demonstrate that the infection of most AAV2 particles was still sensitive to Bafilomycin and Chloroquine at 1hr p.i. and these reagents were still able to partially inhibit (20% of) the viral transduction even added at 2hrs p.i. (Fig.III-12B-a). This observation suggests that some post-entry trafficking events including MT-mediated migration are required for at least a subset, if not all, of the viral particles before endosomal acidification to allow their escape from the late-stage endosomes. In concert with this scenario, disruption of MTs delays the acidification of AAV-containing endosomes and viral escape as demonstrated by the data that administration of anti-MTs reagents (Nocodazole and Vinblastine) resulted in an increased inhibition on viral transduction by adding Chloroquine at 3hrs after pulse infection (Fig.III-12B-b). This is consistent with the earlier reports that AAV2 were routed to late endosomes for their infection (Douar et al. 2001; Ding et al. 2006; Xiao et al. 2011). These results suggest that AAV2 particles traffic on MTs in endosomes from the cell periphery to the peri-nuclear region, where acidification of these membraneous structures and viral escape take place.

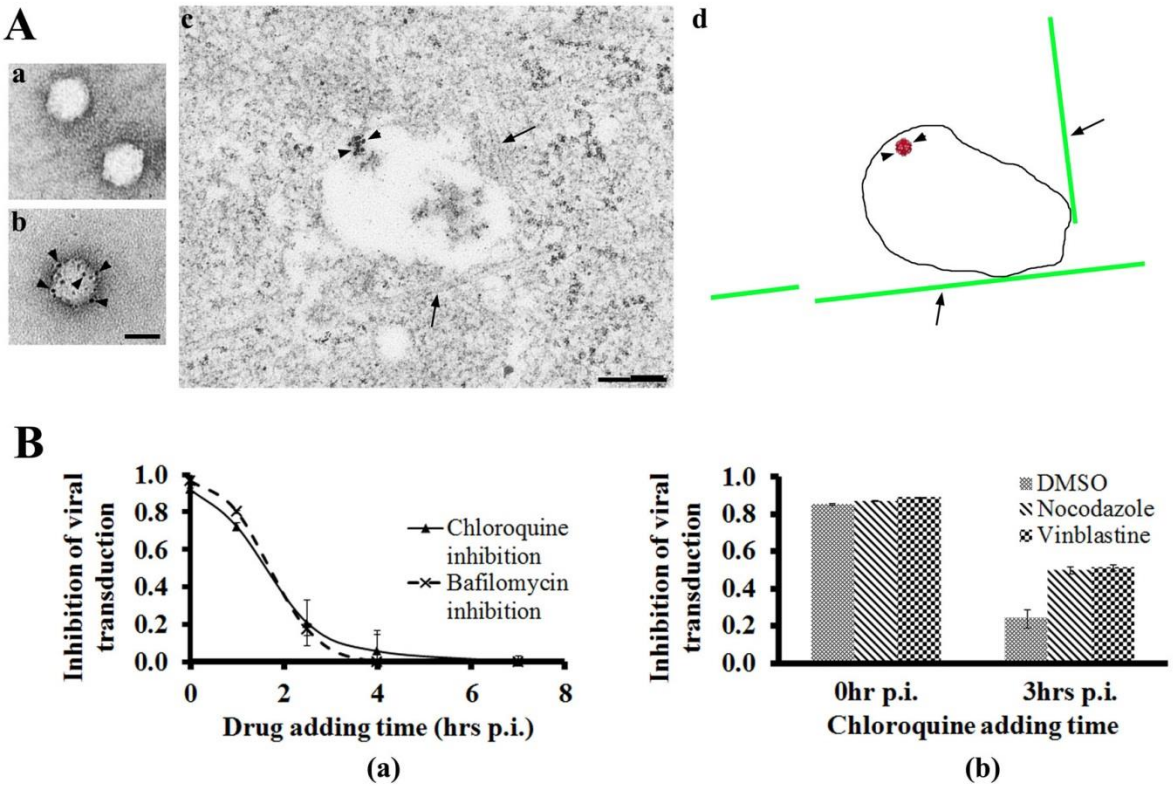


**Figure III-12. Association of AAV2-containing endosome with MTs and delayed endosomal acidification upon MTs disruption.** A) AAV2 particles migrate on MTs in membraneous structures. AAV2 particles before (a) and after (b) labeling of nano-gold were demonstrated by TEM. Bar represents 20nm. (c) Micrograph showing the direct association of AAV-containing endosome with MTs at 1hr after pulse infection of nano-gold labeled AAV2, which is simplified in a cartoon diagram. In the cartoon, MTs are indicated with green lines, endosome membrane is indicated by black line, and virus is in red. (d). Bar represents 200nm. B) Acidification of viral containing endosomes is inhibited by lysosomotropic chemicals at various time points after pulse infection of AAV2 (a). At 1hr after pretreated with anti-MTs drugs (Nocodazole and Vinblastine), Chloroquine was added at 0hr or 3hrs after pulse infection of AAV2. To calculate the inhibition of viral transduction, the expression level of transgene GFP was measured by a flow cytometer and normalized to corresponding treatments without Chloroquine (b).

## Discussion

Cytoplasmic trafficking is critical for most DNA viruses to approach the peri-nuclear region and deposit their genomic DNA in the nucleus of host cells. Previous studies have demonstrated that either actin filaments or microtubules (MTs) are exploited by various viruses to traverse the dense cytoplasm. For AAV, the exact mechanism of cytoplasmic trafficking of this virus remains unclear, due to previous reports that are diametrically opposite in their conclusions (Sanlioglu et al. 2000; Kelkar et al. 2006; Hirosue et al. 2007). Here we have studied the role of MTs on AAV2 transduction and extensively investigated the underlying mechanisms regarding how MTs contribute to viral infection using various pharmacological and microscopy tools. Our data from live cell imaging and flow cytometry analysis determined the involvement of MTs in AAV2 infection, and the data from quantitative 3D microscopy and quantitative PCR analysis demonstrated that intact MT network is required for the nuclear targeting of AAV but not for cell surface attachment or endocytosis of this virus. In the present study, for the first time we have determined that the migration of AAV2 on MT tracks are fast (up to 1.5-3.5 μm/s) which is consistent with dynein-mediated trafficking and are uni-directional which is different from the bi-directional motion of Ad or HSV on MTs. In addition, our study using electron microscopy and pharmacological experiments is the first one to suggest that AAV traffics on MTs in endosomes and acidification of these structures is dependent on intact MT network. The findings herein strongly support an as yet undocumented model in which after internalization, AAV2 exploits MTs for fast and uni-directional trafficking in endosomal compartments towards peri-nuclear region where most viral acidification events take place.

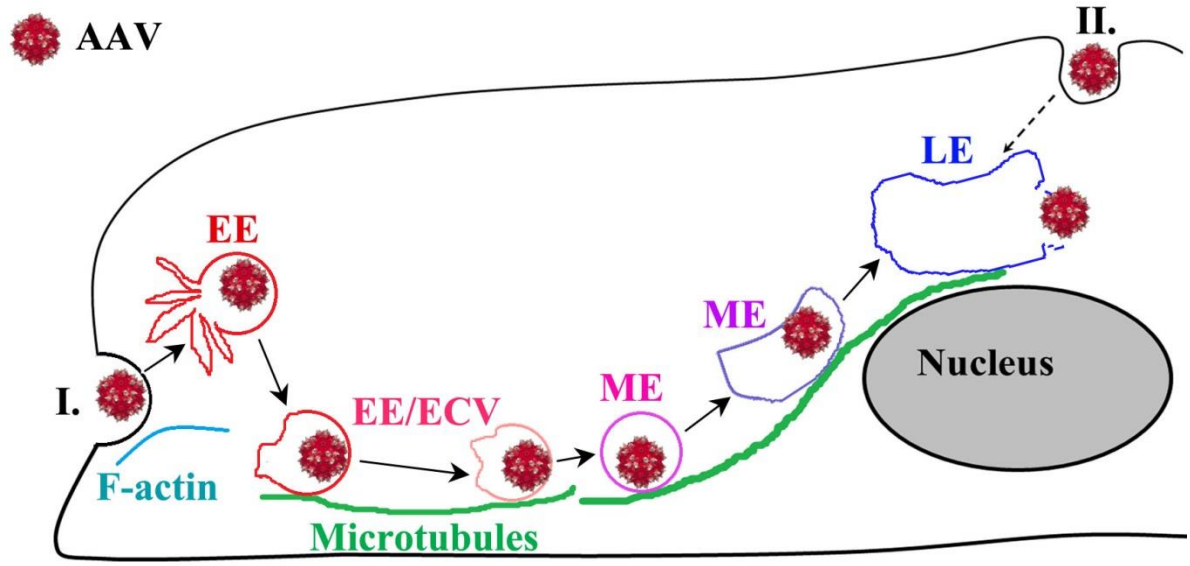


**Figure III-13. A model for the role of microtubules on the cytoplasmic trafficking and endosomal acidification for AAV2 escape.** After binding and endocytosis on cell surface, AAV2 virions may take two possible trafficking routes towards the nucleus. Route I: For these internalized at sites distal from the nucleus, virions migrate on MT tracks in endosomes to traverse the dense cytoplasm towards peri-nuclear region of host cells. Route II: For these internalized at sites close to the nucleus, virions in endocytic vesicles can reach the nucleus by slower MT-independent migration through the cytoplasm between the cytoplasmic membrane and nuclear envelope. For both routes, acidification of AAV2 containing endosomal compartment happens at the peri-nuclear region and allows the escape of viral particles from vesicles, a pre-requisite step for nuclear entry.

Furthermore, our data that MT disruption never completely blocks AAV2 transduction suggests the existence of an alternative MT-independent trafficking pathway for this virus. These data together with earlier studies support a model of AAV2 trafficking during its early infection procedure (Fig.III-13, (Sanlioglu et al. 2000; Douar et al. 2001; Ding et al. 2006; Johnson et al. 2010)).

Both DNA and RNA viruses hijack MTs to achieve productive infection in host cells. Several parvoviruses including CPV and BPV also have been shown to exploit MT network for their transduction (Suikkanen et al. 2003; Dudleenamjil et al. 2010). However, the role(s) of MTs on AAV infection remains controversial. To carefully examine the potential effect of MTs on AAV2 transduction, we employed live cell imaging to monitor the dynamics of transgene GFP expression in real-time as a measurement of successful viral transduction. In contrast to the non-treated cells where GFP fluorescence signal was readily visible as early as 6hrs p.i., GFP expression was much lower in the Nocodazole-treated cells and was barely detectable until 8hrs p.i. (Fig.III-1A). This result is further confirmed by the flow cytometry data that the expression level of transgene GFP is lower in MT disrupted cells compared with control cells (Fig.III-1B). These observations are consistent with the studies from Englehardt's group, supporting the involvement of MTs in AAV transduction (Sanlioglu et al. 2000). In contrast, a previous report concluded that intact MTs were not involved in AAV infection by measuring the percentage of GFP positive cells after inoculation of AAV-GFP (Hirosue et al. 2007). Interestingly, we also observed a similar proportion of GFP positive cells in both Nocodazole and DMSO treated cells with high viral loading (5k-10k vgs/cell), though GFP signal was much weaker in Nocodazole treated cells compared with control cells (Fig.III-1A, and Fig.III-2). It is known that only a few AAV2 particles in nucleus are needed

to turn a cell "green" (regardless how faint this "green" is) and thereby identified by flow cytometer as a "GFP positive cell" ((McCarty et al. 2001; Choi et al. 2005; Ding et al. 2006; Johnson et al. 2009) and data not shown). In addition, our quantitative microscopy data demonstrated that MT disruption only reduced the nuclear entry of AAV2 but didn't completely block this process (Fig.III-7). Under this scenario, it is expected that only a decreased level of GFP fluorescence intensity but not percentage of GFP positive cells will be observed if the reduced number of nuclear virions upon MT disruption is still high enough to turn a cell "green", which is particularly true when a high viral-dosage is used (Fig.III-1, III-2). As a result, GFP mean fluorescence intensity (MFI) is a more reliable measurement to assess AAV transduction in this study. Our data from multiple approaches including live cell imaging, flow cytometry analysis, and quantitative microscopy has strongly suggested that AAV particles exploit MT network during their infection. Additionally, MT disruption only reduced but not fully blocked viral transduction and nuclear entry, which suggests the existence of an alternative but slower trafficking route(s) in addition to MT network for AAV infection (Fig.III-13). And exploration of these potential alternative pathway(s) should shed light on the dynamics of AAV infection in various cell types.

It was previously documented that after disassembled by Nocodazole or cold temperature, MT network can recover to pre-drug level by either washing out the drug or rewarming the cells to 37 $^{o}$C within 10-20 minutes (Cassimeris et al. 1986). We also observed the full recovery of MT network from cold temperature at about 30 minutes after incubation at 37 $^{o}$C (data not shown). Given that the flow cytometry assay was carried out at 10-12hrs after pulse infection, the incubation of cells at 4 $^{o}$C for viral binding should have minimal effects on AAV2 transduction. Consistently, we did not observe significant

difference between pulse infections at 4 $^{o}$C and 37 $^{o}$C on the reduction of viral transduction by Nocodazole treatment (Fig.III-1, III-3). To exclude the potential effect of dead cells on the viral transduction measurement, we washed the cells in each well three times with PBS before harvesting them for flow cytometry analysis to remove any floating or loosely attached cells. In this study, about 95% of cells used for flow cytometry analysis were viable as demonstrated by multiple methods including Trypan blue exclusion or 7-AAD exclusion assays (data not shown). The results and conclusions presented in this study are not influenced by the technical concerns such as contribution of dead cell artifact.

To specifically study the cytoplasmic trafficking of viral particles after internalization, we carried out single particle tracking (SPT) experiments to trace virions at 1-1.5hrs (Fig.III-9) after infection. Besides technical considerations associated with single particle tracking experiments, 1-1.5hrs p.i. is the better time to image MT-mediated AAV2 trafficking for two reasons: first, at this time point, almost all AAV2 particles are internalized (Fig.III-6) and the observation of intracellular trafficking will not be confounded by the viral motions on cell surface typically happened at earlier time point; second, the location of MTOC can be readily visualized by the peri-nuclear accumulation of AAV particles, which will allow one to determine if the MT-mediated migration is towards or away from the peri-nuclear region. As observed in other SPT studies (Akita et al. 2010), our SPT data show that about 8% of viral particles displayed rapid and directional motions with instantaneous speed up to 1.5-3.5μm/s during our observation time in the normal cells. The remaining virions displayed either normal diffusion (Brownian motion) or confined diffusion, as an indication of movement of AAV in cytoplasm or actin filaments. As it takes about 2-4 hours for most virions to finish trafficking from cell periphery to peri-nuclear region (Fig.III-8), it is

expected to observe only a small subset of particles displaying rapid-directional movements on MTs (each event only persists for 5-10 second) in the limited time window (in the order of a minute) that we can trace the virions in the single particle tracking experiment. In addition, the live imaging only allows one to image a subset of viral particles on a certain focal plane in the cell and inevitably the investigator will lose track of other viral particles moving in the same cell at a different plane. Furthermore, fast-directional motion may be interrupted by temporary dissociation of viral particle from MT tracks or alternatively stalled motors (dynein for minus-end directed motion) (Tsai et al. 2000; Leopold et al. 2006). Under these experimental limitations, the "8%" from single particle tracking experiments does not precisely represent the portion of viral particles migrating on the MTs during the observation time, not along the entire viral trafficking period (several hours). Instead, this number is more to show the existence of MT-mediated fast and directional movements in the cells, when compared with the completely absence of such motion in MT disrupted cells. All and all, the window of observation that we utilized while short in duration supported the rapid and uni-directional movement of AAV particles only when MT were intact.

Interestingly, compared with control cells, AAV2 particles in a much smaller proportion were still detected in the nucleus of Nocodazole-treated cells (Fig.III-7). This is consistent with the observation in reporter gene (GFP) assay that AAV2 was still able to transduce cells in the presence of Nocodazole, though in a reduced level compared with control cells (Fig.III-1). One possibility for this observation is related to the inefficient MT-independent trafficking of virions. Under this scenario, AAV2 particles could be internalized in the cell membrane close to the nucleus, where the virions only have to traverse a small distance to reach the nucleus (Fig.III-13 and (Leopold et al. 2006)). Movements over such

short distance (several microns) might be achieved by normal diffusion. Internalization in the sites around nucleus can be achieved by the direct binding of viral particles at these sites or viral surfing on cell membrane to these sites (Neumann et al. 2008). Our studies do not excluded the possibility that AAV2 particles may reach the nucleus through a much slower process by exploiting actin filaments or intermediate filaments (Ohkawa et al. 2010; Schuh 2011). Although, it is not uncommon for viruses to exploit multiple pathways to ensure productive infection, we provide significant data to support the role of MTs whereas other putative pathways require further investigation. All these possible scenarios allow motions with lower velocity and/or directionality toward nucleus, and are supported by our observation that early AAV transduction was delayed in the presence of Nocodazole (Fig.III-1A, 23B).

It was also reported in an *in vitro* binding assay that cytoplasmic dynein can directly bind to AAV2 capsid (Kelkar et al. 2006). An interesting question is whether the rapid-directed motion of AAV2 is mediated by the dynein associated with endosomes or that directly associated with viral capsid. It is known that AAV2 is internalized through clathrin-dynamin mediated pathway into endosome compartments (Duan et al. 1999; Bartlett et al. 2000). While we were not able to definitively determine dynein interaction with AAV-containing endosome *vs* capsid specifically, our data strongly supports the usage of this motor in fast-directed movement of AAV. Interestingly, some dynactin subunits like p62 were demonstrated to have a minimal impact on dynein-mediated functions and suggested to be dispensable for the function of dynactin complex (Quintyne et al. 1999; Schroer 2004). More importantly, recent studies have begun to demonstrate that dynein can directly bind to the pathogen-related cargos and suggest that dynactin may be dispensable especially for the

dynein-mediated pathogen trafficking (Grieshaber et al. 2003; Schroer 2004; Bremner et al. 2009). Careful and sophisticated investigations will be required to address the issues regarding whether and how the dynactin complex contributes to the MT-mediated AAV2 trafficking.

It was interesting to note that AAV particles employed endosome for their transportation on MTs up to peri-nuclear region. We have employed electron microscopy analysis to determine that AAV2 particles are in the endosomal structures when migrating on MTs (Fig.III-12A). It is also known that acidification of endosomes is essential for escape of AAV2 from vesicle into cytoplasm (Bartlett et al. 2000; Douar et al. 2001). Our pharmacological study that MT disruption prolonged the sensitivity of AAV2 infection to Bafilomycin and Chloroquine strongly suggests that prompt acidification of AAV-containing endosomal compartment requires intact MTs (Fig.III-12B). These data altogether suggest an undescribed model for AAV in which after internalization, AAV2 rapidly and uni-directionally traffics on MTs in endosomes directly towards peri-nuclear sites where most viral acidification events happen. This model is in concert with the notion that most acidic endosomes are localized at peri-nuclear sites where viruses escape from these membraneous structures such as influenza (Mellman et al. 1986; Lakadamyali et al. 2003). This model is also consistent with the earlier observations that AAV2 are associated with late endosomes (Ding et al. 2006) and that viral mutants (VP3-only and HD/AN) lacking phospholipase activity can be transported to the peri-nuclear region indistinguishably from parental virions (data not shown and (Johnson et al. 2010)), but remain non-infectious. Interestingly, AAV's helper viruses like Ad and HSV are shown to exploit a different strategy. Instead of moving on MT in membraneous structures, both Ad and HSV have to escape from the endosomes

before trafficking on MTs, which is consistent with their direct interaction with both minus-end-directed and plus-end-directed MT motor proteins, allowing the bi-directional motions documented for both Ad and HSV on these filaments (Dodding et al. 2011; Engelke et al. 2011; Radtke et al. 2011). Typically, the infection of these viruses is not sensitive to the inhibition of endosomal acidification by Bafilomycin or Chloroquine as early as 20-30 minutes after viral inoculation (Greber et al. 1993). In contrast, AAV particles apparently traffic uni-directionally on MTs determined by the interaction between the viral containing endosomes and dynein motors (Lakadamyali et al. 2003). Our data that the majority of AAV2 were still sensitive to both Bafilomycin and Chloroquine at 1hr p.i. implies that a more acidic environment is required for the exposure of Vp1 on viral capsid as well as the viral escape from these membranous structures (Mellman et al. 1986), compared with the early escape of Ad and HSV from endosomes at cell periphery (Sodeik et al. 1997; Leopold et al. 1998; Snyder et al. 2006). This result is consistent with the early notions that multiple viral components including Vp1 and Basic Regions on capsid have to externalize in the endosomes (Sonntag et al. 2006). The observation that, 80% of AAV2 was insensitive to Bafilomycin and Chloroquine treatments at 2hr p.i., indicates that most virions have accomplished all these viral events requiring endosomal acidification, and even may have escaped from the late endosomes. These studies altogether suggest that the rapid-directed motion of AAV2 happens when the viral particles are still inside the endosomes. It should be noted that our data does not exclude the possibility that some AAV2 can escape from the early endosome as an alternative pathway in the cells. Given that cytoplasmic dynein can directly bind to AAV2 capsid *in vitro* (Kelkar et al. 2006; Zhao et al. 2006), it will be of particular interest in the future to identify and mutate the dynein binding sites on AAV2

capsid and further investigate the trafficking of these mutant capsids. Furthermore, understanding the next steps of viral entry (i.e. nuclear entry transition from the peri-nuclear region) may shed critical insights into mechanism that can be exploited for more efficient vector transduction.

The findings reported herein show that microtubule-dependent transport plays an essential role in the viral transduction, especially the early onset of transgene expression. Importantly, the data in this study strongly support an as yet undocumented model in which after internalization, AAV2 exploits fast and uni-directional transportation on MTs in endosomes directly toward the peri-nuclear region where acidification of most AAV-containing endosomal compartments happen. Validating trafficking pathways *in vivo* (Xiao et al. 2011) should allow the research community to enhance the performance of viral vectors by manipulating intracellular events as documented in the *in vitro* studies.

# CHAPTER 4

# PERINUCLEAR RETENTION LIMITS THE INFECTION OF BOTH ENVELOPED AND NON-ENVELOPED VIRUSES


## Summary

Cells have several barriers to restrict viral infection including the plasma membrane, dense cytoplasm, and nuclear envelope. Perinuclear retention of viral particles is a common, but poorly understood, phenomenon observed during the infection of many viruses including Ad, HIV, and parvoviruses. We used the transduction of several recombinant viruses (rAAV, rAd, lentivirus) to test whether perinuclear accumulation acts as a barrier to limit viral infection. Similarly to Ad and HIV, we first demonstrated that parvovirus AAV's perinuclear localization is maintained by microtubules at the microtubule-organization center (MT-MTOC). Disruption of this structure after viral entry led to increased susceptibility to infection of rAAV, rAd, and lentivirus. Using AAV as a model to study the underlying mechanisms, fluorescent microscopy and molecular analyses suggest that the proportion of viral particles entering the nucleus increased following MT-MTOC disruption and that this enhancement was dependent on the AAV capsid's nuclear import signals, indicating the involvement of a nuclear trafficking pathway. Interestingly, after knocking down RhoA or inhibiting its downstream effectors (ROCK and Actin), MT-MTOC disruption did not increase viral transduction or nuclear entry. These data suggest that enhancement of infection

is the result of two consecutive steps: 1) release of viral particles from the perinuclear site upon MT-MTOC disruption, and 2) increased trafficking to the nucleus via the RhoA-ROCK-Actin pathway. We extended the AAV studies *in vivo* and observed that viral transduction of brain, liver, and xenografted tumor tissues was enhanced up to 10-fold by disruption of the MT-MTOC, indicating a similar trafficking mechanism *in vivo*. In summary, this study for the first time experimentally demonstrates that perinuclear accumulation of incoming virions at the MT-MTOC is a barrier limiting infection of most nuclear viruses and more specifically restricting the nuclear entry of AAV, defining a novel defense mechanism by which host cells restrain viral invasion.

## Introduction

Cells have many structures and machineries to protect themselves from exogenous infectious agents (e.g. viruses, bacteria etc.). For example, the plasma membrane is the first structure to restrict viral infection, and molecularly dense cytoplasm and the nuclear envelope sever as additional barriers for viruses to reach their replication sites. As a consequence, viruses have to overcome these cellular barriers in host cells before delivering their genome to the target region for successful infection. Comprehensive knowledge in these barriers and virus-host interactions are critical to improve our understanding of basic virology and viral pathogenesis. Both strengthening these cellular barriers and weakening the viral capacity to penetrate these barriers present potentially powerful means for inhibition of viral infection. On the other hand, attenuating these barriers or designing capsid with enhanced ability to penetrate these barriers will offer promising opportunities to improve current vectors for gene therapy.

The Microtubule-Organization-Center (MTOC) is a subcellular structure at perinuclear region, from which microtubules (MTs) are nucleated to form a radial filamentous network with minus ends anchored at MTOC and plus end reaching cell surface area. Due to these features, MTs and MTOC coordinate, as a trafficking center, the transport of intracellular molecules and organelles between the perinuclear region and other areas of a cell. For instance, intact MTs are required for the nuclear import of several transcription factors (e.g. p53, NF-kB, pRb) and on other hand, these structures are required to sequester other proteins (e.g. c-myc, MIZ-1, smad3) in the cytoplasm to block their nuclear entry (Giannakakou et al. 2000; Niklinski et al. 2000; Ziegelbauer et al. 2001; Roth et al. 2007;

Gong et al. 2011). Numerous studies have also shown that cellular misfolded proteins are transported on the MTs towards MTOC region, where these misfolded proteins are sequestered or degraded by proteasomes and lysosomes at this region (Garcia-Mata et al. 2002; Wileman 2007).

Strikingly, during the early stage of infection, many incoming viruses are also delivered to and retained at a perinuclear site after entering the cells (Sodeik et al. 1997; Dohner et al. 2002; Suikkanen et al. 2002; Mani et al. 2006; Yea et al. 2007; Boisvert et al. 2010; Liu et al. 2012). This perinuclear site has been suggested to be co-localized with the MTOC region and as observed for cellular proteins, transport of these viruses is facilitated by dynein motors and transport along MTs (Fackler et al. 2006; Greber et al. 2006; Wileman 2007). Although this perinuclear retention of incoming virions seems to be a common phenomenon among many viruses, especially those that enter the nucleus, it remains unknown whether this accumulation is beneficial or inhibitory to viral infection (Wileman 2007). Previous studies have shown that several viruses including rotavirus, vaccina and HSV disrupt MTOC during early infection stage for reasons that have not been identified (Avitabile et al. 1995; Ploubidou et al. 2000; Schepis et al. 2006; Liu et al. 2010; Martin et al. 2010). Despite the lack of understanding of the role of such perinuclear retention on viral infection, these observations raise an intriguing hypothesis that MTOC region serves as a subcellular barrier to restrict access of the incoming virions to their replication site (nucleus in this study) during the early stage of viral infection.

On the other hand, during late infection stage, several viruses including HIV, HSV, poliovirus, and norovirus have been suggested to exploit this perinuclear accumulation to concentrate newly synthesized viral components through MTs to facilitate late infection

events including virion replication, assembly, or egress (Sfakianos et al. 2003; Nozawa et al. 2004; Taylor et al. 2009; Hyde et al. 2012). Classical virology assays usually study replication-competent viruses and measure the production of viral progeny as the readout, which is the sum of the total effects of all events in viral infection with these viruses. Given the potential involvement of MTs and MTOC throughout the entire viral infection, this method is unable to precisely dissect the perinuclear retention of incoming virions during early infection stage. Furthermore, viral replication and newly synthesized viral proteins will also confound virion distribution assays which use antibodies (Suikkanen et al. 2002; Boisvert et al. 2010).

Recombinant viruses used as gene therapy vectors (designated as viral vectors) are purposely designed to only exploit the early infection steps including delivering and expressing viral genomes and are deficient in late infection events including viral replication and assembly due to the deletion of critical viral proteins (Xiao et al. 2012). As a result, these viral vectors allow researchers to more precisely separate the early infection steps from the late events, offering a promising opportunity to specifically identify the mechanisms and roles of perinuclear retention on incoming virions. Adeno-associated virus (AAV) is a member in the family *Parvoviridae* and its recombinant form (rAAV) is currently used as a gene therapy vector due to many desirable traits in gene delivery (Xiao et al. 2012). As a gene therapy vector, rAAV does not contain any viral DNA except for two internal repeats (ITR) flanking the exogenous transgene (Xiao et al. 2012). Therefore, rAAV only delivers and expresses transgenes in cells but is incapable of replicating and producing viral progeny. This attribute makes rAAV a useful model to specifically investigate virus-host interplay during the early stage of viral infection. Like many other viruses, its trafficking pathway

typically starts with receptor-mediated endocytosis for cell entry, followed by cytoplasmic trafficking assisted by the endosomal routing system and MT network, and ends with nuclear entry and uncoating for successful transduction (Wang et al. 2011; Nonnenmacher et al. 2012; Xiao et al. 2012).

In this study, we have employed several recombinant viral vectors to investigate the role of perinuclear retention on the infection of both enveloped and non-enveloped viruses, and have further explored the detailed mechanism using Adeno-associated virus (AAV) as a model system. A sensitive and reliable fluorescence imaging platform allowed us to examine viral trafficking in detail over time that has led us to the observation that the majority of viral particles finished cytoplasmic trafficking and localized at perinuclear region by 6-8 hours post infection (p.i.). Manipulating host cells and viral particles using pharmacological interventions around 6-8 hours p.i. allowed us to efficiently investigate the underlying mechanism of perinuclear retention as well as the corresponding impact on viral infection.

## Materials and Methods

**AAV2 production, purification and labeling.** HEK-293 cells were used to produce AAV2 as described previously (Grieger et al. 2006). Briefly, cells were transfected with three plasmids: pXR2 (wt or with BR mutations), pXX680, and a plasmid containing the reporter transgene (GFP or Luciferase) flanked by two ITRs. At 60hrs after transfection, cells were collected and nuclei were isolated using hypotonic buffer and Kontes homogenizer. AAV2 particles were recovered by resuspending the nuclear pellet in PBS with 0.5% Deoxycholate (DOC) and then sonicating for 1min. Highly pure virus was then retrieved as described previously (Xiao et al. 2012). Briefly, after DNase treatment, the virus suspension was subjected to one round of cesium chloride (CsCl) step gradient density fractionation and another round of fractionation using a continuous CsCl gradient. Determination of peak viral fractions, dialysis of virus, and measurement of viral titers by quantitative PCR (qPCR) were performed as previously described. The infectivity of AAV was determined to be approximately 1 transducing unit per 100 particles.

AAV2 was covalently labeled with the Cy5 fluorophores as described in manufacture's protocol with slight modification. Briefly, purified AAV2 were incubated for 2hr at 4℃ in PBS with a 20-fold molar excess of Mono-NHS-Cy5 (GE Healthcare) over capsid protein units. Free dyes were removed from labeled viral particles by dialysis against PBS containing 5% sorbitol and viral solutions were stored at -80℃ as small aliquots. Labeled viral titers were determined by both dot blot (Grieger et al. 2006) and qPCR. Infectivity of the viral particles was determined by GFP reporter gene assay.

**Cell culture, viral infection, and drug treatment.** All cells (American Type Culture Collection) were grown in Dulbecco's modified Eagle medium (DMEM, Invitrogen) with 10% FBS in 5% CO2 incubator. Cells were passaged every 2-3 days for up to ten passages, when new aliquots of frozen cells were recovered from liquid nitrogen.

For pulse infection, cells were seeded on 12-mm glass coverslips at 24hrs before infection. The next day, after incubation in DMEM containing 20mM HEPES at 4℃ for 5min, cells were inoculated with Cy5-AAV2 (~5,000 vgs/cell), non-labeled AAV2 (~1,000-5,000 vgs/cell), recombinant Adenovirus (~20 pfu/cell), or lentivirus (~10 pfu/cell) at 4℃ for another 40min. Cells were then washed with PBS to remove unbound virions and transferred to a 37℃ incubator (regarded as 0hr p.i.). Pharmacological drugs were added at 6-8hrs after pulse infection unless otherwise indicated. The concentrations of drugs were: 30μM Nocodazole, 25μM Colchcine, 10μM Taxol, 10μM Rhizoxin, 10μM Maytansine, 2μM MG132, 20μM ALLN, 10μM H1152, and 10μM Cytochalasin D. The drugs were maintained in the culture for approximately 3 hours unless otherwise indicated.

**Flow cytometry and Immunofluorescence.** To evaluate viral transduction, flow cytometry analysis was used to measure the mean fluorescence intensity (MFI) of GFP expression. To exclude the potential effect of dead cells on the viral transduction measurement, we washed the cells in each well three times with PBS before harvesting for flow cytometry analysis, removing any floating or loosely attached cells. Either Trypan blue exclusion or 7-AAD exclusion assays was used to assure that most cells (~ 95%) used for flow cytometry analysis were viable.

For immunofluorescence, cells were washed with PBS and then fixed with 4% paraformaldehyde (PFA) for 15min at room temperature (RT). The cells were then

permeabilized with 0.2% Triton X-100 in PBS for 5min at RT. After blocking with immunofluorescence buffer (IFB) (5% normal goat serum in PBS containing 0.05% Tween-20) for 1hr at RT, the cells were incubated with primary antibody to detect tubulin (Ab6161, Rat monoclonal from Abcam Inc.), Golgi (Ab24586, Mouse monoclonal from Abcam Inc.) and/or AAV capsid (A20 mouse monoclonal antibody) diluted in 50% IFB for overnight at 4℃. The cells were then incubated with secondary antibody, diluted 1:2,000 in 50% IFB (anti-mouse Alexa-Fluor 488 [Molecular Probes]), for 1hr at RT. After six washes with PBS, coverslips were mounted cell side down on glass slides with mounting medium (Prolong Antifade Gold with DAPI [4',6'- diamidino-2-phenylindole]; Molecular Probes). After images were acquired using confocal microscopy, the existence of perinuclear accumulation in a cell in each image was examined by human eyes.

**Nuclear isolation and viral genome quantification.** Nuclei were isolated from cell fractionations as previously described (Grieger et al. 2006), with minor modifications allowing for viral infection. After incubation with AAV and drugs, cells were washed three times with ice-cold PBS and harvested by centrifugation at 500g for 10 min. The cell pellet was divided into two aliquots: one for direct viral genome extraction and the other for nuclei isolation. One aliquot was resuspended in hypotonic buffer and homogenized on ice using a Kontes homogenizer to the point where ~90% of cells were broken with nuclei remaining intact. The homogenate was spun at 500g for 10 min to separate the nuclei from the cytoplasmic components. The purity of nuclear fraction was assured by phase-contrast microscopy and immunoblotting using anti-tubulin and anti-lamin A/C antibodies.

AAV genomes were recovered from both whole cells and nuclear fraction using DNeasy Blood and Tissue Kit (Qiagen Inc.) according to the manufacturer's protocol. The

copy number of AAV genomes was determined by qPCR on a LightCycler 480 using Sybr green (Roche) as described for viral titering (Grieger et al. 2006).

**Animal studies.** Housing and handling of the BALB/c mice and SCID mice used in the current study were carried out in compliance with National Institutes of Health guidelines and approved by the IACUC at the University of North Carolina-Chapel Hill. To grow xenografted breast cancer tumors, 10^6 ~10^7 MDA-231 breast cancer cells were injected into the mammary fat pad of SCID mice. When the tumor size was about 0.5cm in diameter, the mice were used for intratumoral injection. Recombinant AAV2 vectors packaging luciferase or GFP transgenes were administered through the intravenous route (2e+10vgs into tail vein) in a volume of 200µl PBS or the intratumoral route (1e+10vgs). DMSO or Nocodazole (2mg/kg) were administered via intraperitoneal or intratumoral injection at about 10-12hrs after viral injection. Bioluminescence from luciferase expression was visualized by using a Xenogen IVIS100 imaging system (Caliper Lifesciences) after intraperitoneal injection of luciferin substrate (120 mg/kg of body weight; Nanolight). Image acquisition and analysis were carried out by using Living Image software. Quantitative data are based on values from 3-4 mice per group.

For vector infusions into mouse brain, animals were anesthetized with isoflurane and placed into a stereotaxic frame. Using a 32-gauge stainless steel injector and a Fisher Scientific infusion pump, mice received 1µl per hemisphere (total of 5e+08vgs) into the striatum over 15 min. The injector was left in place for 3 min after infusion to allow diffusion from the site of injection.

To image viral trafficking in mouse tissues, Cy5-AAV2 was administrated through intra-brain, intra-hepatic, or intratumoral routes. DMSO or Nocodazole were administrated

through the intraperitoneal route at about 12hrs after viral inoculation. At 1hr or 12hrs after vector injection or 4-6hrs after Nocodazole injection (16-18hrs after viral injection), animals received an overdose of pentobarbital (100 mg/kg intraperitoneally) and were perfused transcardially with ice-cold 100 mM sodium PBS (pH 7.4), followed by 4% paraformaldehyde in phosphate buffer (PB) (pH 7.4). After tissues were post-fixed for 24hrs at 4℃ in paraformaldehyde (Xiao et al. 2011), 10-20 μm coronal sections were cut using a cryosection microtome and then the slides were directly sealed with mounting medium (Prolong Antifade Gold with DAPI [4',6'- diamidino-2-phenylindole]; Molecular Probes).

**Quantitative 3D microscopy.** Hela cells pulse infected with Cy5-AAV2 were fixed with PFA and mounted to glass slides as described above. The distribution of viral particles in Hela cells were examined using a Zeiss LSM710 laser scanning confocal microscope equipped with a Plan-Apochromat 63×/NA 1.40 oil objective. Stacks of 20-30 focal planes were captured at 0.31μm z-intervals through the depth of the cell. 3D images of the cells were reconstructed using the Z-stacks. All images were acquired at pixel dimensions of 0.13×0.13×0.31μm (X, Y, Z) to fulfill the Nyquist sampling.

Deconvolution was performed by the AutoDeblur software (Media Cybernetics Inc.) using iterative and constrained algorithms as described previously (Xiao et al. 2012). The procedure started with a theoretical PSF derived from the actual settings of Zeiss710 confocal microscope, including NA of the microscope objective, refractive index of the medium, excitation wavelength, emission wavelength, confocal pinhole radius, pixel size, z-axis interval, and microscope type (i.e., wide field, confocal). A new adjusted adaptive PSF derived from the previous deconvolution round was used to generate the next adaptive PSF that fit the real imaging data better than the previous one (termed as one iteration or

deconvolution round). Twelve rounds of iteration were used to deconvolve all the confocal images in this study.

All deconvolved image stacks were processed using the IMARIS software package (Bitplane AG, Zurich, Switzerland) for visualization and quantification as described previously (Xiao et al. 2012). Briefly, each deconvolved image stack was reconstructed using a volume rendering module and smoothed by a 3D-median filter. Subsequently, an isosurface rendering module was applied through thresholding by the fluorescence intensity that was slightly higher than background. For Cy5-AAV2, the isosurface rendering was thresholded at the fluorescence intensity of 2000 a.u. (the upper boundary of background). For DAPI, isosurface rendering was thresholded at the fluorescence intensity of 3200 a.u.. Parameters (volume, MFI, TFI) for these isosurface coated Cy5-AAV2 objects were extracted from the IMARIS program and analyzed to determine the localization of particles as described previously (Xiao et al. 2012).

**Negative staining and electron microscopy.** Purified and dialyzed virus particles in 1× PBS were pipetted onto a glow-discharged copper grid. The grid was washed twice with water and then stained with 2% uranyl acetate. Electron microscopy images were taken with a LEO EM 910 transmission electron microscope at various magnifications.

**Transient transfection of reporter plasmid and siRNA.** For transfection of Hela cells with reporter plasmids, Hela cells were plated at a density of 4e+5 cells/well and 24 hr later were transfected with TR-CMV-EGFP reporter plasmids using PEI. For each well 500 ng DNA was mixed with 5 μl PEI (1 mg/ml) in 100 μl of serum-free DMEM and incubated at room temp for 10 min before addition to cell medium. Culture media was refreshed at 6hrs after transfection. At 16-20hrs after transfection, cells were treated with DMSO or other

drugs as indicated. At about 20hrs post-drug treatments, cells were harvested for flow cytometry analysis of GFP expression as indicated above.

Knockdown of RhoA was obtained by double transfection of siRNA (Dharmacom, Thermo Scientific) using Nucleofector (Lonza Inc.) performed with an Amaxa Electroporator according to the manufacturer's protocol. Knockdown efficiency was verified by Western-blot using RhoA antibody (Abcam Inc.). Efficient knockdown was achieved at two days after the first siRNA transfection. After verifying knockdown, approximately two days post-transfection cells were processed with pulse infection and drug treatments as described above. Viral transduction was analyzed using flow cytometry.

**Statistical analysis.** Experiments were performed in triplicates and repeated at least three times independently, unless otherwise noted. For studies comparing quantification of luciferase or GFP expression in one treatment group to the corresponding control group, a student t-test of the mean expression value was performed. For studies comparing quantification of luciferase or GFP expression in more than two treatments group to the same control group, a one-way analysis of variance (ANOVA) was performed to test the global hypothesis that all mean values are the same across groups. If the global hypothesis is rejected, Dunnett's test was used to compare the mean of each treatment to the mean of control group simultaneously. Luciferase or GFP expression was presented as Mean ± SD (standard deviation) and all tests were considered significant if $p<0.01$, which was indicated by *.

## Results

**Retention of AAV particles at the perinuclear region.** Perinuclear accumulation of many viruses including adenovirus (Ad), HSV, and HIV has been observed in previous studies. Using AAV as a model to study this phenomenon in detail, we first investigated the intracellular trafficking of AAV2 over time using viral particles labeled with Cy5. With our optimized protocol, we were able to visualize a single viral particle and the labeled virions remain as infectious as unlabeled particles. Specifically, homogeneous labeling of virions was achieved as demonstrated by confocal microscopy of labeled particles on glass coverslips (Fig.IV-1A, left). The intensity profile of fluorescent spot followed a single Gaussian distribution, suggesting that the fluorescence signal was from a single particle (Fig.IV-1A, right) (Vonderheit et al. 2005). The signal had a diameter of about 0.4 μm as determined by Full Width at Half Maximum (FWHM), consistent with the fluorescent signal from other nano-sized viruses (Vonderheit et al. 2005). Data from negative staining and electron microscopy demonstrated that the virion structure remained unchanged and that most of the labeled virions were single particles (Fig.IV-1B). To test whether labeling would affect the functionality of the virions, we compared labeled and unlabeled AAV particles in their ability to transduce cells using GFP reporter gene assay. We found that the labeled virions can express GFP transgene as efficiently as the unlabeled ones, indicating that the particles labeled with Cy5 were fully competent at transduction (Fig.IV-1C). It has been relatively difficult to visualize virions on the cell surface presumably because most virions bound as single particles and the visualization method was not sensitive enough to detect them at single particle level (Johnson et al. 2009). In contrast, we were able to visualize the

AAV particles on the cell surface after 40 minutes incubation of cells with Cy5-AAV at 4℃ (Fig.IV-1D, left). In addition, the Cy5 fluorescent signal was successfully co-stained with the signal from monoclonal A20 antibody that specifically recognizes the AAV capsids (Fig.IV-1D, right). These data demonstrate that our labeling and imaging systems are sufficiently robust and reliable to study the viral trafficking and infection at the level of a single particle.

To study the intracellular trafficking of AAV, we synchronized particle trafficking using "pulse infection", in which cells are incubated with virions at 4℃ for 40 minutes and unbound virions are then washed away before cells are transferred to 37℃ for subsequent viral infection. After pulse infection, we studied the distribution of AAV particles at several time points over 12 hours (Fig.IV-2A). During the first 2-4 hours post-infection (p.i.), the majority of viral particles were scattered in the cytoplasm and trafficking towards the perinuclear region. At 4 hours p.i., the majority of viral particles had finished their cytoplasmic trafficking and localized at the perinuclear region in approximately 30-40% of cells. At 8hrs p.i., perinuclear accumulation was observed in over 80% of cells and persisted for over 6 hours, suggesting retention of viral particles at this perinuclear site (arrows in Fig.IV-2A). To specifically investigate the role of the perinuclear retention, we focused on the time period between 6-8 hours after pulse infection, a time point at which, in majority of cells, most virions have finished cytoplasmic trafficking and remain at the perinuclear region.

**Perinuclear retention is dependent on intact MT-MTOC.** Previous studies based on fluorescence signal co-localization have shown that several viruses including Ad and HIV, traffic to a perinuclear region that coincides with the Microtubule-Organization-Center (MTOC). Previous studies have co-localized perinuclear AAV particles to the Golgi apparatus (Johnson et al. 2010; Nonnenmacher et al. 2011), and others have suggested that

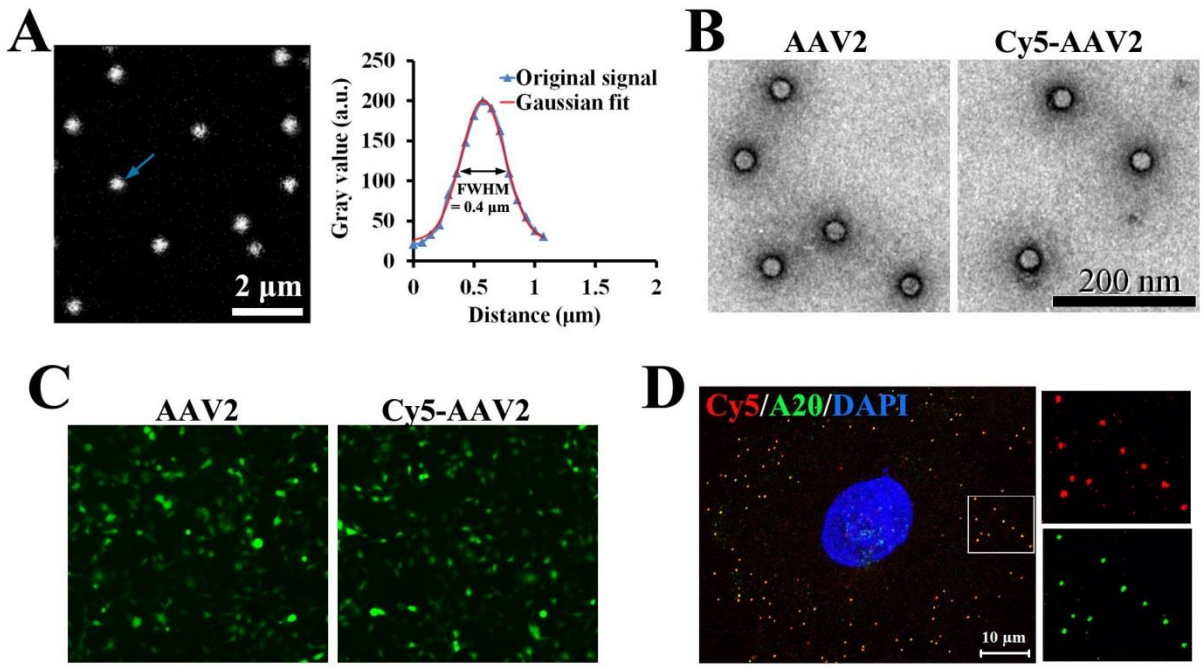


**Figure IV-1. Fluorescent labeling of AAV particles.** A) A representative confocal image (left) showing the fluorescence signal of Cy5-AAV2 bound to coverslip. Right panel: A single Gaussian distribution (red curve) fits the representative distribution of fluorescence intensity (blue curve) from a Cy5-AAV2 particle (arrow in left panel). B) Negative staining and electron micrographs of AAV2 and Cy5-AAV2. C) GFP transgene expression from AAV2 and Cy5-AAV2 as captured with epi-fluorescence microscope. D) A representative confocal image showing the bound Cy5-AAV2 on the surface of Hela cells after 40min incubation at 4 ℃. AAV particles are visualized by Cy5 signal (red) and staining with monoclonal antibody A20 that recognize AAV capsid (green). Nucleus is stained with DAPI (blue).

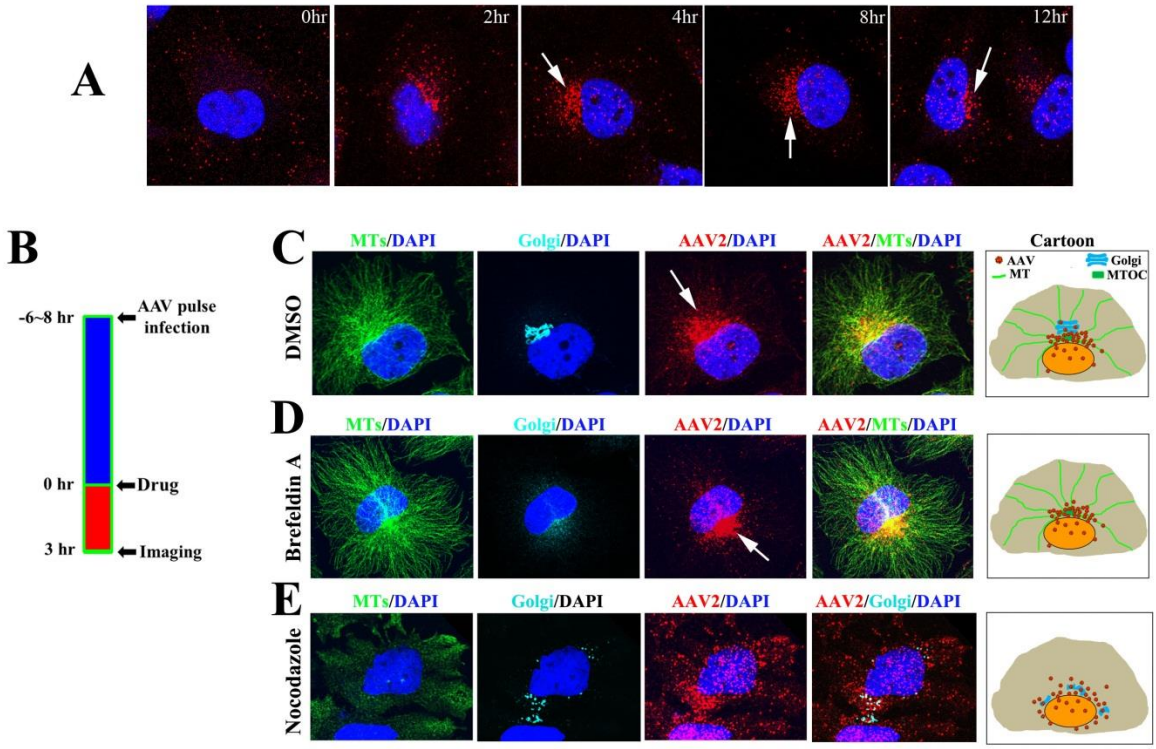


**Figure IV-2. Perinuclear retention of AAV by the MT-MTOC.** Hela cells were fixed to examine the distribution of viral particles at various times after pulse infection. Nuclei were stained with DAPI (blue). A) Representative images showing the distribution of intracellular AAV2 over 12 hours after viral inoculation. Arrows indicate perinuclear accumulation in the cells. B) Schematic diagram showing the procedure used for drug intervention and confocal imaging experiments. C-E) Confocal images showing the localization of the MT-MTOC, Golgi apparatus, and AAV2 when cells treated with DMSO (C), 2 μg/ml Brefeldin-A (D), 30 μM Nocodazole (E). MTs were stained with α-tubulin antibody (green) and Golgi apparatus was stained with Giatin antibody (cyan). Arrows indicate the perinuclear accumulation of AAV. The right most panels in C-E display schematic cartoons showing the localization of AAV particles, Golgi, and MTs in the cells.

these virions may co-localize with the MTOC (Johnson et al. 2011). As the perinuclear region is highly crowded and the resolution of classical fluorescent microscopy is only about 0.3 μm in lateral, images solely generated by such fluorescent microscopy alone could falsely co-localize viral particles with many cellular organelles at perinuclear region, namely Golgi, MTOC, ER etc. (Johnson et al. 2011). To effectively discern which cellular structure(s) at the perinuclear region co-localize with AAV particles and retain these virions, we combined fluorescence microscopy with pharmacological interventions (Fig.IV-2B) to circumvent the above resolution limit issues. Specifically, if AAV particles do co-localize to and are retained by a particular structure at the perinuclear region, we shall be able to predict that: 1) the viral accumulation will be ablated upon the disruption of that structure by pharmacological agents; 2) the majority of virions will still co-localize with that structure after release from the perinuclear region upon disruption of microtubules (MTs) and the MTOC.

Using several antibodies, we demonstrated that AAV particles can be co-stained with markers for Golgi apparatus and MT-MTOC (peri-MTOC microtubules) at the perinuclear region (Fig.IV-2C). To distinguish whether virus localized to the Golgi or MT-MTOC, we used a panel of pharmacological reagents to disrupt these structures individually and visualized the localization of viral particles in each case. Upon Brefeldin-A treatment to specifically disrupt Golgi apparatus, perinuclear accumulation of AAV was not dispersed (Fig.IV-2D). In contrast, when MT-MTOC was fully disrupted by Nocodazole, the perinuclear localization of AAV was ablated and few AAV particles co-localized with dispersed Golgi cisternae (Fig.IV-2E). These data demonstrate that AAV is localized to and retained by the MT-MTOC but not Golgi apparatus at the perinuclear region. This finding is consistent with previous studies that show many other viruses traffic and localize to the

MTOC or MT-MTOC (Sodeik et al. 1997; McDonald et al. 2002; Bailey et al. 2003; Fackler et al. 2006; Greber et al. 2006; Yea et al. 2007).

**MT-MTOC retention limits the transduction of rAAV, rAd, and lentivirus.** Given that the majority of cytoplasmic virions were retained at the MTOC region, we examined the effects of this retention on viral transduction. To do so, we used several anti-MT drugs (AMDs, e.g. Nocodazole, Colchicine, Rhizoxin, and Maytansine) to disrupt MTs at approximately 6-8 hours p.i., after viral particles have completed microtubule-mediated cytoplasmic trafficking to perinuclear region in most cells (Fig.IV-3A). Because our previous study showed that MTs also facilitates viral cytoplasmic trafficking from the cell periphery to the perinuclear region (Xiao et al. 2012), the timing of above treatment allowed us to separate the effects on viral infection of MT mediated cytoplasmic trafficking from those of MT-MTOC dependent perinuclear retention. To exclude potential effects of the reagents on the second strand synthesis of viral DNA, self-complementary AAV (AAV2-CMV-GFPsc) was used in the transduction assay.

Disruption of MTs by Nocodazole treatment at 6~8 hours p.i. induced a 2~4-fold increase in viral transduction in multiple cell lines as measured by the expression of the transgene GFP (Fig.IV-3B). To rule out the possibility that the increased viral transduction was specific to Nocodazole, a panel of ADMs was used (Colchicine, Rhizoxin, Maytansine), all of which disrupt MTs. Similar increases in GFP expression were observed with all of the drugs (Fig.IV-3C). We also tested whether stabilization of MT-MTOC by Taxol would reverse the effect of Nocodazole, through comparing the viral transduction in cells treated with Nocodazole alone or with Nocodazole and Taxol. We found that co-administration of Taxol with Nocodazole restored the enhanced viral transduction to the control

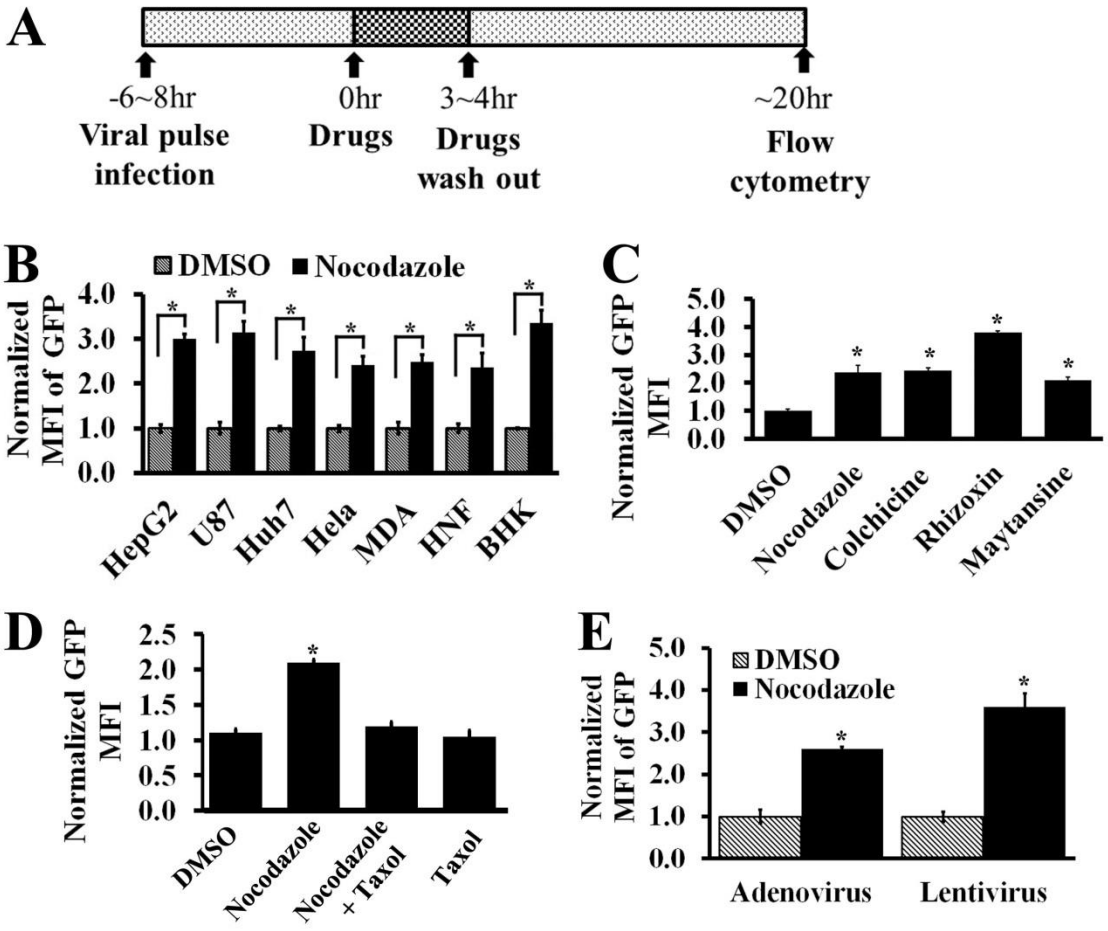


**Figure IV-3. Disruption of MT-MTOC increases transduction of rAAV, rAd, and lentivirus.** A) Schematic diagram showing the procedure used for the experiments in B-E. B) A variety of cell lines used to measure AAV2 transduction with and without Nocodazole treatment. Mean Fluorescence Intensity (MFI) of GFP expression is normalized to the DMSO treatments. C) AAV2 transduction was determined by MFI of GFP expression in Hela cells treated with various AMDs. D) The MFI of GFP expression was measured in cells treated with DMSO, Nocodazole, Nocodazole+Taxol, or Taxol only. E) The MFI of GFP expression from recombinant Adenovirus (rAd) and lentivirus was determined in cells treated with DMSO or Nocodazole. (*) indicates statistically significant difference with $p<0.01$.

level (Fig.IV-3D). Together, these results demonstrated that the increase in AAV transduction was due to MT-MTOC disruption.

As both Ad and HIV accumulate at MTOC in HEK293 cells (McDonald et al. 2002; Yea et al. 2007), we tested whether MT-MTOC disruption can also lead to an increase in transduction of these viruses. Interestingly, treatment of Nocodazole resulted in 2.5-fold and 3.6-fold increases for the transduction of rAd and lentivirus respectively (Fig.IV-3E). This data provides yet another layer of evidence to support the hypothesis that perinuclear retention by MT-MTOC limits viral transduction. Furthermore, this hypothesis holds true for both enveloped and non-enveloped viruses.

**Increased transduction upon MT-MTOC disruption is independent of promoter activity, cell cycle arrest, and viral degradation.** Next, we explored the underlying mechanism associated with the increase in viral transduction induced by MT-MTOC disruption. We envisioned three possible mechanisms for the increase in transgene expression: 1) MT-MTOC disruption leads to the activation of the promoter on the viral transgene cassette; 2) MT-MTOC disruption results in cell cycle arrest which, in turn, leads to increased viral transduction; 3) MT-MTOC disruption affects intracellular viral processing or trafficking. First, we employed *in vitro* plasmid transfection to examine the potential effect of MT-MTOC disruption on promoter activity. Our flow cytometry data demonstrated that MT-MTOC disruption by AMDs did not affect the reporter gene (GFP) expression from the viral transgene cassette, which was directly transfected into the cells using PEI (Fig.IV-4A). This data excludes the possibility of AMD treatment affecting promoter activity (mechanism 1). To test the second possible mechanism, we measured the effects of AMD treatment on viral transduction in cells whose cell cycle was already arrested at S-phase by double

thymidine block, a step preceding the M-phase block caused by AMDs. Our data showed that MT-MTOC disruption also induced an enhancement of viral transduction in these pre-arrested cells, suggesting that the increase in viral transduction was independent of cell cycle arrest induced by disruption of MT-MTOC (mechanism 2, Fig.IV-4B). Additionally, it was previously reported that intracellular degradation of AAV limits viral transduction and its blockage using proteasome inhibitors resulted in dramatic increase in viral transduction (Zhong et al. 2008). It was also previously proposed that MT-MTOC facilitates the degradation of intracellular proteins by transporting these proteins to and retaining proteasome machineries at the perinuclear region. As a result, we tested if MT-MTOC disruption has reduced the AAV degradation. Data from quantitative PCR demonstrate that the amount of AAV measured as genome copy number (vgs/cell) was not significantly changed upon MT-MTOC disruption, suggesting AMD treatment did not affect the viral degradation (Fig.IV-4C). This notion was further supported by our data from pharmacological intervention studies which showed that proteasome inhibitor can further enhance viral transduction if co-administrated with AMDs (Fig.IV-4D). Therefore, we have excluded the hypotheses 1) that MT-MTOC disruption directly increases transgene expression; 2) that MT-MTOC disruption acts to increase transduction through cell cycle arrest; and 3) that MT-MTOC disruption increases AAV transduction by decreasing the degradation of AAV virions.

Interestingly, our (and others') previous studies demonstrated that disruption of MTs during AAV entry has a negative effect on transduction due to impaired cytoplasmic trafficking. Our current findings suggest that: 1) MTs are not required for steps of transduction subsequent to the trafficking to perinuclear region, and 2) though MTs play a

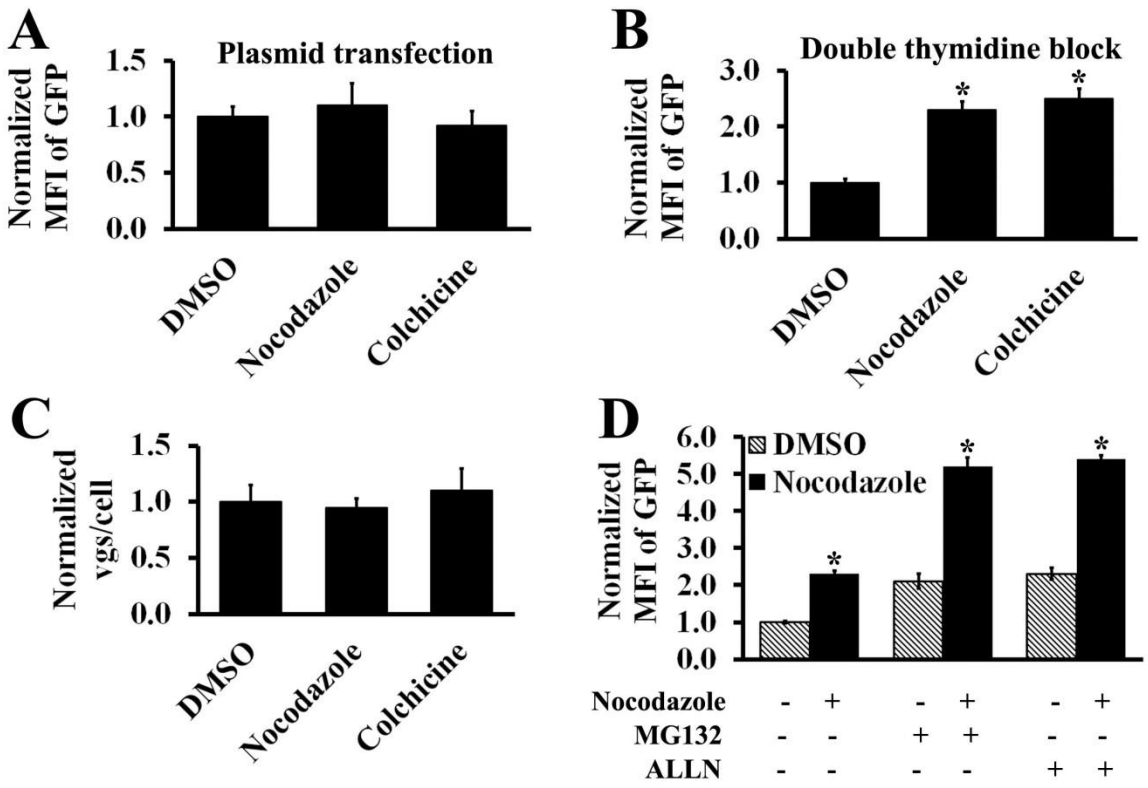


**Figure IV-4. MT-MTOC disruption does not affect promoter activity and viral degradation.** A) At 16-20hrs after transfected with plasmid TR-CMV-GFP using Polyethyleneimine (PEI), Hela cells were treated with drugs for 3hrs. At approximately 20hrs after drug treatments, cells were harvested for flow cytometry analysis to measure the GFP expression. B) Cells were cell cycle arrested using a double thymidine block and then the MT-MTOC was disrupted as in Figure IV-3A and AAV transduction was measured. C) Cells were treated as in Figure IV-1B and quantitative PCR (qPCR) was used to determine the copy number of the viral genome. D) Cells were treated as in Figure IV-3A except that proteasome inhibitors were added with AMD and transduction was measured. (*) indicates statistically significant difference between DMSO and Nocodazole treatments with $p<0.01$.

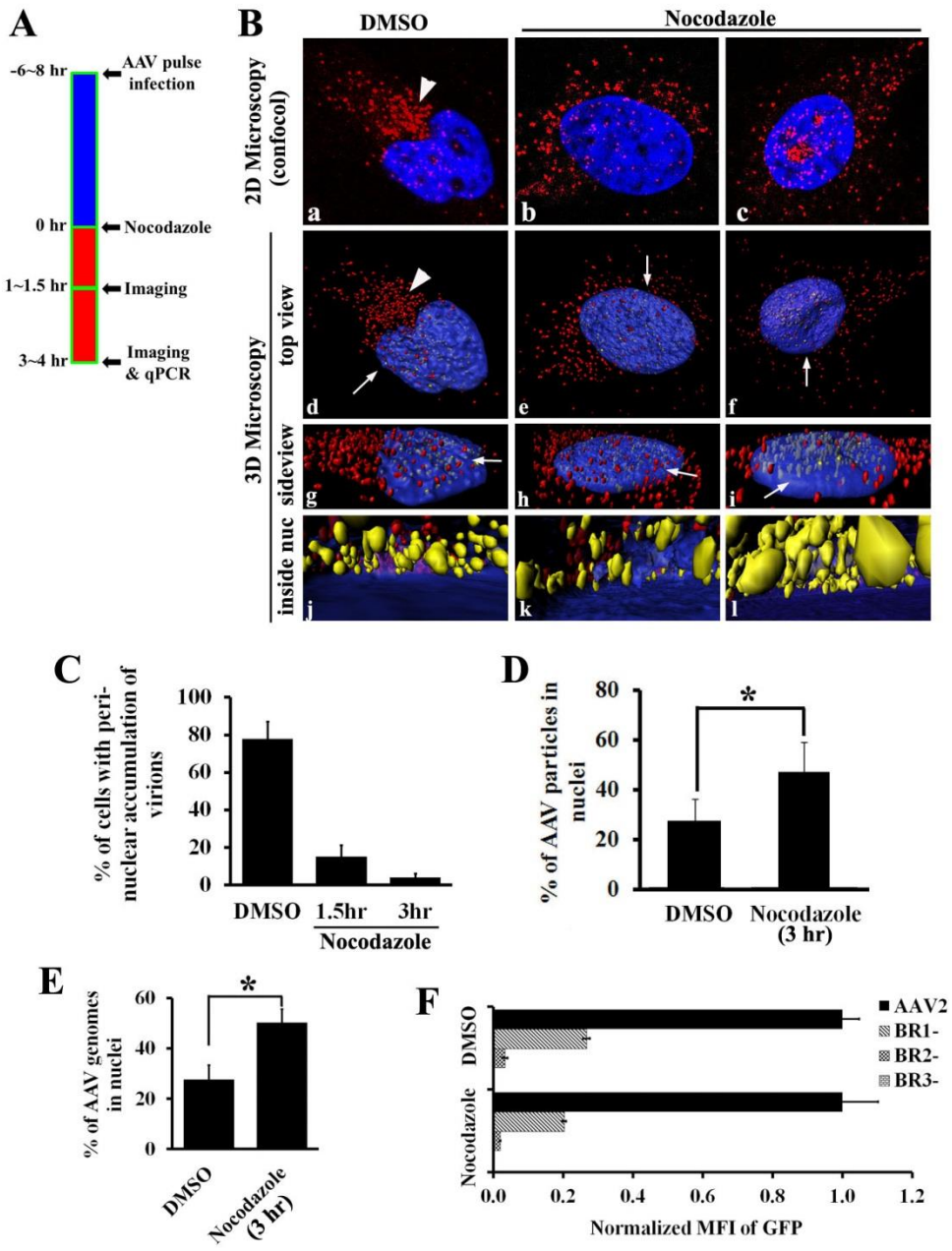


**Figure IV-5. Release of AAV and increased nuclear entry upon MT-MTOC disruption.** A) Schematic diagram showing the procedure for the experiments in B-E. Specifically, Hela cells were treated with DMSO or Nocodazole at 6~8hrs after pulse infection of Cy5-AAV2, and fixed at 1-1.5hrs or 3-4hrs after drug treatments. Nuclei were stained with DAPI (blue). B) Representative images from 2D confocal microscopy of one focal plane (a-c) and 3D images reconstructed from confocal Z-stacks as described in Methods. (d-l) showing the viral distribution in cells treated with DMSO (a,d,g,j), or with Nocodazole for 1-1.5hrs (b,e,h,k) or 3-4hrs (c,f,i,l). d-f are top views, while g-i are magnified side views from directions indicated by arrows in d-f respectively. j-l are views observed inside the nucleus (from the directions indicated by arrows in g-i respectively, between the top and bottom nuclear envelopes, which is indicated by the blue layer based on the DAPI signal). AAV2 particles in cytoplasm are

highlighted as red and those inside the nucleus highlighted as yellow. C) The proportion of cells with perinuclear accumulation of AAV particles after DMSO or Nocodazole treatment (for 1.5hrs or 3hrs) was quantified in 50-100 cells for each group. The perinuclear accumulation is defined as concentrated viral particles at a single perinuclear region (arrows in Fig.IV-2 and arrowheads in Fig.IV-5B). D) The proportion of AAV particles entering nucleus in cells treated with DMSO or Nocodazole at 3hrs was quantified from the 3D microscopy data (Fig.IV-5B). 20-30 cells from each group were used for the 3D quantitative microscopy described in Methods. E) Nuclei were fractioned from cells and qPCR was used to determine the copy number of AAV genomes in the nucleus of cells treated with Nocodazole for 3hrs, in comparison with DMSO treated cells. F) Cells were treated with DMSO or Nocodazole as described in Fig.IV-3A then transduced with AAV or BR mutants of AAV and transduction was analyzed by flow cytometry. GFP expression is normalized to that in DMSO treated group. (*) indicates statistically significant difference between DMSO and Nocodazole treatments with $p<0.01$.

central role in trafficking of the virus to the perinuclear region, at later time points these structures act to retain virions and thus, limit transduction.

**Nuclear entry of AAV is increased upon the disruption of MT-MTOC.** Based on the above findings, the most likely mechanism for elevated viral transduction upon MT-MTOC disruption occurs at the level of trafficking. It has been previously demonstrated that nuclear entry is an essential trafficking event for AAV's infectious pathway (Grieger et al. 2006; Sonntag et al. 2006). Moreover, nuclear entry is the most probable event subsequent to and being limited by perinuclear retention in AAV's infectious trafficking pathway. We hypothesized that the retention of viral particles at the MTOC region may limit the subsequent nuclear trafficking of the virus. To test this hypothesis, we visualized viral trafficking steps with and without Nocodazole treatment by fluorescent confocal microscopy and quantitatively evaluated the distribution of viral particles at different time points after administration of Nocodazole at 6-8 hrs p.i. (Fig.IV-5A). At about 1-1.5 hrs after MT-MTOC disruption (~8-9 hrs p.i.), the perinuclear retention of AAV particles was ablated in most cells examined (Fig.IV-5C) and the viral particles spread around the outside of nucleus (Fig.IV-5B). Later, ~3-4 hours after MT-MTOC disruption (~10-11 hrs p.i.), an approximate 2-fold increase of viral particles was observed in the nucleus as shown by the representative images from confocal microscopy (Fig.IV-5B-c) and quantitative data from 3D microscopy (Fig.IV-5B-f/i/l, and 4D). Increased viral entry into the nucleus was also supported by quantitative PCR analysis of the viral genome copy number in the nuclear fractions of treated and untreated cells (Fig.IV-5E). Together, these results demonstrate that disruption of the MT-MTOC at 6-8hrs p.i. leads to an increase in nuclear entry of AAV particles, explaining the increased transduction we observed (Fig.IV-3).

Three major basic regions (BRs) on the capsid have been shown to function as nuclear localization signals (NLS) with varying strengths (Grieger et al. 2006; Sonntag et al. 2006). AAV mutants with deletions at these regions can still accumulate at the perinuclear region but are unable to enter nucleus (Johnson et al. 2010). To test whether NLS are required for the increased nuclear entry and viral transduction, we examined the effects of MT-MTOC disruption on these BR deletion mutants. In both DMSO and Nocodazole treated cells, BR deletions resulted in the reduced viral transduction (Fig.IV-5F). Importantly, Nocodazole treatment was unable to restore the impaired transduction of these BR mutants, indicating that AMD-induced enhancement of viral transduction and nuclear entry requires the capsid NLSs. These data suggest that MT-MTOC disruption releases AAV to continue down its normal nuclear entry pathway and does not cause AAV's nuclear entry pathway to change.

**AAV is imported into the nucleus via the RhoA-ROCK-Actin pathway upon MT-MTOC disruption.** The above findings suggested that MT-MTOC disruption itself only allows the release of AAV particles from the perinuclear region. The subsequent increase in nuclear entry is achieved by a mechanism that requires the NLS on viral capsid. It is well established that MT disruption can lead to RhoA-ROCK mediated rearrangement of actin filaments (AFs), which in turn affects actin-mediated intracellular trafficking (Krendel et al. 2002; Chang et al. 2008). Perinuclear AFs have been demonstrated to associate with the nuclear envelope and nuclear pore complexes at the nuclear envelope and were proposed to be involved in nuclear import/export of intracellular materials (Hofmann et al. 2001; van Loo et al. 2001; Minakhina et al. 2005; Broers et al. 2006; Favoreel et al. 2007; Schneider et al. 2008). As a result, we tested whether the AFs regulated by the activation of RhoA-ROCK

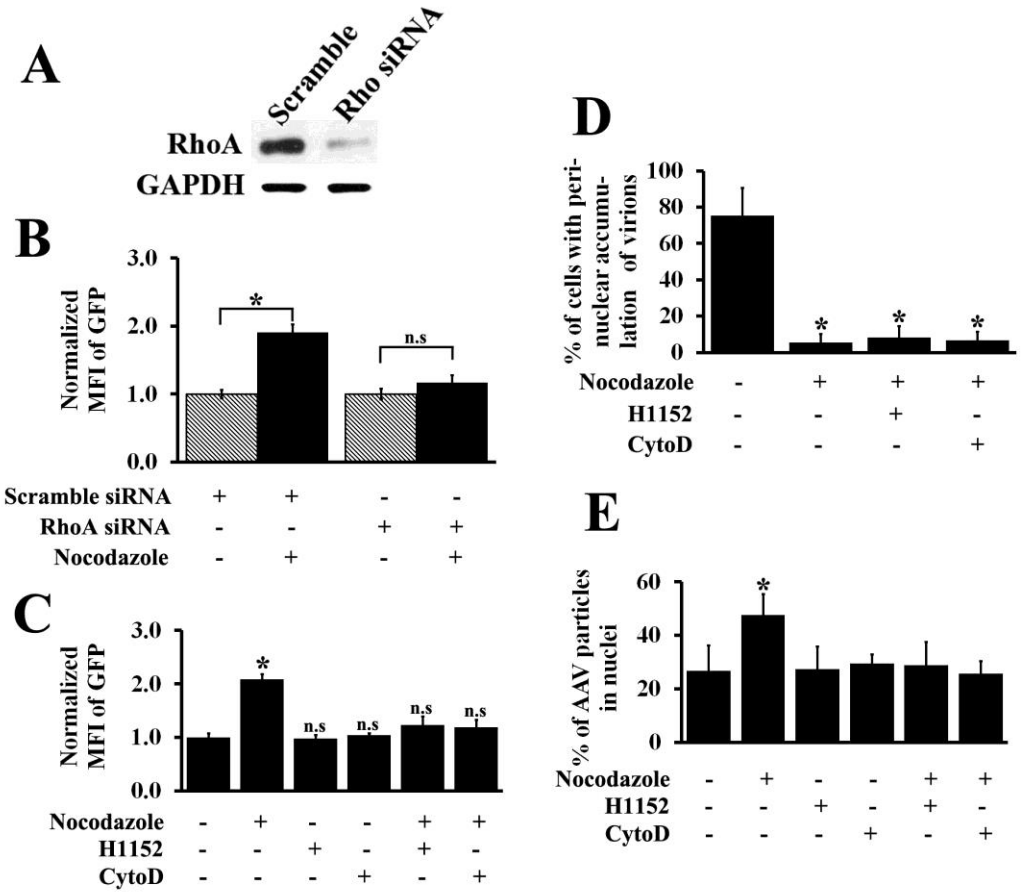


**Figure IV-6. Disruption of the MT-MTOC increases viral transduction and nuclear entry through a RhoA-ROCK-Actin pathway**. A) Immunoblot showing the siRNA-mediated transient knockdown of RhoA protein in Hela cells. Scramble siRNA used as a control. B) The level of AAV transduction was measured in Scramble or RhoA siRNA transfected cells treated with or without Nocodazole treatment at 6-8hrs after AAV infection. C) The level of AAV transduction was determined in cells treated with DMSO or Nocodazole alone or in combination with H1152 or CytoD. D) The proportion of cells with perinuclear accumulation of AAV particles was measured in the presence of DMSO or Nocodazole alone or in combination with H1152 or CytoD. E) The proportion of AAV particles in the nucleus was determined in cells treated with DMSO or Nocodazole alone or in combination with H1152 or CytoD. (*) indicates statistically significant difference between DMSO only and other drug treatments with $p<0.01$.

upon MT disruption contributed to the increased nuclear entry and transduction of AAV we observed. First, we transiently transfected siRNA to knockdown the expression of endogenous RhoA as demonstrated by immunoblotting for the RhoA protein (Fig.IV-6A). Interestingly, treatment with Nocodazole only induced an increase in viral transduction in cells transfected with the control (scrambled) siRNA and had minimal effect in RhoA knockdown cells (Fig.IV-6B). H1152 is a potent inhibitor of ROCK, a downstream effector of RhoA and induces actin filament alterations. Cytochalasin D (CytoD) is an inhibitor of AFs that induces the de-polymerization of these filaments (Schelhaas et al. 2008). Both H1152 and CytoD were found to ablate the transduction enhancement induced by MT-MTOC disruption with Nocodazole; therefore, the enhancement of transduction required that ROCK not be inhibited and that AFs be intact (Fig.IV-6C). These data suggest that the RhoA-ROCK-Actin pathway is required for the increased viral transduction upon MT-MTOC disruption. Visualization of viral particles by fluorescence microscopy revealed that Nocodazole-induced viral dispersion from the perinuclear region was unaffected by co-administration with H1152 or CytoD (Fig.IV-6D). Our data from 3D quantitative microscopy further demonstrated that co-administration of either H1152 or CytoD only blocked the increase in viral nuclear entry after MT-MTOC disruption (Fig.IV-6E). Additionally, administration of H1152 or CytoD alone at 6-8 hrs p.i. did not affect the transduction and nuclear entry of AAV (Fig.IV-6C and E).

Together, the above data suggest a two-step working mechanism for the increased AAV transduction observed upon MT-MTOC disruption: 1) viral particles are released from the perinuclear region and spread around the outside of nucleus upon MT-MTOC disruption;

and 2) some of these viral particles are then transported into the nucleus via the RhoA-ROCK-Actin pathway.

**Perinuclear retention of AAV and Nocodazole-mediated enhancement on viral transduction also occur *in vivo.*** In cell culture, we observed a bottleneck in viral transduction at the stage of accumulation and retention of AAV at MTOC region. rAAV is currently widely used as a gene therapy vector in many clinical trials to tackle a variety of human diseases (Xiao et al. 2012). The effort to improve its efficiency in gene delivery has been compromised by the lack of knowledge about AAV trafficking in *in vivo* settings. With the sensitive imaging technique used in this study, we examined whether perinuclear retention of AAV also acted as a bottleneck *in vivo*. To examine this hypothesis, we injected Cy5-AAV into mouse brain, liver, or xenografted tumor, and determined the viral distribution at different time points after viral infection. At an early stage (~1 hour) after viral inoculation, viral particles were scattered across cells in these tissues, as is clearly observed in the brain image (Fig.IV-7A). Due to the relatively high background fluorescence observed in both liver and xenografted tumor, we were not able to visualize single viral particles in these tissues as observed in brain, and instead were only able to visualize particles at the sites of viral injection, where a higher concentration of labeled virions was present (arrowheads in Fig.IV-7A). At 6-12 hours p.i., a large number of viral particles were observed to accumulate at the perinuclear region, consistent with our *in vitro* studies (Fig.IV-7A). Approximately 60-80% of cells in these tissues had perinuclear accumulation by 12 hours after infection (arrows in Fig.IV-7A).

Furthermore, we tested whether AMD treatment could disrupt this perinuclear retention and increase viral transduction as was observed in our *in vitro* studies.

Approximately 10 hours after viral inoculation, Nocodazole was administrated to the animal through intraperitoneal or intratumoral injection. At 4-6 hours after Nocodazole injection (~14-16 hrs p.i.), perinuclear retention (arrows in Fig.IV-8A) was only observed in DMSO-treated animals and was ablated in the cells of both liver and xenografted breast tumor in Nocodazole-treated animals (Fig.IV-8A). Using GFP as a reporter gene packaged by AAV, a significantly stronger GFP fluorescent signal was observed in the Nocodazole-treated breast tumors (Fig.IV-8B). Moreover, by measuring luciferase activity using the IVIS imaging system, we observed a roughly 10-fold increase of viral transduction in both liver and xenografted tumor of Nocodazole-treated mice (Fig.IV-8C, D). Together, these data suggest that AAV takes a similar subcellular trafficking route in the animal tissues we tested to that we found *in vitro* and is retained at the perinuclear region, a trafficking bottleneck for viral transduction.

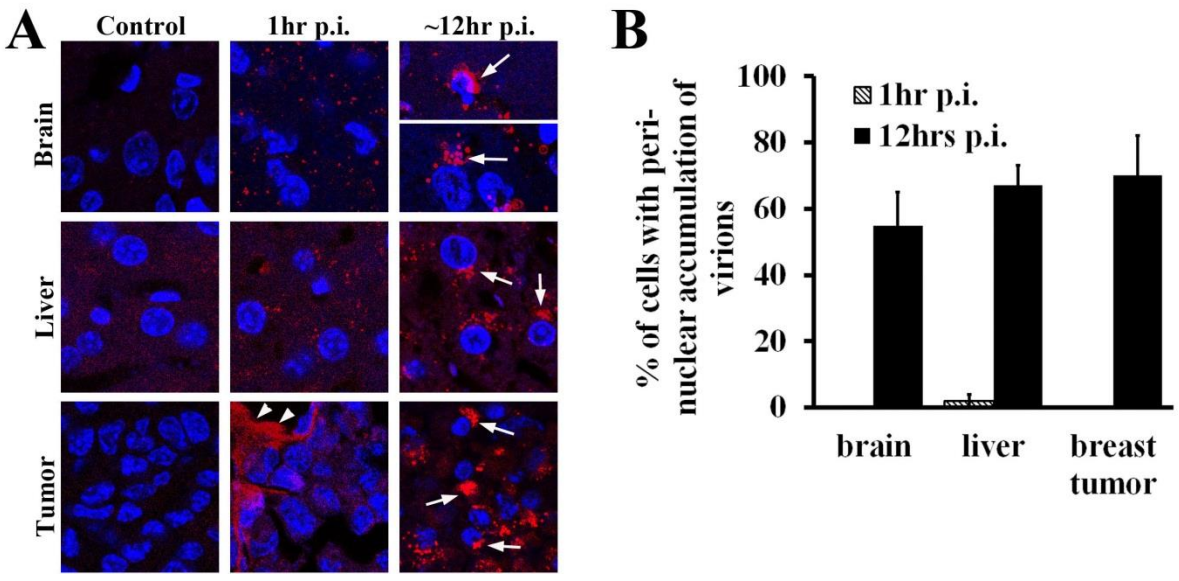


**Figure IV-7. Perinuclear accumulation in mouse tissues.** Mouse tissues (brain (cerebrum), liver, xenografted breast tumor) were removed at 1hr or 12hrs after injection of Cy5-AAV and sectioned using a cryo-microtome. Nuclei are stained with DAPI (blue). The viral particles were visualized by confocal microscopy. A) Representative confocal images showing the viral distribution in uninfected mouse tissues (control), or tissues that were infected with AAV for 1hr or 12hr. Arrowheads indicate concentrated AAV at the injection site. Arrows indicate perinuclear accumulation of virions. B) The percentage of cells with perinuclear accumulation of AAV in each tissue was measured at 1hr p.i. and 12hr p.i.. 50-100 cells were analyzed for each group.

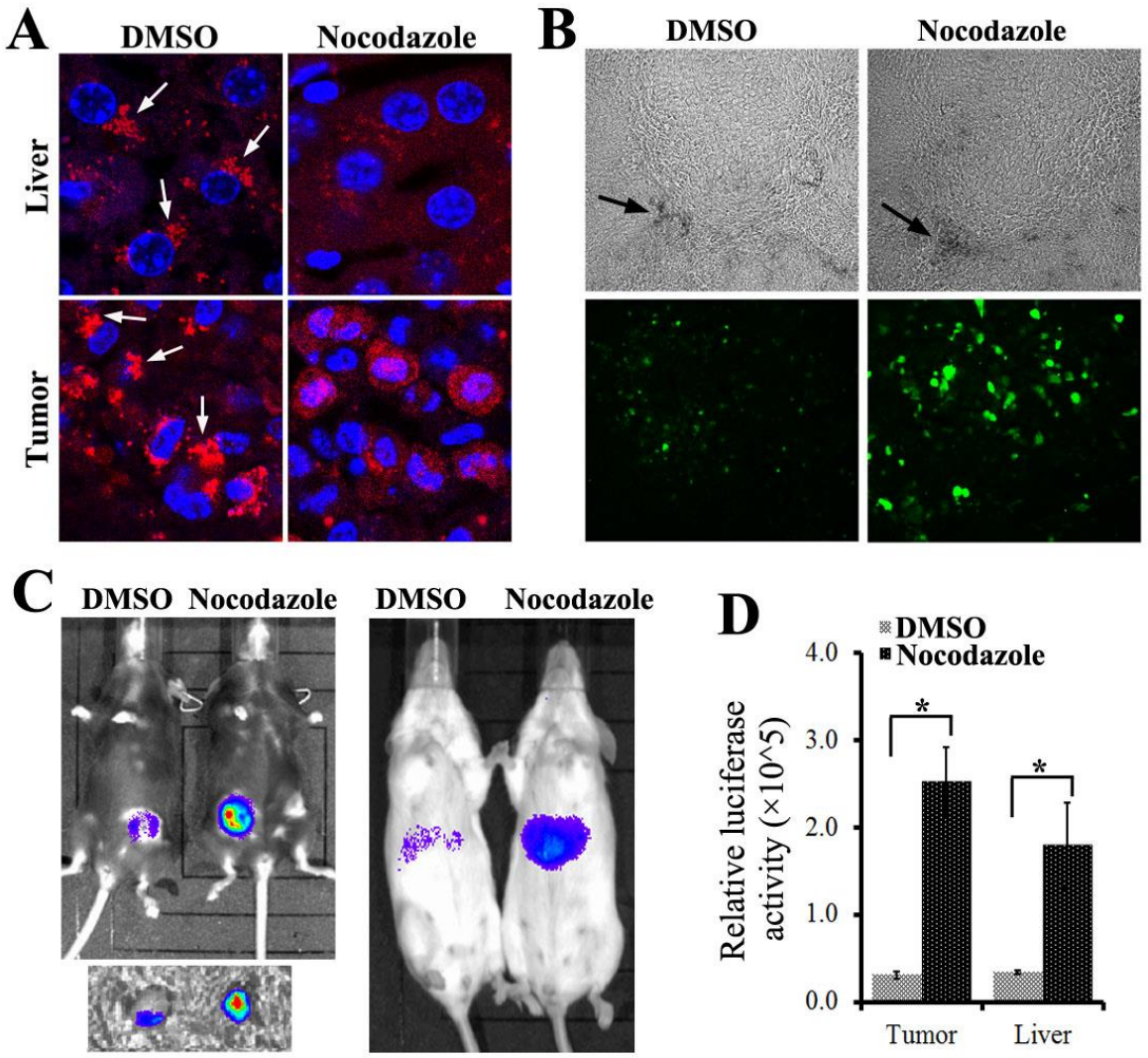


**Figure IV-8. Perinuclear accumulation of AAV particles is disrupted and viral transduction is increased upon Nocodazole treatment in various mouse tissues.** A) Representative images showing the distribution of AAV particles (red) in tissues treated with DMSO or Nocodazole. Nuclei are stained with DAPI (blue). Arrows indicate the perinuclear accumulation of virions. B) Representative images showing the viral injection sites as visualized with injected India ink (arrows on the upper panel) and transgene GFP expression (green in lower panel) in the xenografted tumors. C) IVIS imaging of luciferase signal in xenografted breast tumor and liver at one week after viral injection. Left panel shows the luciferase activity in the xenografted tumor before (upper image) or after (lower image) removal from the mice. Right panel shows the luciferase activity from liver expression. D) The relative luciferase activity in the tumor and liver were quantitated as photons/sec/cm^2 (n=3-4). (*) indicates statistically significant difference between DMSO and Nocodazole treatments with $p<0.01$.

## Discussion

Viral accumulation at the perinuclear region is commonly observed during the infection of many viruses (e.g. Ad, HSV, HIV, influenza, parvoviruses) (Dohner et al. 2002; McDonald et al. 2002; Mani et al. 2006; Yea et al. 2007; Boisvert et al. 2010). However, it remains unclear regarding whether and how this accumulation affects viral infection. Two plausible hypotheses are (Wileman 2007): 1) viruses exploit the cellular protein-trafficking machineries to approach the replication site or to concentrate viral components for viral replication and later virion assembly, thus supporting viral infection; 2) perinuclear accumulation represents an innate cellular response that recognizes virus components as foreign or misfolded proteins and targets them for sequestration and degradation at the perinuclear region, thus interfering with viral infection. Our present study has supported the hypothesis that perinuclear accumulation is a cellular defense mechanism to sequester virions in order to limit the infection of both enveloped virus (HIV) and non-enveloped viruses (Ad and AAV).

Both Golgi and MTOC are perinuclear structures that coincidentally colocalize at the perinuclear region with many viruses (Sodeik et al. 1997; Dohner et al. 2002; Mani et al. 2006; Yea et al. 2007; Boisvert et al. 2010; Liu et al. 2012). However, prior to this study, it remained unclear which cellular structure maintains perinuclear accumulation of AAV. Earlier studies have suggested that the perinuclear viral particles co-localize to the Golgi apparatus (Johnson et al. 2010; Nonnenmacher et al. 2011). Another study suggests that these virions may co-localize with the MTOC (Johnson et al. 2011). In this study, to examine which structure was involved, we combined confocal fluorescence microscopy with

pharmacological intervention to circumvent the difficulties in studying the interactions between virions and cellular structures at the highly crowded perinuclear region caused by the resolution limits of classical fluorescence microscopy (~ 0.3 μm in lateral). Our results demonstrate that it is MT-MTOC but not the Golgi that co-localize with and retain the AAV particles at perinuclear region (Fig.IV-2). Consistent with our findings, many other viruses including Ad, HSV, and HIV have also been shown to move on MTs to the MTOC region and associated with MT-MTOC (Sodeik et al. 1997; McDonald et al. 2002; Bailey et al. 2003; Fackler et al. 2006; Greber et al. 2006; Leopold et al. 2006; Yea et al. 2007). Furthermore, figure IV-2E shows that only a small portion of viral particles co-localized with the dispersed Golgi cisternae which are released from highly packed MTOC region upon MT-MTOC disruption. This suggests that few particles physically localize in the Golgi apparatus. Consistent with previous reports, we did find disruption of the Golgi apparatus at an earlier time during infection can impair AAV transduction. These data indicate that the Golgi does play a role in viral infection, probably through viral capsid modifying critical for viral infection, but is dispensable for perinuclear retention of incoming virions. Further investigation of the exact role of the Golgi apparatus on the infection of AAV and other viruses may advance our current knowledge of virology.

Our results, together with previous studies strongly suggest that perinuclear retention at MTOC during early infection serves as a cellular barrier limiting viral transportation to the replication sites, and leads to decreased viral transduction. During early infection stage, in which a virus delivers its genome to the target site for replication, accumulation of incoming virions at MTOC region is observed for most viruses that exploit MTs for earlier cytoplasmic trafficking (Sodeik et al. 1997; Dohner et al. 2002; McDonald et al. 2002; Suikkanen et al.

2002; Mani et al. 2006; Yea et al. 2007; Boisvert et al. 2010). Combining our observations with these previously published findings prompted us to test whether the MT-MTOC serves as a subcellular barrier restricting access of the virions to their replication site (nucleus in this study) during the early stage of viral infection. In order to do so, we have disrupted MT-MTOC using AMDs specifically at about 6-8 hours p.i. to exclude the potential complications from earlier MT-mediated cytoplasmic trafficking. In addition, we have utilized recombinant viruses to rule out the potential complications from viral replication and assembly. Using these experimental strategies, we demonstrated that retention of AAV by MT-MTOC limits viral transduction. Additionally, both Ad and HIV are also known to accumulate at MTOC region in HEK293 cells (McDonald et al. 2002; Yea et al. 2007), and the nuclear delivery of their components is essential for infection (Goff 2001). Interestingly, our data shows that disruption of MT-MTOC during infection with these viruses also led to an increase in viral transduction (Fig.IV-4E). Though further studies are required to demonstrate the mechanism in each of these cases, these findings are consistent with our observations using AAV and the model that retention of incoming virions at MTOC region during early infection limits transduction. Strikingly, some viruses may have evolved to overcome the MTOC retention by breaking MTs during their infection (Avitabile et al. 1995; Ploubidou et al. 2000; Schepis et al. 2006; Liu et al. 2010; Martin et al. 2010). For instance, HSV dismantle the MT-MTOC after entering the cells as one of the functions of viral protein ICP0 and deletion of ICP0 seems to limit viral infection (Liu et al. 2010).

Our current study raises an interesting question for future exploration, which is whether and how the endosomal vesicles at MTOC region may contribute to the transduction enhancement observed upon MT-MTOC disruption. A reasonable hypothesis is that at 6-8

hrs p.i., some viral particles observed at the MTOC region still remain inside the MT-localized endosomes/lysosomes (Ding et al. 2006; Xiao et al. 2012), while others have escaped the endosomes and directly associate with MTs. Direct interaction between MTs and the AAV capsid has been demonstrated previously (Kelkar et al. 2006). Both endosomal and escaped viral particles would be released from the MTOC region upon MT-MTOC disruption. Using AAV mutants with defects in the phospholipase (PLA) domain, we determined that MT-MTOC disruption was unable to rescue the impaired viral transduction of these mutants (data not shown), which suggests that MT-MTOC disruption does not promote the escape of AAV from endosomes. Furthermore, increased viral particles reaching the nucleus upon disruption of MT-MTOC are most likely the subset of virions that have escaped from endosomes and are directly associated with MTs. Those virions that failed to escape endosomes are not eligible for nuclear entry regardless of the integrity of MT-MTOC. This notion is consistent with our observation that the proportion of nuclear particles only increases from about 30% to 50%, potentially because about 30-40% of virions are still inside the endo/lysosomes at 8 hrs p.i. (Xiao et al. 2012). In the future, it will be interesting to investigate the potential role of endo/lysosomal vesicles on viral retention at the perinuclear region, which would add valuable information to the mechanism of this perinuclear phenomenon.

Actin filaments (AFs) and small Rho GTPases have been shown to be involved in viral infection including cell entry, cytoplasmic trafficking, and nuclear entry (Lehmann et al. 2005; Favoreel et al. 2007; Schelhaas et al. 2008; Ohkawa et al. 2010; Nonnenmacher et al. 2011). Recently, perinuclear and nuclear AFs were shown to associate with the nuclear envelope and nuclear pore complex, and were suggested to be involved in nuclear transport

of macromolecules and viral particles (Hofmann et al. 2001; van Loo et al. 2001; Minakhina et al. 2005; Broers et al. 2006; Favoreel et al. 2007; Schneider et al. 2008). In addition, AAV, as well as other viruses, has been suggested to utilize AFs to enter nucleus during an earlier stage of infection when MTs were disrupted (Xiao et al. 2012). Furthermore, the disruption of MTs leads to a RhoA-ROCK mediated rearrangement of AFs (Krendel et al. 2002; Chang et al. 2008). Consistent with these studies, our data show that AFs may facilitate the increase in nuclear entry through the RhoA-ROCK pathway upon MT-MTOC disruption (Fig.IV-6). Interruption of this pathway in the presence of intact MTs does not affect the level of viral transduction. This finding indicates that, at this time point, nuclear import of AAV by AFs only occurs upon the disruption of the MT-MTOC. It is possible that the AAV capsid has a much higher binding affinity for MTs than for AFs, and therefore remains associated with MT-MTOC. Moreover, the requirement of RhoA and ROCK activity indicates that MT disruption-induced alterations of AFs are necessary for the increase in viral nuclear entry and transduction. One possibility is that activated RhoA-ROCK results in more AFs connecting to the nuclear pore complex, which in turn transports more AAV particles into the nucleus. Further study of this mechanism will add more detail to current knowledge of viral nuclear entry as well as the biology of cellular cytoskeletons.

Although tremendous progress has been made in understanding the trafficking of AAV virions in cell culture, little is known about the trafficking pattern of this virus *in vivo*. This has limited one's ability to improve the efficiency of viral transduction for gene delivery in its natural environment. In this study, we examined the trafficking of AAV in mouse tissues including brain, liver, and xenografted tumors. In each of these tissues the viral particles accumulate at a perinuclear site, resembling our *in vitro* observations (Fig.IV-7).

Treatment with Nocodazole was able to disrupt the perinuclear retention of AAV and increase the viral transduction in all tissues tested (Fig.IV-8). Although further investigations are needed to refine the details of viral trafficking in these tissues, to our best knowledge, this is the first study to verify an *in vitro* trafficking pathway in *in vivo* settings. Additionally, the data showing that Nocodazole treatment can enhance AAV transduction in breast cancer cells indicates that there may be a synergistic effect between chemotherapeutic drugs, such as AMDs, and AAV-mediated gene therapy in treating cancer patients.

In summary, our current study examined the mechanism of perinuclear retention of the parvovirus AAV and the corresponding effects on viral infection. Our data demonstrated that perinuclear retention by MT-MTOC serves as a subcellular barrier and limits viral infection, specifically at the step of nuclear entry, providing a novel host defense mechanism to sequester incoming virions. Our observations with Ad and HIV suggest a similar mechanism is active during the infection of these viruses as well, expanding our findings to both non-enveloped and enveloped viruses. These studies may shed light on mechanisms of viral pathogenesis, especially under circumstances of MT disassembly during cell division and that of MTOC malfunction caused by misfolded-protein diseases or treatment with chemotherapy drugs. Moreover, further understanding the determinants on the virus responsible for perinuclear retention may also lead to novel strategies for the enhancement of vectors for gene delivery.

# CHAPTER 5

# CONCLUSIONS AND FUTHER EXPLORATIONS

## Summary of results

Gene therapy, an idea conceived several decades ago to introduce a functional copy of nucleic acid sequences into patients with genetically defects, is gaining momentum as a method to treat human diseases. AAV is a promising viral vector to deliver therapeutic genes. Like many other viruses, AAV has to interact with and travel through a variety of cellular organelles in order to successfully deliver its genetic material into host nucleus. Understanding how this virus transits from cell surface to deposit its genome in nucleus is the central research in AAV biology and vectorology. Importantly, understanding how nanoparticles travel through the cellular structures and how pharmacological reagents can affect viral trafficking is essential for the development of enhanced gene therapy vectors (Torchilin 2006; Breunig et al. 2008). For instance, attenuating the barriers of viral trafficking or designing capsid with enhanced ability to penetrate these barriers will offer promising opportunities to improve current vectors for gene therapy. Consequently, development of therapeutic delivery vectors has concentrated on pharmacological reagents and vector variants that affect these pathways (Duan et al. 2000; Maheshri et al. 2006; Asokan et al. 2009; Yang et al. 2009). In this dissertation, we have sought to establish a reliable methodology to effectively study the vector trafficking (chapter-2), study the role of

MTs on AAV trafficking (chapter-3), and finally highlighted a novel trafficking barrier during AAV infection (chapter-4). Using our quantitative 3D microscopy as well as other experimental tools, we determined that after internalization AAV particles inside endosomes migrate on MTs toward perinuclear region and its nuclear entry is then restricted by MTOC retention, illustrating the fine tuning of AAV infection by MT system (Fig.V-1).

Effective achievement of such efforts requires quantitatively evaluating the biological effect(s) of those reagents or vector variants on these complex trafficking routes and bio-distribution of delivery vehicles. In chapter-2, based on recent advances with computational image processing(Sedarat et al. 2004; Feng et al. 2007), we developed a sensitive and reliable methodology by integrating single particle imaging and 3D quantification into classical immunofluorescence to quantitate the trafficking kinetics and bio-distribution of nanoparticles in three dimensional animal cells and tissues. Using Cy5-labeled AAV as a working model, we quantitatively investigated the nuclear entry kinetics and bio-distribution of AAV2 in human cells and mouse tissues. We uncovered an as yet uncharacterized rate-limiting step during viral cell entry, while delineating nuclear accumulation of virions during the first 8hrs post-infection. Additionally, our studies revealed for the first time that following intramuscular injection, AAV spread progressively across muscle tissues through endomysium between myofibers instead of traversing through target cells. This observation supports a hypothesis that, unlike in cultured cells, viral particles *in vivo* can persist in myofibers potentially providing a temporal reservoir of virus. These virions may traffic to the nucleus and contribute to viral transduction at later times (over 2 weeks), which also could be an explanation to the observed AAV transduction profile in muscle (Fisher et al. 1997; Chao et al. 2000) . These findings both support the current working knowledge of AAV biology

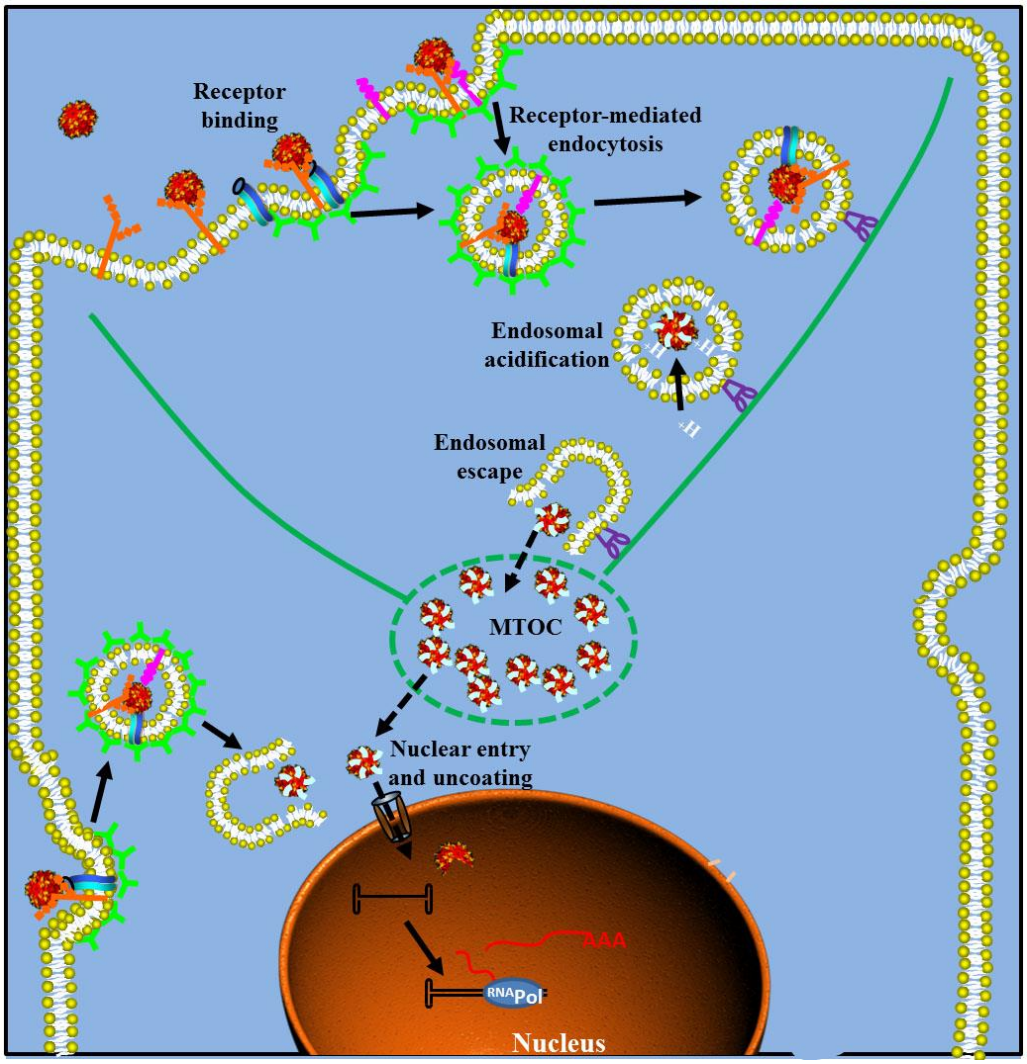


**Figure V-1. Updated scheme for AAV trafficking.** After binding to the heparan sulfate proteoglycan (HSPG) on cell surface, AAV2 interacts with cell surface receptors (i.e. integrin and FGFR) and is internalized through clathrin-dependent and independent endocytosis. After binding and endocytosis on cell surface, AAV2 virions may take two possible trafficking routes towards the nucleus. Route I: For these internalized at sites distal from the nucleus, virions migrate on MT tracks in endosomes to traverse the dense cytoplasm towards peri-nuclear region of host cells. Route II: For these internalized at sites close to the nucleus, virions in endocytic vesicles can reach the nucleus by slower MT-independent migration through the cytoplasm between the cytoplasmic membrane and nuclear envelope. For both routes, acidification of AAV2 containing endosomal compartment happens at the peri-nuclear region and allows the escape of viral particles from vesicles, a pre-requisite step for nuclear entry. After cytoplasmic trafficking, most virions are retained by MT-MTOC, which restricts the nuclear entry of viral particles. Nuclear entry of viral genome is regarded as an essential event for successful AAV transduction. Currently, it remains unclear whether nuclear entry is through the nuclear pore complex or other routes. It is also unknown when and where and how genome uncoating takes place.

and provide a better mechanistic insight into the behavior of this viral vector *in vitro* and *in vivo*. This study demonstrates the potential of this methodology in screening pharmacological reagents and vector variants for the development of therapeutic-material delivery strategies, as well as in understanding the intracellular behavior of delivery viral vectors *in vitro* and *in vivo*.

Cytoplasmic trafficking is critical for most DNA viruses to approach the peri-nuclear region and deposit their genomic DNA in the nucleus of host cells. Previous studies have demonstrated that either actin filaments or microtubules (MTs) are exploited by various viruses to traverse the dense cytoplasm. For AAV, the exact mechanism of cytoplasmic trafficking of this virus remains unclear, due to previous reports that are diametrically opposite in their conclusions (Sanlioglu et al. 2000; Kelkar et al. 2006; Hirosue et al. 2007). In chapter-3 we have studied the role of MTs on AAV2 transduction and extensively investigated the underlying mechanisms regarding how MTs contribute to viral infection using various pharmacological and microscopy tools. Our data from live cell imaging and flow cytometry analysis have determined the involvement of MTs in AAV2 infection, and the data from quantitative 3D microscopy and quantitative PCR analysis have demonstrated that intact MT network is required for the nuclear targeting of AAV but not for cell surface attachment or endocytosis of this virus. In this study, for the first time we have determined that the migration of AAV2 on MT tracks are fast (up to 1.5-3.5 μm/s) which is consistent with dynein-mediated trafficking and are uni-directional which is different from the bi-directional motion of Ad or HSV on MTs. In addition, our study using electron microscopy and pharmacological experiments is the first one to suggest that AAV traffics on MTs in endosomes and acidification of these structures is dependent on intact MT network. The

findings herein strongly support an as yet undocumented model in which after internalization, AAV2 exploits MTs for fast and uni-directional trafficking in endosomal compartments towards peri-nuclear region where most viral acidification events take place. Furthermore, our findings that MT disruption never completely blocks AAV2 transduction suggest the existence of an alternative MT-independent trafficking pathway for this virus. These data together with earlier studies support a model of AAV2 trafficking during its early infection procedure (Fig.III-13, (Sanlioglu et al. 2000; Douar et al. 2001; Ding et al. 2006; Johnson et al. 2010)).

Like many other viruses (e.g. Ad, HSV, HIV, influenza, parvoviruses), after MT-mediated cytoplasmic trafficking, AAV particles accumulate at the perinuclear region. However, it remains unclear regarding whether and how this accumulation affects viral infection. Two plausible hypotheses are (Wileman 2007): 1) viruses exploit the cellular protein-trafficking machineries to approach the replication site or to concentrate viral components for viral replication and later virion assembly, thus supporting viral infection; 2) perinuclear accumulation represents an innate cellular response that recognizes virus components as foreign or misfolded proteins and targets them for sequestration and degradation at the perinuclear region, thus interfering with viral infection. In chapter-4, we test the hypothesis that perinuclear accumulation is a cellular defense mechanism to sequester virions in order to limit the infection of both enveloped virus (HIV) and non-enveloped viruses (Ad and AAV). In this study, we first demonstrate that, similarly to Ad and HIV, parvovirus AAV's perinuclear localization is maintained by microtubules at the microtubule-organization center (MT-MTOC). Disruption of this structure after viral entry leads to increased susceptibility to infection of rAAV, rAd, and lentivirus. We further used AAV as a

study model and fluorescent microscopy and molecular analyses as experimental approaches to study the underlying mechanisms. The results suggest that the proportion of viral particles entering the nucleus increases following MT-MTOC disruption and that this enhancement is dependent on the AAV capsid's nuclear import signals, indicating the involvement of a nuclear trafficking pathway. Interestingly, after knocking down RhoA or inhibiting its downstream effectors (ROCK and Actin), MT-MTOC disruption did not increase viral transduction or nuclear entry. These data suggest a two-step mechanism for the enhancement of infection: 1) release of viral particles from the perinuclear site upon MT-MTOC disruption, and 2) increased trafficking to the nucleus via the RhoA-ROCK-Actin pathway. Furthermore, we extended the AAV studies *in vivo* and observed that viral transduction of brain, liver, and xenografted tumor tissues was enhanced up to 10-fold by disruption of the MT-MTOC, indicating a similar trafficking mechanism *in vivo*. In summary, this study for the first time experimentally demonstrates that perinuclear accumulation of incoming virions at the MT-MTOC is a barrier limiting the infection of most nuclear viruses and more specifically restricting the nuclear entry of AAV, defining a novel defense mechanism by which host cells restrain viral invasion.

All in all, our studies documented in this dissertation, through three chapters (chapter 2-4), create a robust microscopy method for viral trafficking and exploit this method together with other experimental tools to dissect the intracellular trafficking of AAV in detail. Briefly, in chapter-2, by exploiting recent advances with computational image processing and fluorescence labeling, we developed a sensitive and reliable methodology by integrating single particle imaging and 3D quantification into classical immunofluorescence to quantitate the trafficking kinetics and bio-distribution of nanoparticles in three dimensions. The

associated studies demonstrate the potential of this methodology in screening pharmacological reagents and vector variants for the development of therapeutic-material delivery strategies, as well as in understanding the intracellular behavior of delivery viral vectors *in vitro* and *in vivo*. In chapter-3, we employed the 3D quantitative microscopy together with multiple other techniques including confocal microscopy, live cell imaging, single particle tracking, electron microscopy, and pharmacological analysis to examine the role(s) of MTs during AAV infection and to investigate the underlying mechanisms in detail. Besides providing a comprehensive understanding of the role of MTs on AAV trafficking, the findings in the study also suggest an as yet undescribed model in which after internalization, AAV2 exploits MTs for rapid cytoplasmic trafficking in endosomal compartments uni-directionally towards peri-nuclear region where most acidification events for viral escape take place. In chapter-4, we investigated the role and mechanism of perinuclear accumulation of AAV, a subcellular event that is subsequent to the MT-mediated cytoplasmic trafficking documented in chapter-3 and is associated the nuclear entry. In this study, we experimentally demonstrates that perinuclear MT-MTOC retains incoming virions and serves as a barrier to limit the infection of most nuclear viruses and more specifically restrict the nuclear entry of AAV, suggesting a novel host defense mechanism against viral invasions. Our above studies will advance the current model of AAV infectious pathway by adding the roles of MTs into the trafficking picture (Fig.V-1). I personally believe the work described in this dissertation have advanced our knowledge in AAV biology and vectorology, as well as provided some critical insights for several research fields including virology, cell biology, biophysics, and gene therapy.

## Unpublished data and future directions

Our above studies demonstrate the roles of MTs on AAV trafficking and transduction in the host cells. It should be noticed that these studies mostly focused on the behavior of AAV particles during the interphase of cultured cells. Although AAV is not a popular vector for gene delivery into the dividing cells in our body, it is yet a quite interesting question whether and how MTs may play roles on AAV trafficking during cell division. The MT dynamics is critical to the mitotic process as evidenced by the appearance of high tubulin turnover in MTs during mitosis. During prophase, the long interphase MTs start to disappear and are replaced with astral MTs, the major component of the spindle. These mitotic MTs nucleated from the centrosomes are more numerous, shorter, and less stable than interphase ones. Typically, the average lifetime of a MT diminished from about 10 minutes in interphase cells to roughly 30 seconds in the mitotic spindle. To study whether such change in MT dynamics will alter the trafficking or distribution of viral particles in host cells, we observed Cy5 labeled AAV in mitotic cells (Fig.V-2). In mitotic cells, most virions are associated with MTs especially those at the mitotic spindle that are ‘corresponding’ to the MTOC in the interphase cells. However, a surprising observation is that a lot of virions are not confined to the perinuclear region in the mitotic cells, differing from our previous results in interphase cells where most of the virions are retained at the perinuclear MTOC region (Fig.V-2b, 2d, 2e). An immediate question is how these virions that originally localized at the perinuclear region spread out into the cytoplasm. One possible mechanism could be that these unstable and highly dynamic mitotic MTs are less efficient to hold viral particles at the perinuclear region. It is also known that the nuclear envelope will be dissolved during prometaphase, a stage that is exploited by some retroviruses to import viral materials into the nucleus. As a result, another interesting

hypothesis is that host cells utilize MTs to temporally move virions away from the perinuclear region to reduce the opportunistic nuclear entry of AAV particles when nuclear envelope is broken down during cell division. In this case, a positive-end MT motor like kinesin may mediate the movement of AAV on the MTs away from the perinuclear region. While addressing this question will not necessarily be directly relevant to the vector development, it may advance our knowledge on AAV biology, especially the interaction between this virus and its host.

Interestingly, in chapter-3, we notice that AAV2 particles in a much smaller proportion were still detected in the nucleus of Nocodazole-treated cells (Fig.III-7). This is consistent with the observation in reporter gene (GFP) assay that AAV2 was still able to transduce cells in the absence of MTs, though in a reduced level compared with control cells (Fig.III-1). One possibility for this observation is related to the inefficient MT-independent trafficking of virions. Under this scenario, AAV2 particles could be internalized in the cell membrane close to the nucleus, where the virions only have to traverse a small distance to reach the nucleus (Fig.III-13 and (Leopold et al. 2006)). Movements over such short distance (several microns) might be achieved by normal diffusion (Fig.III-13, V-1). Internalization in the sites around nucleus can be achieved by the direct binding of viral particles at these sites or viral surfing on cell membrane to these sites (Neumann et al. 2008). Current work does not exclude the possibility that AAV2 particles may reach the nucleus through a much slower process by exploiting actin filaments or intermediate filaments (Ohkawa et al. 2010; Schuh 2011). It is not uncommon for viruses to exploit multiple pathways to ensure productive infection. Further explorations are needed to validate these putative pathways and may bring new insights into the infectious pathway of AAV particles.

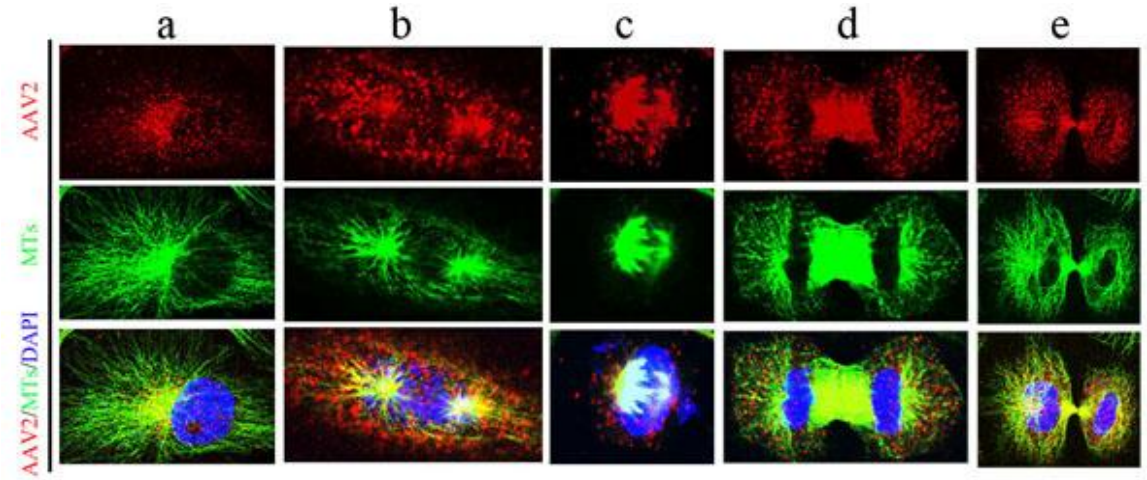


**Figure V-2. Peri-nuclear localization of AAV2 requires intact MTs and associated with MTs throughout cell cycle.** 8hrs after incubation with AAV, cells were fixed and stained with α-tubulin antibody for MTs (green), Giatin antibody for Golgi (Cyan), and DAPI for Nuclei (blue). A) Hela cells were pulse infected with Cy5-AAV2 (red) and drugs were administrated at 7-10hrs after infection. Upper panel: Disruption of Golgi apparatus by Brefeldin A did not ablate the peri-nuclear localization of AAV2 particles. Lower panel: Peri-nuclear localization of AAV2 was ablated by the disruption of intact MTs using Nocodazole (30 μM). B) AAV2 is associated with MTs throughout all stages of cell cycle. Hela cells were pulse infected with Cy5-AAV2 (red) and fixed at 6hrs after pulse infection. Confocal images were taken to examine the distribution of viral particles at various stages of cell cycle: a) interphase, b) prometaphase, c) metaphase and anaphase, d) telophase, e) post-telophase.

After internalized, AAV has to traffic through a variety of endocytic vesicles, including early endosome, late endosome, recycling endosome, and so on. Dr. John Engelhardt's group and others reported that AAV particles were found in various endosomes and might take different endosomal trafficking routes at different viral dosages (Douar et al. 2001; Ding et al. 2006). However, the details about AAV trafficking in endosomes remain unknown. A previously debating issue is whether AAV escapes from early endosomes or late endosomes, both of which are supported by literatures (Bartlett et al. 2000; Douar et al. 2001; Ding et al. 2006). For its helper viruses like Ad and HSV, the virions escape from early endosomes before their migration on the MTs (Dodding and Way 2011; Engelke, Burckhardt et al. 2011; Radtke, Kieneke et al. 2011). Our studies in chapter-3 demonstrate that AAV does not escape from endosome until it finishes MT trafficking from cell periphery to perinuclear region where most endosomal acidification takes place and late endosomes localized (Mellman, Fuchs et al. 1986; Lakadamyali, Rust et al. 2003). This is in concert with the notion that endosomal acidification is required for AAV escape and supports that AAV escape from acidic late endosomes. To further look into the details regarding how AAV particles transit between different endosomes, we used confocal microscopy to lively track the viral particles in cells expressing fluorescence protein fused Rab proteins (Fig.V-3). At perinuclear region, an AAV virion is observed to reside in a Rab5-associated early endosome and then transit into a Rab7-associated endosome. This transition seems to be really fast as it only takes about 10 seconds. This also supports the notion that AAV particles escape from the late endosomes instead of early ones.

It should be noted that our current data does not exclude the possibility that some AAV2 can escape from the early endosome as an alternative pathway in the cells. Given that

cytoplasmic dynein can directly bind to AAV2 capsid *in vitro* (Kelkar et al. 2006; Zhao et al. 2006), it will be of particular interest in the future to identify and mutate the dynein binding sites on AAV2 capsid and further investigate the trafficking of these mutant AAVs. There might be of some interest to study whether the rapid-directed motion of AAV2 is mediated by the dynein associated with endosomes or that directly associated with viral capsid. It is known that AAV2 is internalized through clathrin-dynamin mediated pathway into endosome compartments (Duan et al. 1999; Bartlett et al. 2000).While we were not able to definitively determine dynein interaction with AAV-containing endosome *vs* capsid specifically, our data strongly supports the usage of this motor in fast-directed movement of AAV. Interestingly, some dynactin subunits like p62 were demonstrated to have a minimal impact on dynein-mediated functions and suggested to be dispensable for the function of dynactin complex (Quintyne et al. 1999; Schroer 2004). More importantly, recent studies have begun to demonstrate that dynein can directly bind to the pathogen-related cargos and suggest that dynactin may be dispensable especially for the dynein-mediated pathogen trafficking (Grieshaber et al. 2003; Schroer 2004; Bremner et al. 2009). Careful and sophisticated investigations will be required to address the issues regarding whether and how the dynactin complex contributes to the MT-mediated AAV2 trafficking.

Our observations in this dissertation also raise an interesting question for future exploration, which is how and when the AAV particles escape from endosomal vesicles at perinuclear MTOC region. How this mechanism may contribute to the transduction enhancement observed upon MT-MTOC disruption. A reasonable hypothesis is that at 6-8 hrs p.i., some viral particles observed at the MTOC region still remain inside the MT-localized endosomes/lysosomes (Ding et al. 2006; Xiao et al. 2012), while others have

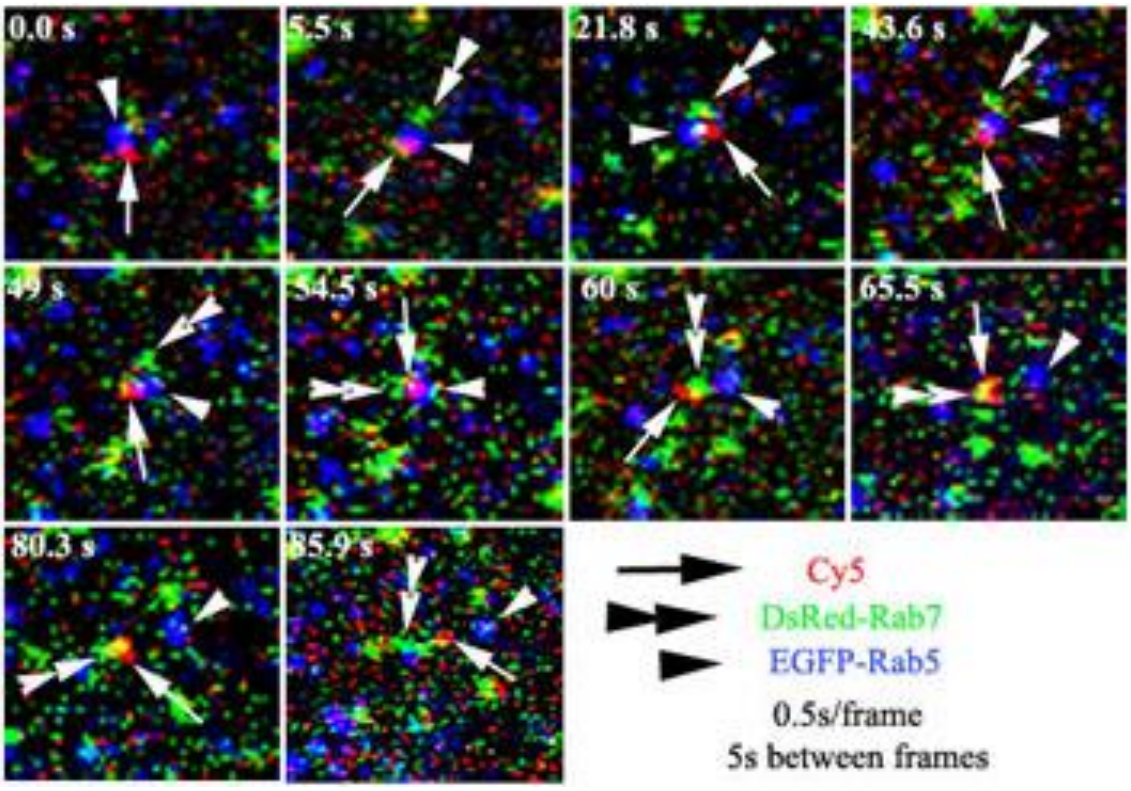


**Figure V-3. Transition of AAV particles from early endosome to late endosome.** Video from zeiss510 confocal microscopy was captured at 0.5s per frame and 5s between two frames. Selected frames with indicated time point are displayed. AAV particles are visualized by Cy5 fluorescence (red, arrow), early endosomes are visualized by EGFP fused Rab5 (blue, arrowhead), and late endosomes are visualized by DsRed fused Rab7 (green, double arrowhead).

escaped the endosomes and directly associate with MTs. Direct interaction between MTs and the AAV capsid has been demonstrated previously (Kelkar et al. 2006). Both endosomal and escaped viral particles would be released from the MTOC region upon MT-MTOC disruption. Using AAV mutants with defects in the phospholipase (PLA) domain, we determined that MT-MTOC disruption was unable to rescue the impaired viral transduction of these mutants, which suggests that MT-MTOC disruption does not promote the escape of AAV from endosomes. Furthermore, increased viral particles reaching the nucleus upon disruption of MT-MTOC are most likely the subset of virions that have escaped from endosomes and are directly associated with MTs. Those virions that failed to escape endosomes are not eligible for nuclear entry regardless of the integrity of MT-MTOC. This notion is consistent with our observation that the proportion of nuclear particles only increases from about 30% to 50%, potentially because about 30-40% of virions are still inside the endo/lysosomes at 8 hrs p.i. (Xiao et al. 2012). In the future, it will be interesting to investigate the potential role of endo/lysosomal vesicles on viral retention at the perinuclear region, which would add valuable information to the mechanism of endosomal trafficking and perinuclear accumulation.

Both Golgi and MTOC are perinuclear structures that coincidentally colocalize at the perinuclear region with many viruses (Sodeik et al. 1997; Dohner et al. 2002; Mani et al. 2006; Yea et al. 2007; Boisvert et al. 2010; Liu et al. 2012). However, prior to this work, it remained unclear which cellular structure maintains perinuclear accumulation of AAV. Earlier studies have suggested that the perinuclear viral particles co-localize to the Golgi apparatus (Johnson et al. 2010; Nonnenmacher et al. 2011). Another study suggests that these virions may co-localize with the MTOC (Johnson et al. 2011). In chapter-4, we determined

that it is MT-MTOC but not the Golgi that co-localize with and retain the AAV particles at perinuclear region. Consistent with our findings, many other viruses including Ad, HSV, and HIV have also been shown to move on MTs to the MTOC region and associated with MT-MTOC (Sodeik et al. 1997; McDonald et al. 2002; Bailey et al. 2003; Fackler et al. 2006; Greber et al. 2006; Leopold et al. 2006; Yea et al. 2007). Our observation that only a small portion of viral particles co-localized with the dispersed Golgi cisternae which are released from highly packed MTOC region upon MT-MTOC disruption further suggests that few particles physically localize in the Golgi apparatus. Consistent with previous reports, we did find disruption of the Golgi apparatus at an earlier time during infection can impair AAV transduction. These data indicate that the Golgi does play a role in viral infection, probably through viral capsid modifying critical for viral infection, but is dispensable for perinuclear retention of incoming virions. Further investigation of the exact role of the Golgi apparatus on the infection of AAV and other viruses may advance our current knowledge of virology.

Actin filaments (AFs) and small Rho GTPases have been shown to be involved in viral infection including cell entry, cytoplasmic trafficking, and nuclear entry (Lehmann et al. 2005; Favoreel et al. 2007; Schelhaas et al. 2008; Ohkawa et al. 2010; Nonnenmacher et al. 2011). Recently, perinuclear and nuclear AFs were shown to associate with the nuclear envelope and nuclear pore complex, and were suggested to be involved in nuclear transport of macromolecules and viral particles (Hofmann et al. 2001; van Loo et al. 2001; Minakhina et al. 2005; Broers et al. 2006; Favoreel et al. 2007; Schneider et al. 2008). In addition, AAV, as well as other viruses, has been suggested to utilize AFs to enter nucleus during an earlier stage of infection when MTs were disrupted (Xiao et al. 2012). Furthermore, the disruption of MTs leads to a RhoA-ROCK mediated rearrangement of AFs (Krendel et al. 2002; Chang

et al. 2008). Consistent with these studies, our data show that AFs may facilitate the increase in nuclear entry through the RhoA-ROCK pathway upon MT-MTOC disruption (Fig.IV-6). Interruption of this pathway in the presence of intact MTs does not affect the level of viral transduction. This finding indicates that, at this time point, nuclear import of AAV by AFs only occurs upon the disruption of the MT-MTOC. It is possible that the AAV capsid has a much higher binding affinity for MTs than for AFs, and therefore remains associated with MT-MTOC. Moreover, the requirement of RhoA and ROCK activity indicates that MT disruption-induced alterations of AFs are necessary for the increase in viral nuclear entry and transduction. One possibility is that activated RhoA-ROCK results in more AFs connecting to the nuclear pore complex, which in turn transports more AAV particles into the nucleus. Further study of this mechanism will add more detail to current knowledge of viral nuclear entry as well as the biology of cellular cytoskeletons.

Nuclear entry is regarded as the most critical and rate-limiting step for the life cycle of most DNA viruses (e.g. adenovirus, herpesvirus and parvovirus) (Whittaker et al. 2000; Greber et al. 2009). Blocking the nuclear entry is an alternative way to block viral replication (Haffar et al. 2005; Boulo et al. 2007; Hindley et al. 2007; Greber et al. 2009), and on the other hand, facilitating the nuclear entry of viruses has been a promising strategy to improve viral vectors for gene delivery (Hansen et al. 2000; Suzuki et al. 2007; Johnson et al. 2008; Mudhakir et al. 2009). Several groups have suggested that AAV entered nucleus as intact virions (Bartlett et al. 2000; Sonntag et al. 2006; Johnson et al. 2008). In chapter-2, while characterizing the kinetics of AAV nuclear targeting, in dose response studies, the number of virions in the nucleus does not increase linearly with the number of nuclear membrane associated virions at 2hrs p.i. (Fig.II-10D). This result suggests that there may be limited

sites/routes for AAV2 nuclear entry through the nuclear membrane, and provides a sound explanation for the observation that the fold increase in virion dosage does not translate to equivalent fold increase in transduction (Fig.II-11).

Nuclear pore complex (NPC) is designed for the transportation of cellular materials into and out of nucleus, and is also exploited by many viruses to deposit their genetic materials in the nucleus. Both NPC-dependent and independent pathways have been proposed and reported for the nuclear entry of DNA viruses. The strong association of virus particles with MT structures throughout the cell cycle suggests that AAV is unlikely to exploit the breakdown of nuclear envelope during mitosis (Fig.V-2). In figure V-4, we first tested the co-localization between AAV2 and NPC. Viral particles were co-localized with NPC and representing virions were highlighted by arrowheads in figure V-4. Consistently, our electron microscopy (EM) data also demonstrate the close association between AAV2 particles and NPC (Fig.V-4B). It was previously demonstrated that while docking at the NPC to release the genome, HSV interacts with the cytoplasmic filaments (30-50 nm in length) and typically sits about 40-80 nm away from the luminal spoke rings of the NPC (Peng et al. 2010). Our EM image suggests an interaction between AAV2 and cytoplasmic filaments for the viral access to the nuclear pore (Fig.V-4B, C). Further we used a recent established 3D microscopy method to study the localization between AAV2 and those NPCs on nuclear envelope in the DMSO or Nocodazole treated cells. In DMSO-treated cells, more viral particles were associated with the NPCs close to the peri-nuclear viral accumulation site than with those at the distal site. In contrast, viral particles evenly co-localized with NPCs across the entire nuclear membrane in Nocodazole treated cells (Fig.V-4D).

Both our confocal fluorescence imaging and electron microscopy data demonstrate the association of AAV particles with NPC, indicating the potential involvement of NPC in viral nuclear entry. Although the diameter of the opening of NPC is about 9nm compared to 20nm-sized AAV particles, it has been suggested that the pore can be dilated up to 26nm which would potentially allow for the nuclear import of AAV (Dworetzky et al. 1988). In addition, the increased association of AAV2 particles we observed with NPC especially at distal site of MTOC after disruption resulted in both enhancement of viral nuclear entry consistent with the barrier hypothesis. Although a previous study using isolated nuclei suggested that nuclear pore is not required for the nuclear entry of AAV2 virions (Hansen et al. 2001), this premise has not been formerly tested in intact cells. In addition, other DNA viruses have been shown to deliver viral genomes into the nucleus through NPC (Greber et al. 1997; Ojala et al. 2000), so it remains to be determined what contribution the NPC may play in the nuclear entry of AAV in intact cells. Examination of the roles of nuclear import machinery on AAV transduction and nuclear entry is essential. Better understanding the mechanism of viral nuclear entry could potentially increase our ability to improve vector performance by either manipulating the cellular machinery for nuclear import or designing better capsids.

Another important but under-studied research direction is the trafficking of AAV particles in animal tissues. Although tremendous progress has been made in understanding the trafficking of AAV virions in cell culture, little is known about the trafficking pattern of this virus *in vivo*. This has limited one's ability to improve the efficiency of viral transduction for gene delivery in its natural environment, as the *in vivo* setting provides the most applicable information for the development of efficient gene delivery vectors. However,

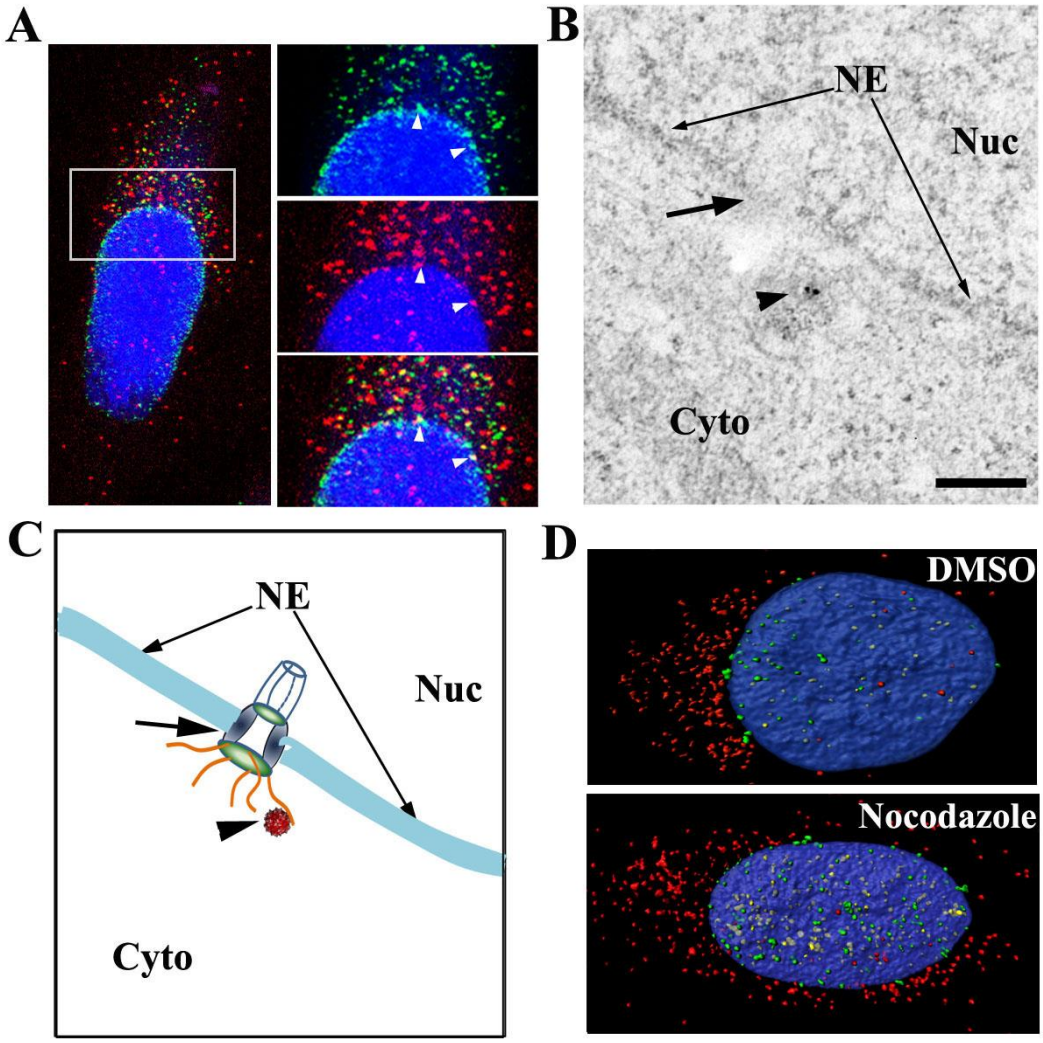


**Figure V-4. AAV2 co-localizes with nuclear pore complex (NPC) and disruption of viral accumulation at MTOC results in viral access to the NPC distal from this region.** A) Confocal image showing colocalization between NPC (green) and Cy5-AAV2 (red) at 6hrs after pulse infection. Nuclei were stained with DAPI (blue). In the magnified right panel, viral particles co-localized with NPC were highlighted by arrowheads. B) Electron microscopy graph showing the close association between AAV2 particles (labeled with nanogold, arrowhead) and NPC (indicated by arrow as a discontinuous region on nuclear envelope, short for NE)., Cyto: cytoplasm, Nuc: nucleus. Bar represents 200 nm. C) A cartoon illustrates the content in B. AAV particle is associated with NPC through the cytoplasmic filaments (in orange) of the pore complex. D) At 6hrs p.i., AAV2 access to the NPCs that mostly locate on nuclear envelope next to the peri-nuclear viral accumulation in DMSO treated cells (upper panel). At 1-1.5hrs after Nocodazole treatment, virions are evenly co-localized with NPCs across the entire nuclear envelope. Cy5-AAV2 in red, those inside the nucleus are in yellow, and those co-colocalize with NPC on nuclear envelope are highlighted as green. Nuclei were stained with DAPI (blue).

studying viral trafficking is an extremely challenging task with current experimental tools.

By employing the newly established imaging method described in chapter-2, we have attempted to study the distribution of AAV2 particles in animal tissues and made several intriguing discoveries. In chapter-2, we for the first time showed that the AAV2 particles were localized at the injection site during the first 30 minutes and then uniformly spread through tissues up to three muscle fibers away from the injection site over 4hrs (Fig.II-12B). This result is significant in that it allows one to correlate viral spread with expression and should provide insight into vector tropism when studying capsid variants specific for muscle or various tissues such as brain and eye (Kessler et al. 1996; Fisher et al. 1997; Gregorevic et al. 2004; Sun et al. 2005; Wang et al. 2005). We also addressed the question how the viruses traffic to the cells distal from the injection site (Kessler et al. 1996; Fisher et al. 1997; Gregorevic et al. 2004; Sun et al. 2005; Wang et al. 2005; Di Pasquale et al. 2006) by showing that most AAV2 particles traffic through the endomysium between muscle fibers instead of traversing through myofibers as proposed by previous studies (Bomsel et al. 2003; Di Pasquale et al. 2006; Bhat et al. 2007). Additionally, at 6 days after injection, AAV2 particles were also detected inside of the muscle fibers/cells (Fig.II-12C). This observation supports a hypothesis that, unlike in cultured cells, viral particles *in vivo* can persist in myofibers potentially providing a temporal reservoir of virus. And these virions may traffic to the nucleus and contribute to viral transduction at later times (over 2 weeks), which also could be an explanation to the observed AAV transduction profile in muscle (Fisher et al. 1997; Chao et al. 2000). In chapter-4, we briefly examined the trafficking of AAV in several mouse tissues including brain, liver, and xenografted tumors. Our study show that AAV also experiences perinuclear accumulation resembling our *in vitro* observations and disruption of

this perinuclear retention increases the viral transduction in all tissues tested. Although further investigations are needed to refine the details of viral trafficking in these tissues, to our best knowledge, this is the first study to verify an *in vitro* trafficking pathway in *in vivo* settings.

It is an interesting question how AAV particles traffic in brain tissue, particularly the shuttling between different brain regions (e.g. from Thalamus to Cortex or Substantial Nigra (SN); from Striatum to Cortex, Thalamus, or SN). It is proposed that such trafficking is mediated by axonal antegrade or retrograde transportation. We have also studied the trafficking of AAV in rat cerebrum after striatum injection (Fig.V-5). At 1hr after viral injection, while most virions are remain at the injection site, many particles spread out into the brain tissue and distributed in a gradually reduced density as the distance from injection site increases. At 24hrs, virions start to accumulate at the perinuclear region of neuronal cells within regions at various distances from injection site except the region that is immediately next to the injection site. This observation implies that the virions can reach the cells right next to the injection site through a MT-independent route, but may have to migrate on MTs in the axons to reach those neurons that are away from the injection site. It is likely that the axonal mediated retrograde transportation is exploited by AAV to infect those cells that localized away from the virion reservoir. However, we didn't find any viral particles at SN, a distal site from the injection site. This does not necessary mean that the axonal mediated retrograde transportation from Striatum to SN is not utilized by AAV. A likely explanation could be that the sensitivity of tissue imaging is insufficient to detect viral particles at low abundance in SN. The axonal mediated transportation is also varying among different AAV serotypes. More investigations are needed to better understand the AAV trafficking

mechanism in brain, which shall greatly advance our knowledge on the application and development of this vector for neuronal gene delivery.

Both fluorophore labeling and fluorescent imaging are the mainstay in understanding the virus and host interactions, especially the trafficking of virions in host cells. In chapter-2, we described a quantitative 3D microscopy to study viral trafficking and distribution both *in vitro* and *in vivo*. The data acquired in our study was not limited by traditional light microscope and incorporation of deconvolution technique improves the contrast and resolution of digital images by correcting image distortions, making the fluorescence images suitable for quantitative measurement. In the future, super-resolution microscopes (e.g. STORM, STED, PALM) shall provide additional means to improve the quantification of fluorescence images (Huang et al. 2008; Huang et al. 2009). At the moment, these super-resolution microscopes typically require longer time to capture images and access is limited for most virology labs. For further studying the distribution of viral particles in tissues, two-photon microscopy will enable this method to deal with much thicker tissues by providing larger imaging depth.

In summary, with the studies documented in this dissertation, we have refined the protocols for vector preparation and purification, advanced current methodologies to study the virus-host interactions, and provided an approach to effectively evaluate the effects of pharmacological reagents or vector variants on the delivery efficiency of viral vectors in cultured cells as well as animal tissues. In addition, studies on MT-mediated cytoplasmic trafficking of AAV have advanced our understanding of AAV trafficking dynamics and elaborated the roles of cellular machinery specifically MTs and MT-associated structures on AAV transportation and infection. Furthermore, our study has also identified

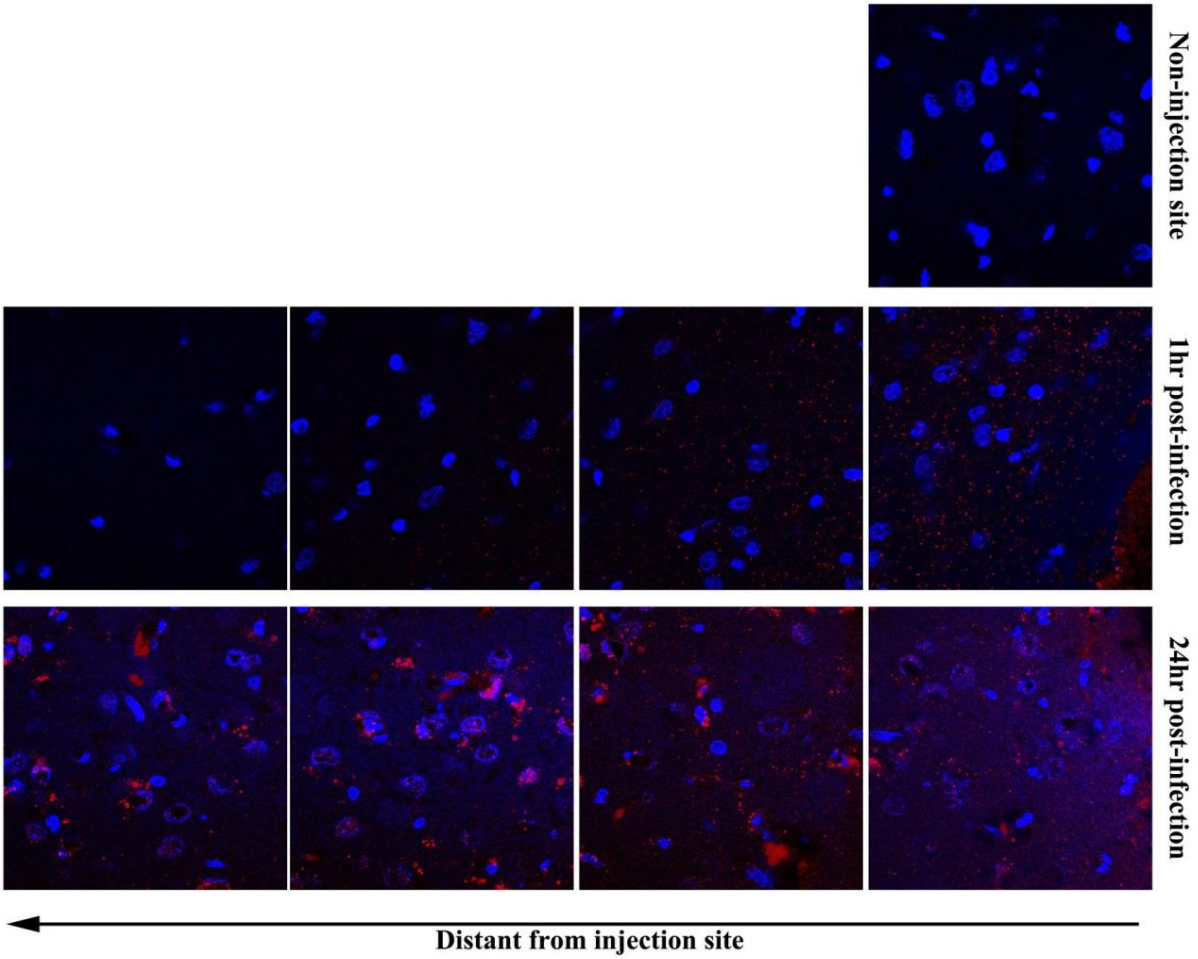


**Figure V-5. AAV trafficking in rodent cerebrum.** Viral particles are visualized by Cy5 fluorescence and nuclei are visualized by DAPI signal. Top panel is micrograph of a control slide without viral injection. Middle panel is the distribution of AAV particles at various distances from injection site at 1hr after viral inoculation. Bottom panel is the distribution of AAV particles at various distances from injection site at 24hr after viral inoculation. Right side is most close to the injection site and left side is most distant from the injection site.

perinuclear retention as a novel subcellular barrier that limits AAV infection, specifically at the step of nuclear entry, which provides a new host defense mechanism to sequester incoming virions. Altogether, these studies may shed light on mechanisms of viral pathogenesis especially under the circumstances of MT disassembly during cell division and that of MTOC malfunction caused by misfolded-protein diseases or treatments with chemotherapy drugs. Further understandings of the determinants on the virus responsible for perinuclear retention may also facilitate the development of viral variants with enhanced delivery efficiency using rational design. Lastly, this work has significantly advances our knowledge regarding the trafficking of AAV2 particles in animal tissues, the natural environment of this virus.

This dissertation provides valuable research tools, rationales, and assays for future exploration of the details of AAV trafficking. It is my personal prediction that such exploration shall focus on the details of endosomal trafficking, cytoskeleton-mediated cellular trafficking, nuclear importation, intra-nuclear processing of virions, as well as the associated determinants on AAV capsid. Meanwhile, validating trafficking pathways *in vivo* shall draw the attention of the research community as such information is more critical to enhance the performance of AAV vector for gene therapy. I sincerely believe that the comprehensive combination of multi-principle methodologies including those in cell biology, virology, biophysics, chemistry, applied math, statistics, and pharmacology will pickup the power in advancing the field of vector research and development.

## APPENDICES: PLASMIDS

### For production of AAV virions

TR-promoter-gene, the vector plasmid provides the transgene cassette flanked by TRs at both ends to be packaged into the virions. Plasmid ‘pTR-CBA-ssDNA’ (map provided in Fig.S-1) provides a single stranded genomic DNA to be packaged in the virions, and plasmid ‘dsEMBL-TR-CMV-EGFPsc’ (map provided in Fig.S-1) provides a self-complementary genomic DNA to be packaged in the virions.

pXR(s), packaging plasmid expresses the viral proteins (Rep78/68/52/40 and VP1/2/3) that are essential to make virions. Plasmid ‘pXRs’ (map provided in Fig.S-2) contains a ‘Rep’ coding sequence from serotype-2 and a ‘Cap’ coding sequence from various serotypes. The ‘Rep’ coding sequence encodes all the essential ‘Rep’ proteins as non-structural proteins for virion production. The ‘Cap’ sequence encodes the structural proteins to make virions and thus determines the serotype of virions made from the ‘pXRs’ plasmid.

HEK-293 (ATCC, cat. no. CRL-1573, provides E1a and E1b) and plasmid pXX680 (provides E2a, E4, and VA) together to provide Ad helper function for the expression of AAV proteins from packaging plasmid, essential processing of vector plasmid into a packageble viral genomic DNA, assembly of virions, and packaging of genomic DNA. pXX680 plasmid is composed of E2a, E4, and VA from Adenovirus genome and the backbone of Bluescript KS(+) II as illustrated in figure S-3.

**For endosomal trafficking**

EGFP-Rab5, a plasmid used to be expressed in live cells and highlight the Rab5-associated early endosomes. This plasmid was constructed by inserting the human Rab5 coding sequence into mono-clonal-site (MCS) of construct pEGFP-C3 using restriction enzyme Hind III and BamH I. The representative map is shown in figure S-4.

DsRed-Rab7, a plasmid used to be expressed in live cells and highlight the Rab7-associated late endosomes. This plasmid was constructed by inserting the human Rab7 coding sequence into mono-clonal-site (MCS) of construct pDsRed2-C1 using restriction enzyme Hind III and BamH I. The representative map is shown in figure S-5.

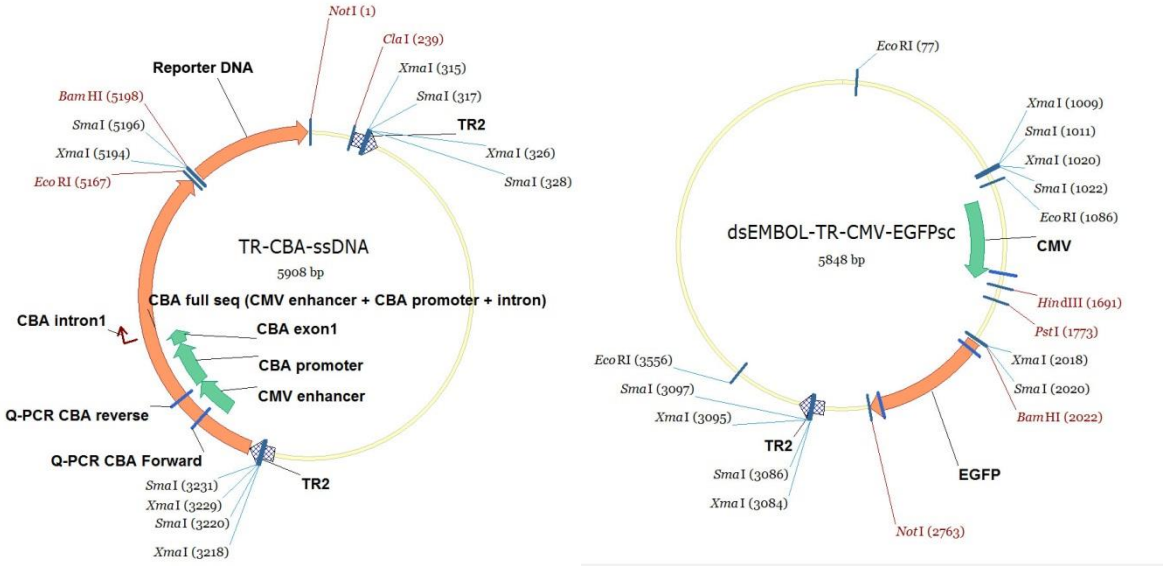


**Figure S-1. Maps of TR-CBA-ssDNA and dsEMBOL-TR-CMV-EGFPsc.** Plasmid 'TR-CBA-ssDNA' provides a single stranded genomic DNA for packaging where 'ssDNA' part can be reporter genes (e.g. GFP, Luciferase) or therapeutic genes. Plasmid 'TR-CMV-EGFPsc' provides a double stranded genomic DNA for packaging where 'EGFPsc' may be replaced by other reporter genes or therapeutic genes.

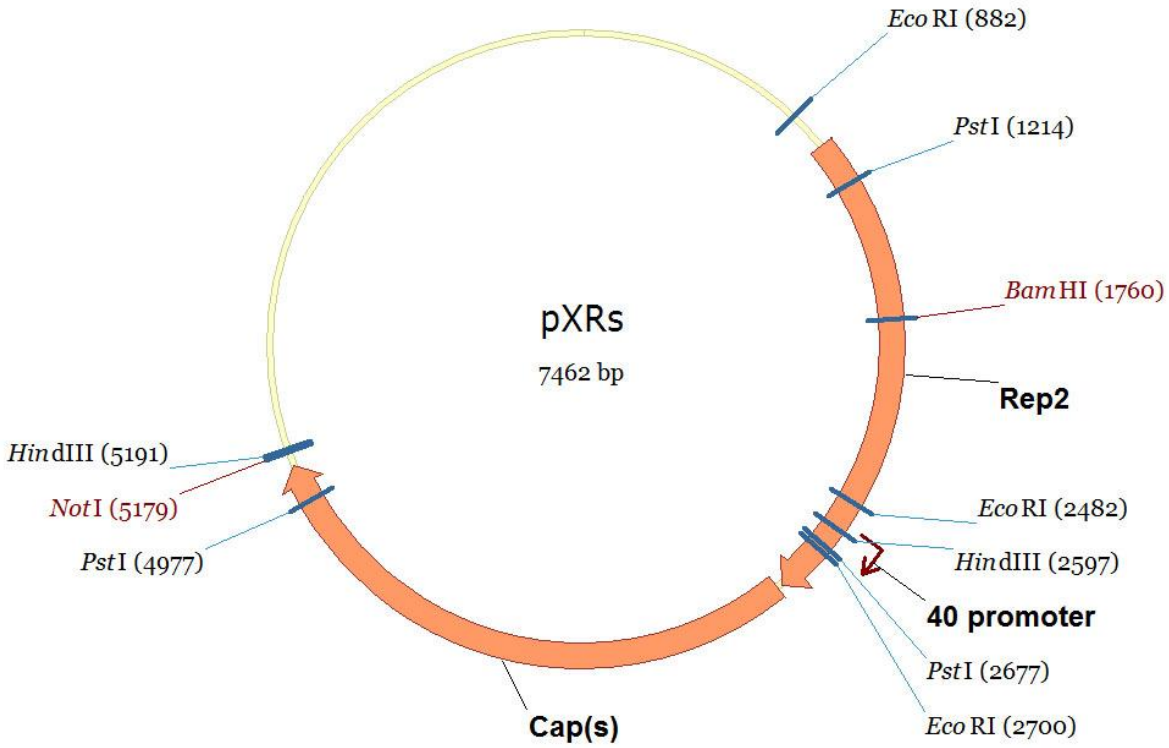


**Figure S-2. The map of packaging plasmid 'pXRs'.** Rep2 is from AAV2 and Cap(s) can be from any serotypes.

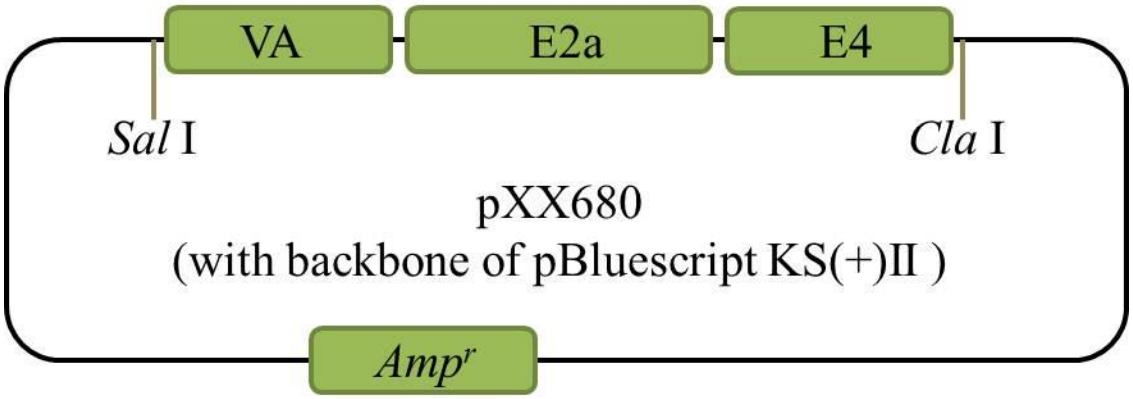


**Figure S-3. The representative map of Ad helper plasmid pXX680.**

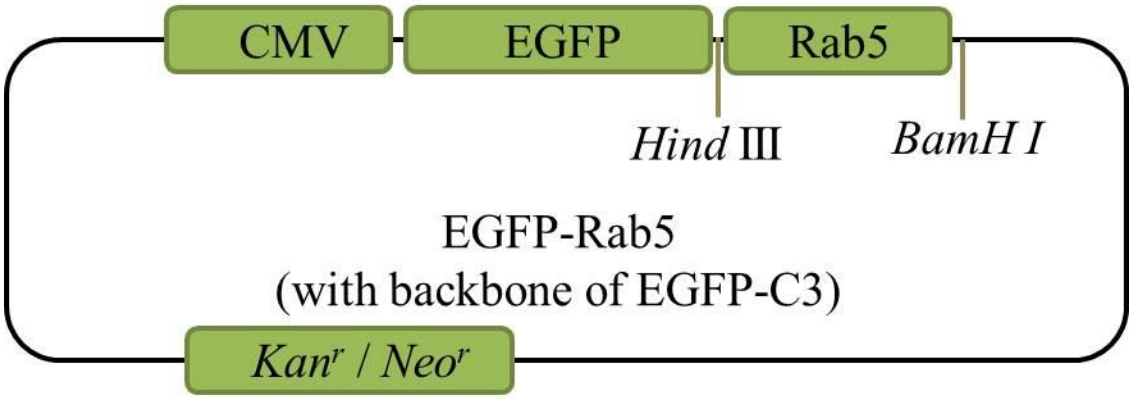


**Figure S-4. The representative map of plasmid EGFP-Rab5.**

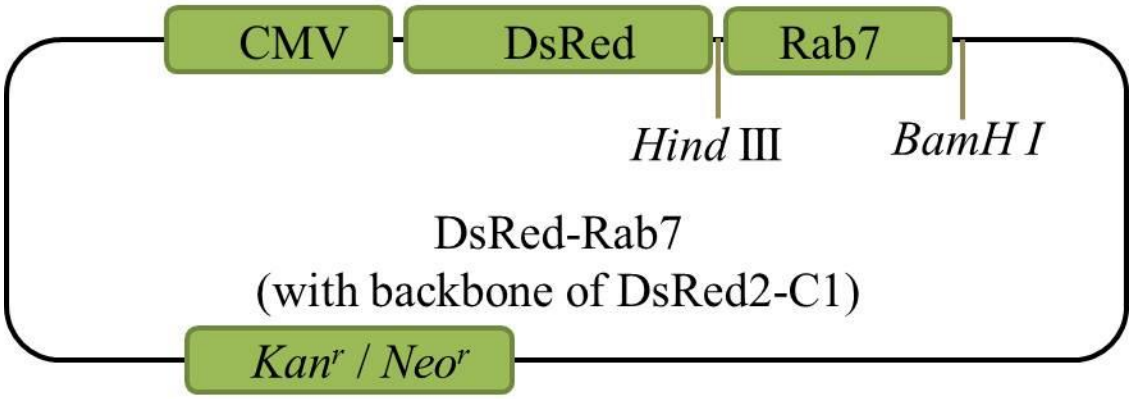


**Figure S-5. The representative map of plasmid EGFP-Rab7.**

## REFERENCES


Acland, G. M., G. D. Aguirre, et al. (2001). "Gene therapy restores vision in a canine model of childhood blindness." Nat Genet **28**(1): 92-5.

Aitken, M. L., R. B. Moss, et al. (2001). "A phase I study of aerosolized administration of tgAAVCF to cystic fibrosis subjects with mild lung disease." Hum Gene Ther **12**(15): 1907-16.

Akita, H., K. Enoto, et al. (2010). "Particle tracking of intracellular trafficking of octaarginine-modified liposomes: a comparative study with adenovirus." Mol Ther **18**(5): 955-64.

Akita, H., R. Ito, et al. (2004). "Quantitative three-dimensional analysis of the intracellular trafficking of plasmid DNA transfected by a nonviral gene delivery system using confocal laser scanning microscopy." Mol Ther **9**(3): 443-51.

Asokan, A., J. C. Conway, et al. (2009). "Reengineering a receptor footprint of adeno-associated virus enables selective and systemic gene transfer to muscle." Nat Biotechnol.

Asokan, A., J. C. Conway, et al. (2010). "Reengineering a receptor footprint of adeno-associated virus enables selective and systemic gene transfer to muscle." Nat Biotechnol.

Atchison, R. W., B. C. Casto, et al. (1965). "Adenovirus-Associated Defective Virus Particles." Science **149**(3685): 754-6.

Avitabile, E., S. Di Gaeta, et al. (1995). "Redistribution of microtubules and Golgi apparatus in herpes simplex virus-infected cells and their role in viral exocytosis." J Virol **69**(12): 7472-82.

Bahner, I., T. Sumiyoshi, et al. (2007). "Lentiviral vector transduction of a dominant-negative Rev gene into human CD34+ hematopoietic progenitor cells potently inhibits human immunodeficiency virus-1 replication." Mol Ther **15**(1): 76-85.

Bailey, C. J., R. G. Crystal, et al. (2003). "Association of adenovirus with the microtubule organizing center." J Virol **77**(24): 13275-87.

Bainbridge, J. W., A. J. Smith, et al. (2008). "Effect of gene therapy on visual function in Leber's congenital amaurosis." N Engl J Med **358**(21): 2231-9.

Bank, A., R. Dorazio, et al. (2005). "A phase I/II clinical trial of beta-globin gene therapy for beta-thalassemia." Ann N Y Acad Sci **1054**: 308-16.

Bantel-Schaal, U. and H. zur Hausen (1984). "Characterization of the DNA of a defective human parvovirus isolated from a genital site." Virology **134**(1): 52-63.

Bartel, M., D. Schaffer, et al. (2011). "Enhancing the Clinical Potential of AAV Vectors by Capsid Engineering to Evade Pre-Existing Immunity." Front Microbiol **2**: 204.

Bartlett, J. S., R. J. Samulski, et al. (1998). "Selective and rapid uptake of adeno-associated virus type 2 in brain." Hum Gene Ther **9**(8): 1181-6.

Bartlett, J. S., R. Wilcher, et al. (2000). "Infectious entry pathway of adeno-associated virus and adeno-associated virus vectors." J Virol **74**(6): 2777-85.

Berns, K. I., T. C. Pinkerton, et al. (1975). "Detection of adeno-associated virus (AAV)-specific nucleotide sequences in DNA isolated from latently infected Detroit 6 cells." Virology **68**(2): 556-60.

Bhat, P. and D. A. Anderson (2007). "Hepatitis B virus translocates across a trophoblastic barrier." J Virol **81**(13): 7200-7.

Bieber, T., W. Meissner, et al. (2002). "Intracellular route and transcriptional competence of polyethylenimine-DNA complexes." J Control Release **82**(2-3): 441-54.

Bleker, S., F. Sonntag, et al. (2005). "Mutational analysis of narrow pores at the fivefold symmetry axes of adeno-associated virus type 2 capsids reveals a dual role in genome packaging and activation of phospholipase A2 activity." J Virol **79**(4): 2528-40.

Boisvert, M., S. Fernandes, et al. (2010). "Multiple pathways involved in porcine parvovirus cellular entry and trafficking toward the nucleus." J Virol **84**(15): 7782-92.

Bomsel, M. and A. Alfsen (2003). "Entry of viruses through the epithelial barrier: pathogenic trickery." Nat Rev Mol Cell Biol **4**(1): 57-68.

Bonci, D., A. Cittadini, et al. (2003). "'Advanced' generation lentiviruses as efficient vectors for cardiomyocyte gene transduction in vitro and in vivo." Gene Ther **10**(8): 630-6.

Boucas, J., K. Lux, et al. (2009). "Engineering adeno-associated virus serotype 2-based targeting vectors using a new insertion site-position 453-and single point mutations." J Gene Med **11**(12): 1103-13.

Boulo, S., H. Akarsu, et al. (2007). "Nuclear traffic of influenza virus proteins and ribonucleoprotein complexes." Virus Res **124**(1-2): 12-21.

Bowles, D. E., S. W. McPhee, et al. (2011). "Phase 1 Gene Therapy for Duchenne Muscular Dystrophy Using a Translational Optimized AAV Vector." Mol Ther.

Brandenburg, B. and X. Zhuang (2007). "Virus trafficking - learning from single-virus tracking." Nat Rev Microbiol **5**(3): 197-208.

Brantly, M. L., J. D. Chulay, et al. (2009). "Sustained transgene expression despite T lymphocyte responses in a clinical trial of rAAV1-AAT gene therapy." Proc Natl Acad Sci U S A **106**(38): 16363-8.

Brantly, M. L., L. T. Spencer, et al. (2006). "Phase I trial of intramuscular injection of a recombinant adeno-associated virus serotype 2 alphal-antitrypsin (AAT) vector in AAT-deficient adults." Hum Gene Ther **17**(12): 1177-86.

Bremner, K. H., J. Scherer, et al. (2009). "Adenovirus transport via direct interaction of cytoplasmic dynein with the viral capsid hexon subunit." Cell Host Microbe **6**(6): 523-35.

Breunig, M., S. Bauer, et al. (2008). "Polymers and nanoparticles: intelligent tools for intracellular targeting?" Eur J Pharm Biopharm **68**(1): 112-28.

Broers, J. L., F. C. Ramaekers, et al. (2006). "Nuclear lamins: laminopathies and their role in premature ageing." Physiol Rev **86**(3): 967-1008.

Buning, H., M. Braun-Falco, et al. (2004). "Progress in the use of adeno-associated viral vectors for gene therapy." Cells Tissues Organs **177**(3): 139-50.

Campos, S. K. and M. A. Barry (2007). "Current advances and future challenges in Adenoviral vector biology and targeting." Curr Gene Ther **7**(3): 189-204.

Carlsson, T., T. Bjorklund, et al. (2007). "Restoration of the striatal dopamine synthesis for Parkinson's disease: viral vector-mediated enzyme replacement strategy." Curr Gene Ther **7**(2): 109-20.

Cartier, N., S. Hacein-Bey-Abina, et al. (2009). "Hematopoietic stem cell gene therapy with a lentiviral vector in X-linked adrenoleukodystrophy." Science **326**(5954): 818-23.

Cassimeris, L. U., P. Wadsworth, et al. (1986). "Dynamics of microtubule depolymerization in monocytes." J Cell Biol **102**(6): 2023-32.

Cavazzana-Calvo, M. and A. Fischer (2007). "Gene therapy for severe combined immunodeficiency: are we there yet?" J Clin Invest **117**(6): 1456-65.

Chang, L. S. and T. Shenk (1990). "The adenovirus DNA-binding protein stimulates the rate of transcription directed by adenovirus and adeno-associated virus promoters." J Virol **64**(5): 2103-9.

Chang, Y. C., P. Nalbant, et al. (2008). "GEF-H1 couples nocodazole-induced microtubule disassembly to cell contractility via RhoA." Mol Biol Cell **19**(5): 2147-53.

Chao, H., Y. Liu, et al. (2000). "Several log increase in therapeutic transgene delivery by distinct adeno-associated viral serotype vectors." Mol Ther **2**(6): 619-23.

Chen, H. H., Y. P. Ho, et al. (2008). "Quantitative comparison of intracellular unpacking kinetics of polyplexes by a model constructed from quantum dot-FRET." Mol Ther **16**(2): 324-32.

Chen, H. H., L. M. Mack, et al. (1997). "Persistence in muscle of an adenoviral vector that lacks all viral genes." Proc Natl Acad Sci U S A **94**(5): 1645-50.

Chen, T., Z. Wang, et al. (2007). "Polyethylenimine-DNA solid particles for gene delivery." J Drug Target **15**(10): 714-20.

Chinen, J., J. Davis, et al. (2007). "Gene therapy improves immune function in preadolescents with X-linked severe combined immunodeficiency." Blood **110**(1): 67-73.

Choi, V. W., R. J. Samulski, et al. (2005). "Effects of adeno-associated virus DNA hairpin structure on recombination." J Virol **79**(11): 6801-7.

Christine, C. W., P. A. Starr, et al. (2009). "Safety and tolerability of putaminal AADC gene therapy for Parkinson disease." Neurology **73**(20): 1662-9.

Cideciyan, A. V., T. S. Aleman, et al. (2008). "Human gene therapy for RPE65 isomerase deficiency activates the retinoid cycle of vision but with slow rod kinetics." Proc Natl Acad Sci U S A **105**(39): 15112-7.

Clemente, R. and J. C. de la Torre (2009). "Cell entry of Borna disease virus follows a clathrin-mediated endocytosis pathway that requires Rab5 and microtubules." J Virol **83**(20): 10406-16.

Cohen, S., A. R. Behzad, et al. (2006). "Parvoviral nuclear import: bypassing the host nuclear-transport machinery." J Gen Virol **87**(Pt 11): 3209-13.

Cooper, M., S. Nayak, et al. (2009). "Improved Induction of Immune Tolerance to Factor IX by Hepatic AAV-8 Gene Transfer." Human Gene Therapy **20**(7): 767-776.

Davidson, B. L., C. S. Stein, et al. (2000). "Recombinant adeno-associated virus type 2, 4, and 5 vectors: transduction of variant cell types and regions in the mammalian central nervous system." Proc Natl Acad Sci U S A **97**(7): 3428-32.

de Bruin, K., N. Ruthardt, et al. (2007). "Cellular dynamics of EGF receptor-targeted synthetic viruses." Mol Ther **15**(7): 1297-305.

Dean, D. A., D. D. Strong, et al. (2005). "Nuclear entry of nonviral vectors." Gene Ther **12**(11): 881-90.

den Hollander, A. I., R. Roepman, et al. (2008). "Leber congenital amaurosis: genes, proteins and disease mechanisms." Prog Retin Eye Res **27**(4): 391-419.

Desai, A. and T. J. Mitchison (1997). "Microtubule polymerization dynamics." Annu Rev Cell Dev Biol **13**: 83-117.

Di Pasquale, G. and J. A. Chiorini (2006). "AAV transcytosis through barrier epithelia and endothelium." Mol Ther **13**(3): 506-16.

Ding, W., L. Zhang, et al. (2005). "Intracellular trafficking of adeno-associated viral vectors." Gene Ther **12**(11): 873-80.

Ding, W., L. N. Zhang, et al. (2006). "rAAV2 traffics through both the late and the recycling endosomes in a dose-dependent fashion." Mol Ther **13**(4): 671-82.

DiPrimio, N., A. Asokan, et al. (2008). "Surface loop dynamics in adeno-associated virus capsid assembly." J Virol **82**(11): 5178-89.

DiPrimio, N., S. W. McPhee, et al. (2010). "Adeno-associated virus for the treatment of muscle diseases: toward clinical trials." Curr Opin Mol Ther **12**(5): 553-60.

Dodding, M. P. and M. Way (2011). "Coupling viruses to dynein and kinesin-1." Embo J **30**(17): 3527-39.

Dohner, K., A. Wolfstein, et al. (2002). "Function of dynein and dynactin in herpes simplex virus capsid transport." Mol Biol Cell **13**(8): 2795-809.

Douar, A. M., K. Poulard, et al. (2001). "Intracellular trafficking of adeno-associated virus vectors: routing to the late endosomal compartment and proteasome degradation." J Virol **75**(4): 1824-33.

Douglas, J. T. (2007). "Adenoviral vectors for gene therapy." Mol Biotechnol **36**(1): 71-80.

Duan, D., Q. Li, et al. (1999). "Dynamin is required for recombinant adeno-associated virus type 2 infection." J Virol **73**(12): 10371-6.

Duan, D., P. Sharma, et al. (1999). "Formation of adeno-associated virus circular genomes is differentially regulated by adenovirus E4 ORF6 and E2a gene expression." J Virol **73**(1): 161-9.

Duan, D., Y. Yue, et al. (2000). "Endosomal processing limits gene transfer to polarized airway epithelia by adeno-associated virus." J Clin Invest **105**(11): 1573-87.

Dudleenamjil, E., C. Y. Lin, et al. (2010). "Bovine parvovirus uses clathrin-mediated endocytosis for cell entry." J Gen Virol **91**(Pt 12): 3032-41.

Dworetzky, S. I., R. E. Lanford, et al. (1988). "The effects of variations in the number and sequence of targeting signals on nuclear uptake." J Cell Biol **107**(4): 1279-87.

Eberling, J. L., W. J. Jagust, et al. (2008). "Results from a phase I safety trial of hAADC gene therapy for Parkinson disease." Neurology **70**(21): 1980-3.

Ellis, J. (2005). "Silencing and variegation of gammaretrovirus and lentivirus vectors." Hum Gene Ther **16**(11): 1241-6.

Engelke, M. F., C. J. Burckhardt, et al. (2011). "The dynactin complex enhances the speed of microtubule-dependent motions of adenovirus both towards and away from the nucleus." Viruses **3**(3): 233-53.

Excoffon, K. J., J. T. Koerber, et al. (2009). "Directed evolution of adeno-associated virus to an infectious respiratory virus." Proc Natl Acad Sci U S A **106**(10): 3865-70.

Fackler, O. T. and H. G. Krausslich (2006). "Interactions of human retroviruses with the host cell cytoskeleton." Curr Opin Microbiol **9**(4): 409-15.

Favoreel, H. W., L. W. Enquist, et al. (2007). "Actin and Rho GTPases in herpesvirus biology." Trends Microbiol **15**(9): 426-33.

Feng, D., D. Marshburn, et al. (2007). "Stepping into the third dimension." J Neurosci **27**(47): 12757-60.

Ferrari, F. K., T. Samulski, et al. (1996). "Second-strand synthesis is a rate-limiting step for efficient transduction by recombinant adeno-associated virus vectors." J Virol **70**(5): 3227-34.

Fink, D. J. and J. C. Glorioso (1997). "Engineering herpes simplex virus vectors for gene transfer to neurons." Nat Med **3**(3): 357-9.

Fisher, K. J., G. P. Gao, et al. (1996). "Transduction with recombinant adeno-associated virus for gene therapy is limited by leading-strand synthesis." J Virol **70**(1): 520-32.

Fisher, K. J., K. Jooss, et al. (1997). "Recombinant adeno-associated virus for muscle directed gene therapy." Nat Med **3**(3): 306-12.

Flotte, T. R., M. L. Brantly, et al. (2004). "Phase I trial of intramuscular injection of a recombinant adeno-associated virus alpha 1-antitrypsin (rAAV2-CB-hAAT) gene vector to AAT-deficient adults." Hum Gene Ther **15**(1): 93-128.

Flotte, T. R., T. J. Conlon, et al. (2007). "Preclinical characterization of a recombinant adeno-associated virus type 1-pseudotyped vector demonstrates dose-dependent injection site inflammation and dissemination of vector genomes to distant sites." Hum Gene Ther **18**(3): 245-56.

Flotte, T. R. and C. Mueller (2011). "Gene therapy for alpha-1 antitrypsin deficiency." Hum Mol Genet **20**(R1): R87-92.

Flotte, T. R., B. C. Trapnell, et al. (2011). "Phase 2 clinical trial of a recombinant adeno-associated viral vector expressing alpha1-antitrypsin: interim results." Hum Gene Ther **22**(10): 1239-47.

Flotte, T. R., P. L. Zeitlin, et al. (2003). "Phase I trial of intranasal and endobronchial administration of a recombinant adeno-associated virus serotype 2 (rAAV2)-CFTR vector in adult cystic fibrosis patients: a two-part clinical study." Hum Gene Ther **14**(11): 1079-88.

Fraefel, C., S. Song, et al. (1996). "Helper virus-free transfer of herpes simplex virus type 1 plasmid vectors into neural cells." J Virol **70**(10): 7190-7.

Gao, G., L. H. Vandenberghe, et al. (2004). "Clades of Adeno-associated viruses are widely disseminated in human tissues." J Virol **78**(12): 6381-8.

Gao, G. P., M. R. Alvira, et al. (2002). "Novel adeno-associated viruses from rhesus monkeys as vectors for human gene therapy." Proc Natl Acad Sci U S A **99**(18): 11854-9.

Garcia-Mata, R., Y. S. Gao, et al. (2002). "Hassles with taking out the garbage: aggravating aggresomes." Traffic **3**(6): 388-96.

Gaspar, H. B., K. L. Parsley, et al. (2004). "Gene therapy of X-linked severe combined immunodeficiency by use of a pseudotyped gammaretroviral vector." Lancet **364**(9452): 2181-7.

Geller, A. I. (1997). "Herpes simplex virus-1 plasmid vectors for gene transfer into neurons." Adv Neurol **72**: 143-8.

Ghosh, S. S., P. Gopinath, et al. (2006). "Adenoviral vectors: a promising tool for gene therapy." Appl Biochem Biotechnol **133**(1): 9-29.

Giannakakou, P., D. L. Sackett, et al. (2000). "p53 is associated with cellular microtubules and is transported to the nucleus by dynein." Nat Cell Biol **2**(10): 709-17.

Gilbert, J. and T. Benjamin (2004). "Uptake pathway of polyomavirus via ganglioside GD1a." J Virol **78**(22): 12259-67.

Giraud, C., E. Winocour, et al. (1995). "Recombinant junctions formed by site-specific integration of adeno-associated virus into an episome." J Virol **69**(11): 6917-24.

Girod, A., M. Ried, et al. (1999). "Genetic capsid modifications allow efficient re-targeting of adeno-associated virus type 2." Nat Med **5**(9): 1052-6.

Girod, A., C. E. Wobus, et al. (2002). "The VP1 capsid protein of adeno-associated virus type 2 is carrying a phospholipase A2 domain required for virus infectivity." J Gen Virol **83**(Pt 5): 973-8.

Goff, S. P. (2001). Retroviridae: the retroviruses and their replication. Fields Virology. D. M. Knipe and P. M. Howley. Philadelphia, Pa, Lippincott-Raven Publishers**:** 1871-1940.

Gong, K., D. Xing, et al. (2011). "cGMP inhibits TGF-beta signaling by sequestering Smad3 with cytosolic beta2-tubulin in pulmonary artery smooth muscle cells." Mol Endocrinol **25**(10): 1794-803.

Gorlich, D. and U. Kutay (1999). "Transport between the cell nucleus and the cytoplasm." Annu Rev Cell Dev Biol **15**: 607-60.

Gray, S. J., B. L. Blake, et al. (2009). "Directed Evolution of a Novel Adeno-associated Virus (AAV) Vector That Crosses the Seizure-compromised Blood-Brain Barrier (BBB)." Mol Ther.

Gray, S. J. and R. J. Samulski (2008). "Optimizing gene delivery vectors for the treatment of heart disease." Expert Opin Biol Ther **8**(7): 911-22.

Greber, U. F. and D. Puntener (2009). "DNA-tumor virus entry--from plasma membrane to the nucleus." Semin Cell Dev Biol **20**(5): 631-42.

Greber, U. F., M. Suomalainen, et al. (1997). "The role of the nuclear pore complex in adenovirus DNA entry." Embo J **16**(19): 5998-6007.

Greber, U. F. and M. Way (2006). "A superhighway to virus infection." Cell **124**(4): 741-54.

Greber, U. F., M. Willetts, et al. (1993). "Stepwise dismantling of adenovirus 2 during entry into cells." Cell **75**(3): 477-86.

Gregorevic, P., M. J. Blankinship, et al. (2004). "Systemic delivery of genes to striated muscles using adeno-associated viral vectors." Nat Med **10**(8): 828-34.

Grieger, J. C., V. W. Choi, et al. (2006). "Production and characterization of adeno-associated viral vectors." Nat Protoc **1**(3): 1412-28.

Grieger, J. C., S. Snowdy, et al. (2006). "Separate basic region motifs within the adeno-associated virus capsid proteins are essential for infectivity and assembly." J Virol **80**(11): 5199-210.

Griesenbach, U. and E. W. Alton (2012). "Progress in gene and cell therapy for cystic fibrosis lung disease." Curr Pharm Des **18**(5): 642-62.

Grieshaber, S. S., N. A. Grieshaber, et al. (2003). "Chlamydia trachomatis uses host cell dynein to traffic to the microtubule-organizing center in a p50 dynamitin-independent process." J Cell Sci **116**(Pt 18): 3793-802.

Grifman, M., M. Trepel, et al. (2001). "Incorporation of tumor-targeting peptides into recombinant adeno-associated virus capsids." Mol Ther **3**(6): 964-75.

Grimm, D. and M. A. Kay (2003). "From virus evolution to vector revolution: use of naturally occurring serotypes of adeno-associated virus (AAV) as novel vectors for human gene therapy." Curr Gene Ther **3**(4): 281-304.

Grimm, D., J. S. Lee, et al. (2008). "In vitro and in vivo gene therapy vector evolution via multispecies interbreeding and retargeting of adeno-associated viruses." J Virol **82**(12): 5887-911.

Grossman, Z., E. Winocour, et al. (1984). "Recombination between simian virus 40 and adeno-associated virus: virion coinfection compared to DNA cotransfection." Virology **134**(1): 125-37.

Gupta, B., T. S. Levchenko, et al. (2005). "Intracellular delivery of large molecules and small particles by cell-penetrating proteins and peptides." Adv Drug Deliv Rev **57**(4): 637-51.

Haffar, O. and M. Bukrinsky (2005). "Nuclear translocation as a novel target for anti-HIV drugs." Expert Rev Anti Infect Ther **3**(1): 41-50.

Hajjar, R. J., K. Zsebo, et al. (2008). "Design of a phase 1/2 trial of intracoronary administration of AAV1/SERCA2a in patients with heart failure." J Card Fail **14**(5): 355-67.

Hansen, J., K. Qing, et al. (2000). "Impaired intracellular trafficking of adeno-associated virus type 2 vectors limits efficient transduction of murine fibroblasts." J Virol **74**(2): 992-6.

Hansen, J., K. Qing, et al. (2001). "Infection of purified nuclei by adeno-associated virus 2." Mol Ther **4**(4): 289-96.

Hashida, M., M. Nishikawa, et al. (2001). "Cell-specific delivery of genes with glycosylated carriers." Adv Drug Deliv Rev **52**(3): 187-96.

Hauck, B., L. Chen, et al. (2003). "Generation and characterization of chimeric recombinant AAV vectors." Mol Ther **7**(3): 419-25.

Heim, R., A. B. Cubitt, et al. (1995). "Improved green fluorescence." Nature **373**(6516): 663-4.

Herson, S., F. Hentati, et al. (2012). "A phase I trial of adeno-associated virus serotype 1-gamma-sarcoglycan gene therapy for limb girdle muscular dystrophy type 2C." Brain.

High, K. A. (2011). "Gene therapy for haemophilia: a long and winding road." J Thromb Haemost **9 Suppl 1**: 2-11.

Hindley, C. E., F. J. Lawrence, et al. (2007). "A role for transportin in the nuclear import of adenovirus core proteins and DNA." Traffic **8**(10): 1313-22.

Hirosue, S., K. Senn, et al. (2007). "Effect of inhibition of dynein function and microtubule-altering drugs on AAV2 transduction." Virology **367**(1): 10-8.

Hoen, D. R., K. C. Park, et al. (2006). "Transposon-mediated expansion and diversification of a family of ULP-like genes." Mol Biol Evol **23**(6): 1254-68.

Hofherr, S. E., K. E. Adams, et al. "Real-time dynamic imaging of virus distribution in vivo." PLoS One **6**(2): e17076.

Hofmann, W., B. Reichart, et al. (2001). "Cofactor requirements for nuclear export of Rev response element (RRE)- and constitutive transport element (CTE)-containing retroviral RNAs. An unexpected role for actin." J Cell Biol **152**(5): 895-910.

Hoggan, M. D., N. R. Blacklow, et al. (1966). "Studies of small DNA viruses found in various adenovirus preparations: physical, biological, and immunological characteristics." Proc Natl Acad Sci U S A **55**(6): 1467-74.

Huang, B., M. Bates, et al. (2009). "Super-resolution fluorescence microscopy." Annu Rev Biochem **78**: 993-1016.

Huang, B., S. A. Jones, et al. (2008). "Whole-cell 3D STORM reveals interactions between cellular structures with nanometer-scale resolution." Nat Methods **5**(12): 1047-52.

Huotari, J. and A. Helenius (2011). "Endosome maturation." Embo J **30**(17): 3481-500.

Hyde, J. L., L. K. Gillespie, et al. (2012). "Mouse norovirus 1 utilizes the cytoskeleton network to establish localization of the replication complex proximal to the microtubule organizing center." J Virol **86**(8): 4110-22.

Janson, C., S. McPhee, et al. (2002). "Clinical protocol. Gene therapy of Canavan disease: AAV-2 vector for neurosurgical delivery of aspartoacylase gene (ASPA) to the human brain." Hum Gene Ther **13**(11): 1391-412.

Johnson, J. S., M. Gentzsch, et al. (2011). "AAV exploits subcellular stress associated with inflammation, endoplasmic reticulum expansion, and misfolded proteins in models of cystic fibrosis." PLoS Pathog **7**(5): e1002053.

Johnson, J. S., C. Li, et al. (2010). "Mutagenesis of adeno-associated virus type 2 capsid protein VP1 uncovers new roles for basic amino acids in trafficking and cell-specific transduction." J Virol **84**(17): 8888-902.

Johnson, J. S. and R. J. Samulski (2008). "Enhancement of AAV infection by mobilizing capsids into and out of the nucleolus." J Virol.

Johnson, J. S. and R. J. Samulski (2009). "Enhancement of adeno-associated virus infection by mobilizing capsids into and out of the nucleolus." J Virol **83**(6): 2632-44.

Kaludov, N., E. Padron, et al. (2003). "Production, purification and preliminary X-ray crystallographic studies of adeno-associated virus serotype 4." Virology **306**(1): 1-6.

Kaminsky, P. M., N. W. Keiser, et al. (2012). "Directing Integrin-linked Endocytosis of Recombinant AAV Enhances Productive FAK-dependent Transduction." Mol Ther.

Kaplitt, M. G., A. Feigin, et al. (2007). "Safety and tolerability of gene therapy with an adeno-associated virus (AAV) borne GAD gene for Parkinson's disease: an open label, phase I trial." Lancet **369**(9579): 2097-105.

Kass, S. U., N. Landsberger, et al. (1997). "DNA methylation directs a time-dependent repression of transcription initiation." Curr Biol **7**(3): 157-65.

Kawabata, K., Y. Takakura, et al. (1995). "The fate of plasmid DNA after intravenous injection in mice: involvement of scavenger receptors in its hepatic uptake." Pharm Res **12**(6): 825-30.

Kay, M. A., C. S. Manno, et al. (2000). "Evidence for gene transfer and expression of factor IX in haemophilia B patients treated with an AAV vector." Nat Genet **24**(3): 257-61.

Kelkar, S., B. P. De, et al. (2006). "A common mechanism for cytoplasmic dynein-dependent microtubule binding shared among adeno-associated virus and adenovirus serotypes." J Virol **80**(15): 7781-5.

Kern, A., K. Schmidt, et al. (2003). "Identification of a heparin-binding motif on adeno-associated virus type 2 capsids." J Virol **77**(20): 11072-81.

Kessler, P. D., G. M. Podsakoff, et al. (1996). "Gene delivery to skeletal muscle results in sustained expression and systemic delivery of a therapeutic protein." Proc Natl Acad Sci U S A **93**(24): 14082-7.

Koerber, J. T., J. H. Jang, et al. (2008). "DNA Shuffling of Adeno-associated Virus Yields Functionally Diverse Viral Progeny." Mol Ther.

Kotchey, N. M., K. Adachi, et al. "A Potential Role of Distinctively Delayed Blood Clearance of Recombinant Adeno-associated Virus Serotype 9 in Robust Cardiac Transduction." Mol Ther.

Kotin, R. M., R. M. Linden, et al. (1992). "Characterization of a preferred site on human chromosome 19q for integration of adeno-associated virus DNA by non-homologous recombination." Embo J **11**(13): 5071-8.

Kovesdi, I., D. E. Brough, et al. (1997). "Adenoviral vectors for gene transfer." Curr Opin Biotechnol **8**(5): 583-9.

Krendel, M., F. T. Zenke, et al. (2002). "Nucleotide exchange factor GEF-H1 mediates cross-talk between microtubules and the actin cytoskeleton." Nat Cell Biol **4**(4): 294-301.

Kronenberg, S., B. Bottcher, et al. (2005). "A conformational change in the adeno-associated virus type 2 capsid leads to the exposure of hidden VP1 N termini." J Virol **79**(9): 5296-303.

Kronenberg, S., J. A. Kleinschmidt, et al. (2001). "Electron cryo-microscopy and image reconstruction of adeno-associated virus type 2 empty capsids." EMBO Rep **2**(11): 997-1002.

Kyostio, S. R., R. A. Owens, et al. (1994). "Analysis of adeno-associated virus (AAV) wild-type and mutant Rep proteins for their abilities to negatively regulate AAV p5 and p19 mRNA levels." J. Virol. **68**(5): 2947-2957.

Lakadamyali, M., M. J. Rust, et al. (2003). "Visualizing infection of individual influenza viruses." Proc Natl Acad Sci U S A **100**(16): 9280-5.

Lehmann, M. J., N. M. Sherer, et al. (2005). "Actin- and myosin-driven movement of viruses along filopodia precedes their entry into cells." J Cell Biol **170**(2): 317-25.

Leone, P., C. G. Janson, et al. (1999). "Global CNS gene transfer for a childhood neurogenetic enzyme deficiency: Canavan disease." Curr Opin Mol Ther **1**(4): 487-92.

Leopold, P. L., B. Ferris, et al. (1998). "Fluorescent virions: dynamic tracking of the pathway of adenoviral gene transfer vectors in living cells." Hum Gene Ther **9**(3): 367-78.

Leopold, P. L., G. Kreitzer, et al. (2000). "Dynein- and microtubule-mediated translocation of adenovirus serotype 5 occurs after endosomal lysis." Hum Gene Ther **11**(1): 151-65.

Leopold, P. L. and K. K. Pfister (2006). "Viral strategies for intracellular trafficking: motors and microtubules." Traffic **7**(5): 516-23.

Lerch, T. F., Q. Xie, et al. (2009). "Twinned crystals of adeno-associated virus serotype 3b prove suitable for structural studies." Acta Crystallogr Sect F Struct Biol Cryst Commun **65**(Pt 2): 177-83.

Li, M. J., J. Kim, et al. (2005). "Long-term inhibition of HIV-1 infection in primary hematopoietic cells by lentiviral vector delivery of a triple combination of anti-HIV shRNA, anti-CCR5 ribozyme, and a nucleolar-localizing TAR decoy." Mol Ther **12**(5): 900-9.

Li, W., A. Asokan, et al. (2008). "Engineering and selection of shuffled AAV genomes: a new strategy for producing targeted biological nanoparticles." Mol Ther **16**(7): 1252-60.

Li, W., L. Zhang, et al. (2009). "Generation of novel AAV variants by directed evolution for improved CFTR delivery to human ciliated airway epithelium." Mol Ther **17**(12): 2067-77.

Lilley, C. E., F. Groutsi, et al. (2001). "Multiple immediate-early gene-deficient herpes simplex virus vectors allowing efficient gene delivery to neurons in culture and widespread gene delivery to the central nervous system in vivo." J Virol **75**(9): 4343-56.

Limberis, M. P., L. H. Vandenberghe, et al. (2008). "Transduction Efficiencies of Novel AAV Vectors in Mouse Airway Epithelium In Vivo and Human Ciliated Airway Epithelium In Vitro." Mol Ther **17**(2): 294-301.

Lipskaia, L., E. R. Chemaly, et al. (2010). "Sarcoplasmic reticulum Ca(2+) ATPase as a therapeutic target for heart failure." Expert Opin Biol Ther **10**(1): 29-41.

Liu, F., L. M. Shollenberger, et al. (2007). "Mechanism of naked DNA clearance after intravenous injection." J Gene Med **9**(7): 613-9.

Liu, M., E. E. Schmidt, et al. (2010). "ICP0 dismantles microtubule networks in herpes simplex virus-infected cells." PLoS One **5**(6): e10975.

Liu, S. L., Z. L. Zhang, et al. (2012). "Effectively and efficiently dissecting the infection of influenza virus by quantum-dot-based single-particle tracking." ACS Nano **6**(1): 141-50.

Lombardo, E., J. C. Ramirez, et al. (2000). "A beta-stranded motif drives capsid protein oligomers of the parvovirus minute virus of mice into the nucleus for viral assembly." J Virol **74**(8): 3804-14.

Lombardo, E., J. C. Ramirez, et al. (2002). "Complementary roles of multiple nuclear targeting signals in the capsid proteins of the parvovirus minute virus of mice during assembly and onset of infection." J Virol **76**(14): 7049-59.

Lu, Y., Y. K. Choi, et al. (2006). "Therapeutic level of functional human alpha 1 antitrypsin (hAAT) secreted from murine muscle transduced by adeno-associated virus (rAAV1) vector." J Gene Med **8**(6): 730-5.

Luo, D. and W. M. Saltzman (2000). "Synthetic DNA delivery systems." Nat Biotechnol **18**(1): 33-7.

Luo, J., M. G. Kaplitt, et al. (2002). "Subthalamic GAD gene therapy in a Parkinson's disease rat model." Science **298**(5592): 425-9.

Lux, K., N. Goerlitz, et al. (2005). "Green fluorescent protein-tagged adeno-associated virus particles allow the study of cytosolic and nuclear trafficking." J Virol **79**(18): 11776-87.

Maguire, A. M., F. Simonelli, et al. (2008). "Safety and efficacy of gene transfer for Leber's congenital amaurosis." N Engl J Med **358**(21): 2240-8.

Maheshri, N., J. T. Koerber, et al. (2006). "Directed evolution of adeno-associated virus yields enhanced gene delivery vectors." Nat Biotechnol **24**(2): 198-204.

Mani, B., C. Baltzer, et al. (2006). "Low pH-dependent endosomal processing of the incoming parvovirus minute virus of mice virion leads to externalization of the VP1 N-terminal sequence (N-VP1), N-VP2 cleavage, and uncoating of the full-length genome." J Virol **80**(2): 1015-24.

Manno, C. S., A. J. Chew, et al. (2003). "AAV-mediated factor IX gene transfer to skeletal muscle in patients with severe hemophilia B." Blood **101**(8): 2963-2972.

Manno, C. S., G. F. Pierce, et al. (2006). "Successful transduction of liver in hemophilia by AAV-Factor IX and limitations imposed by the host immune response." Nat Med **12**(3): 342-7.

Marks, W. J., Jr., J. L. Ostrem, et al. (2008). "Safety and tolerability of intraputaminal delivery of CERE-120 (adeno-associated virus serotype 2-neurturin) to patients with idiopathic Parkinson's disease: an open-label, phase I trial." Lancet Neurol **7**(5): 400-8.

Martin, D., M. Duarte, et al. (2010). "Sequestration of free tubulin molecules by the viral protein NSP2 induces microtubule depolymerization during rotavirus infection." J Virol **84**(5): 2522-32.

Martin, K. R., R. L. Klein, et al. (2002). "Gene delivery to the eye using adeno-associated viral vectors." Methods **28**(2): 267-75.

Mata-Espinosa, D. A., V. Mendoza-Rodriguez, et al. (2008). "Therapeutic effect of recombinant adenovirus encoding interferon-gamma in a murine model of progressive pulmonary tuberculosis." Mol Ther **16**(6): 1065-72.

McCarty, D. M., H. Fu, et al. (2003). "Adeno-associated virus terminal repeat (TR) mutant generates self-complementary vectors to overcome the rate-limiting step to transduction in vivo." Gene Ther **10**(26): 2112-8.

McCarty, D. M., P. E. Monahan, et al. (2001). "Self-complementary recombinant adeno-associated virus (scAAV) vectors promote efficient transduction independently of DNA synthesis." Gene Ther **8**(16): 1248-54.

McDonald, D., M. A. Vodicka, et al. (2002). "Visualization of the intracellular behavior of HIV in living cells." J Cell Biol **159**(3): 441-52.

McPhee, S. W., C. G. Janson, et al. (2006). "Immune responses to AAV in a phase I study for Canavan disease." J Gene Med **8**(5): 577-88.

Mease, P. J., K. Hobbs, et al. (2009). "Local delivery of a recombinant adenoassociated vector containing a tumour necrosis factor alpha antagonist gene in inflammatory arthritis: a phase 1 dose-escalation safety and tolerability study." Ann Rheum Dis **68**(8): 1247-54.

Mellman, I., R. Fuchs, et al. (1986). "Acidification of the endocytic and exocytic pathways." Annu Rev Biochem **55**: 663-700.

Mendell, J. R., K. Campbell, et al. (2011). "Dystrophin immunity in Duchenne's muscular dystrophy." N Engl J Med **363**(15): 1429-37.

Mendell, J. R., L. R. Rodino-Klapac, et al. (2009). "Limb-girdle muscular dystrophy type 2D gene therapy restores alpha-sarcoglycan and associated proteins." Ann Neurol **66**(3): 290-7.

Mendell, J. R., L. R. Rodino-Klapac, et al. (2010). "Sustained alpha-sarcoglycan gene expression after gene transfer in limb-girdle muscular dystrophy, type 2D." Ann Neurol **68**(5): 629-38.

Miao, C. H., R. O. Snyder, et al. (1998). "The kinetics of rAAV integration in the liver." Nat Genet **19**(1): 13-5.

Michelfelder, S., J. Kohlschutter, et al. (2009). "Successful expansion but not complete restriction of tropism of adeno-associated virus by in vivo biopanning of random virus display peptide libraries." PLoS One **4**(4): e5122.

Michelfelder, S., M. K. Lee, et al. (2007). "Vectors selected from adeno-associated viral display peptide libraries for leukemia cell-targeted cytotoxic gene therapy." Exp Hematol **35**(12): 1766-76.

Miller, D. G., M. A. Adam, et al. (1990). "Gene transfer by retrovirus vectors occurs only in cells that are actively replicating at the time of infection." Mol Cell Biol **10**(8): 4239-42.

Miller, D. G., G. D. Trobridge, et al. (2005). "Large-scale analysis of adeno-associated virus vector integration sites in normal human cells." J Virol **79**(17): 11434-42.

Miller, E. B., B. Gurda-Whitaker, et al. (2006). "Production, purification and preliminary X-ray crystallographic studies of adeno-associated virus serotype 1." Acta Crystallogr Sect F Struct Biol Cryst Commun **62**(Pt 12): 1271-4.

Minakhina, S., R. Myers, et al. (2005). "Crosstalk between the actin cytoskeleton and Ran-mediated nuclear transport." BMC Cell Biol **6**: 32.

Mingozzi, F. and K. A. High (2011). "Immune responses to AAV in clinical trials." Curr Gene Ther **11**(4): 321-30.

Mingozzi, F., M. V. Maus, et al. (2007). "CD8(+) T-cell responses to adeno-associated virus capsid in humans." Nat Med **13**(4): 419-22.

Mingozzi, F., J. J. Meulenberg, et al. (2009). "AAV-1-mediated gene transfer to skeletal muscle in humans results in dose-dependent activation of capsid-specific T cells." Blood **114**(10): 2077-86.

Mitchell, M., H. J. Nam, et al. (2009). "Production, purification and preliminary X-ray crystallographic studies of adeno-associated virus serotype 9." Acta Crystallogr Sect F Struct Biol Cryst Commun **65**(Pt 7): 715-8.

Miyoshi, H., U. Blomer, et al. (1998). "Development of a self-inactivating lentivirus vector." J Virol **72**(10): 8150-7.

Mochizuki, H. and Y. Mizuno (2003). "Gene therapy for Parkinson's disease." J Neural Transm Suppl(65): 205-13.

Mori, S., L. Wang, et al. (2004). "Two novel adeno-associated viruses from cynomolgus monkey: pseudotyping characterization of capsid protein." Virology **330**(2): 375-83.

Moss, R. B., C. Milla, et al. (2007). "Repeated aerosolized AAV-CFTR for treatment of cystic fibrosis: a randomized placebo-controlled phase 2B trial." Hum Gene Ther **18**(8): 726-32.

Moss, R. B., D. Rodman, et al. (2004). "Repeated adeno-associated virus serotype 2 aerosol-mediated cystic fibrosis transmembrane regulator gene transfer to the lungs of patients with cystic fibrosis: a multicenter, double-blind, placebo-controlled trial." Chest **125**(2): 509-21.

Mudhakir, D. and H. Harashima (2009). "Learning from the viral journey: how to enter cells and how to overcome intracellular barriers to reach the nucleus." Aaps J **11**(1): 65-77.

Mueller, C. and T. R. Flotte (2008). "Clinical gene therapy using recombinant adeno-associated virus vectors." Gene Ther **15**(11): 858-63.

Muller, O. J., F. Kaul, et al. (2003). "Random peptide libraries displayed on adeno-associated virus to select for targeted gene therapy vectors." Nat Biotechnol **21**(9): 1040-6.

Muramatsu, S., K. Fujimoto, et al. (2010). "A phase I study of aromatic L-amino acid decarboxylase gene therapy for Parkinson's disease." Mol Ther **18**(9): 1731-5.

Nakai, H., X. Wu, et al. (2005). "Large-scale molecular characterization of adeno-associated virus vector integration in mouse liver." J Virol **79**(6): 3606-14.

Nakai, H., S. R. Yant, et al. (2001). "Extrachromosomal recombinant adeno-associated virus vector genomes are primarily responsible for stable liver transduction in vivo." J Virol **75**(15): 6969-76.

Nam, H.-J., M. D. Lane, et al. (2007). "Structure of Adeno-Associated Virus Serotype 8, a Gene Therapy Vector." J. Virol. **81**(22): 12260-12271.

Nathwani, A. C., E. G. Tuddenham, et al. (2011). "Adenovirus-Associated Virus Vector-Mediated Gene Transfer in Hemophilia B." N Engl J Med.

Neumann, A. K., N. L. Thompson, et al. (2008). "Distribution and lateral mobility of DC-SIGN on immature dendritic cells--implications for pathogen uptake." J Cell Sci **121**(Pt 5): 634-43.

Nicklin, S. A., H. Buening, et al. (2001). "Efficient and selective AAV2-mediated gene transfer directed to human vascular endothelial cells." Mol Ther **4**(3): 174-81.

Nigg, E. A. (1997). "Nucleocytoplasmic transport: signals, mechanisms and regulation." Nature **386**(6627): 779-87.

Niklinski, J., G. Claassen, et al. (2000). "Disruption of Myc-tubulin interaction by hyperphosphorylation of c-Myc during mitosis or by constitutive hyperphosphorylation of mutant c-Myc in Burkitt's lymphoma." Mol Cell Biol **20**(14): 5276-84.

Nonnenmacher, M. and T. Weber (2011). "Adeno-Associated Virus 2 Infection Requires Endocytosis through the CLIC/GEEC Pathway." Cell Host Microbe **10**(6): 563-76.

Nonnenmacher, M. and T. Weber (2012). "Intracellular transport of recombinant adeno-associated virus vectors." Gene Ther **19**(6): 649-58.

Nonnenmacher, M. and T. Weber (2012). "Intracellular transport of recombinant adeno-associated virus vectors." Gene Ther.

Nozawa, N., Y. Yamauchi, et al. (2004). "Formation of aggresome-like structures in herpes simplex virus type 2-infected cells and a potential role in virus assembly." Exp Cell Res **299**(2): 486-97.

O'Donnell, J., K. A. Taylor, et al. (2009). "Adeno-associated virus-2 and its primary cellular receptor--Cryo-EM structure of a heparin complex." Virology **385**(2): 434-43.

Ohkawa, T., L. E. Volkman, et al. (2010). "Actin-based motility drives baculovirus transit to the nucleus and cell surface." J Cell Biol **190**(2): 187-95.

Ojala, P. M., B. Sodeik, et al. (2000). "Herpes simplex virus type 1 entry into host cells: reconstitution of capsid binding and uncoating at the nuclear pore complex in vitro." Mol Cell Biol **20**(13): 4922-31.

Opie, S. R., K. H. Warrington, Jr., et al. (2003). "Identification of amino acid residues in the capsid proteins of adeno-associated virus type 2 that contribute to heparan sulfate proteoglycan binding." J Virol **77**(12): 6995-7006.

Osten, P., V. Grinevich, et al. (2007). "Viral vectors: a wide range of choices and high levels of service." Handb Exp Pharmacol(178): 177-202.

Osterman, J. V., A. Waddell, et al. (1971). "Gene therapy systems: the need, experimental approach, and implications." Ann N Y Acad Sci **179**: 514-9.

Ouzilou, L., E. Caliot, et al. (2002). "Poliovirus transcytosis through M-like cells." J Gen Virol **83**(Pt 9): 2177-82.

Pacak, C. A., C. S. Mah, et al. (2006). "Recombinant adeno-associated virus serotype 9 leads to preferential cardiac transduction in vivo." Circ Res **99**(4): e3-9.

Pawley, J. B. (2006). Handbook of Biological Confocal Microscopy. New York, Springer.

Pelkmans, L., J. Kartenbeck, et al. (2001). "Caveolar endocytosis of simian virus 40 reveals a new two-step vesicular-transport pathway to the ER." Nat Cell Biol **3**(5): 473-83.

Peng, L., S. Ryazantsev, et al. (2010). "Three-dimensional visualization of gammaherpesvirus life cycle in host cells by electron tomography." Structure **18**(1): 47-58.

Perabo, L., H. Buning, et al. (2003). "In vitro selection of viral vectors with modified tropism: the adeno-associated virus display." Mol Ther **8**(1): 151-7.

Perabo, L., J. Endell, et al. (2006). "Combinatorial engineering of a gene therapy vector: directed evolution of adeno-associated virus." J Gene Med **8**(2): 155-62.

Petrs-Silva, H., A. Dinculescu, et al. (2009). "High-efficiency transduction of the mouse retina by tyrosine-mutant AAV serotype vectors." Mol Ther **17**(3): 463-71.

Ploubidou, A., V. Moreau, et al. (2000). "Vaccinia virus infection disrupts microtubule organization and centrosome function." Embo J **19**(15): 3932-44.

Pollard, H., J. S. Remy, et al. (1998). "Polyethylenimine but not cationic lipids promotes transgene delivery to the nucleus in mammalian cells." J Biol Chem **273**(13): 7507-11.

Pruchnic, R., B. Cao, et al. (2000). "The use of adeno-associated virus to circumvent the maturation-dependent viral transduction of muscle fibers." Hum Gene Ther **11**(4): 521-36.

Qing, K., C. Mah, et al. (1999). "Human fibroblast growth factor receptor 1 is a co-receptor for infection by adeno-associated virus 2." Nat Med **5**(1): 71-7.

Quesada, O., B. Gurda, et al. (2007). "Production, purification and preliminary X-ray crystallographic studies of adeno-associated virus serotype 7." Acta Crystallogr Sect F Struct Biol Cryst Commun **63**(Pt 12): 1073-6.

Quintyne, N. J., S. R. Gill, et al. (1999). "Dynactin is required for microtubule anchoring at centrosomes." J Cell Biol **147**(2): 321-34.

Rabinowitz, J. E., D. E. Bowles, et al. (2004). "Cross-dressing the virion: the transcapsidation of adeno-associated virus serotypes functionally defines subgroups." J Virol **78**(9): 4421-32.

Rabinowitz, J. E., F. Rolling, et al. (2002). "Cross-packaging of a single adeno-associated virus (AAV) type 2 vector genome into multiple AAV serotypes enables transduction with broad specificity." J Virol **76**(2): 791-801.

Radtke, K., D. Kieneke, et al. (2011). "Plus- and minus-end directed microtubule motors bind simultaneously to herpes simplex virus capsids using different inner tegument structures." PLoS Pathog **6**(7): e1000991.

Rissanen, T. T. and S. Yla-Herttuala (2007). "Current status of cardiovascular gene therapy." Mol Ther **15**(7): 1233-47.

Robbins, P. D. and S. C. Ghivizzani (1998). "Viral vectors for gene therapy." Pharmacol Ther **80**(1): 35-47.

Rogers, G. L., A. T. Martino, et al. (2011). "Innate Immune Responses to AAV Vectors." Front Microbiol **2**: 194.

Rogers, S. (1971). "Gene therapy: a potentially invaluable aid to medicine and mankind." Res Commun Chem Pathol Pharmacol **2**(4): 587-600.

Roohvand, F., P. Maillard, et al. (2009). "Initiation of hepatitis C virus infection requires the dynamic microtubule network: role of the viral nucleocapsid protein." J Biol Chem **284**(20): 13778-91.

Rosenberg, S. A., P. Aebersold, et al. (1990). "Gene transfer into humans--immunotherapy of patients with advanced melanoma, using tumor-infiltrating lymphocytes modified by retroviral gene transduction." N Engl J Med **323**(9): 570-8.

Roth, D. M., G. W. Moseley, et al. (2007). "A microtubule-facilitated nuclear import pathway for cancer regulatory proteins." Traffic **8**(6): 673-86.

Roth, J. A. (2006). "Adenovirus p53 gene therapy." Expert Opin Biol Ther **6**(1): 55-61.

Rutledge, E. A., C. L. Halbert, et al. (1998). "Infectious clones and vectors derived from adeno-associated virus (AAV) serotypes other than AAV type 2." J Virol **72**(1): 309-19.

Samulski, R. J., K. I. Berns, et al. (1982). "Cloning of adeno-associated virus into pBR322: rescue of intact virus from the recombinant plasmid in human cells." Proc Natl Acad Sci U S A **79**(6): 2077-81.

Samulski, R. J., L. S. Chang, et al. (1989). "Helper-free stocks of recombinant adeno-associated viruses: normal integration does not require viral gene expression." J Virol **63**(9): 3822-8.

Samulski, R. J., A. Srivastava, et al. (1983). "Rescue of adeno-associated virus from recombinant plasmids: gene correction within the terminal repeats of AAV." Cell **33**(1): 135-43.

Samulski, R. J., X. Zhu, et al. (1991). "Targeted integration of adeno-associated virus (AAV) into human chromosome 19." Embo J **10**(12): 3941-50.

Sanlioglu, S., P. K. Benson, et al. (2000). "Endocytosis and nuclear trafficking of adeno-associated virus type 2 are controlled by rac1 and phosphatidylinositol-3 kinase activation." J Virol **74**(19): 9184-96.

Schelhaas, M., H. Ewers, et al. (2008). "Human papillomavirus type 16 entry: retrograde cell surface transport along actin-rich protrusions." PLoS Pathog **4**(9): e1000148.

Schepis, A., B. Schramm, et al. (2006). "Vaccinia virus-induced microtubule-dependent cellular rearrangements." Traffic **7**(3): 308-23.

Schneider, M., A. A. Noegel, et al. (2008). "KASH-domain proteins and the cytoskeletal landscapes of the nuclear envelope." Biochem Soc Trans **36**(Pt 6): 1368-72.

Schnell, T., P. Foley, et al. (2000). "Development of a self-inactivating, minimal lentivirus vector based on simian immunodeficiency virus." Hum Gene Ther **11**(3): 439-47.

Schroer, T. A. (2004). "Dynactin." Annu Rev Cell Dev Biol **20**: 759-79.

Schuh, M. (2011). "An actin-dependent mechanism for long-range vesicle transport." Nat Cell Biol.

Sedarat, F., E. Lin, et al. (2004). "Deconvolution of confocal images of dihydropyridine and ryanodine receptors in developing cardiomyocytes." J Appl Physiol **97**(3): 1098-103.

Seisenberger, G., M. U. Ried, et al. (2001). "Real-time single-molecule imaging of the infection pathway of an adeno-associated virus." Science **294**(5548): 1929-32.

Sfakianos, J. N. and E. Hunter (2003). "M-PMV capsid transport is mediated by Env/Gag interactions at the pericentriolar recycling endosome." Traffic **4**(10): 671-80.

Shen, S., K. D. Bryant, et al. "Terminal N-linked galactose is the primary receptor for adeno-associated virus 9." J Biol Chem **286**(15): 13532-40.

Shi, W., G. S. Arnold, et al. (2001). "Insertional mutagenesis of the adeno-associated virus type 2 (AAV2) capsid gene and generation of AAV2 vectors targeted to alternative cell-surface receptors." Hum Gene Ther **12**(14): 1697-711.

Shi, W. and J. S. Bartlett (2003). "RGD inclusion in VP3 provides adeno-associated virus type 2 (AAV2)-based vectors with a heparan sulfate-independent cell entry mechanism." Mol Ther **7**(4): 515-25.

Shi, Y., E. Seto, et al. (1991). "Transcriptional repression by YY1, a human GLI-Kruppel-related protein, and relief of repression by adenovirus E1A protein." Cell **67**(2): 377-88.

Simonelli, F., A. M. Maguire, et al. (2010). "Gene therapy for Leber's congenital amaurosis is safe and effective through 1.5 years after vector administration." Mol Ther **18**(3): 643-50.

Snyder, A., T. W. Wisner, et al. (2006). "Herpes simplex virus capsids are transported in neuronal axons without an envelope containing the viral glycoproteins." J Virol **80**(22): 11165-77.

Sodeik, B., M. W. Ebersold, et al. (1997). "Microtubule-mediated transport of incoming herpes simplex virus 1 capsids to the nucleus." J Cell Biol **136**(5): 1007-21.

Song, S., M. Scott-Jorgensen, et al. (2002). "Intramuscular administration of recombinant adeno-associated virus 2 alpha-1 antitrypsin (rAAV-SERPINA1) vectors in a nonhuman primate model: safety and immunologic aspects." Mol Ther **6**(3): 329-35.

Sonntag, F., S. Bleker, et al. (2006). "Adeno-associated virus type 2 capsids with externalized VP1/VP2 trafficking domains are generated prior to passage through the cytoplasm and are maintained until uncoating occurs in the nucleus." J Virol **80**(22): 11040-54.

Sonntag, F., K. Kother, et al. (2011). "The assembly-activating protein promotes capsid assembly of different adeno-associated virus serotypes." J Virol **85**(23): 12686-97.

Sonntag, F., K. Schmidt, et al. (2010). "A viral assembly factor promotes AAV2 capsid formation in the nucleolus." Proc Natl Acad Sci U S A **107**(22): 10220-5.

Stein, L., K. Roy, et al. (2011). "Clinical gene therapy for the treatment of RPE65-associated Leber congenital amaurosis." Expert Opin Biol Ther **11**(3): 429-39.

Stone, E. M. (2007). "Leber congenital amaurosis - a model for efficient genetic testing of heterogeneous disorders: LXIV Edward Jackson Memorial Lecture." Am J Ophthalmol **144**(6): 791-811.

Stroes, E. S., M. C. Nierman, et al. (2008). "Intramuscular administration of AAV1-lipoprotein lipase S447X lowers triglycerides in lipoprotein lipase-deficient patients." Arterioscler Thromb Vasc Biol **28**(12): 2303-4.

Strunze, S., L. C. Trotman, et al. (2005). "Nuclear targeting of adenovirus type 2 requires CRM1-mediated nuclear export." Mol Biol Cell **16**(6): 2999-3009.

Suikkanen, S., T. Aaltonen, et al. (2003). "Exploitation of microtubule cytoskeleton and dynein during parvoviral traffic toward the nucleus." J Virol **77**(19): 10270-9.

Suikkanen, S., K. Saajarvi, et al. (2002). "Role of recycling endosomes and lysosomes in dynein-dependent entry of canine parvovirus." J Virol **76**(9): 4401-11.

Summerford, C., J. S. Bartlett, et al. (1999). "AlphaVbeta5 integrin: a co-receptor for adeno-associated virus type 2 infection." Nat Med **5**(1): 78-82.

Summerford, C. and R. J. Samulski (1998). "Membrane-associated heparan sulfate proteoglycan is a receptor for adeno-associated virus type 2 virions." J Virol **72**(2): 1438-45.

Sun, B., H. Zhang, et al. (2005). "Efficacy of an adeno-associated virus 8-pseudotyped vector in glycogen storage disease type II." Mol Ther **11**(1): 57-65.

Sun, M., G. R. Zhang, et al. (2003). "Correction of a rat model of Parkinson's disease by coexpression of tyrosine hydroxylase and aromatic amino acid decarboxylase from a helper virus-free herpes simplex virus type 1 vector." Hum Gene Ther **14**(5): 415-24.

Sun, X., B. Pawlyk, et al. (2010). "Gene therapy with a promoter targeting both rods and cones rescues retinal degeneration caused by AIPL1 mutations." Gene Ther **17**(1): 117-31.

Suzuki, M., E. A. Chiocca, et al. (2008). "Stable transgene expression from HSV amplicon vectors in the brain: potential involvement of immunoregulatory signals." Mol Ther **16**(10): 1727-36.

Suzuki, Y. and R. Craigie (2007). "The road to chromatin - nuclear entry of retroviruses." Nat Rev Microbiol **5**(3): 187-96.

Taylor, M. P., T. B. Burgon, et al. (2009). "Role of microtubules in extracellular release of poliovirus." J Virol **83**(13): 6599-609.

Torchilin, V. P. (2006). "Recent approaches to intracellular delivery of drugs and DNA and organelle targeting." Annu Rev Biomed Eng **8**: 343-75.

Towers, G. J. (2007). "The control of viral infection by tripartite motif proteins and cyclophilin A." Retrovirology **4**: 40.

Tsai, M. Y., G. Morfini, et al. (2000). "Release of kinesin from vesicles by hsc70 and regulation of fast axonal transport." Mol Biol Cell **11**(6): 2161-73.

Van de Walle, G. R., H. W. Favoreel, et al. (2001). "Involvement of cellular cytoskeleton components in antibody-induced internalization of viral glycoproteins in pseudorabies virus-infected monocytes." Virology **288**(1): 129-38.

van Loo, N. D., E. Fortunati, et al. (2001). "Baculovirus infection of nondividing mammalian cells: mechanisms of entry and nuclear transport of capsids." J Virol **75**(2): 961-70.

Vandervoort, H. T. M. and K. C. Strasters (1995). "Restoration of Confocal Images for Quantitative Image-Analysis." Journal of Microscopy-Oxford **178**: 165-181.

Vaughan, J. C., B. Brandenburg, et al. (2009). "Rapid actin-dependent viral motility in live cells." Biophys J **97**(6): 1647-56.

Vihinen-Ranta, M., L. Kakkola, et al. (1997). "Characterization of a nuclear localization signal of canine parvovirus capsid proteins." Eur J Biochem **250**(2): 389-94.

Vihinen-Ranta, M., A. Kalela, et al. (1998). "Intracellular route of canine parvovirus entry." J Virol **72**(1): 802-6.

Vonderheit, A. and A. Helenius (2005). "Rab7 associates with early endosomes to mediate sorting and transport of Semliki forest virus to late endosomes." PLoS Biol **3**(7): e233.

Wagner, J. A., A. H. Messner, et al. (1999). "Safety and biological efficacy of an adeno-associated virus vector-cystic fibrosis transmembrane regulator (AAV-CFTR) in the cystic fibrosis maxillary sinus." Laryngoscope **109**(2 Pt 1): 266-74.

Wagner, J. A., I. B. Nepomuceno, et al. (2002). "A phase II, double-blind, randomized, placebo-controlled clinical trial of tgAAVCF using maxillary sinus delivery in patients with cystic fibrosis with antrostomies." Hum Gene Ther **13**(11): 1349-59.

Walters, R. W., M. Agbandje-McKenna, et al. (2004). "Structure of Adeno-Associated Virus Serotype 5." J. Virol. **78**(7): 3361-3371.

Walz, C., A. Deprez, et al. (1997). "Interaction of human papillomavirus type 16 and adeno-associated virus type 2 co-infecting human cervical epithelium." J Gen Virol **78 ( Pt 6)**: 1441-52.

Wang, J., S. M. Faust, et al. (2011). "The next step in gene delivery: molecular engineering of adeno-associated virus serotypes." J Mol Cell Cardiol **50**(5): 793-802.

Wang, Z., T. Zhu, et al. (2005). "Adeno-associated virus serotype 8 efficiently delivers genes to muscle and heart." Nat Biotechnol **23**(3): 321-8.

Warrington, K. H., Jr. and R. W. Herzog (2006). "Treatment of human disease by adeno-associated viral gene transfer." Hum Genet **119**(6): 571-603.

Waterkamp, D. A., O. J. Muller, et al. (2006). "Isolation of targeted AAV2 vectors from novel virus display libraries." J Gene Med **8**(11): 1307-19.

Watson, P., A. T. Jones, et al. (2005). "Intracellular trafficking pathways and drug delivery: fluorescence imaging of living and fixed cells." Adv Drug Deliv Rev **57**(1): 43-61.

Weinberg, M. S., R. J. Samulski, et al. (2012). "Adeno-associated virus (AAV) gene therapy for neurological disease." Neuropharmacology.

Wells, D. J. (2010). "Electroporation and ultrasound enhanced non-viral gene delivery in vitro and in vivo." Cell Biol Toxicol **26**(1): 21-8.

White, A. F., M. Mazur, et al. (2008). "Genetic modification of adeno-associated viral vector type 2 capsid enhances gene transfer efficiency in polarized human airway epithelial cells." Hum Gene Ther **19**(12): 1407-14.

White, S. J., S. A. Nicklin, et al. (2004). "Targeted gene delivery to vascular tissue in vivo by tropism-modified adeno-associated virus vectors." Circulation **109**(4): 513-9.

Whittaker, G. R., M. Kann, et al. (2000). "Viral entry into the nucleus." Annu Rev Cell Dev Biol **16**: 627-51.

Wileman, T. (2007). "Aggresomes and pericentriolar sites of virus assembly: cellular defense or viral design?" Annu Rev Microbiol **61**: 149-67.

Williams, D. A. (2009). "ESCGT 2008: progress in clinical gene therapy." Mol Ther **17**(1): 1-2.

Wolff, J., D. L. Lewis, et al. (2005). "Non-viral approaches for gene transfer." Acta Myol **24**(3): 202-8.

Work, L. M., H. Buning, et al. (2006). "Vascular bed-targeted in vivo gene delivery using tropism-modified adeno-associated viruses." Mol Ther **13**(4): 683-93.

Wu, P., W. Xiao, et al. (2000). "Mutational analysis of the adeno-associated virus type 2 (AAV2) capsid gene and construction of AAV2 vectors with altered tropism." J Virol **74**(18): 8635-47.

Wu, Z., A. Asokan, et al. (2006). "Single amino acid changes can influence titer, heparin binding, and tissue tropism in different adeno-associated virus serotypes." J Virol **80**(22): 11393-7.

Wu, Z., A. Asokan, et al. (2006). "Adeno-associated virus serotypes: vector toolkit for human gene therapy." Mol Ther **14**(3): 316-27.

Xiao, P. J., L. Hu, et al. (2007). "NSSR1 is regulated in testes development and cryptorchidism and promotes the exon 5-included splicing of CREB transcripts." Mol Reprod Dev **74**(11): 1363-72.

Xiao, P. J., T. B. Lentz, et al. (2012). "Recombinant adeno-associated virus: clinical application and development as a gene-therapy vector." Therapeutic Delivery **3**(7): 835-856.

Xiao, P. J., C. Li, et al. (2011). "Quantitative 3D Tracing of Gene-delivery Viral Vectors in Human Cells and Animal Tissues." Mol Ther.

Xiao, P. J., C. Li, et al. (2012). "Quantitative 3D tracing of gene-delivery viral vectors in human cells and animal tissues." Mol Ther **20**(2): 317-28.

Xiao, P. J., Z. Y. Peng, et al. (2011). "Dephosphorylated NSSR1 is induced by androgen in mouse epididymis and phosphorylated NSSR1 is increased during sperm maturation." PLoS One **6**(9): e25667.

Xiao, P. J. and R. J. Samulski (2012). "Cytoplasmic trafficking, endosomal escape, and perinuclear accumulation of adeno-associated virus type 2 particles are facilitated by microtubule network." J Virol **86**(19): 10462-73.

Xiao, W., K. H. Warrington, Jr., et al. (2002). "Adenovirus-facilitated nuclear translocation of adeno-associated virus type 2." J Virol **76**(22): 11505-17.

Xiao, X., J. Li, et al. (1998). "Production of high-titer recombinant adeno-associated virus vectors in the absence of helper adenovirus." J Virol **72**(3): 2224-32.

Xiao, X., W. Xiao, et al. (1997). "A novel 165-base-pair terminal repeat sequence is the sole cis requirement for the adeno-associated virus life cycle." J Virol **71**(2): 941-8.

Xie, Q., W. Bu, et al. (2002). "The atomic structure of adeno-associated virus (AAV-2), a vector for human gene therapy." Proc Natl Acad Sci U S A **99**(16): 10405-10.

Yakobson, B., T. Koch, et al. (1987). "Replication of adeno-associated virus in synchronized cells without the addition of a helper virus." J Virol **61**(4): 972-81.

Yalkinoglu, A. O., R. Heilbronn, et al. (1988). "DNA amplification of adeno-associated virus as a response to cellular genotoxic stress." Cancer Res **48**(11): 3123-9.

Yang, L., J. Jiang, et al. (2009). "A myocardium tropic adeno-associated virus (AAV) evolved by DNA shuffling and in vivo selection." Proc Natl Acad Sci U S A **106**(10): 3946-51.

Yazawa, H., T. Murakami, et al. (2006). "Hydrodynamics-based gene delivery of naked DNA encoding fetal liver kinase-1 gene effectively suppresses the growth of pre-existing tumors." Cancer Gene Ther **13**(11): 993-1001.

Yea, C., J. Dembowy, et al. (2007). "Microtubule-mediated and microtubule-independent transport of adenovirus type 5 in HEK293 cells." J Virol **81**(13): 6899-908.

Yu, C. Y., Z. Yuan, et al. (2009). "A muscle-targeting peptide displayed on AAV2 improves muscle tropism on systemic delivery." Gene Ther **16**(8): 953-62.

Yu, W., N. Zhang, et al. (2009). "Saccharide modified pharmaceutical nanocarriers for targeted drug and gene delivery." Curr Pharm Des **15**(32): 3826-36.

Zadori, Z., J. Szelei, et al. (2001). "A viral phospholipase A2 is required for parvovirus infectivity." Dev Cell **1**(2): 291-302.

Zeltner, N., E. Kohlbrenner, et al. (2010). "Near-perfect infectivity of wild-type AAV as benchmark for infectivity of recombinant AAV vectors." Gene Ther **17**(7): 872-9.

Zenklusen, D., D. R. Larson, et al. (2008). "Single-RNA counting reveals alternative modes of gene expression in yeast." Nat Struct Mol Biol **15**(12): 1263-71.

Zhang, H. G., J. Xie, et al. (2002). "Addition of six-His-tagged peptide to the C terminus of adeno-associated virus VP3 does not affect viral tropism or production." J Virol **76**(23): 12023-31.

Zhao, W., L. Zhong, et al. (2006). "Role of cellular FKBP52 protein in intracellular trafficking of recombinant adeno-associated virus 2 vectors." Virology **353**(2): 283-93.

Zhong, L., B. Li, et al. (2008). "Tyrosine-phosphorylation of AAV2 vectors and its consequences on viral intracellular trafficking and transgene expression." Virology **381**(2): 194-202.

Zhong, L., B. Li, et al. (2008). "Next generation of adeno-associated virus 2 vectors: point mutations in tyrosines lead to high-efficiency transduction at lower doses." Proc Natl Acad Sci U S A **105**(22): 7827-32.

Ziegelbauer, J., B. Shan, et al. (2001). "Transcription factor MIZ-1 is regulated via microtubule association." Mol Cell **8**(2): 339-49.